Steric Control of the Formation of Metallosupramolecular Complexes

---

A thesis submitted in partial fulfilment of the requirements for the degree of

Master of Science in **Chemistry**

University of Canterbury

Samantha Ellen Bodman

2014

“Character cannot be developed in ease and quiet. Only through experience of trial and suffering can the soul be strengthened, ambition inspired, and success achieved.”

Helen Keller

Acknowledgements

First and foremost, I would like to thank my research supervisor, Dr. Chris Fitchett for his expertise, knowledge, patience and support throughout not only my master's thesis but throughout my studies at the University of Canterbury.

To the past and present members of the Fitchett group and Steel group, as well as those in office 832, who have created a friendly working environment throughout the past two years. I would like to extend my thank you to Siji Rajan for her help and knowledge with my never ending questions, as well as to Robbie Currie, Will Kerr, Shane Verma and Rob Staniland for knowledge in the lab and constant banter. To Sian Davies for all the coffee breaks and listening to my chemistry highs and lows.

I am grateful to the academic staff, in the Chemistry Department who have passed on their knowledge to me throughout my studies at Canterbury. I would like to extend my thanks to Dr. Marie Squire for all your help with NMR, Mass Spectrometry and your constant support throughout, we both know I wouldn't be here without you. Thank you to all the technical staff, especially to Wayne Mackay and Rob McGregor. A special mention to Andy Pratt and Jan Wikaira for taking your time to share your extensive knowledge and support with me throughout this journey.

Thank you to all my friends outside the chemistry department, especially Lanette Shute for all your encouragement, wine nights and keeping me in touch with reality, you may not have understood entirely what I was doing but thank you for taking the time to listen. A huge thank you to Tammi van Niekerk, for always being there for me.

I extend a very special thank-you to my family for their constant love, belief and encouragement not just through this process, but in all my endeavours. Thank you for helping shape me into the person I am today.

Lastly, to my wonderful Graeme, thank you for believing in me and for your constant support and love in everything I do.

Table of Contents

Acknowledgements……iii

Table of Contents……iv

Abstract……...vi

Abbreviations……vii

Chapter 1: Introduction……....1

1.1 Supramolecular Chemistry……...2
1.2 Metallosupramolecular Chemistry..…….....4
1.3 Supramolecular Grids…….…..5
1.4 Supramolecular Helicates…….…....8
1.5 Inter-conversion between metallogrids and helicates……10
1.6 Pyridazines……12
1.7 Ligands synthesised in this study…….……12
1.8 Scope of thesis, methods of synthesis and data collection……16

Chapter 2: Silver Complexes……..……....18

2.1 Introduction…….....19
2.2 Solution Studies…….....22
2.3 Coordination Complexes I……..26
2.4 Synthesis of L13 – L16…….....48
2.5 Coordination Complexes II……50
2.6 Summary…….....53

Chapter 3: Copper Complexes…….....57

3.1 Introduction…….....58
3.2 Coordination Complexes…….....61
3.3 Summary…….....76

Chapter 4: Zinc Complexes…….....78

4.1 Introduction…….....79
4.2 Coordination Complexes…….....81

4.3 Summary…….....113

Chapter 5: Conclusion and Future Work……..117

Chapter 6: Experimental…….....120

6.1 General Experimental…….....121
6.2 Ligands…….....122
6.3 Silver Complexes…….....126
6.4 Copper Complexes…….....131
6.5 Zinc Complexes…….....134

References…….....138

Appendix 1: Crystal data and structure refinement details……..145

Abstract

This thesis describes the preparation of a series of metallosupramolecular architectures formed with three selected d^{10} metals, silver(I), copper(I) and zinc(II). A total of sixteen rigid ligands were synthesised, with hindering substituents introduced to the central pyridazine ring, resulting in an interesting series of complexes.

Chapter one outlines an introduction to the topic discussed in this study providing examples from the literature. This also includes an in-depth background of the complex work reported for previously synthesised ligands. *Chapter two* details metallosupramolecular self-assembled architectures with silver(I); with solution studies and single crystal X-ray crystallography determinations of the complexes formed. *Chapter three* presents crystallographically characterised discrete and polymeric species with copper(I) as the metal. *Chapter four* shows an interesting series of zinc(II) complexes with each characterised by NMR spectroscopy, UV-Visible spectrophotometry and single crystal X-ray diffraction determination. *Chapter five* concludes the results as a whole and potential future direction of this work. *Chapter six* outlines the synthesis, characterisation of the new and modified synthesis of the ligands and complexes in this study.

Twenty-five coordination complexes are prepared, characterised by X-ray crystallography and determination of the structures in solution are investigated.

Abbreviations

^{1}H-NMR: Proton Nuclear Magnetic Resonance

^{13}C-NMR: Carbon Nuclear Magnetic Resonance

UV-Vis: Ultraviolet-Visible

ESI-MS: Electrospray Ionisation Mass Spectrometry

MP: Melting Point

IR: Infrared

s: strong (IR)

m: medium (IR)

w: weak (IR)

br: broad (IR)

Atom Colour Scheme

Black: Carbon

Blue: Nitrogen

White: Hydrogen

Red: Oxygen

Dark Green: Chlorine

Light Green: Fluorine

Yellow: Sulfur

Pink: Phosphate

Light Grey: Boron

Purple: Iodine

Magenta: Silver

Dark Orange: Copper

Gold: Zinc

CHAPTER ONE

Introduction

1.1 Supramolecular Chemistry

Supramolecular chemistry has emerged as an important field of chemistry over the past few decades. It has been defined in many ways, firstly described by Lehn in 1988 as "chemistry beyond the molecule".[1] However, a more suitable definition may be: the properties of supramolecular molecules are the chemical, physical and biological features of intermolecular bonds, formed by the association of two or more molecules.[1,2,3] More traditional molecular chemistry is focused on atoms held together by strong covalent bonds,[4] where, supramolecular chemistry concerns the weaker interactions between molecules that give rise to larger assemblies.

Pioneers in this field were Cram,[5] Lehn[1] and Pedersen,[6] whose work in the area of host-guest chemistry, "spherands", "cryptands" and "crown-ethers", respectively, resulted in them receiving the Nobel Prize for Chemistry in 1987 *"for their development and use of molecules with structure-specific interactions of high selectivity"*. The molecular components are held together and organised by non-covalent interactions, which are a fundamental concept in the understanding and interpretation of the function of supramolecular architectures. These interactions include van der Waal, charge transfer, electrostatic, π-π and hydrogen-bonding; their principle characteristics are shown in table 1.1.[7-9] Discussed further are those interactions relevant to this research (see below).

Interaction Type	Distance Range (Å)	Energy Range
Coordination Bond	~1.8 – 2.5	~ 50 – 500 kJ mol^{-1-}
Classical Hydrogen Bond (N, O donor/acceptors)	≤ 3.2 (D···A)	10 – 30 kJ mol^{-1}
Non-classical Hydrogen Bond (C N O donor/acceptors)	3 – 3.5 (D···A)	8 – 15 kJ mol^{-1}
C-H···π interaction (edge to face [a])	3.5 – 3.8 (C···π)	2 – 8 kJ mol^{-1}
Π-π(Offset face to face [a])	3.3 – 3.8 (interplanar)	2 – 50 kJ mol^{-1}

[a]Terms explained in π-π interactions below.

Table 1.1: Summarises the key bonding interactions, bond lengths and energies that are commonly encountered for metallosupramolecular interactions.[7,9-11] Hydrogen bonding interactions can exhibit bond dissociation enthalpies of over 150 kJ/mol, however the scope of these interactions lies outside this work.[7]

π-π Interactions:

Interactions between aromatic rings are prevalent in nature, with DNA being the classic example. It has been proven that the twisting of the helix is due to the π-stacking of the base pairs.[9,12] In supramolecular chemistry, aromatic systems can interact in a similar way. There are two types of π-

π interactions, face-to-face and edge-to-face which are shown in figure 1.1. In the former, the π-systems are involved in a parallel stacking interaction, which, when partially off-set, maximises the interaction and minimises the π-electron repulsion that occurs. Alternatively, a proton on one aromatic ring can be positioned adjacent to the face of a neighbouring aromatic ring with a π-π interaction observed.

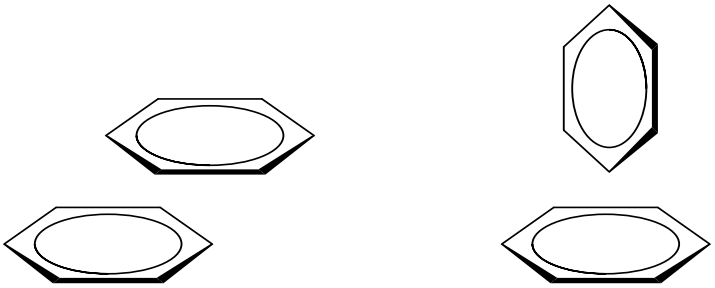

(a) **(b)**

Figure 1.1: The configurations of the benzene dimer showing π-π stacking occurring between the aromatic rings involving, (a) face-to-face, and (b) edge-to-face interactions.

Hydrogen Bonding:

Hydrogen bonding is one of the most important non-covalent interactions in the design of supramolecular architectures because of its strength and its high degree of directionality.[13] There are many definitions that have been used to describe this interaction since its discovery over a century ago.[10] A practically useful definition is *"An X-H···A interaction is called a "hydrogen bond", if (1) It constitutes a local bond, and (2) X-H acts as a proton donor to A".*[10] There are four different types of accepted hydrogen bonds reviewed by Nishio *et al.*,[11] as shown in figure 1.2: (i) X-H···X bond, where the X is an electronegative atom, oxygen, nitrogen or fluorine, and due to the polarity of the X in the X-H bond results in a positively charged hydrogen atom; (ii) a weaker non-classical hydrogen-bond, X-H···π, where again X is an electronegative atom and the π system acts as a H-acceptor; (iii) C-H···n, where the carbon acts as a proton donor and a lone pair of electrons on *n* as the acceptor; (iv) an even weaker molecular force C-H···π interactions involving a sp^3 or sp^2 CH group as the H-donor interacting with a π system, this interaction is also referred to as a π-π edge to face interaction (as described previously).

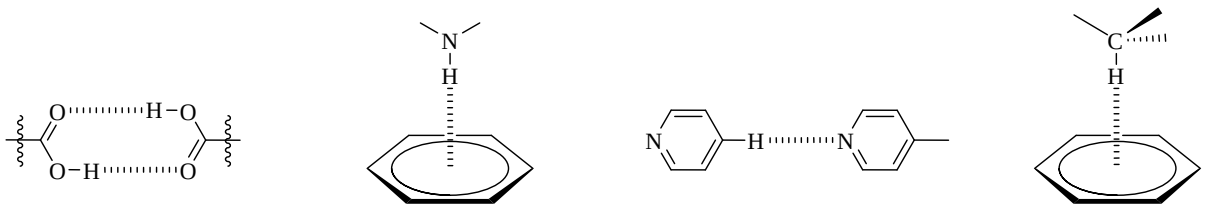

Figure 1.2: The different types of hydrogen bonding. (a) X-H···X, (b) X-H···π, (c) C-H···n and (d) C-H···π.

1.2 Metallosupramolecular Chemistry

Metallosupramolecular chemistry is a subsection of supramolecular chemistry which involves the use of bridging organic ligands in combination with metallic units to synthesise discrete or polymeric assemblies. The term 'metallosupramolecular" was first introduced in 1994 by Constable,[14] and is used to describe the self-assembly of metal-mediated structures. A vast number of metallosupramolecular aggregates have been investigated with a large variation in the topologies found. Not only do these architectures have varied aesthetically pleasing structures, but they possess interesting physical and chemical properties.

One of the key concepts in supramolecular chemistry is the reversibility of bond formation. As covalent bonds typically exhibit strong interactions and are less likely to be reversible, weak interactions show reversibility that rapidly equilibrates to give the most thermodynamically favourable state, rather than the kinetically favourable product, which will more likely be short lived. This concept is called self-assembly,[15] which involves the spontaneous self-organisation of a number of components into a single aggregated structure.[16] Self-assembly processes are generally efficient because the products are usually both enthalpically and entropically favoured.

The consideration of the building blocks (synthons) is an essential part of the design, one being the metal ion and the other an organic molecule.[7] The metal atoms have different properties which allow the choices for specific applications. *Lability* of the coordination bonds (metal-to-ligand) contributes to the overall structure forming the most stable thermodynamic product. Metals chosen to prepare assemblies usually have preferred coordination geometries and numbers, which often dictate the final structure observed. The most common metal atom coordination geometries are shown in figure 1.3. The organic ligands are carefully designed with features appropriate for

bonding to the metal ions, which are selected for their coordination number and stereochemical preferences.[17]

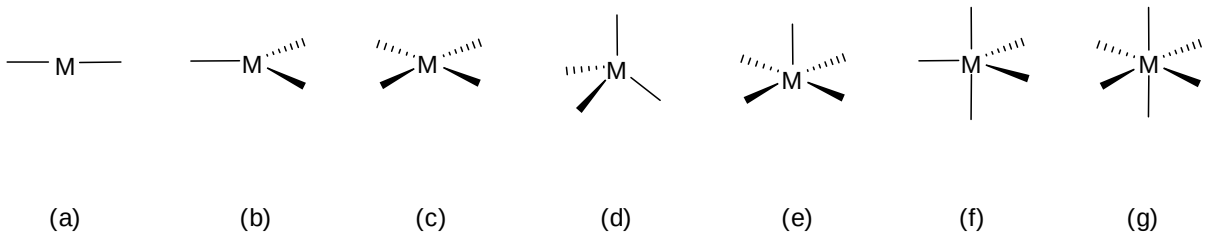

Figure 1.3: Coordination geometries of metal atoms commonly used in metallosupramolecular chemistry; (a) linear; (b) trigonal planar; (c) square planar; (d) tetrahedral; (e) square pyramidal; (f) trigonal bipyramidal; (g) octahedral.

The metals chosen for this study, silver(I), copper(I) and zinc(II) are all d^{10} transition metals and have different preferences for coordination. The geometries associated with silver(I) metal ions are commonly (**a**) or (**b**). Although silver is promiscuous, it can adopt other coordinate geometries as well, with up to nine donor atoms.[18-20] Copper(I) shows a preference for four-coordinate tetrahedral geometry (**d**), however, copper(II), being a d^9 metal ion, can adopt a variety of coordination geometries, from four-coordinate through to six-coordinate.[21] Zinc(II), prefers an octahedral arrangement (**g**), but also is seen in complexes that are tetrahedral four-coordinate (**d**) depending on the nature of the ligands.[21] A discussion of each metal is included at the beginning of each chapter.

The metal-to-ligand bond strength varies with different metal atoms. The metallosupramolecular assemblies have functional properties due to the different metal atoms they possess, including photophysical, photochemical, electrochemical and magnetic for applications such as in molecular electronics,[22-24] sensors,[22,24-27] solid state memory,[23] and for catalysis.[22,24,26,28,29]

Metal-directed self-assembly is a rich area of supramolecular chemistry that has led to the development of chemical architectures including grids,[14] boxes,[30] rotaxanes,[31,32] catenanes,[32,33] and helicates,[34,35] where grids and helical structures will be the focus of this research. The remainder of the discussion of self-assembly will be limited to grid-like and helical coordination complexes.

1.3 Supramolecular Grids

The term "metallogrid" is used to describe a metal ion complex in which the arrays of organic components are essentially planar and the metal ions are considered to define a junction in a square or rectangular grid. The formation of grid-like structures involves the subtle control and

manipulation of steric, electronic, enthalpic and entropic factors of both the ligands and metal atoms used. The different components featured can lead to the formation of other architectures. Lehn and co-workers have formed several grid-like complexes with examples of [2 x 2], [3 x 3] and [4 x 4] grid based architectures.[30,36-45]

There are three factors that influence the self-assembly of metallosupramolecular architectures in the generation of grid-type arrays:

i. A set of coordination interactions that impose the correct geometry on the structure which drives the process of self-assembly based on the principle of full occupancy of the binding sites;[46]
ii. Internal factors (including steric factors) hindering formation of other products or stabilizing interactions that proceed to form the desired product;
iii. External factors that help favour the formation of the chosen product, these include binding of solvent molecule(s), counter-ion(s) or other chemical species in the environment. Entropy also plays a role in the product formation.

The first reported formation of a [2 x 2] metallogrid was in 1992 by Osborn *et al.*[30] This architecture contains four metal ions with four deliberately designed rigid ditopic ligands of 3,6-bis(2-pyridyl)pyridazine, where the nitrogen atoms in the heterocycle donate a pair of electrons to the metal in a tetrahedral geometry. Both Cu(I)[30] (Figure 1.4) and Ag(I)[36] (Chapter 2) metallogrids spontaneously form when the metal and ligand components are mixed in a 1:1 stoichiometry.

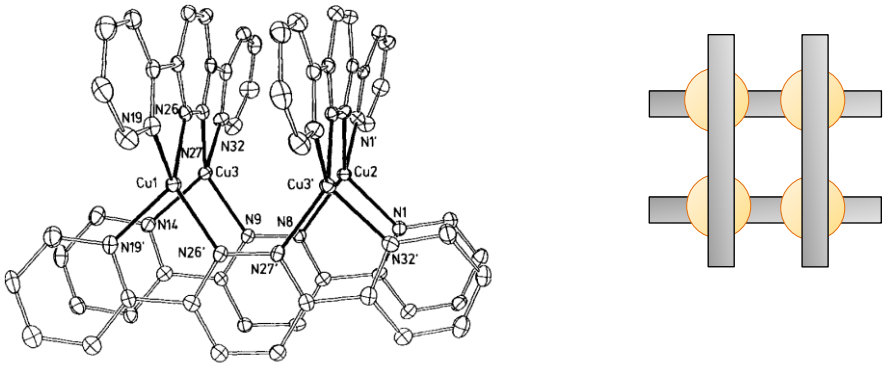

Figure 1.4: Structure of the first reported grid-like structure (left).[30] Cartoon representation of the structure, Cu(I) metal atoms represented as orange spheres and the lines correspond to the ligands (right).

[3 x 3] Metallogrids consist of nine metals and six ligands which are synthetically more challenging.[41] The first in this class of grids was reported by Baxter *et al.*,[37] with the supramolecular

system utilising the self-assembly process of geometric, recognition, thermodynamic and entropic effects.[16,37] This grid-like array (figure 1.5) was formed with the ligand, 6,6'-bis[2-(6-methylpyridyl)]-3,3'-bipyridazine reacted with the silver triflate metal salt. These types of grids have also been formed with tridentate ligands and different metals, Mn(II), Cu(II), Co(II), Ni(II), Fe(III).[40,41,43,47]

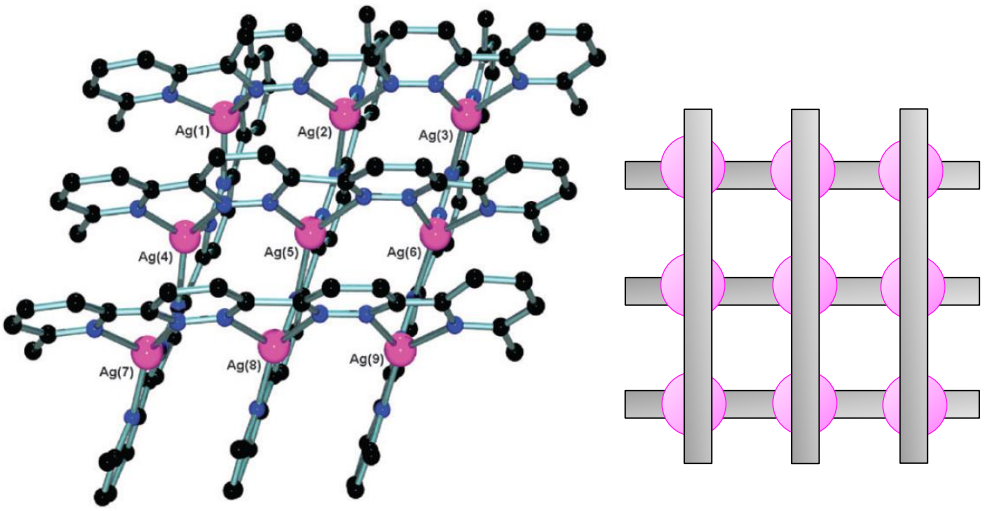

Figure 1.5: Structure of the first [3 x 3] metallogrid (Left).[37,41] *Cartoon representation of the structure, Ag(I) metal atoms represented as mangeta spheres and the lines correspond to the ligand (right).*

Squares [*n* x *n*] (*n* > 3) require that the ligands are symmetrical and the core donor units bridge an even number of metals. [4 x 4] Grids have been explored with metals with octahedral preferred geometries, Pb(II),[44] Cu(II) and Mn(II).[41]

The three types of metallogrid assemblies mentioned above, [2 x 2], [3 x 3] and [4 x 4] can form exclusively, while [5 x 5] grids have proven more difficult to form. The synthesis of a pentatopic pyridazine ligand by Lehn *et al.* did not produce the desired [5 x 5] grid, but instead led to two oligomers, incomplete grids [4 x 5] and quadruple helicates.[38] However, CITS (current imaging tunnelling spectroscopy) clearly showed Mn_{16} and M_{25} [*n* x *n*] structural motifs, reported by Thompson *et al.*[42]

Grid-like metal ion arrays have several attractive features including:

i. Their redox, magnetic and spin-state transitions between adjacent metal atoms;
ii. Well defined structural motifs that resemble strongly binary coded matrices for information storage and processing technology;

iii. They can be arranged into extended two-dimensional ensembles and deposited onto surfaces. Over a decade ago, the two-dimensional grid motif was the structural base to the molecular 64-bit logic and storage device.[43]

Applications for metallogrids include nanoscale electronics and spintropic devices as well as biological applications that have been outlined in a review published by Hardy.[48]

1.4 Supramolecular Helicates

Helical molecular structures have been observed on numerous occasions in nature; with the most well studied examples being deoxyribonucleic acid (DNA), α-helical proteins and collagen.[1,49] Helices have a particular shape, which commonly involved hydrogen bonding interactions and/or metal ion coordination. The term "helicate" specifically refers to the metal ions involvement and was coined by Lehn in 1987.[49] Work was occurring before this term was coined, however, expansion in this field did not occur until the late 1980's.[34] A helicate is a discrete helical supramolecular complex containing one or more covalent organic strands that is wrapped around and coordinated to a series of metal ions defining a *helical axis*.[49-51] The helical axis is the instantaneous axis of rotation, which the strands twist around. A helix can be characterised by the helical axis as well as the pitch (the distance taken to complete a full rotation of the strand about the helical axis). A helix may be right-handed (*plus, P*) or left-handed (*minus, M*), according to whether the rotation is clockwise or anticlockwise, demonstrated in figure 1.6. The assignment of which way the helix twists is considered from the viewer's eye towards a distant point looking down the helical axis.[50]

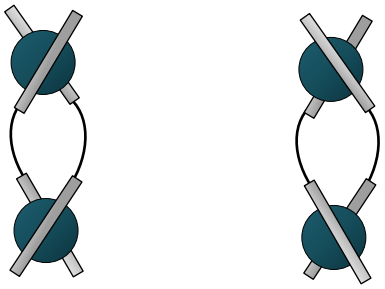

Figure 1.6: (a) Right handed helicate (Δ = P) (b) The left handed helicate (Λ = M).

The helix has become a useful building block for metallosupramolecular chemistry due to the structural architecture and the non-covalent interactions associated with complex structures. The synthesis of artificial helical molecules can utilise H-bonding, π-stacking and metal-coordination to mimic both structurally and functionally the macromolecules found in nature. The helicate structure

is formed by a strict self-assembly process which leads to the most stable thermodynamic architecture. However, changing the information of one of the building-block components can lead to different structural outcomes.

There are two requirements for a supramolecular structure to be defined as a helicate:[50]

i. One or more organic acyclic ligand strands are twisted and coordinated to cations or anions by coordinate bonds;
ii. The helicate must contain a minimum of two ions and form a discrete polynuclear structure.

There are four terms that can help to distinguish between different helical structures[50] (Figure 1.7):

i. The number of different strands: single-, double-, triple- or quadruple-stranded;
ii. The nature of the strands; homotopic (ligand contains identical binding units) or heterotopic (ligand contains different binging units);
iii. The orientation of the strands in the helicate: H= head-to-head, T= head-to-tail;
iv. The metal ion can have ancillary ligands coordinated to satisfy the desired coordination; saturated (no extra ligands) or unsaturated (one or more ancillary ligands are coordinated to the metal).

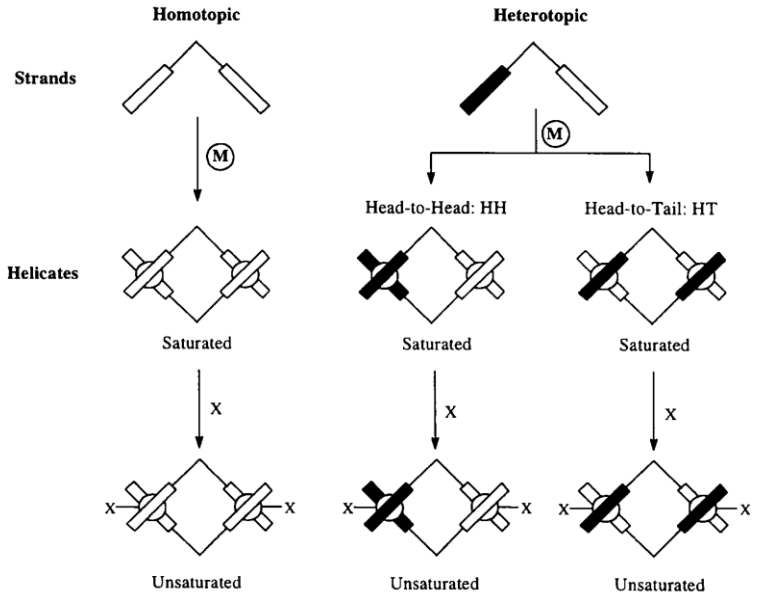

Figure 1.7: Classification of various helicates.[50]

Helicates are of interest in the development and the understanding of processes involved in supramolecular chemistry. The influence of non-covalent interactions can be investigated by studying helicates as simple model systems to give information on the stereochemistry and

regiochemistry of supramolecular architectures.[34] It also aids with the understanding of self-assembly, organization and recognition.

1.5 Inter-conversion between metallogrids and helicates

It has proven possible to form metallogrids and helicates by means of deliberate design of ligands and choice of specific metal ions. There are several examples of the same reactant ligands forming both grid-like and helical arrays, and their inter-conversion. In 2000, Lehn *et al.,*[39] showed the possibility of this, using a pentatopic ligand reacting with Ag(I) to form two polynuclear architectures, a [4 x 5] metallogrid and a quadruple-helicate obtained from the same reaction solution. The grid-like structure crystallises as pale yellow rhombohedra, while the helicate as orange blocks. Firstly, this study involved a $^{109}Ag^{+}$-NMR spectroscopic investigation, where an ^{1}H-NMR titration was performed with the stoichiometry between metal-to-ligand ranging from 2:1 – 2.5:1. To begin, a 2:1 metal-ligand ratio showed a very complex spectrum with the presence of slowly exchanging species. With an increase to 2.2:1 (M:L) ratio caused a "dramatic simplification" and at the ratio 2.5:1 (M:L), which is the required ratio for the grid, the spectrum was interpreted as the ligand in three different environments indicating three different coordinating ligand environments. A variable temperature ^{1}H-NMR study (70°C, 25°C and -17.5°C) was completed to obtain information about these species present in this spectrum, the results showed an approximately 2:1 mixture of two species that are in slow exchange. They then predicted the possible solid-state structure; at low temperature the species could be a quadruple helicate which has four ligands, each in two different environments and the high temperature spectra corresponded to either a [2 x 2] grid or "to a pool of exchanging grid-type or other species". Neither [4 x 5] grid nor the [5 x 5] grid are observed in significant quantity in the proton spectrum. X-ray crystallography confirmed the two structures as a [4 x 5] metallogrid and the helicate. The authors argued that the grid structure obtained possesses more interesting features, with two [2 x 5] rectangular subgrids that are located on opposite sides of a plane (figure 1.8), which could be addressed as a potential value for information handling and switching devices.[39]

Another example of inter-conversion between these two architectural arrays (figure 1.9) is the redox chemistry of copper as a tetranuclear Cu(II) grid and a binuclear Cu(I) double helicate.[52] This is made possible by the metal ion coordination preferences, for octahedral geometry (Cu^{2+}), versus the tetrahedral geometry (Cu^{+}), and the reorganization of the ligand to change the coordination modes from tridentate in the grid compared to the bidentate coordination in the helicate. The preferred geometries are crucial for the functioning of certain molecular machines, for example motional

devices based on catenanes, rotaxanes and molecular shuttles.[32] Similar to the inter-conversion discussed above, X-ray crystallography and NMR spectroscopy were completed to determine the structure of the complexes. The [2 x 2] grid complex structure was determined and the crystals dissolved in CD_3NO_2 and a ^{1}H-NMR spectrum taken. A double helicate was confirmed to form by NMR and ESI-MS studies, however attempts to grow crystals of the double helicate resulted in the formation of the grid. This oxidation of Cu(I) to Cu(II) in solution was due to traces of oxygen.

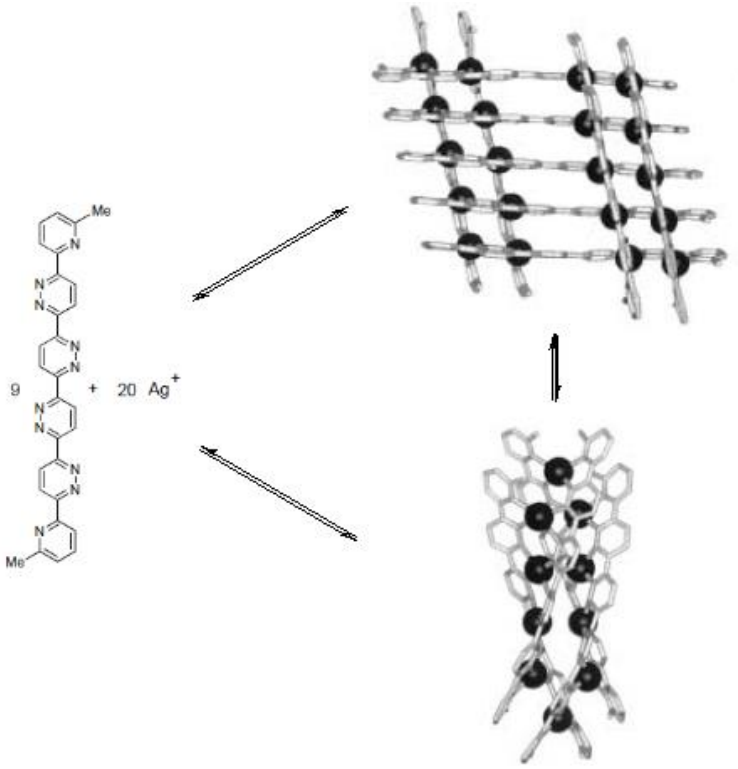

Figure 1.8: The inter-conversion of the pentatopic ligand with Ag(I) as investigated by Lehn et al.[39]

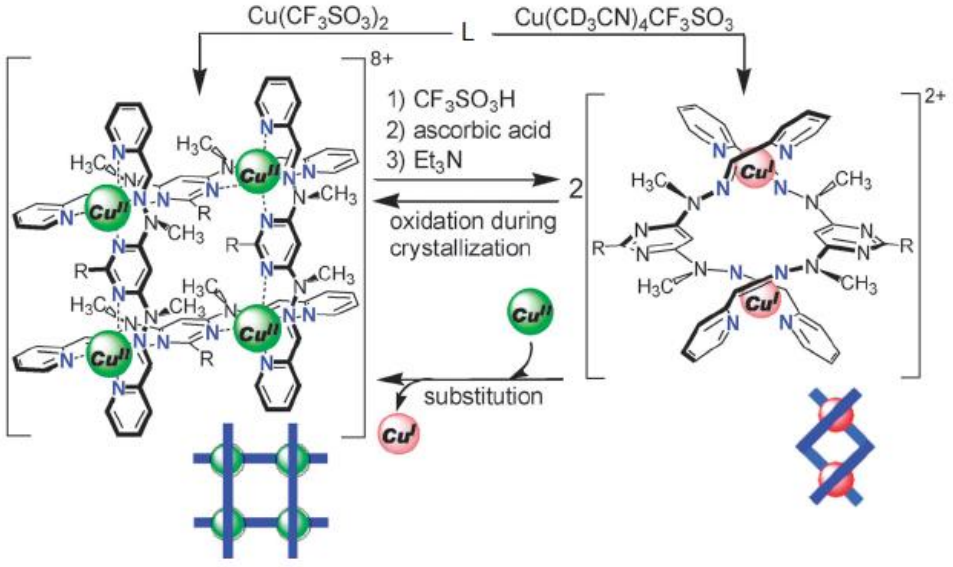

Figure 1.9: The oxidation and reduction of copper forming the two different architectural assemblies as reported in literature.[52]

Nanosized molecular structures are expected to display intriguing photochemical properties and have the potential to be created for molecular-level devices.[39] However, due to the overall low yields of multistep synthetic reactions required for ligand preparation, may limit the practical purpose of these molecular architectures.

1.6 Pyridazines

Pyridazine, also known as 1,2-diazine, is a heterocyclic aromatic organic molecule that contains a six-membered ring with two adjacent nitrogen atoms. Pyridazines are planar, but have a slightly distorted geometry due to the differing bond lengths, as observed by electron diffraction and microwave spectroscopy.[53] Pyridazine derivatives can be synthesised using [4+2]-cycloaddition reactions, using tetrazine as the 4π electron component. Pyridazines have two adjacent donor atoms and are often used as bi- or tri-dentate ligands because of this, different pendent heterocycles (eg. pyridine, dimethylpyrazole or pyrdazine as used in this regard) in the 3- and 6- positions of the pyridazine ring can impact on the binding to a metal, as bis-chelation can occur (figure 1.10). Substituted pyridazine-based compounds are extensively studied with regard to the varying and versatile applications, and have proven particularly popular for gird formation (see above).

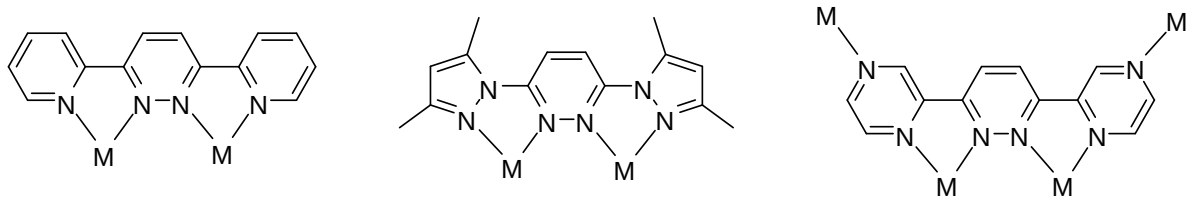

(a) (b) (c)

Figure 1.10: Coordination chemistry of molecules explored in this study, the pyridazine ring structure with different pendant heterocycles in the 3 and 6 position, (a) 2-pyridine; (b) 1-(3,5-dimethylpyrazole); (c) 2-pyrazine.

1.7 Ligands synthesised in this study

There are three series of molecules that have been synthesised for this study. Each group is based on the different pendant groups as shown in figure 1.11 with fused rings; (cyclopentene, cyclohexene, cycloheptene and acenapthylene) on the 4- and 5- positions of the pyridazine ring. Literature procedures have been adopted to synthesise **L1-L12**[54-60] with a modified synthesis for **L6** and **L12**. Similar methods have been used to synthesise new molecules **L13-L16** (See Chapter 2)

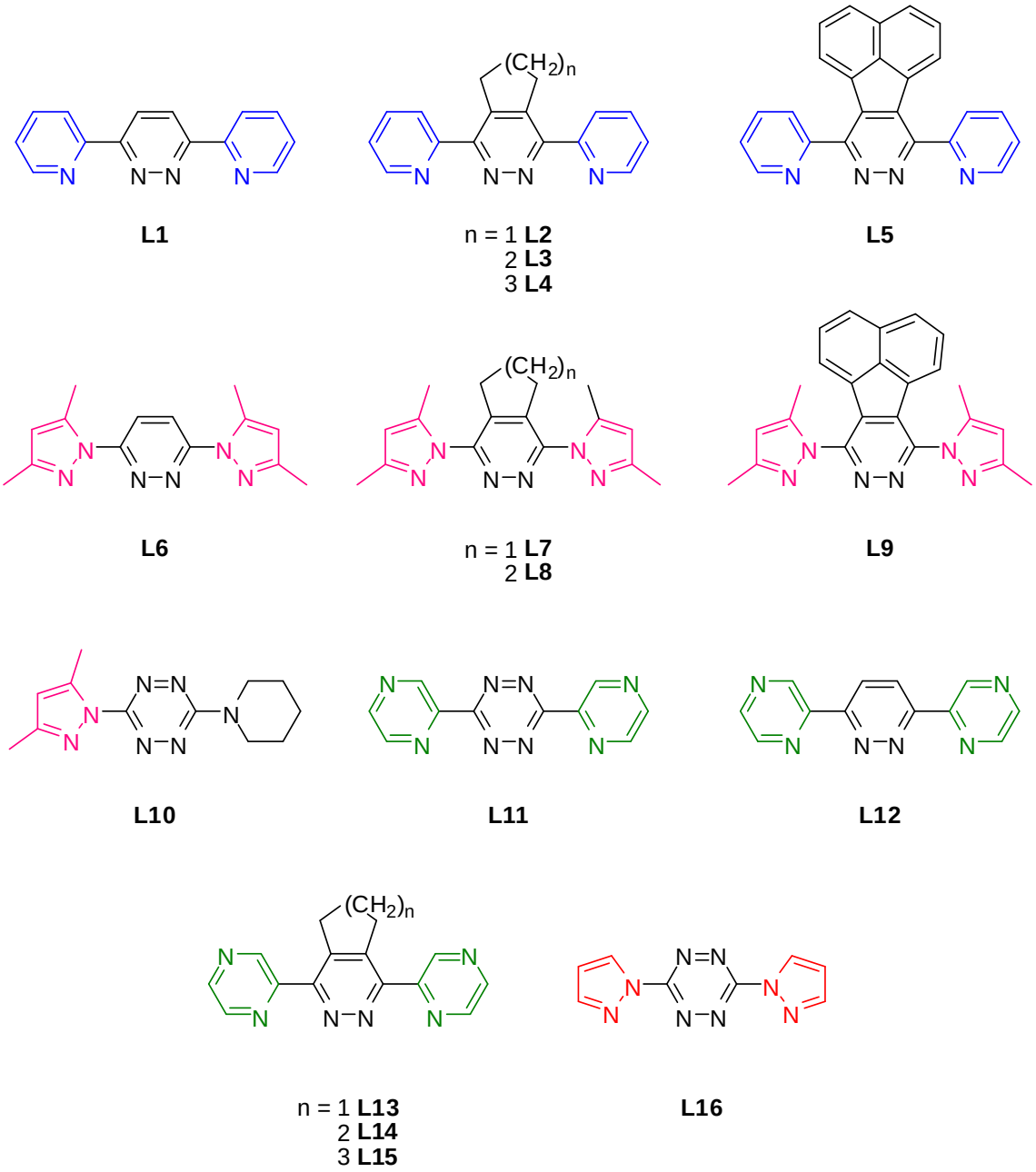

Figure 1.11: Molecules synthesised for this study with the selected labelling for each. Each pendant group shown in a different colour, 2-pyridyl (blue), 1-dimethylpyrazolyl (pink), 2-pyrazinyl (green) and 1-pyrazole (red).

3,6-Bis-(2-pyridyl)-pyridazine (**L1**) has been proven a popular ligand for metallosupramolecular complexes. Pyridazine, **L1** has been reacted with a total of thirteen different metals, Cu(I),[30] Ag(I),[36,61] Cu(II),[62,63] Ni(II),[64,65] Co(II),[65] Mn(II),[66] Pd(II),[67] Pt(II),[68] Ru(II),[69] Rh(III),[70] Ir(III),[71] Mo(0),[72] Cr(0).[72] Constable *et al.* has shown a side-by-side complex of **L1** with silver triflate.[61] Three years later in 2006, Schottel *et al*. investigated anion-π interactions as a controlling element in Ag(I) supramolecular complexes (See Chapter 2).[36] However, the other metals mentioned have

had their coordination chemistry examined. The other ligands in the pyridyl series that have been previously complexed with metals are summarised in table 1.2.

Ligand	Metal Coordinated
L1	Cu(I), Ag(I),[36,61] Cu(II),[62,63] Ni(II),[64,65] Co(II), Mn(II), Pd(II), Pt(II), Ru(II), Rh(III), Ir(III), Mo(0), Cr(0).[30,36,61-72]
L2	Ru(II), Rh(II), Ir(III), Pt(II), Pd(II).[73-75]
L3	Pt(II), Pd(II), Rh(II).[73,74]
L4	Pt(II), Pd(II), Rh(II).[73,74]
L5	Ru(II), Cu(I), Pt(II), Mo(0), Cr(0), W(0).[72,76,77]

Table 1.2: Summary of metals that have been previously complexed with the molecules containing pyridine as the pendant group.

Of the pyrazole containing series only, 3,6-bis(3,5-dimethylpyrazolyl)pyridazine (**L6**) has been investigated with the formation of Ag(I),[78] Cu(I),[79] Ru(II),[80] Co(II)[81] and Cu(II)[82-85] complexes. A copper(I) [2 x 2] grid was obtained with **L6** by Manzano *et al.* in 2008 (See Chapter 3).[79] The Ag(I) complex with **L6** by Yu *et al.* is a one-dimensional linear helical polymer, with each silver atom coordinated to two nitrogen atoms from the pendant groups and there is an interaction between the Ag(I) and the two pyridazine nitrogen atoms from each ligand. The ligands are oriented *trans* on the metal, as shown in figure 1.12a. Tetrazine, **L10** was synthesised to examine the coordination of the dimethylpyrazole group substituted on a tetrazine ring in the 3-position and with a piperidyl group in the 6-position leaving only one site for chelation. Previous coordination of this ligand with Co(II) was studied by Cherdantseva *et al.* looking into the magnetic and ESR resonance properties.[86] The structure contained metals in two different environments, one cobalt atom being four coordinate, bound to four chlorine atoms, and the other cobalt six coordinate, bound to four nitrogen atoms and two chlorine atoms that bridge between the two metals (figure 1.12b).

Pyrazine substituted, **L11** and **L12**, have been investigated by complexation with Ag(I)[87,88] forming coordination polymers. Tetrazine, **L11** has also been shown to form coordination polymers with Co(II) and Cd(II),[89] and the coordination chemistry with Ru(II) and Re(II) has been reported.[90,91]

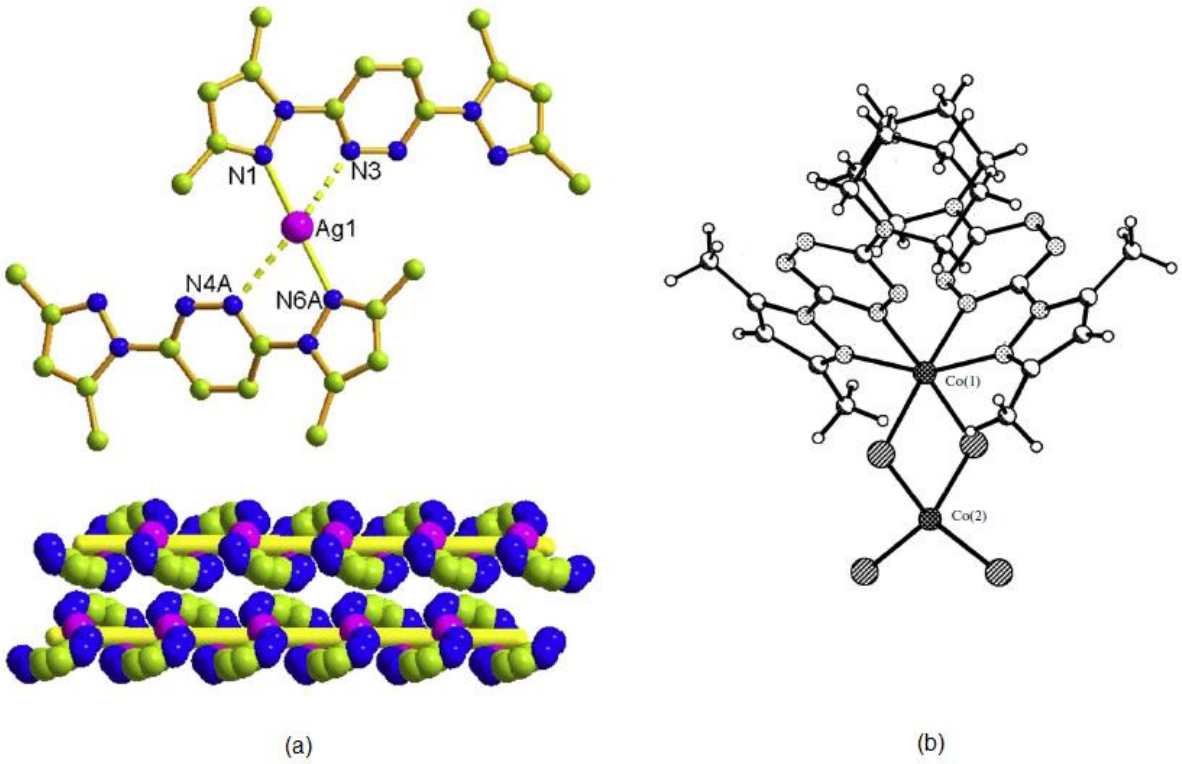

*Figure 1.12: (a) One-dimensional polymeric structure formed when **L6** is reacted with silver perchlorate;[78](b) Discrete structure of Co(II) and **L10**.[92]*

The molecules **L13** - **L16** have not yet been synthesised, see Chapter 2 for a discussion of synthesis.

Previous work on grid-like arrays within the Fitchett group[60] has involved the use of a rigid ligand, with the substitution of a cyclopentene ring fused on a pyridazine ring (**L2**). The same structural motif is observed with molecule **L1**, as reported by Youinou *et al.*[30] When **L2** is reacted with silver tetrafluoroborate, a [2 x 2] grid like architecture is observed, as shown in figure 1.13, causing slight twisting of the pyridine pendant groups (~24°) due to the sterically hindering fused ring.

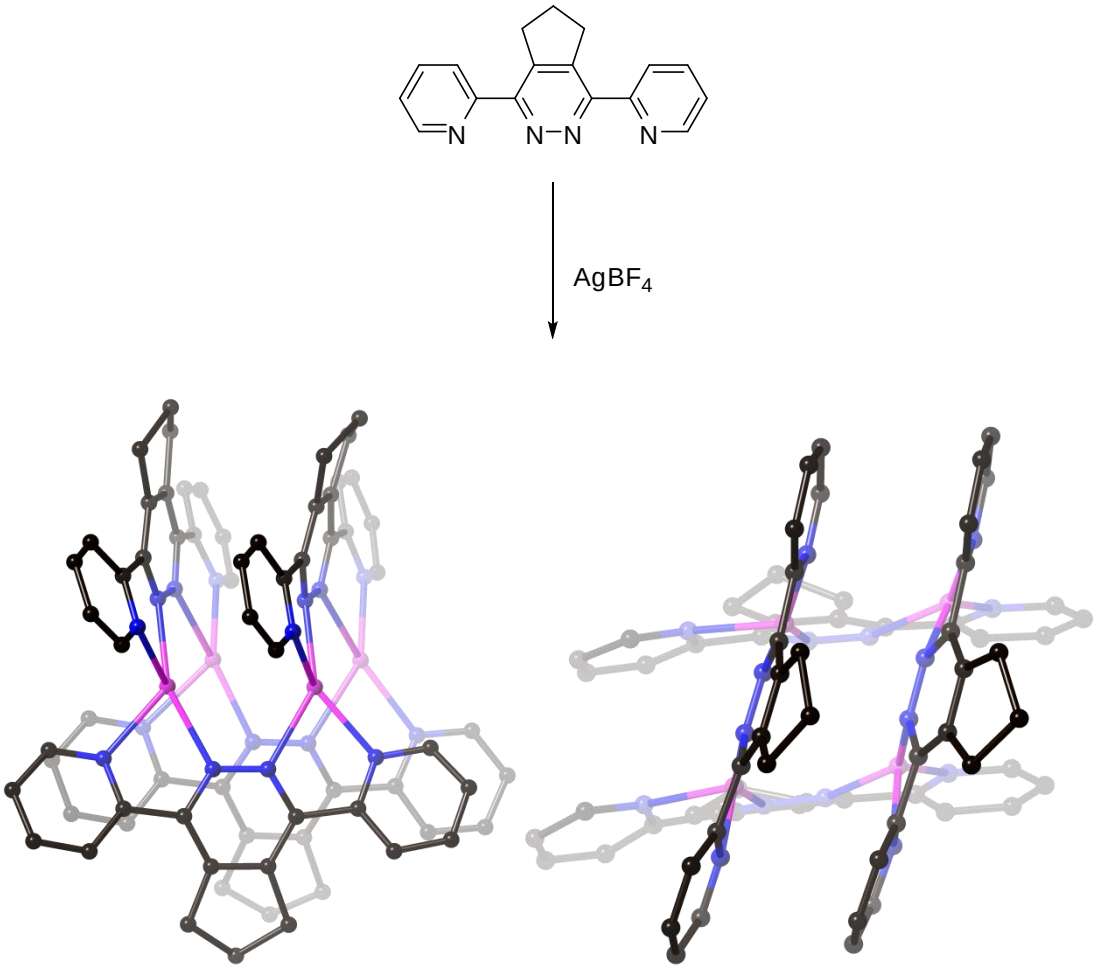

*Figure 1.13: Grid-like Ag(I) structure formed by the reaction of **L2** with silver tetrafluoroborate.*

1.8 Scope of thesis, methods of synthesis and data collection

The aims of the study are to investigate the effect of complex formation when substituting different fused rings, *viz* cyclopentene, cyclohexene, cycloheptene and acenapthylene at the 4- and 5-positions of the pyridazine ring, and the substitution of different pendant groups; pyridine, dimethylpyrazole and pyrazine. The study also explores the structural effects of complexes formed by the reaction of these molecules with d^{10} metals, Ag(I), Cu(I) and Zn(II). The comparisons between the complexes in solution and solid state have been analysed and a possible association between the structures from the solution studies investigated.

Chapter Two investigates Ag(I) with ten different ligands. NMR and ESI-MS were collected for the solution studies and characterisation of each complex was done by X-ray crystallography.

Chapter Three investigates complexes formed with Cu(I). $Cu(MeCN)_4BF_4$ and CuI were the two metal salts used. Seven complexes formed with six different ligands. X-ray crystallography was the main tool used within this chapter.

Chapter Four explores complex formation of Zn(II) with eight different ligands. NMR, UV-Visible spectroscopy and ESI-MS were the solution studies carried out and X-ray crystallography was completed elucidating the structures in the solid state.

All organic precursors and products have been fully characterised using nuclear magnetic resonance (NMR), electrospray ionisation mass spectrometry (ESI-MS), infrared spectroscopy (IR), UV-Visible Spectroscopy, melting point analysis (Mp), single crystal X-ray determination and microanalysis.

The crystallographic refinements and data are located in the crystallographic tables in Appendix 1.

CHAPTER TWO

Silver Complexes

2.1 Introduction

Silver(I) ions have proven extremely popular in metallosupramolecular chemistry. This is due to the d^{10} electronic configuration resulting in a coordination sphere that allows a range of different geometries to be observed.[20] Due to the nature of this metal, the self-assembled product is influenced by the ligands used,[93] solvent[60] and anions[94] more so than other metal ions. Ag(I) is flexible in its choice of coordination number, ranging from 2-8. The lower coordination numbers are more common, with linear three and tetrahedral four coordinate geometries being predominant. The self-assembly of Ag(I) adopts a tetrahedral geometry when the ligands used are rigid, linear polytopic and contain bidentate chelating sites forming architectures like metallogrids.[39,43] Ag(I) can self-assemble into helicates[50] with more flexible ligands, or the metal ion can fix adjacent ligands together in a side by side arrangement.[50,95] The latter is more favourable when steric factors play a role in the architecture formation.

As previously mentioned, 3,6-bis-(2-pyridyl)-pyridazine (**L1)** has previously been complexed with a range of different Ag(I) salts, with metallogrid architectures forming regardless of the anion present. Dunbar *et al.* showed that the 3,6-bis-(2-pyridyl)-1,2,4,5-tetrazine to **L1** (figure 2.1) results in the formation of different assemblies; polymers, planar dinuclear, propeller-type, dinuclear depending on the anion.[36] The difference is due to the higher acidic character of the tetrazine ring compared to the more electron rich pyridazine ring. With this in mind, the tetrazine is more likely to participate in anion-π interactions than the π-π interactions, with all the complexes obtained, showing multiple and shorter anion-π interactions between the anions and the central tetrazine core. However in the grid-like structures the intramolecular π-π interactions are maximised at the expense of the anion-π interactions, as shown in figure 2.2.

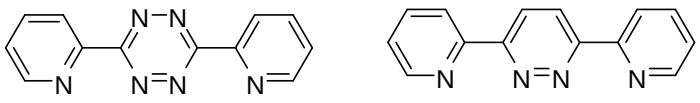

3,6-bis-(2-pyridyl)-1,2,4,5-tetrazine **L1**

*Figure 2.1: Structure of the 3,6-bis-(2-pyridyl)-1,2,4,5-tetrazine and **L1** that have been complexes with Ag(I).[36]*

The reactions of related rigid ligands with Ag(I) have proven a fruitful area of reseach. Brooker *et al.* published an example of increasing the steric interactions on the ligand with the loss of a metallogrid architecture (figure 2.2a). The increase in the steric factors was done by substitution of bulky ortho-methyl substituents which in turn removed the planarity and conjugation of the ligand with production of the side-by-side interaction with metal ions (figure 2.2b).[95]

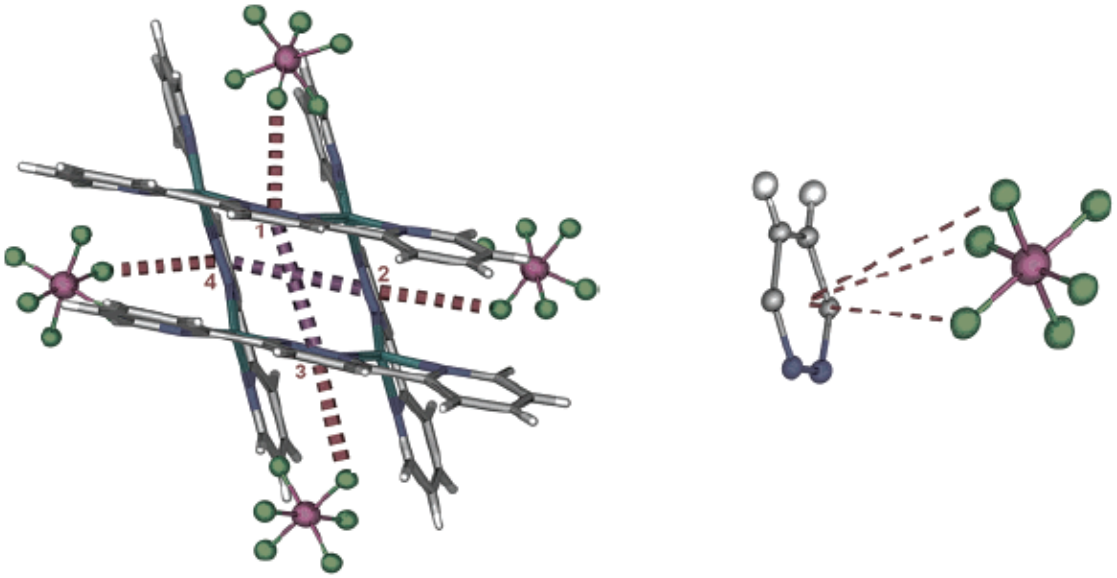

Figure 2.2: The grid-like structure of $[Ag_4(\mathbf{L1})_3][PF_6]_4$ *showing (a) the π-π interactions and anion-π interactions; and (b) the pyridazine ring of one of the ligands with a* PF_6 *anion displaying three anion-π interactions with the fluorine atoms.*[36]

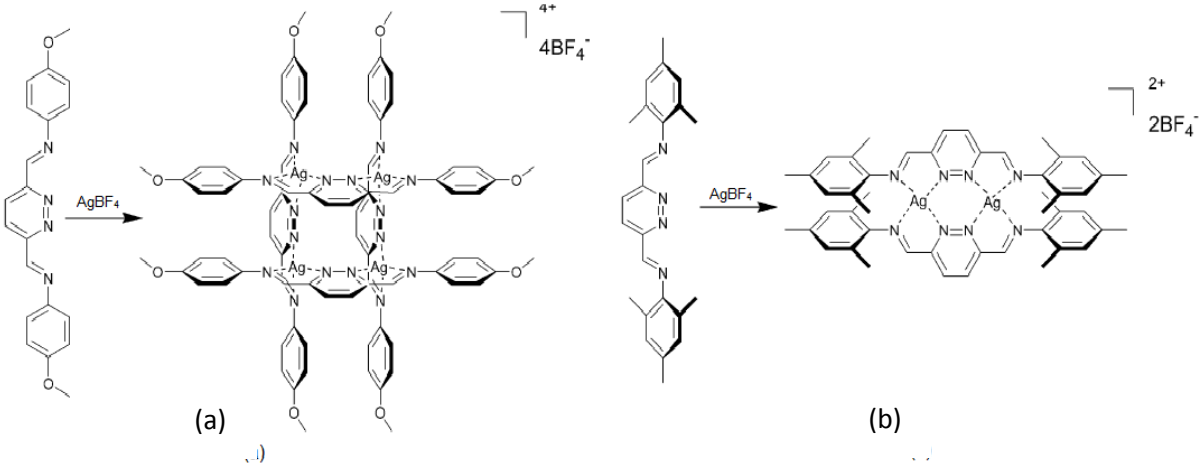

Figure 2.3: (a) The planar bidentate pyridazine-based ligand forming a [2 x 2] grid with $AgBF_4$*; (b) With the addition of the bulky groups disrupts the planarity of the ligand forming the side-by-side structure with* $AgBF_4$*.*[95]

This Chapter will explore the concepts, by introducing sterically hindering components to determine their possible implications on the supramolecular assemblies formed with a range of different silver metal ion salts.

Previous results in the Fitchett group[60] have successfully shown the formation of metallogrids, as previously mentioned (figure 1.13). Along with this interesting architecture, was the formation of side by side complexes with two different silver salts, hexafluorophosphate (**C2.2**) and perchlorate

(**C2.3**) (figure 2.4). Other heterocyclic ligands explored by the Fitchett group showed that supramolecular aggregation can be controlled by anions in Ag(I) complexes.[94]

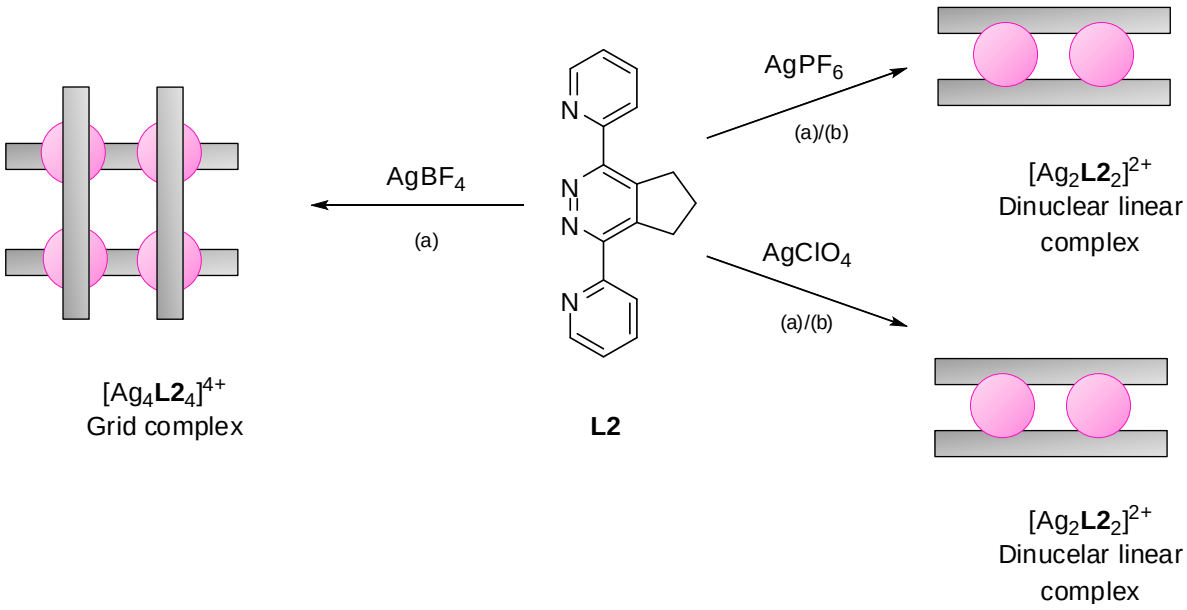

*Figure 2.4: Schematic summarising the structures of the complexes identified by X-ray crystallography when **L2** was reacted with different silver salts in CH_2Cl_2:CH_3CN (9:1) with a 1:1 metal-to-ligand stoichiometry.*

We decided to first investigate if the solution structures matched the solid state structure. Firstly the solution studies by NMR were completed, with the Fitchett groups' previous complexes. The same ligand molecule, **L2** reacted with a range of Ag(I) metal salts, under the same conditions has been investigated (**C2.2**, **C2.3**, **C2.4**). We then decided to increase the sterically hindering rings fused to the 4- and 5- position on the pyridazine ring, to **L3, L4** and **L5**.

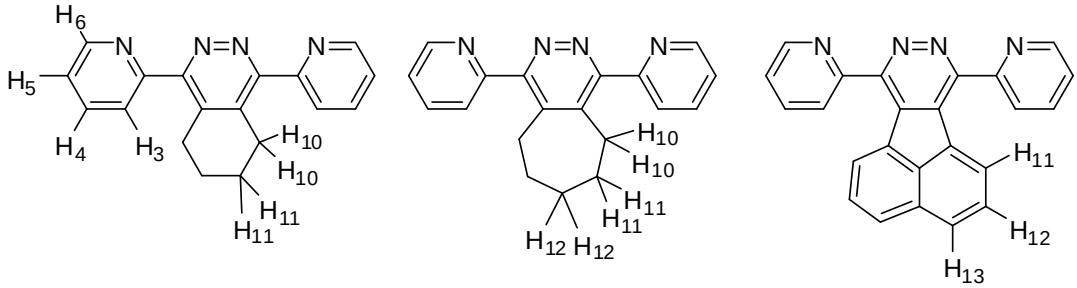

*Figure 2.5: Selected proton labelling of molecules **L3**-**L5**.*

2.2 Solution studies

Complex 2.1 - **L2** + silver tetrafluoroborate

The initial complex with **L2** was obtained from a solvent mixture of dichloromethane: acetonitrile (9:1) and crystals were obtained after vapour diffusion of pentane into the reaction mixture. This complex was dissolved in d_6-DMSO and a ^{1}H-NMR spectrum obtained that showed uncoordinated ligand, likely due to the strong donor solvent, DMSO.

In order to observe the complex formation in solution a ^{1}H-NMR titration was carried out. This was done by addition of 20 µL 0.05 mol L^{-1} $CDCl_3$:CD_3CN (9:1) aliquots of silver tetrafluoroborate salt solution to a 500 µL of 0.01 mol L^{-1} $CDCl_3$:CD_3CN (9:1) solution of **L2** until a 1:1 metal to ligand ratio was obtained. An extra equivalent of metal salt solution was added to ensure the reaction was complete. The ^{1}H-NMR spectra recorded for the titration of complex **2.1** are shown in figure 2.6. With the addition of 0.2 equivalence (eq.) of metal salt solution, the spectra showed symmetrical coordination with the pyridine rings equivalent throughout. With the continuous addition of 0.2 eq., coordination induced shifts (CIS) are observed until the metal-to-ligand ratio is 1:1, and these are summarised in table 2.1 (1:1 metal-ligand ratio spectra).

	H3	H4	H5	H6	H10	H11
L2	8.51	7.98	7.47	8.76	3.49	2.14
C2.1	7.96	7.96	7.47	8.56	3.39	2.23
CIS[b]	-0.55	-0.02	-	-0.20	-0.10	+0.09

[a] For deuterated acetonitrile solutions. [b] CIS= $^{\delta}$complex-$^{\delta}$ligand.

*Table 2.1: ^{1}H-NMR Chemical shifts[a] and Coordination Induced Shifts[b] of complex **2.1**.*

The CIS observed in the titration show the greatest shift for proton H3 upfield by 0.55 ppm. The ligands bind to the Ag(I) in a symmetrical fashion in all spectra taken in the titration, and the overall structure observed has a 1:1 metal-to-ligand stoichiometry.

The ^{1}H-NMR titration for complex **2.1** indicates a 1:1 metal to ligand stoichiometry which is the same stoichiometry observed in the solid state structure. The upfield CIS of H3 and H6 are related to the free ligand, as H3 moves from the de-shielding zone to being shielded, as shown in figure 2.7. This also has an effect on H6 as the metal coordination makes H6 electron deficient. The shifts of H10 could be due to possible interactions with H3.The symmetry and CIS observed are consistent with the solid state structure of **2.1**.

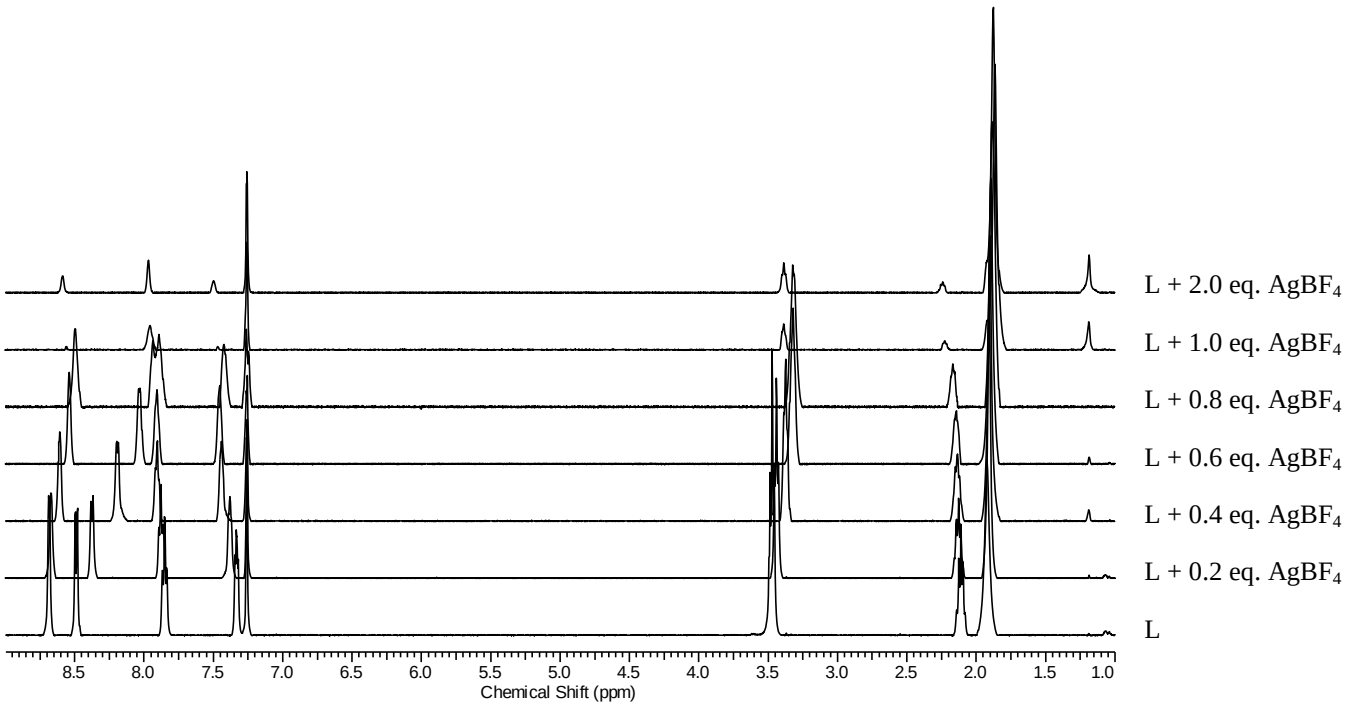

*Figure 2.6: NMR titration to form complex 2.1 of **L2** with $AgBF_4$.*

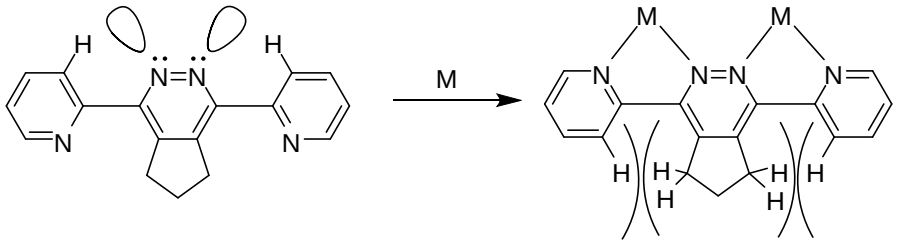

Figure 2.7: A possible explanation for the shifts observed in this solution state complex, with H3 having a stronger shielding effect when complexes with a metal such as Ag(I).

Complex 2.2 - **L2** + silver hexafluorophosphate

As previously mentioned, the Fitchett group has had success in growing crystals suitable for single crystal X-ray determination of the product of the reaction between silver hexafluorophosphate and **L2**. The structure was determined to be a side-by-side dimer (figure 2.8) with the same structure observed when the crystals were obtained under different conditions; using both acetonitrile, as well as a mixture of dichloromethane:acetonitrile (9:1). Solution studies were completed including full NMR characterisation and a ^{1}H-NMR titration.

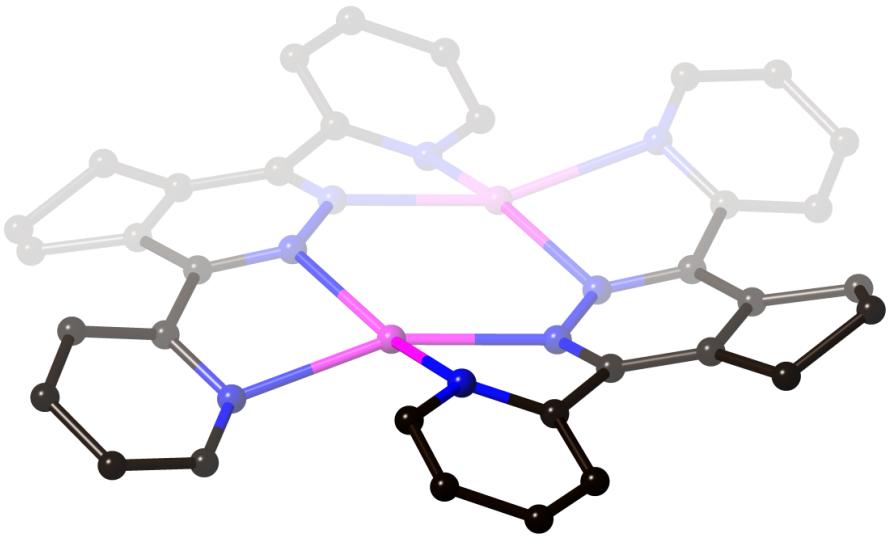

Figure 2.8: Structure of the side-by-side dimer of complex 2.2.[60] The anions, solvates and hydrogen atoms have been omitted for clarity.

Complex **2.2** was dissolved in d_3-acetonitrile and a ^{1}H-NMR spectrum collected and compared with the ligand spectrum. The coordination induced shifts are summarised in table 2.2. The results show the greatest CIS is experienced by H3, 0.41 ppm upfield. The other protons experience a small CIS of 0.06 ppm – 0.15 ppm, however not as significant as H3. This trend is similar to what is observed in complex **2.1**, the same ligand with a different silver salt.

The ^{1}H-NMR titration was done by addition of 20 µL 0.05 mol L^{-1} acetonitrile aliquots of silver hexafluorophosphate salt solution to a 500 µL of 0.01 mol L^{-1} acetonitrile solution of **L2** until a 1:1 metal to ligand ratio was obtained. An extra equivalence of metal salt was added to confirm the spectrum did not change further. The ^{1}H-NMR titration that was performed is shown in figure 2.9. Throughout the titration a symmetrical molecule is observed as the two pendant heterocycle's pyridine rings are equivalent. The overall titration indicates a 1:1 metal-to-ligand stoichiometry for complex formation.

	H3	H4	H5	H6	H10	H11
L2	8.51	7.98	7.47	8.76	3.49	2.14[c]
C2.2	8.10	8.07	7.62	8.70	3.34	2.17[c]
CIS[b]	-0.41	+0.09	+0.15	-0.06	-0.15	+0.03[c]

[a] For deuterated acetonitrile solutions. [b] CIS= $^{\delta}$complex-$^{\delta}$ligand. [c] Water overlap.

*Table 2.2: ^{1}H-NMR Chemical shifts[a] and Coordination Induced Shifts[b] of complex **2.2**.*

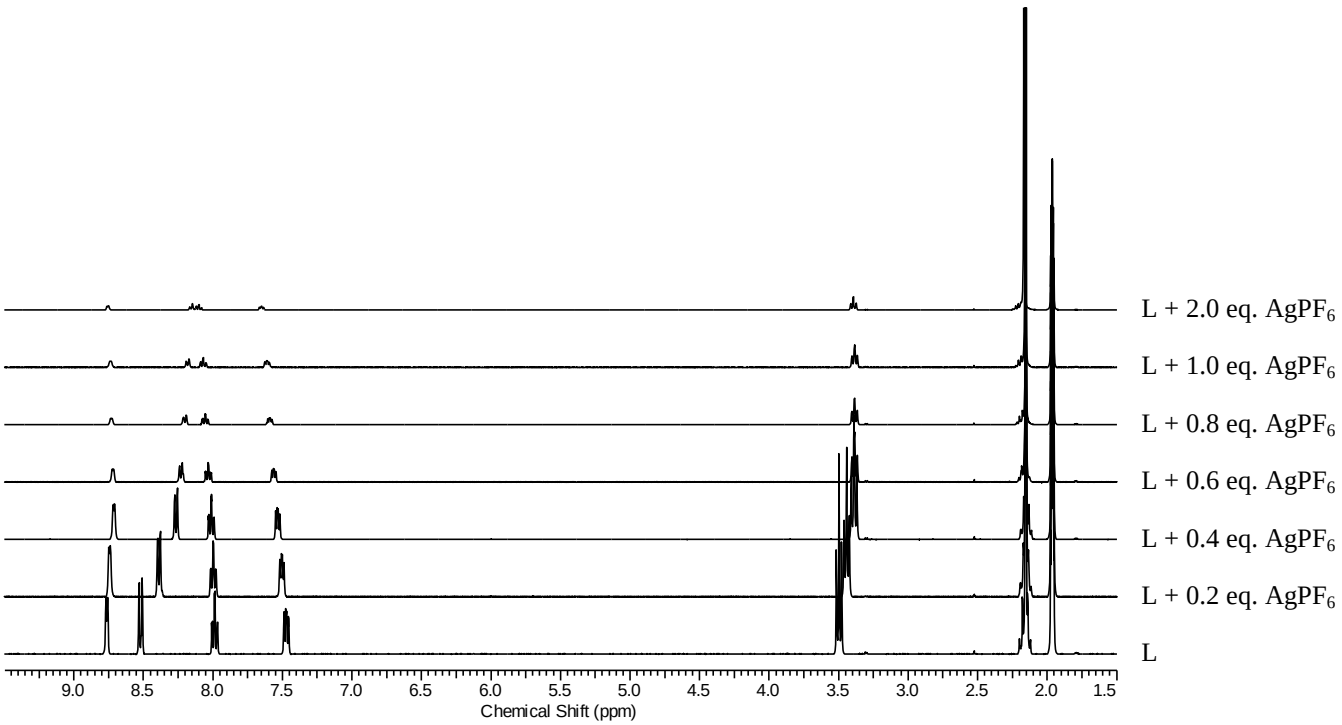

*Figure 2.9: NMR titration to form complex 2.2 of **L2** and $AgPF_6$.*

Complex 2.3 - **L2** + silver perchlorate

Solution studies were completed for complex **2.3**, the reaction between **L2** and silver perchlorate. Crystallography of this complex has been previously determined in the Fitchett group and the resulting architecture is the same as **2.2**, with a side-by-side structure. The results from the comparison of the complex with the ligand in d_3-acetonitrile showed similar coordination induced shifts as complex **2.2**, as well as the same results for the ^{1}H-NMR titration. The coordination induced shifts for complex **2.3** are summarised in table 2.2 and will not be discussed any further.

	H3	H4	H5	H6	H10	H11[c]
L2	8.51	7.98	7.47	8.76	3.49	2.14[c]
C2.3	8.09	8.07	7.62	8.69	3.34	2.18[c]
CIS[b]	-0.42	+0.09	+0.15	-0.07	-0.15	+0.04

[a] For deuterated acetonitrile solutions. [b] CIS= $^{\delta}$complex-$^{\delta}$ligand. [c] Deuterated acetonitrile overlap.

*Table 2.2: ^{1}H-NMR Chemical shifts[a] and Coordination Induced Shifts[b] of complex **2.3***

Complex **2.2** and **2.3** show very similar coordination induced shifts and are very similar to complex **2.1**. The ligand structures are very similar as when coordinated to the metal, having the greatest

effect on H3. The titrations indicate a 1:1 metal-to-ligand stoichiometries, which could show either the metallogrid (Ag_4L_4) and the side-by-side complex (Ag_2L_2) have formed in solution.

2.3 Coordination complexes I

Complex 2.4 - **L2** + silver tetrafluoroborate

Solution studies were carried out using NMR spectroscopy for complex **2.4**. The complex was dissolved in d_3-acetonitrile and a ^{1}H-NMR spectrum collected, analysed and compared with the ligand spectrum. The coordinated induced shifts are shown in table 2.4.

	H3	H4	H5	H6	H10	H11[c]
L2	8.51	7.98	7.47	8.76	3.49	2.14[c]
C2.4	8.03	8.02	7.56	8.61	3.28	2.13[c]
CIS[b]	-0.48	+0.04	+0.09	-0.13	-0.21	-0.01

[a] For deuterated acetonitrile solutions. [b] CIS= $^{\delta}$complex-$^{\delta}$ligand. [c] Deuterated acetonitrile overlap.

*Table 2.4: ^{1}H-NMR Chemical shifts[a] and Coordination Induced Shifts[b] of complex **2.4***

When complex **2.4** forms there is a minor coordination induced shift for most of the protons on the ligand, however, one proton, H3 on the pyridine ring has the greatest upfield shift of 0.48 ppm compared to 0.04, 0.09 and 0.13 ppm for the other pyridine ring protons, H4, H5 and H6, respectively. The fused cyclopentene protons, H10 experiences a shift upfield 0.21 ppm, whereas the H11 protons do not experience a shift (0.01 ppm). The effect in which the H3 experiences could be due to change in environment, becoming shielded as the chelation occurs, and the possible interactions with the alkyl protons (H10) which also show a greater coordination induced shift (figure 2.7). These shifts are similar to those observed in complexes **2.2** and **2.3**, which could indicate a side-by-side complex with a 1:1 metal-ligand stoichiometry. The ^{1}H-NMR titration was performed shown in figure 2.10, using the same procedure as described in complex **2.2**. The results show a similar trend for this molecule (**L2**) with the different silver salts (**C2.2** and **C2.3**), with binding of Ag(I) ions in a symmetrical fashion. With the addition of the first equivalence of metal (0.2 eq.), a small CIS is observed and these small shifts continue to be seen until the metal to ligand ratio is 1:1.

The high resolution electrospray ionisation mass spectrometry (ESI-MS) is consistent with the ^{1}H-NMR titration with the complex having a 1:1 stoichiometry, [Ag(**L2**)] and [Ag_2(**L2**)$_2$]. However,

due to the comparisons with this ligand to the other silver salt structures elucidated, the side-by-side complex is more likely, with similar shifts being observed to that of the grid structure.

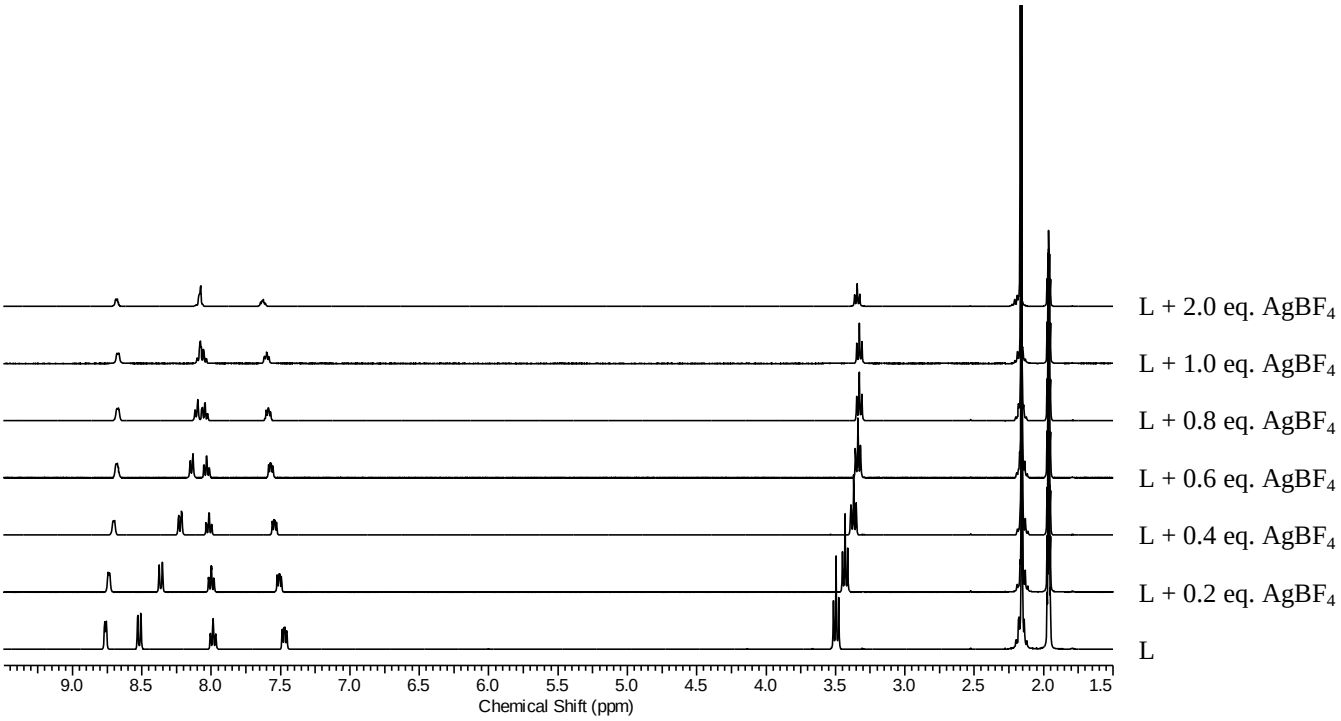

*Figure 2.10: NMR titration to form complex **2.4** of **L2** + $AgBF_4$.*

The reaction of **L2** and silver tetrafluoroborate in acetonitrile gave complex **2.4.** Bright yellow needles were obtained from a solution prepared for NMR analysis standing overnight in d_3-acetonitrile and these were suitable for single crystal X-ray determination. However, due to the small amount of crystals obtained, these were regrown and this solid was analysed with a 1:1 metal-ligand stoichiometry.

This complex crystallised in the triclinic space group P-1 with an asymmetric unit containing one silver metal, two molecules of **L2** and one non-coordinated tetrafluoroborate anion, clearly different from the analysis results. This is due to the solid analysed being different from the crystals obtained from the NMR solvent, same conditions were employed however slightly different concentrations and the vial used will be the effect of this.

The silver has a distorted square based pyramidal geometry, as shown in figure 2.11, and is bound to five nitrogen atoms as a dimer, with the two other pyridine ring nitrogen atoms being non-coordinated. The nitrogen bond lengths to silver in the chelating component, from the pyridazine nitrogen are shorter than that from the pyridyl ring, 2.2738(12) Å and 2.2779(12) Å compared to 2.4931(14) Å and 2.4848(13) Å. The coordinated pyridine rings are twisted relative to the central pyridazine ring, 38.10(4)° and 27.69(5)°, in order to relieve the steric clash between the hydrogen atoms and the fused cyclopentene ring, which influences the Ag-N bond length of the pyridine-ring.

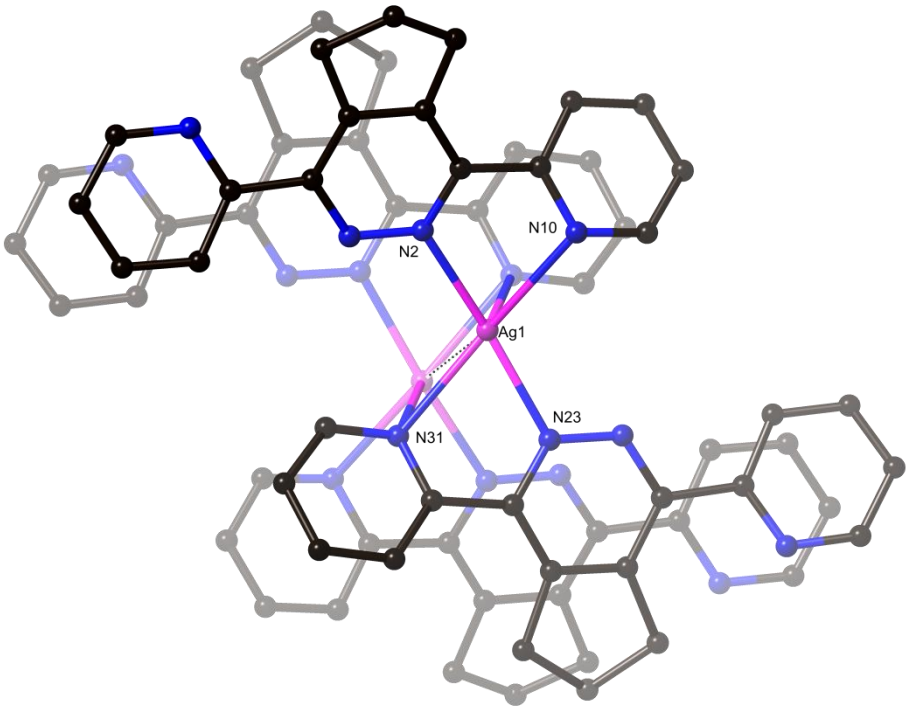

Figure 2.11: Perspective view of the dimer of complex ***2.4*** *showing π-π stacking and pyramidilisation of the nitrogen with the selected atomic labelling. The anion and hydrogen bonds have been omitted for clarity. Selected bond lengths (Å):* Ag1-N2 2.2738(12), Ag1-N10 2.4931(14), Ag1-N23 2.2779(12), Ag1-N31 2.4848(13), Ag'-N31 2.6575(14) *and angles (°):* N2-Ag1-N10 69.49(5), N23-Ag1-N31 70.80(4).

Interestingly, the non-coordinated pyridine rings are twisted at angles of 156.93(5)° and 161.88(5)° relative to the pyridazine core. This observation is common for the conformation of biheterocycles (figure 2.6).[96] The twisting of the coordinated pyridine rings leads to pyramidilisation of the nitrogen atoms which bifurcate two silver atoms, as shown in figure 2.12. The silver has a weak Ag-Ag interaction of 2.9868(3) Å due to the metallo-macrocycle pulling the silver metals closer togther. In the dimer the ligands are off-set stacked with parallel arrangement due to the π-π stacking interaction with centroid-centroid distances of the three heterocyclic rings being 3.5683(9) Å, 3.7757(8) Å and 3.7723(10) Å.

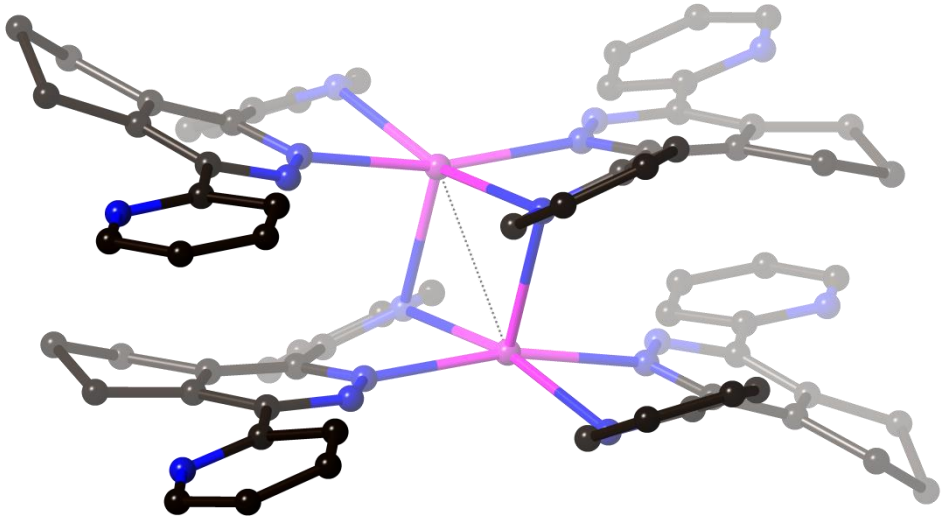

Figure 2.12: Dimer of complex 2.4 showing Ag-Ag interaction, nitrogen pyramidilisation and stacking of the ligands. Hydrogen atoms and non-coordinated anion have been omitted for clarity. Ag···Ag 2.9868(3) Å *selected distance.*

The solid state structure is not consistent with the results obtained in the solution studies. The solution studies show symmetrical pyridine proton peaks which indicates the silver metals are coordinated to both rings, however in the solid state this is not the case. The *trans* coordination of the ligands would show non-symmetrical pyridine rings as they are in different environments.

Complex 2.5 – **L3** + silver triflate

Crystals of complex **2.5** suitable for single crystal X-ray structure determination were obtained by vapour diffusion of diisopropyl ether into the reaction mixture of **L3** and silver trifluoromethanesulfonate in dichloromethane/acetonitrile (9:1). This complex analysed with a 1:1 metal-to-ligand stoichiometry.

Solution studies of complex **2.5** were completed as described for complex **2.4** with coordination induced shifts summarised in table 2.5. The protons that experience the greatest CIS are protons H3, H6 and H10, which move upfield by 0.11 ppm, 0.16 ppm and 0.15 ppm, respectively, while the other protons experience relatively small shifts. The H6 proton experiences could be due to this proton facing into a shielding zone of a nearby aromatic ring as it is the greatest CIS for this complex.

The ^{1}H-NMR titration completed for complex **2.5** is shown in figure 2.12. The titration was carried out the same way as described in complex **2.2**, with the addition of metal to ligand until the ratio

was 1:1 and then the extra equivalent of metal salt added to ensure no change in the spectrum. Similarities to the previous complex, **2.4**, are seen. In all the spectra collected a symmetrical molecule is observed as well as the same resulting stoichiometry indicating a 1:1 metal to ligand complex formed in solution. The ESI-MS results confirms the possibility of a 1:1 metal-ligand stoichiometry, however these could be fragments of complex **2.4**, as $[Ag_2(\mathbf{L3})_2]^{2+}$ or $[Ag_2(\mathbf{L3})_3]^{2+}$.

	H3	H4	H5	H6	H10	H11
L3	7.88	7.98	7.48	8.72	2.94	1.80
C2.5	7.77	8.01	7.52	8.56	2.79	1.76
CIS[b]	-0.11	+0.03	+0.04	-0.16	-0.15	-0.04

[a] For deuterated acetonitrile solutions. [b] CIS= $^{\delta}$complex-$^{\delta}$ligand.

*Table 2.5: ^{1}H-NMR Chemical shifts[a] and Coordination Induced Shifts[b] of complex **2.5***

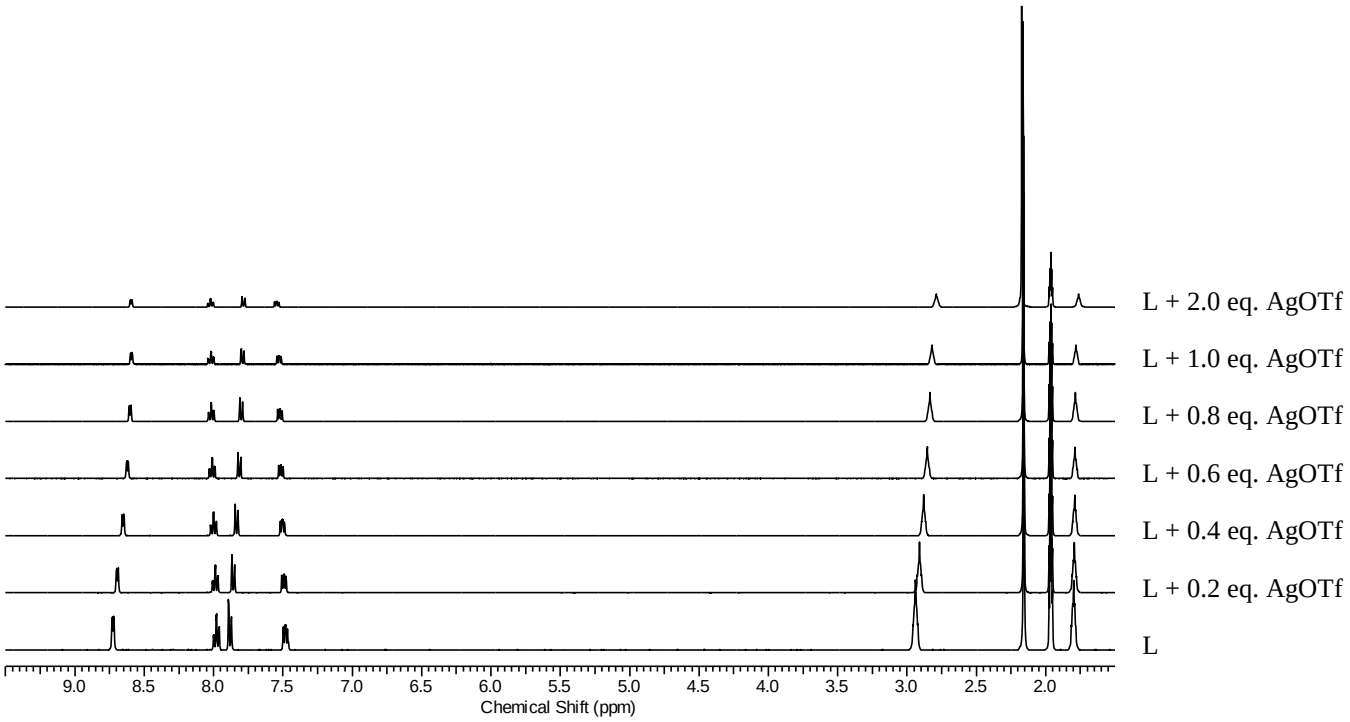

*Figure 2.12: NMR titration to form complex 2.5 of **L3** with AgOTf.*

This complex crystallises in the monoclinic space group $P2_1/c$, and has a one-dimensional polymeric structure. The asymmetric unit contains two silver metals, one molecule of **L3** and two coordinated triflate anions.

The silver atoms in the $Ag_4(\mathbf{L3})_2$ subunit of the polymer (figure 2.13) are four coordinate with a distorted tetrahedral geometry. The silver atoms are held in close proximity (3.0836(3) Å) by the ligand subunits, showing a relatively weak Ag···Ag interaction. Each metal is coordinated by two oxygen atoms from the triflate anions present and two nitrogen atoms from different ligands, one

from the pyridazine central ring and one pyridine ring. The Ag-N bond lengths range from 2.273(2) Å – 2.367(2) Å. The nitrogen atoms on the pyridyl groups are twisted out of the plane of the pyridazine core (57.44(8)° and 60.60(8)°) forming the Ag_4(**L3**)$_2$ subunit within the polymer, with the molecules of **L3** tetra-bridging, which is unusual. This twisting is due to the interactions of the hydrogen atoms between the pyridine rings and the fused cyclohexene ring. The distances from the closest pyridyl carbon to the fused cyclohexene ring carbon shows a distance in which is the result of the twisting of the pyridine groups (C8-C19 3.159(4) Å, C5-C13 3.193(4) Å).

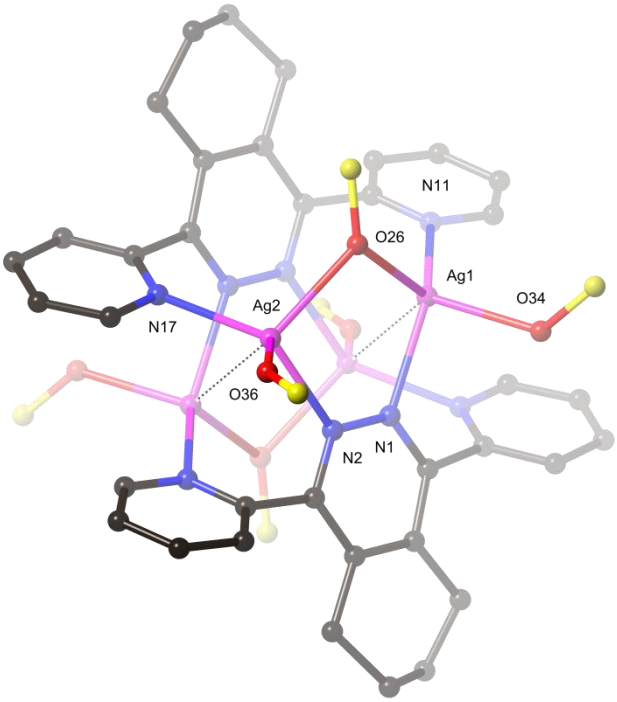

Figure 2.13: The Ag_4(**L3**)$_2$ *subunit of complex* ***2.5*** *highlighting the coordination of the silver atoms, with coordinated oxygen and sulfur atoms of triflate anions shown. Minor disorder, hydrogen atoms and non-coordinating components of the triflate anions have been removed for clarity. Selected bond lengths (Å):* Ag1-N1 2.367(2), Ag1-N11 2.273(2), Ag1-O26 2.420(2), Ag1-O34 2.420(2), Ag2-N2 2.303(2), Ag1-N17 2.273(2), Ag2-O26 2.413(2), Ag2-O36 2.246(2) *and angles (°):* N11-Ag1-O34 116.57(8), N11-Ag1-O26 110.49(7), N11-Ag1-Ag2 69.71(5), N11-Ag1-N1 132.68(7), O36-Ag2-O26 107.09(8), O36-Ag2-N17 96.97(8), O36-Ag2-Ag1 128.84(6), O36-Ag2-N2 102.94(8), O26-Ag2-Ag1 123.93(5), Ag1-Ag2-N2 67.29(5), Ag1-Ag2-O36 128.84(6), Ag1-Ag2-N17 69.75(5), Ag2-Ag1-N11 69.71(5), Ag2-Ag1-O34 128.27(6), Ag2-Ag1-O26 118.12(5), Ag2-Ag1-N1 63.61(5).

The cyclohexene ring fused to the pyridazine ring is distorted over two sites, which have the different half-chair conformations of cyclohexene (figure 2.14), with the larger occupancy being 64%. The structure is a one-dimensional polymer which propagates along the *a*-axis of the cell.

Figure 2.14: The two possible chair conformations of the cyclohexene fused ring located on the back of the pyridazine core.

There are four triflate anions, two of which bifurcate between two metals and the other two which bridge between the two subunits, with the Ag-O bond lengths ranging from 2.246(2) Å – 2.420(2) Å. The bridging triflate is a key component to the polymer formation as it bridges the two silver atoms from the different Ag_4(**L3**)$_2$ subunits, as shown in figure 2.15.

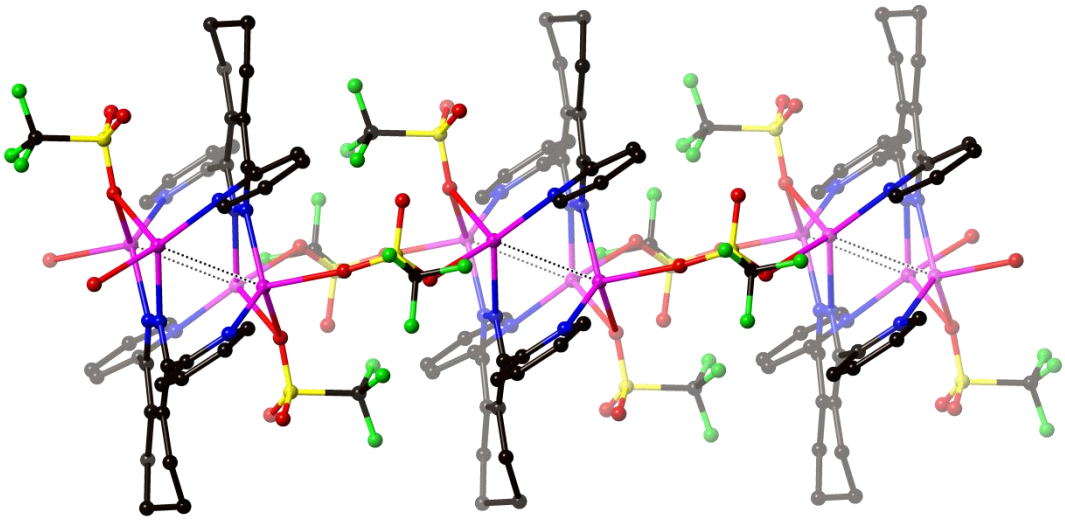

Figure 2.15: 1-D polymeric structure of complex **2.5** *showing the connectivity of the triflate anions between the* Ag_4***(L3)***$_2$ *subunits. The hydrogen atoms have been omitted for clarity.*

The ^{1}H-NMR titration for complex **2.5** indicates a 1:1 metal to ligand stoichiometry; however in the solid state the stoichiometry is 2:1. The CIS of H6 shows an upfield shift which in the solid state located over an aromatic ring at a distance of 3.4827(10) Å and 3.5869(10) Å, however, this distance is too long as is it more likely due to the nitrogen binding to the metal making the proton electron deficient.

Complex 2.6 – **L4** + silver hexafluorophosphate

Large crystals of complex **2.6** were obtained by diffusion of pentane into the reaction mixture with a 1:1 metal-ligand ratio of molecule **L4** and silver hexafluorophosphate in acetonitrile. This complex analysed with a 2:1 metal to ligand stoichiometry.

NMR spectroscopy was carried out for complex **2.6** with the same procedures used as previously described. Shown in table 2.6 are the coordination induced shifts for complex **2.6**, with the greatest CIS for this complex observed for proton H3, 0.23 ppm downfield, followed by 0.16 ppm upfield for proton H6 and H10 which experience a 0.13 ppm shift upfield, similar to that observed previously.

	H3	H4	H5	H6	H10	H11	H12
L4	7.86	7.98	7.49	8.73	3.00	1.71	1.89
C2.6	7.63	8.01	7.54	8.57	2.87	1.69	1.92
CIS[b]	-0.23	+0.03	+0.05	-0.16	-0.13	-0.02	+0.03

[a] For deuterated acetonitrile solutions. [b] CIS= $^{\delta}$complex-$^{\delta}$ligand. [c] Deuterated acetonitrile interruption.

*Table 2.6: ^{1}H-NMR Chemical shifts[a] and Coordination Induced Shifts[b] of complex **2.6**.*

The ^{1}H-NMR titration, displayed in figure 2.16 showed similarities between this complex and the

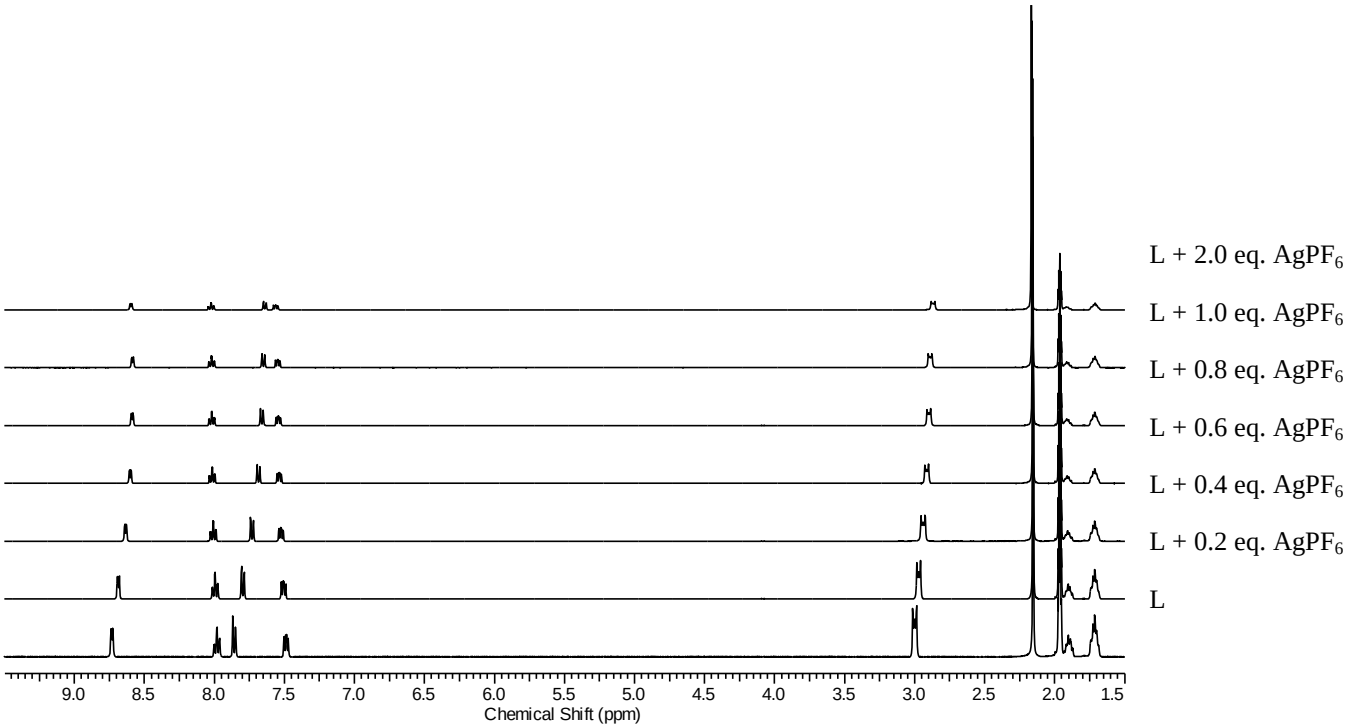

*Figure 2.16: ^{1}H-NMR titration to form complex **2.6** of **L4** with $AgPF_6$.*

previous two complexes, **2.4** and **2.5**. With the addition of 0.2 eq., a small CIS is observed with continued shifting of these peaks until the 1:1 metal to ligand ratio is completed. The ESI-MS shows the possibility of a $[Ag(\mathbf{L3})]^{+}$ complex as well as $[Ag_2(\mathbf{L3})_2]^{2+}$ complex however, these could be fragmented components of the complex.

The complex **2.6** crystallises in a triclinic space group P-1 as chunky crystals. The asymmetric unit is made up of two silver atoms, one molecule of **L4**, three coordinated acetonitrile molecules, two non-coordinated hexafluorophosphate anions and one uncoordinated dichloromethane solvate. The discrete complex structure, $Ag_4(\mathbf{L3})_2$ is displayed in figure 2.17. The silver metals within this complex are four coordinate with a distorted tetrahedral geometry, with each bound to four nitrogen atoms; one from each ligand and two from acetonitrile solvates. The angles around the silver metals range from 92.75(8)° - 134.03(7)° which indicate the distorted coordination geometry. There is also a Ag-Ag interaction that is fairly weak (3.0192(3) Å), giving the structure a similar motif to complex **2.5**.

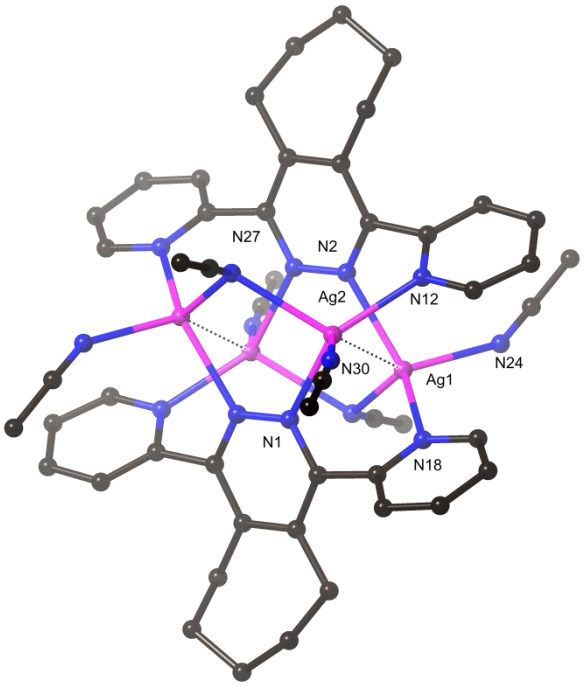

Figure 2.17 Discrete structure of complex 2.6. Hydrogen atoms, solvent molecules and anions have been omitted for clarity. Selected bond lengths (Å): Ag1-N2 2.418(2), Ag1-N18 2.319(2), Ag1-N24 2.313(3), Ag1-N27 2.405(3), Ag2-N1 2.334(2), Ag2-N27 2.536(3), Ag2-N12 2.296(2), Ag2-N30 2.269(3) *and angles(°):*N2-Ag1-N18 134.03(7), N24-Ag1-N18 105.20(10), N2-Ag1-N24 102.54(9), N18-Ag1-N27 115.55(9), N2-Ag1-N27 93.09(8), N24-Ag1-N27 102.15(10), N1-Ag2-N12 133.62(7), N12-Ag2-N17 115.34(9), N1-Ag2-N27 92.75(8), N12-Ag2-N30 105.06(10), N1-Ag2-N30 106.49(9), N27-Ag2-N30 98.10(11).

The sterically hindered backbone stops the complex from chelating and the Ag_4(**L4**)$_2$ complex is formed instead of a grid. The molecule of **L4** is tetra-bridging to four silver atoms with twisting of the pyridine rings out of the plane of the pyridazine core (61.85(5)° and 65.84(8)°) caused by the steric interaction of the fused ring.

As previously mentioned, there are three coordinated acetonitrile solvates within the asymmetric unit. Two of these solvate molecules are coordinated to a single silver metal; with the other bifurcating two silver metals. This is reflected in the bond lengths associated with the different connectivity; the bifurcating acetonitrile has longer bond lengths of 2.405(3) Å and 2.536(3) Å compared to the bond lengths of the two singly coordinated acetonitrile, 2.313(3) Å and 2.269(3) Å.

The conformation of the fused cycloheptene ring and the coordinated solvate molecules creates an interesting bowl shape that one of the PF_6 anions is situated, as shown in figure 2.18. The other anions and solvates do not show any significant interactions and are located in space between subunits.

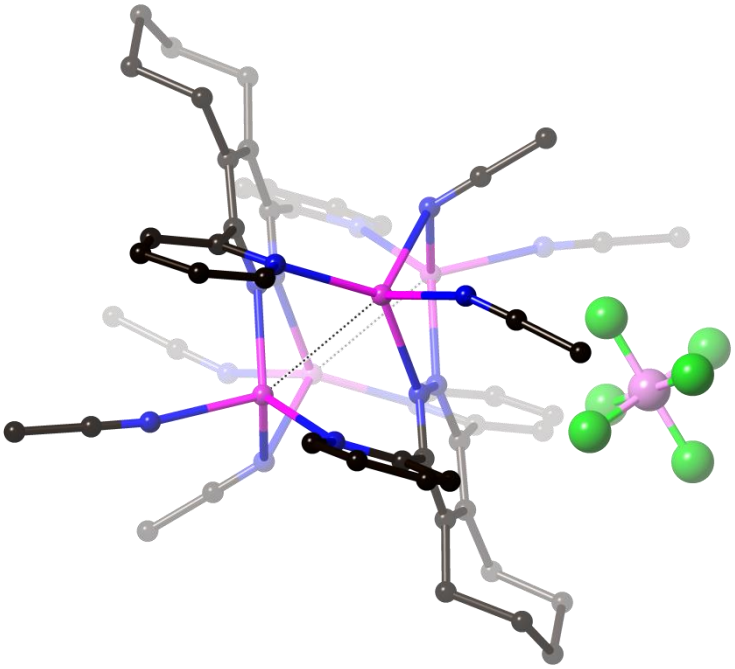

Figure 2.18: *Perspective view of bowl shape formed by the acetonitrile and the fused cycloheptene ring where the one of the PF_6 anions is located. Other non-coordinated anions and solvates have been removed for clarity.*

Complex **2.6** solution studies were consistent with complex **2.5**. The twisting of the pyridyl rings are greater for complex **2.6** compared to the other complexes **2.1** – **2.5** and this is an effect of the larger fused ring (cycloheptene) to the pyridazine ring.

Complex 2.7 – **L5** + silver triflate

Small crystals suitable for single crystal X-ray structure determination of complex **2.7** were obtained after vapour diffusion of diisopropyl ether into the reaction mixture in a solvent mixture (dichloromethane/acetonitrile, 9:1) containing silver triflate and **L5**. The solid analysed with a 1:1 metal-ligand stoichiometry.

NMR spectroscopy of complex **2.7** showed only uncoordinated ligand. Complex **2.7** was insoluble in most common NMR solvents; nevertheless, the complex was able to be dissolved in d_6-DMSO. A ^{1}H-NMR titration was unsuccessful even using a solvent mixture due to both **L5** and the metal salt being insoluble in the same solvent. The titration resulted in precipitation occurring almost immediately upon addition of the metal salt solution to the ligand solution. ESI-MS shows four possible complexes, $[Ag(\mathbf{L5})_2]^+$, $[Ag_2(\mathbf{L5})_3]^{2+}$ and $[Ag(\mathbf{L5})]^+/[Ag_2(\mathbf{L5})_2]^{2+}$, again as previously, these could be fragmented components.

Complex **2.7** crystallises in the triclinic space group P-1, with an asymmetric unit consisting of two molecules of **L5**, two silver metals, two non-coordinated triflate anions, one non-coordinated dichloromethane and one non-coordinated acetonitrile. The silver metals are disordered over two sites with the largest having an occupancy of 92%. This complex is a discrete $Ag_4(\mathbf{L5})_4$ structure, as seen in figure 2.19.

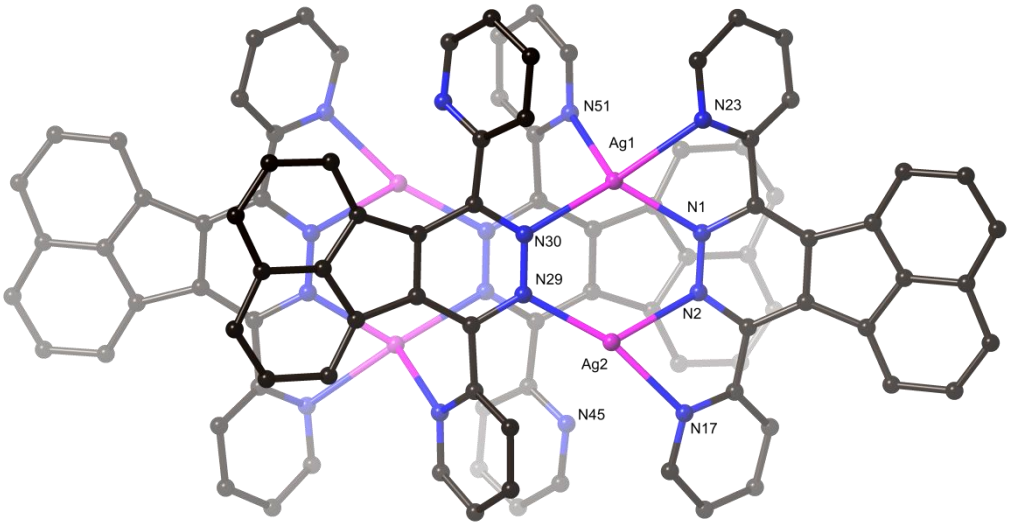

*Figure 2.19: Discrete structure of complex **2.7**. Minor occupancies of the Ag atoms, hydrogen atoms, solvent molecules and anions have been omitted for clarity. Selected bond lengths (Å):* Ag1-N1 2.305(5), Ag1-N23 2.459(6), Ag1-N30 2.364(6), Ag1-N51 2.367(6), Ag2-N2 2.330(6), Ag2-N17 2.301(6), Ag2-N29 2.228(6) *and angles(°):* N1-Ag1-N23 69.28(19), N17-Ag2-N2 71.5(2).

The two silver metals have different coordination geometries; one having a distorted trigonal geometry while the other has a distorted tetrahedral geometry. This difference is a result of the sterically hindering fused acenaphthylene ring and the twisting of the pyridyl groups. There is one pyridyl group in the Ag_4(**L5**)$_4$ discrete structure where the nitrogen is not coordinated to the silver metal. The distance from this non-coordinated nitrogen (N45) to the closest silver atom (Ag2) is 3.588(7) Å, thus being too long to consider coordination to occur.[97] The twisting of the pyridine group results in this larger distance. The pyridine rings of **L4** are twisted out of the plane of the pyridazine core at angles of 37.2(2)° and 38.5(2)° for the ligand that has two chelating sites. The other ligand that contains only one chelating site has twists of 50.0(2)° and 59.2(2)°.

Packing of these discrete structures (figure 2.20) shows a π-π stacking interaction of 3.787(4) Å between the fused acenapthyl rings of different discrete structures. The acetonitrile solvates are located in the pockets formed by the fused acenapthyl-group and the nitrogen is facing towards to silver atom. The acetonitrile is said to be non-coordinated as it is modelled to be coordinated to one of the minor occupied silver metals (very low occupancy of 8%).

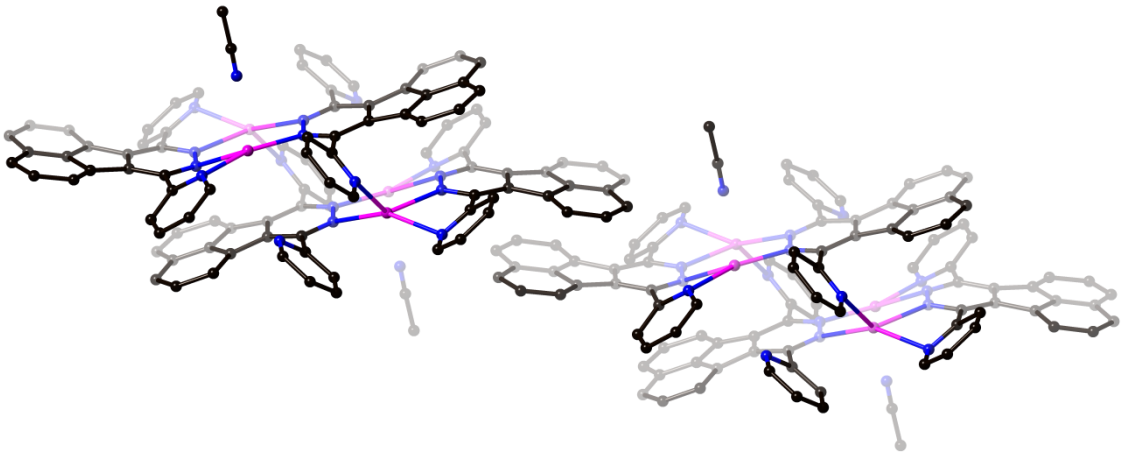

*Figure 2.20: Packing of the complex **2.7**, showing π-π interactions between the discrete structures and the acetonitrile solvates facing towards the silver metal. Hydrogen atoms, anions and minor occupancies have been removed for clarity.*

The 2-pyridyl series of ligands with Ag(I) have shown a range of different self-assembled structures, with examples of side-by-side, metallogrids, tetra-bridging ligands and polymeric complexes . When increasing the hindering fused rings from **L2** to **L3** to **L4** and **L5**, increased the twisting of the pyridine ring, causing the interesting tetra-bridging structures and non-coordinating groups (**C2.7**). Due to the versatile structures observed we decided to increase the hindrance on the pendant group, changing to 1-dimethylpyrazole to see what effect this has.

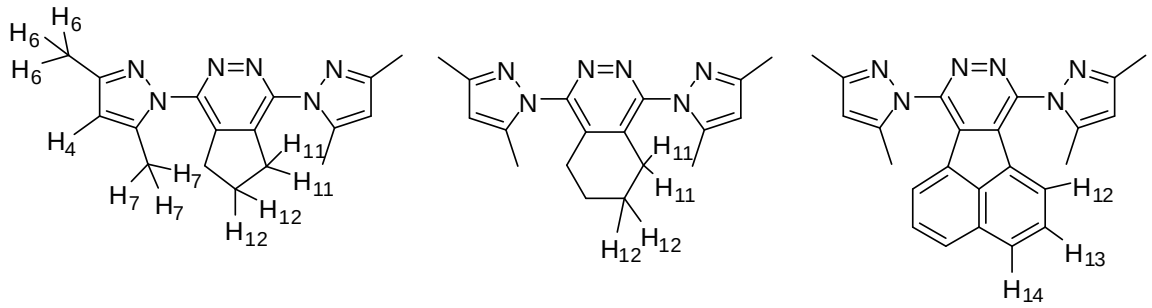

L7 **L8** **L9**

*Figure 2.21: Selected proton labelling and structures of **L7**-**L9**.*

Complex 2.8 – **L7** + silver triflate

The reaction of **L7** with silver triflate resulted in complex **2.8**. Crystals were obtained by vapour diffusion of diisopropyl ether into the reaction mixture in acetonitrile. This solid analysed with a 1:1 metal-ligand stoichiometry.

The same solution studies as previously described, NMR Spectroscopy and Mass Spectrometry were carried out for complex **2.7**. The complex was dissolved in d_3-acetonitrile and a ^{1}H NMR spectrum collected and compared to the ligand spectrum. The coordination induced shifts are shown in table 2.7. All the protons exhibit small CIS, making it difficult to determine if there is a coordination of the metal as determined by NMR. A ^{1}H-NMR titration was completed which confirms the same observation. ESI-MS shows most likely fragmented components as $[Ag(\mathbf{L7})_2]^+$ and $[Ag(\mathbf{L7})]^+/[Ag_2(\mathbf{L7})_2]^{2+}$.

	H4	H6	H7	H11	H12[c]
L7	6.13	2.26	2.50	3.23	2.20[c]
C2.5	6.18	2.28	2.47	3.18	2.20[c]
CIS[b]	+0.05	+0.02	-0.03	-0.05	-

[a] For deuterated acetonitrile solutions. [b] CIS= $^{\delta}$complex-$^{\delta}$ligand. [c] Water overlap.

*Table 2.7: ^{1}H-NMR Chemical shifts[a] and Coordination Induced Shifts[b] of complex **2.5***

Complex **2.8** crystallises in the monoclinic space group $P2_1/c$. The asymmetric unit contains one ligand (**L7**), two silver metals, two coordinated acetonitrile solvate molecules (one to each metal) and two triflate anions; one coordinated and one non-coordinated. The complex has a $Ag_4(\mathbf{L7})_2$ structure, as shown in figure 2.22.

The substituted pyrazole groups are twisted out of the plane of the pyridazine core, 58.49(13)° and 59.95(13)° due to the steric interactions between the fused cyclopentene ring and the methyl groups on the pyrazole groups, giving a discrete structure where the ligand coordinates to all four metals.

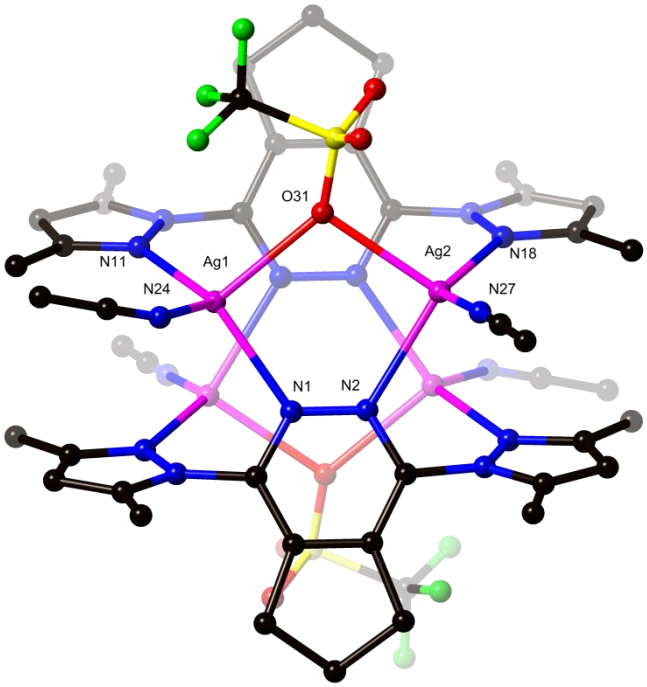

Figure 2.22: Discrete structure of complex 2.8. Hydrogen atoms, non-coordinated anions have been omitted for clarity. Selected bond lengths (Å): Ag1-N24 2.311(5), Ag1-N11 2.219(3), Ag1-N1 2.375(3), Ag1-O31 2.480(3), Ag2-N18 2.226(3), Ag2-N2 2.463(3), Ag2-N27 2.234(4), Ag2-O31 2.507(3) *and angles(°):* N1-Ag1-N11 134.92(12), N2-Ag2-N18 128.98(12), Ag1-O31-Ag2 105.94(11).

The silver metals have a distorted tetrahedral geometry and are coordinated by three nitrogen atoms (one from each ligand and the other from the coordinated solvate) and one oxygen from the triflate anion. The coordinated anions bifurcate two silver atoms (2.480(3) Å and 2.507(3) Å). There is also a very weak Ag···Ag interaction of 3.2114(4) Å, giving a similar structural motif to complex **2.5**. The bond lengths from silver to the pyridazine nitrogen are longer than the nitrogen bound to the pyrazole group, 2.375(3) Å and 2.463(3) Å, compared to 2.219(3) Å and 2.226(3) Å. The coordinated acetonitrile bond lengths to silver are similar to those of the pyrazole group. The coordination of the bridging anion between two of the metals is an essential component to this structure.

Complex 2.9 – **L8** + silver triflate

Vapour diffusion of petroleum ether into the reaction mixture of **L8** and silver triflate yielded block-like colourless crystals of complex **2.9** that were suitable for X-ray crystallography. These crystals were analysed with a 1:2 metal to ligand stoichiometry.

Solutions studies as previously described were completed for complex **2.9** showing similar results to complex, **2.8**. Coordination induced shifts are summarised in table 2.8, showing that H4 and H11 have slight shifts of 0.05 ppm downfield and 0.03 ppm upfield, respectively. Thus, analysis of the silver metals coordination is difficult to determine. The ^{1}H-NMR titration supports the shifts mentioned. ESI-MS shows the same results as the previous complex, **2.8,** $[Ag(\mathbf{L7})_2]^+$ and $[Ag(\mathbf{L7})]^+/[Ag_2(\mathbf{L7})_2]^{2+}$.

	H4	H6[c]	H7[c]	H11	H12
L8	6.11	2.26[c]	2.26[c]	2.67	1.78
C2.9	6.16	2.28[c]	2.28[c]	2.64	1.78
CIS[b]	+0.05	+0.02	+0.02	-0.05	-

[a] For deuterated acetonitrile solutions. [b] CIS= $^{\delta}$complex-$^{\delta}$ligand. [c] Water overlap

*Table 2.8: ^{1}H-NMR Chemical shifts[a] and Coordination Induced Shifts[b] of complex **2.9***

Complex **2.9**, crystallises in the monoclinic space group C2/c. The asymmetric unit consists of two metals, one **L8** molecule, two coordinated acetonitrile solvates and two triflate anions; one bifurcating two metals and one non-coordinated. The dimeric structure is the same as previously seen in complex **2.8**, a discrete $Ag_4(\mathbf{L8})_2$ structure with the triflate anion bridging the two silver metals, as shown in figure 2.23.

The silver metals have the same geometry and connectivity as described in complex **2.8**, with each metal having a tetrahedral geometry, bound to three nitrogen atoms and one oxygen atom. The fused cyclohexene ring on the ligand is in the two half-chair conformations (figure 2.14) highest occupancy being 65%. This effect has been evident in the previous fused cyclohexene ring complex, **2.5** (figure 2.13). The two pendant heterocycles are twisted 86.43(18)° and 89.72(19)°, relative to the pyridazine core structure. This is the largest twisting that has been seen so far and confirms that this twist relieves the strain between the fused ring and the sterically substituted pyrazole rings. The distance from the methyl groups to the fused cyclohexene ring show adequate distance lengths removing this strain (C24-C8 3.829(8) Å and C17-C5 3.799(9) Å) due to the twisting of the pendant groups.

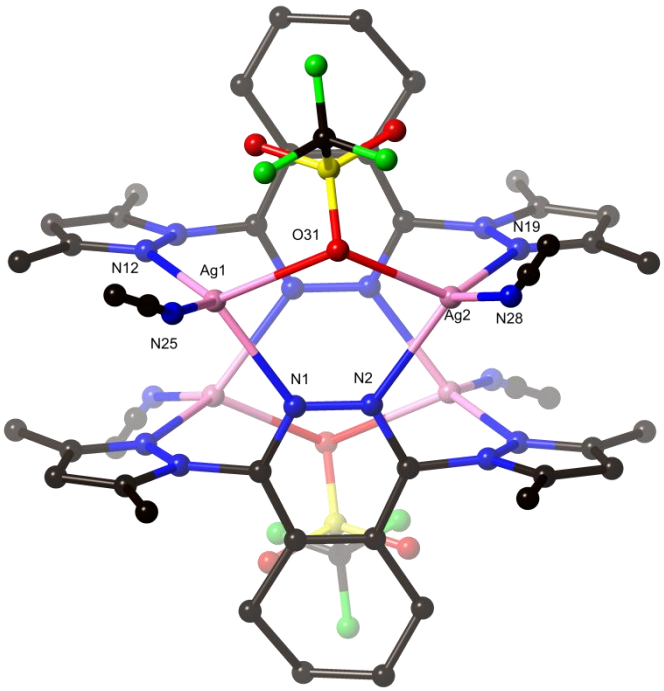

Figure 2.23: Discrete structure of complex **2.9**. *Hydrogen atoms, non-coordinated anions have been omitted for clarity. Selected bond lengths (Å):* Ag1-N1 2.393(4), Ag1-N12 2.236(4), Ag1-N25 2.296(5), Ag1-O31 2.492(5), Ag2-N2 2.395(4), Ag2-N19 2.226(4), Ag2-N28 2.272(5), Ag2-O31 2.591(5), *and angles(°):* N1-Ag1-N12 117.33(13), N2-Ag2-N19 116.42(14).

There is a pocket formed within the subunits, where a cluster of water molecules is located. The non-coordinated anion is located in space and has no significant interactions, with distances to the closest atoms C24-to-O42 3.428(8) Å and C24-to-O41 3.815(10) Å.

When the same ligand, **L8** was reacted with silver perchlorate the same structural motif was observed, the only difference being the oxygen atom of the perchlorate anion bifurcates two silver metals, rather than the triflate. Similar bond lengths, angles and twisting of the pendant group with respect to the pyridazine ring are observed. Other silver salts containing non-coordinating anions were investigated, although no solid product was obtained.

There is no significant link between the solution studies and solid state for complex **2.9**; nevertheless, the structure is the same motif as observed in complex **2.5**, **2.6** and **2.8**.

Complex 2.10 - **L9** + silver triflate

Complex **2.10**, was grown by vapour diffusion of petroleum ether into the reaction mixture of **L9** and silver triflate in dichloromethane and acetonitrile (9:1) producing yellow crystals suitable for single X-ray analysis. The complex was analysed with a 2:1 metal to ligand stoichiometry

The same solution studies were completed for this complex giving interesting results. Firstly, the complex was dissolved in d_3-acetonitrile and a ^{1}H-NMR spectrum collected and compared with the free ligand. The coordination induced shifts are summarised in table 2.9. All the protons experience an upfield CIS when Ag(I) is coordinated. H14 experiences the largest shift of 0.16 ppm, with all other protons experiencing CIS between 0.05 ppm – 0.09 ppm.

	H4	H6	H7	H12	H13	H14
L9	6.42	2.53	2.53	8.36	7.90	8.08
C2.10	6.37	2.44	2.44	8.30	7.82	7.92
CIS[b]	-0.05	-0.09	-0.09	-0.06	-0.08	-0.16

[a] For deuterated acetonitrile solutions. [b] CIS= $^{\delta}$complex-$^{\delta}$ligand.

*Table 2.9: ^{1}H-NMR Chemical shifts[a] and Coordination Induced Shifts[b] of complex **2.10**.*

A ^{1}H-NMR titration was then carried out as previously described with the addition of the metal salt to the ligand in acetonitrile with the results shown in figure 2.24b. The titration is similar to what has been observed in the other Ag(I) complexes, in this work however the complex spectra, shown in figure 2.24a, have the same peaks as the titration when 0.6 eq. of metal salt is added indicating that the complex has already formed even though the spectrum is still changing with extra addition of metal salt until the metal-to-ligand ratio is 1:1. The ESI-MS results show $[Ag(\mathbf{L9})_3]^+$, $[Ag_2(\mathbf{L9})_3]^{2+}$, $[Ag_2(\mathbf{L9})_2]^{2+}$, $[Ag(\mathbf{L9})_2]^+$ and $[Ag(\mathbf{L9})]^+$, which could possibly be complexes or fragmented components.

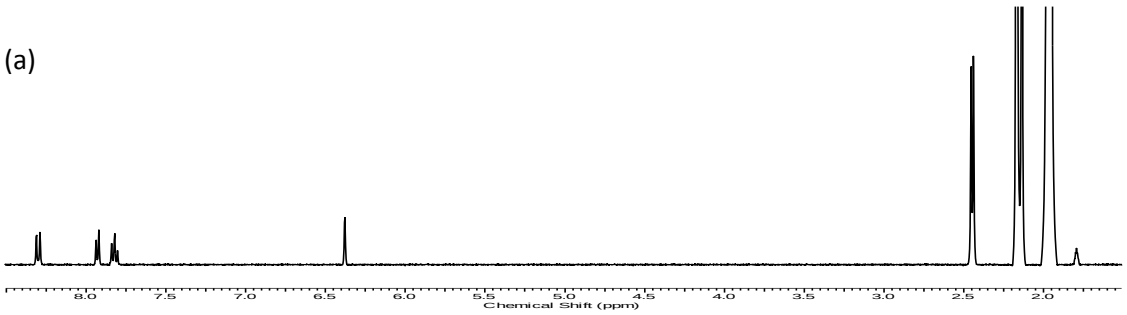

Figure 2.24(a): Complex ^{1}H NMR spectra dissolved in acetonitrile.

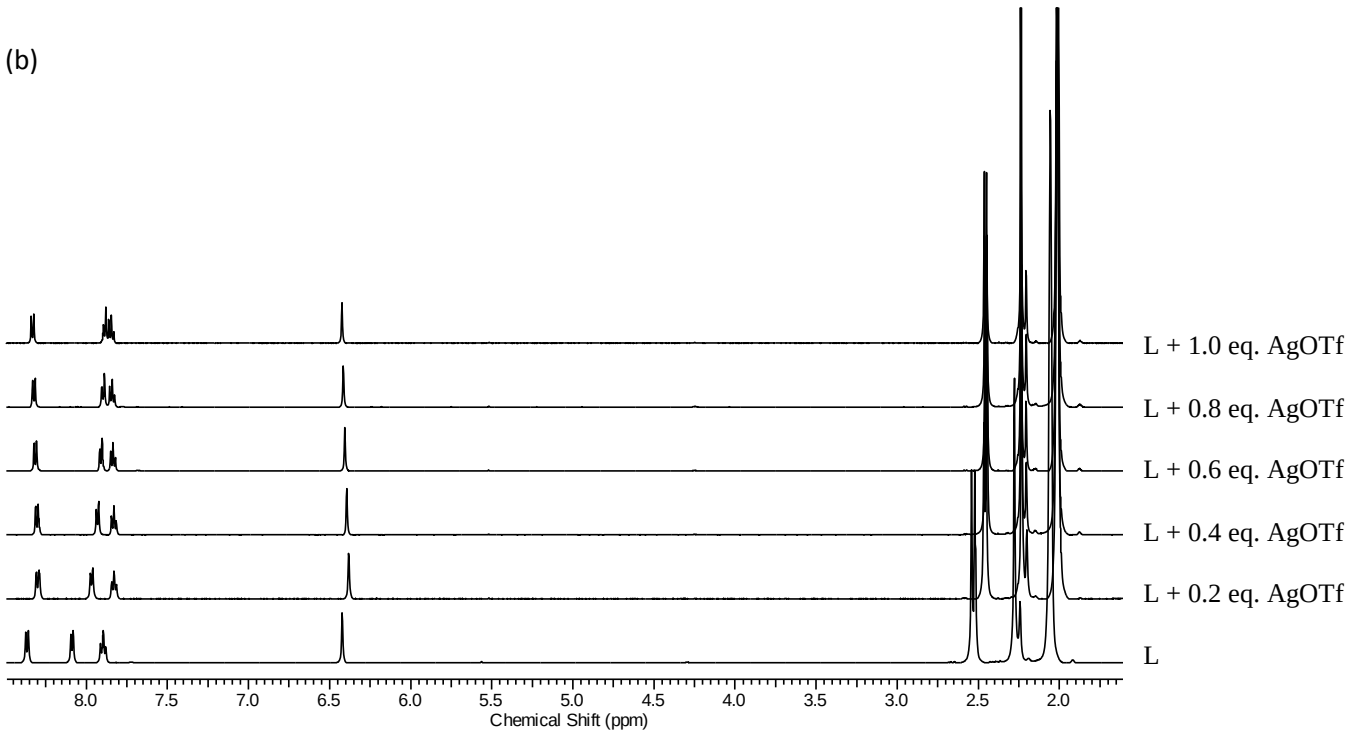

Figure 2.24(b): ^{1}H-NMR titration to form complex 2.10.

Complex **2.10** crystallises in the triclinic space group P-1, with the asymmetric unit containing one molecule of **L9**, two silver metals with two coordinated water molecules and one coordinated acetonitrile. There are also two non-coordinated triflate anion and two non-coordinated water molecules in the asymmetric unit. The X-ray crystallographic structure is $Ag_4(\mathbf{L9})_2$ displayed in figure 2.25.

The silver metals have a tetrahedral geometry with angles ranging from 94.46(7)° - 135.76(6)°, are coordinated to one oxygen atom from a water molecule and three nitrogen atoms; one pyridazine-nitrogen, one pendant pyrazolyl-nitrogen and bifurcating acetonitrile solvate. The dimethylpyrazole groups are twisted out of the plane of the pyridazine core by ~68°, this twist is due to both the fused acenaphthyl-group to relieve the steric interaction between the hydrogen atoms, as well as the methyl groups that sterically hinder the pyrazole pendant heterocycle. Tetra-bridging is observed due to this twisting (68.01(9)°, 68.94(7)°).

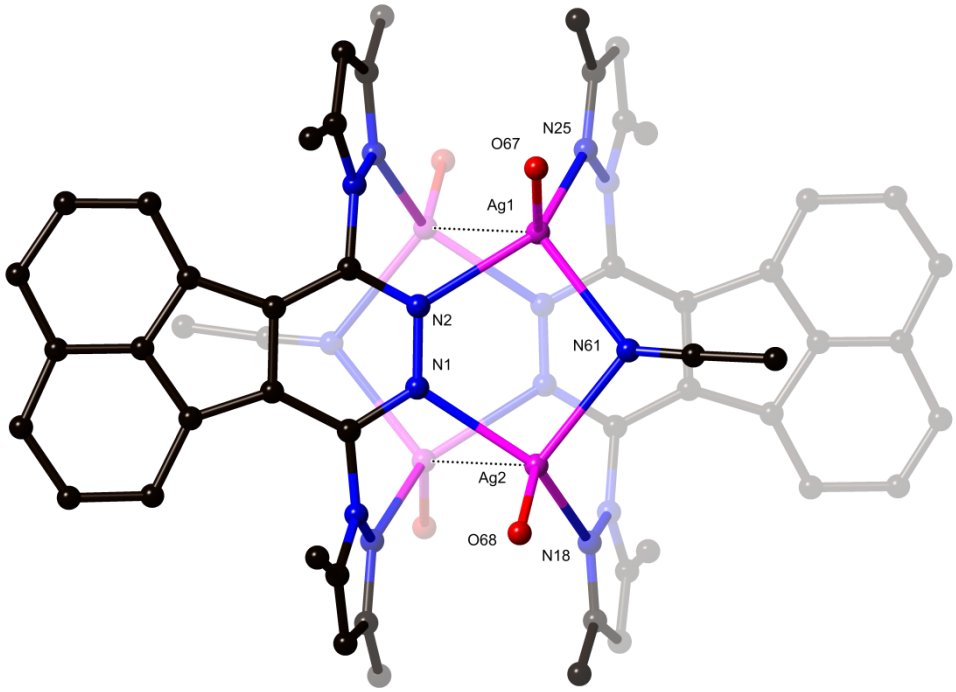

Figure 2.25: Discrete structure of complex ***2.10****. Hydrogen atoms, anions, non-coordinated water have been omitted for clarity. Selected bond lengths (Å):* Ag1-N2 2.3610(16), Ag1-N25 2.2422(17), Ag1-N61 2.487(2), Ag1-O67 2.3383(18), Ag2-N1 2.3575(16), Ag2-N18 2.2294(17), Ag2-N61 2.474(2), Ag2-O68 2.3585(18), *interactions (Å)* Ag1···Ag2 3.2092(2), *angles (°)* O67-Ag1-N2 97.94(6), O67-Ag1-N61 104.61(8), N2-Ag1-N61 94.98(7), N25-Ag1-O67 110.94(7), N25-Ag1-N2 134.61(6), N25-Ag1-N61 109.82(7), O68-Ag2-N61 108.40(8), N1-Ag2-O68 92.93(6), N1-Ag2-N61 94.46(7), N18-Ag2-O78 114.81(7), N18-Ag2-N1 135.77(6), N18-Ag2-N61 107.22(7) *and twisting of the pendant-groups (°)* 68.01(9), 68.94(7).

The non-coordinated solvates and anions are situated in space between the discrete structures with the two triflate anions being in close proximity to the coordinated waters. Two oxygen atoms on one of the triflate anions are involved in hydrogen bonding interactions, with three in total in this complex. These interactions are summarised in table 2.16 and shown in figure 2.26.

-H···A	D-A(Å)	D-H···A(°)
O67-H67A···O82	2.733(4)	175.01(14)
O68-H68A···O81	2.726(3)	151.59(16)
O68-H68B···O72	2.829(3)	173.24(14)

Table 2.10: *Hydrogen bonding interactions observed in complex* ***2.10****.*

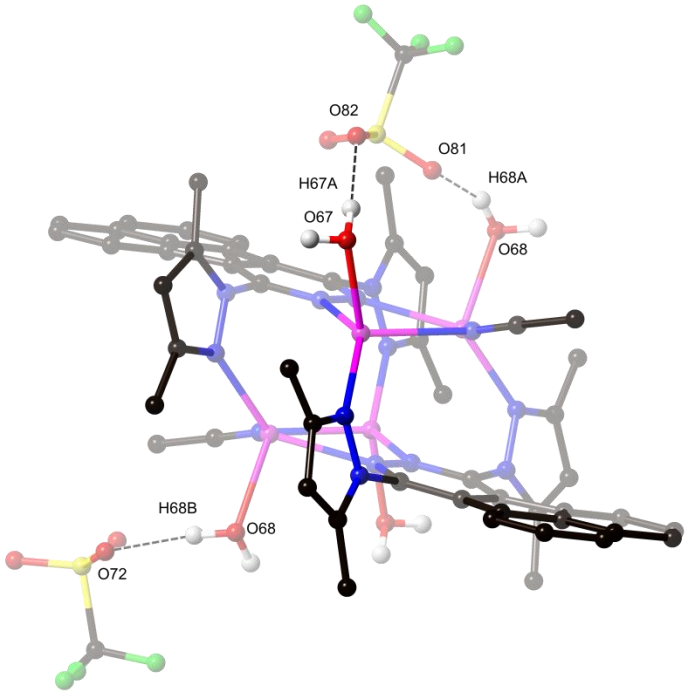

Figure 2.26: Structure showing the hydrogen bonding interactions between the water molecules and the anions. All other hydrogen atoms and non-coordinated solvate molecules have been removed for clarity.

Complex 2.11 – **L10** + silver hexafluorophosphate

The dimethylpyrazole complexes **2.8**, **2.9** and **2.10** show tetrabridging due to the more hindering groups introduced to the ligand. Molecule **L10** was complexed with Ag(I) to observe if chelation occurs without the sterically hindering fused components.

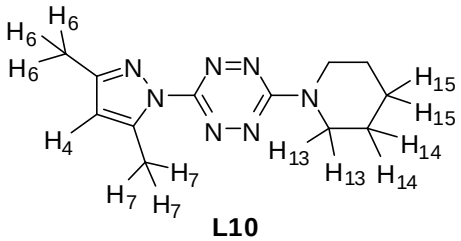

L10

*Figure 2.27: Structure and selected proton labelling of molecule **L10**.*

Bright red crystals of complex **2.11** were grown by vapour diffusion of diisopropyl ether into the reaction mixture containing molecule **L10** and silver hexafluorophosphate in acetonitrile. These crystals were suitable for X-ray crystallography. Unfortunately microanalysis was unable to be recorded as attempts to regrow these crystals met with no success.

Solution studies were completed for complex **2.11**, as previously described. Complex **2.11** was dissolved in d_3-acetonitrile and a ^{1}H-NMR spectrum collected and compared to the ligand spectrum. The coordination induced shifts are summarised in table 2.11. Proton H4 experiences the greatest shift of 0.11 ppm downfield, followed by the methyl group protons, H6 and H7 both experiencing a small downfield shift of 0.06 ppm. The protons on the piperidyl ring experience a very small shift of 0.03 ppm upfield for H13, however, the other protons do not experience a coordination induced shift.

	H4	H6	H7	H13	H14	H15
L10	6.15	2.27	2.44	3.98	1.78	1.72
C2.11	6.26	2.33	2.50	3.95	1.78	1.72
CIS[b]	+0.11	+0.06	+0.06	-0.03	-	-

[a] For deuterated acetonitrile solutions. [b] CIS= $^{\delta}$complex-$^{\delta}$ligand.

*Table 2.11: ^{1}H-NMR Chemical shifts[a] and Coordination Induced Shifts[b] of **complex 2.11***

A ^{1}H-NMR titration (figure 2.28) was carried out for complex **2.11** using the same procedures as previously described and the results are consistent with the comparison of the complex to the ligand stated above. When 0.2 eq. of metal is added to the ligand there is a small coordination induced shift and these shifts are observed until the 1:1 metal to ligand stoichiometry is completed. ESI-MS results show the complex possibilities of $[Ag(\mathbf{L10})_2]^+$, $[Ag(\mathbf{L10})CH_3CN)]^+$ and $[Ag(\mathbf{L10})]^+$.

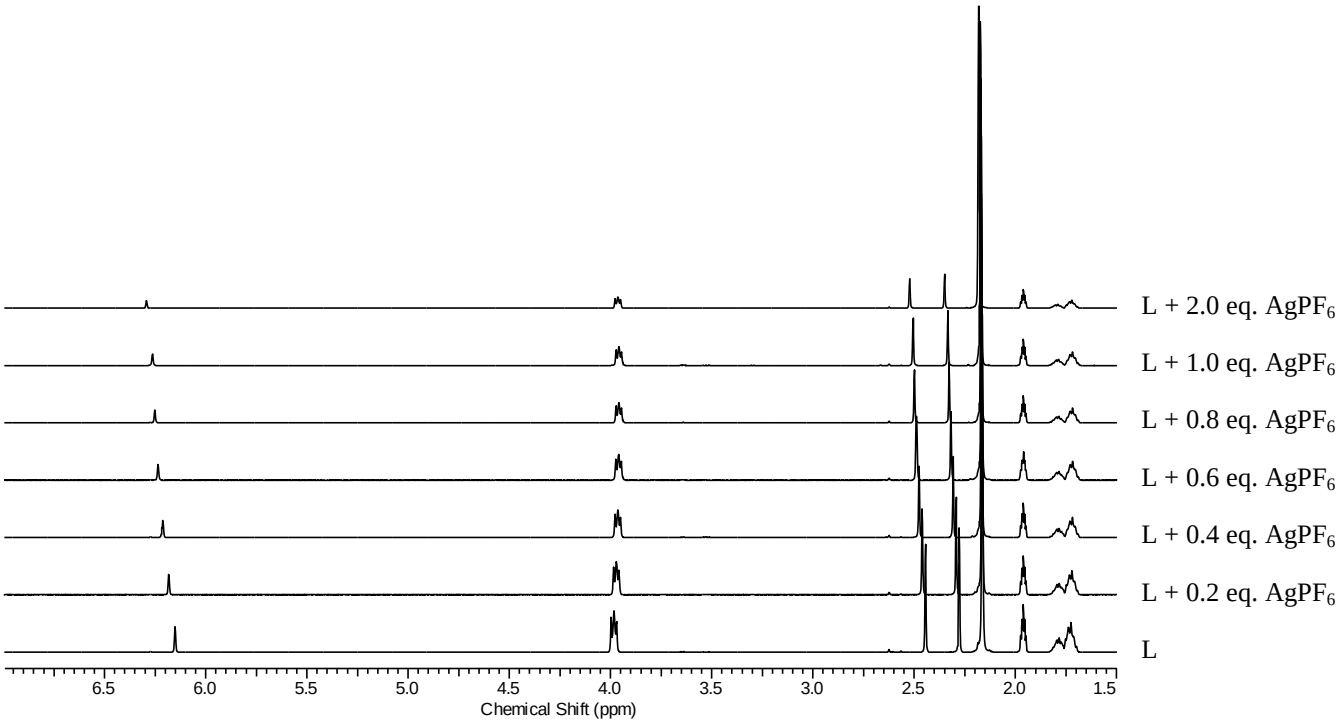

*Figure 2.28: NMR titration to form complex **2.11** of L10 with $AgPF_6$.*

The complex **2.11** crystallised in the triclinic space group P-1, with the asymmetric unit containing eight molecules of **L10**, four silver metals and four non-coordinated hexafluorophosphate anions. Two ligands and one metal coordinate to form four separate structures within the asymmetric unit.

Two of the silver metals are two coordinate; bound to one nitrogen from the pyridazine core of one ligand and one nitrogen from the dimethylpyrazole group of another ligand. This coordination has been seen previously by Yu *et al.*, with **L6** and Ag(I), see figure 1.12a.[78] The other two metals are three coordinate; bound to one nitrogen from the pyridazine core of one ligand, and a chelation occurs to the other ligand. The two coordinating types are shown in figure 2.29. The angle between the two coordinated pyrazole nitrogen atoms is ~175° for all the four structures. The pyridazine-nitrogen atoms are involved in Ag···N interactions ranging from 2.645(4) Å – 2.810(4) Å. The pendant heterocycles have twists ranging from 3.41(18)° - 35.79(17)° out of the plane of the tetrazine ring. The larger twists cause the Ag(I) atoms to be two coordinate and the three coordinate Ag(I) are observed when there is the smaller twisting.

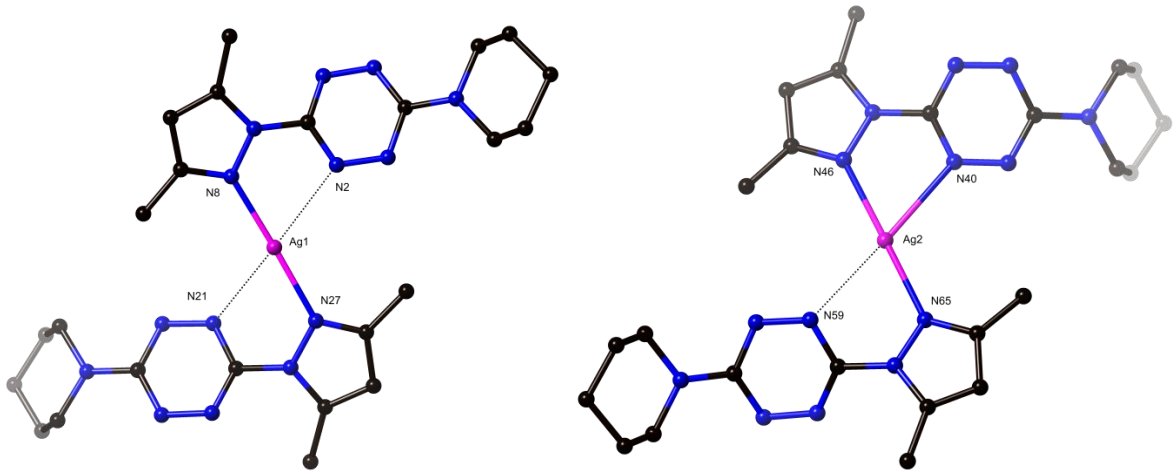

*Figure 2.29: Structure of complex **2.11** showing the different coordinating modes of the silver atoms. Selected bond lengths (Å):* Ag1-N8 2.183(4), Ag1-N27 2.169(4), Ag2-N40 2.577(4), Ag2-N46 2.223(4), Ag2-N65 2.202(4), Ag3-N78 2.634(4), Ag3-N84 2.211(4), Ag3-N103 2.214(4), Ag4-N122 2.167(4), Ag4-N141 2.154(4) *interactions(Å):* Ag1···N2 2.660(4), Ag1···N21 2.706(4), Ag2···N59 2.745(4), Ag3···N97 2.663(4), Ag4···N116 2.645(4), Ag4···N135 2.810(4); *angles(°):* N40-Ag2-N46 67.89(14), N78-Ag3-N84 66.20(44), N8-Ag1-N27 175.35(15), N46-Ag2-N65 177.08(14), N84-Ag3-N103 174.91(14), N122-Ag4-N141 176.61(14).

The structures are "stacked" on top of one another, shown in figure 2.30, with the perchlorate anions situated in space around the structures with no significant interactions. In the stacked structures there is a silver-nitrogen interaction between two of the side-by-side structures, Ag3-N137 2.662(4) Å.

For the complexes **2.8 - 2.11**, which all contain the same pendant group, 1-(3,5-dimethylpyrazole), the solution studies do not give information about the solution product. Due to extension of the fused rings on the pyridazine ring and the sterically hindering methyl groups on the pyrazole ring we have shown that the pendant groups show larger twisting with respect to the pyridazine ring and the ligands are tetrabridging in complexes **2.8 - 2.10** with no chelation. Complex **2.11** was studied as a model compound to confirm the twisting of one pendant group and to see if this effect is because of the fused ring component. This was shown to be confirmed with slight twisting of the pendant groups, though in complex **2.11** only half the Ag(**L10**)$_2$ structures showed chelation.

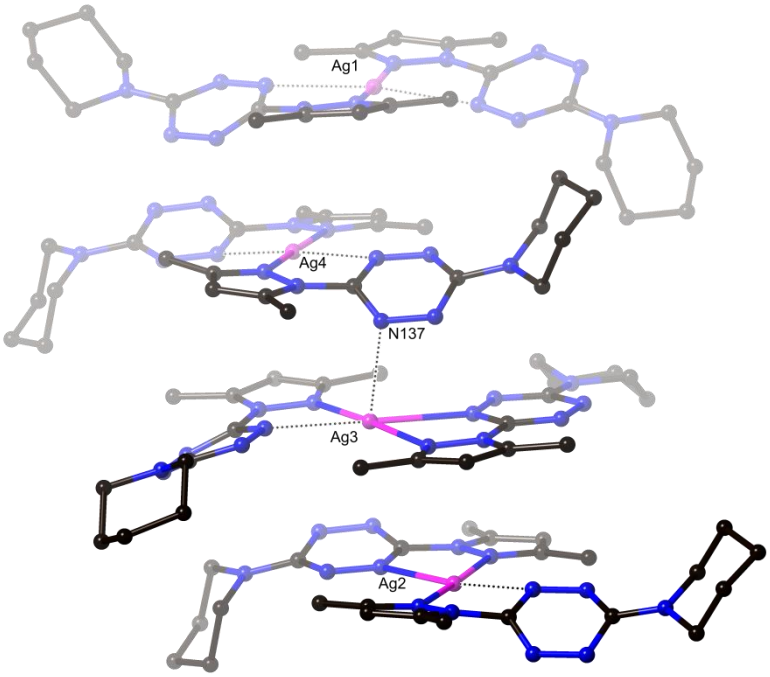

Figure 2.30: Perspective view of the four stacked structures. Non-coordinated anions and hydrogen atoms have been removed for clarity. Selected interaction (Å): Ag3-N137 2.662(4) *and twisting of the pendant groups(°):* Ag1 26.56(17) and 23.24(17), Ag2 14.32(18) and 35.79(17), Ag3 3.41(18) and 20.85(19), Ag4 23.76(18) and 26.07(17).

2.4 Synthesis of L13 - L16

The increase in donor atoms as previously mentioned can lead to polymeric structures or bridging between subunits. Molecules **L13** and **L15** were synthesised by adopting methods reported by Xie *et al*.[54] Molecule **L14** was synthesised by a new method as described below.

1,4-Bis(2-pyrazinyl)-6,7-dihydro-5*H*-cyclopenta[*d*]pyridazine (**L13**) and 1,4-di(2-pyrazinyl)-6,7,8,9-tetrahydro-5H-cyclohepta[*d*]pyridazine (**L15**) were synthesised from the tetrazine precursor, 3,6-bis(2-pyrazinyl)-1,2,4,5-tetrazine, with cyclopentanone for **L13** and cycloheptanone for **L15** and proline in a schlenk tube under N_2. The products were isolated after a Diels-Alder reaction in modest overall yields of 50% (**L13**) and 48% (**L15**), as a light brown solid and an off white solid, respectively. The recrystallization of **L13** was done using methanol, while, no recrystallization was necessary for **L15**, as once filtered and washed with cold methanol it yielded pure product.

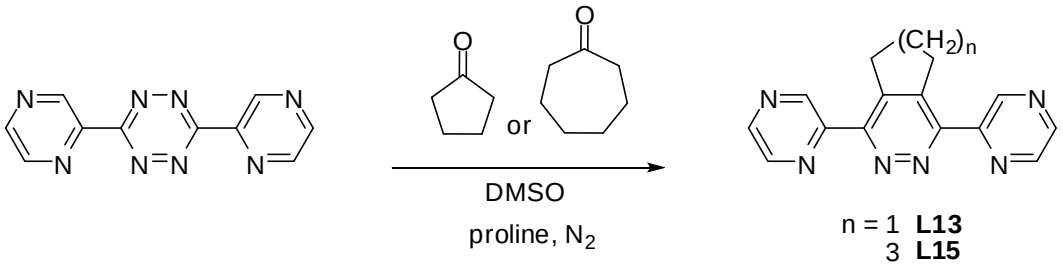

Scheme 2.1

1,4-Di(2-pyrazinyl)-5,6,7,8-tetrahydrophthalazine (**L14**) was synthesised by a Diels-Alder reaction using cyclohexene and the tetrazine precursor in a sealed tube with toluene. The resulting oily product was washed with hot methanol, impurities were filtered and the solvent removed under reduced pressure. The product was isolated in lower yield (38%) as an off white solid.

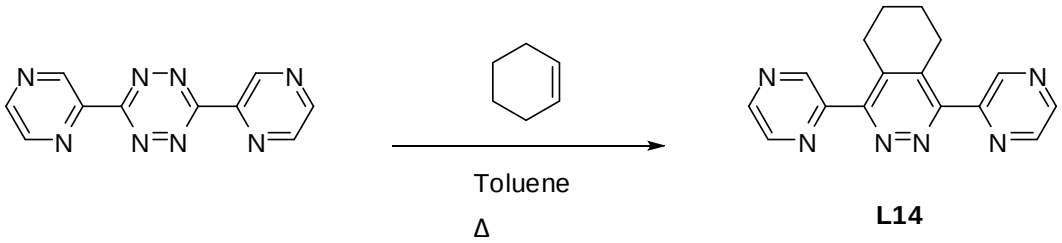

Scheme 2.2

Another new ligand, 3,6-bis(pyrazolyl)-1,2,4,5-tetrazine (**L16**) was synthesised by the reaction of 3,6-bis(3,5-dimethylpyrazol-1-yl)-1,2,4,5-tetrazine with excess of pyrazole under N_2. The mixture was kept in a molten state at 100°C. Once cooled to room temperature, the solid remains were washed with petroleum ether and acetonitrile. The remaining solid was extracted into dichloromethane and washed with water to remove any excess pyrazole. The organic layer was then separated, dried and removed under reduced pressure with the potential ligand being isolated in moderate yield (63%) as a pink powder. Unfortunately, due to time restrictions, no complexes were obtained with this molecule.

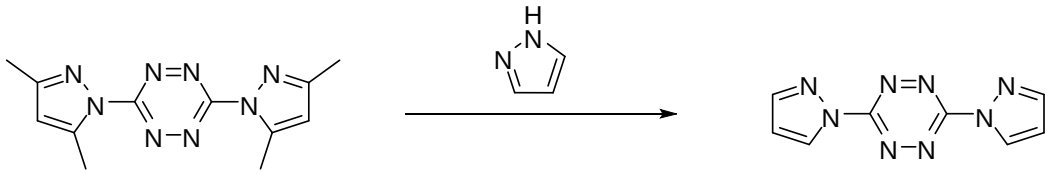

L16

Scheme 2.3

The new molecules described above have been characterised by NMR spectroscopy, IR spectroscopy, Mass Spectrometry, UV-Visible Spectrophotometry, melting point, microanalysis and X-ray crystallography. Crystal structures of the four new ligands were obtained, however these are not described in this thesis due to space restrictions.

2.5 Coordination Complexes II

Complex 2.12 – **L13** + silver triflate

Complex **2.12** was obtained after vapour diffusion of diethyl ether into the reaction mixture of **L13** and silver triflate in acetonitrile. The complex analysed with a 1:1 metal-ligand stoichiometry.

Using the method described previously, solution studies for complex **2.12** were carried out. Unfortunately due to the solubility of the ligand and the complex, CIS could not be completed. However a ^{1}H-NMR of the complex is shown in figure 2.31, which indicates that a symmetrical complex is formed due to the pyrazine rings on the ligand being equivalent. ESI-MS results show $[Ag_2(\mathbf{L7})_2(OTf)]^+$, $[Ag(\mathbf{L13})_2]^+$ and $[Ag(\mathbf{L13})]^+/[Ag_2(\mathbf{L13})_2]^{2+}$, showing possible complexes and fragmented components.

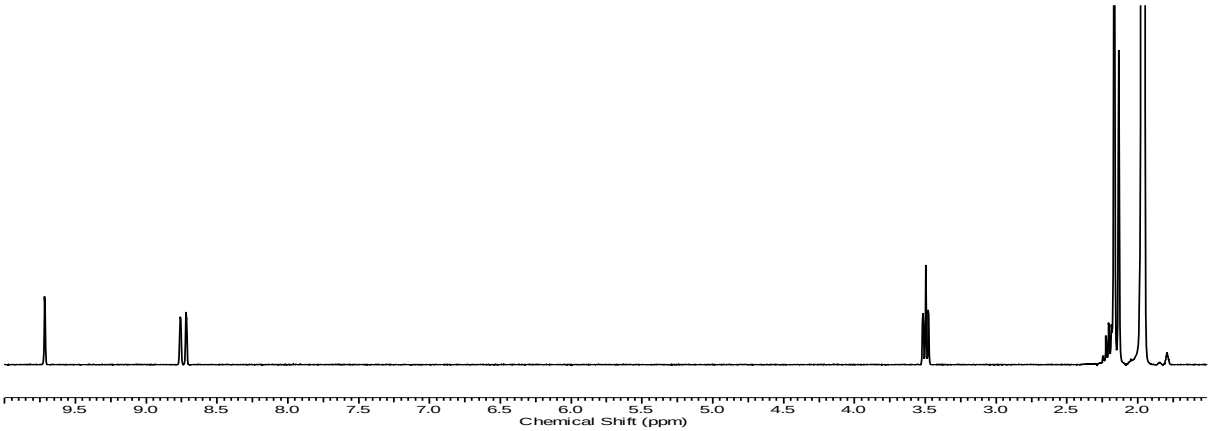

*Figure 2.31: ^{1}H-NMR of complex **2.12** in CD_3CN.*

Complex **2.12** crystallises in the triclinic space group P-1, with the asymmetric unit consisting of one molecule of **L13**, one metal and one coordinated triflate anion. The complex is a Ag_2(**L13**)$_2$ dimer, as shown in figure 2.32. An inversion centre relates the two halves of the complex, with each symmetry related ligand chelating two metal atoms, with bite angles of 67.3(7)° and 69.9(7)°.

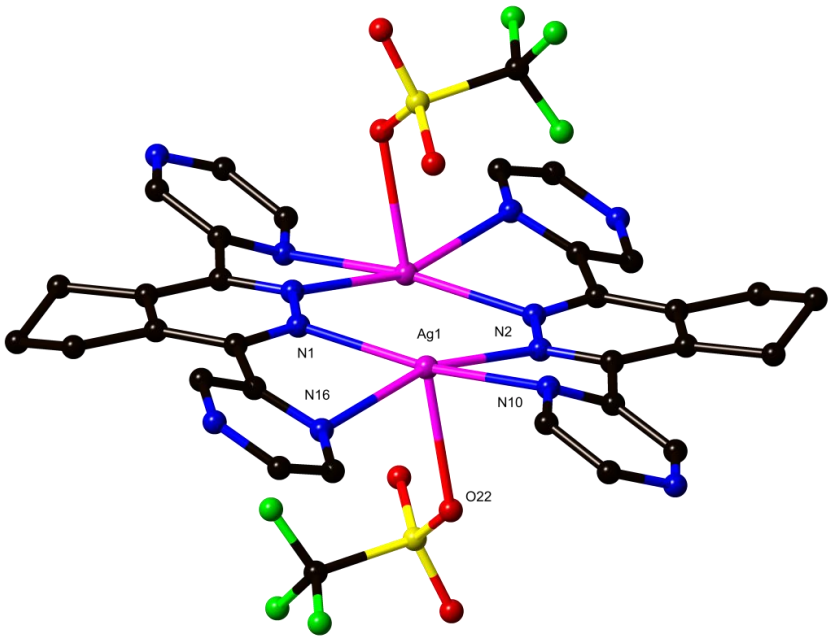

*Figure 2.32: Dimer of complex **2.12**. Selected bond lengths (Å):* Ag1-N1 2.38(2), Ag1-N2 2.28(2), Ag1-N10 2.58(2), Ag1-N16 2.39(2), Ag1-O22 2.557(19) *and angles(°):* N2-Ag1-N10 67.3(7), N1-Ag1-N16 69.9(7).

The silver atoms are in a distorted square pyramidal geometry, coordinated to four nitrogen atoms (bond lengths ranging from 2.28(2) Å - 2.58(2) Å) in the based plane and the apical site occupied by the triflate anion with a longer bond length of 2.557(19) Å. The pyrazine rings are twisted much less (26.4(8)° and 30.6(9)°) than previously observed for the complexes within this chapter. The twisting however is not due to the difference in pendant groups rather the steric clash of this group with the fused CH_2- of the alkyl ring with distance measuring C5-to-C12 3.13(3) Å and C7-to-C18 3.16(4) Å.

The change to the pyrazine-ring as the pendant group was synthesised to form coordination polymers or larger structures that contain bridging components. Unfortunately this complex did not form in such a way, instead giving a side-by-side Ag_2(**L13**)$_2$ complex. The solution studies showed a possible 1:1 stoichiometry which was confirmed in the solid state structure.

Complex 2.13 – **L14** + silver hexafluorophosphate

Crystals of complex **2.13** suitable for single X-ray crystallography were grown from vapour diffusion of diisopropyl ether into the reaction mixture of **L14** and silver hexafluorophosphate in acetonitrile. The complex was analysed with a 1:1 metal-ligand stoichiometry.

Solution studies of complex **2.13** were completed as previously described. The NMR results of the complex and the ^{1}H-NMR titration showed no CIS indicating no coordination of metal to the ligand. The ESI-MS showed two fragmented components; $[Ag(\mathbf{L14})_2]^+$ and $[Ag(\mathbf{L14})]^+/[Ag_2(\mathbf{L14})_2]^{2+}$.

Complex **2.13** crystallises in the triclinic space group, P-1. The asymmetric unit consists of one silver metal, one molecule of **L14**, one coordinated acetonitrile solvate and two non-coordinated components; one hexafluorophosphate anion, half an acetonitrile and half of a water molecule. Selected atomic labelling is shown in figure 2.33. The silver metals are in a distorted tetrahedral geometry coordinated to four nitrogen atoms, with angles around the silver metals ranging from 94.4(5)° - 130.6(4)°. This is one of the less distorted coordinate geometries of the silver complexes. The bond lengths from the silver metal to the nitrogen atoms range from 2.263(12) Å – 2.403(14) Å with the largest bond length associated with the coordinated acetonitrile.

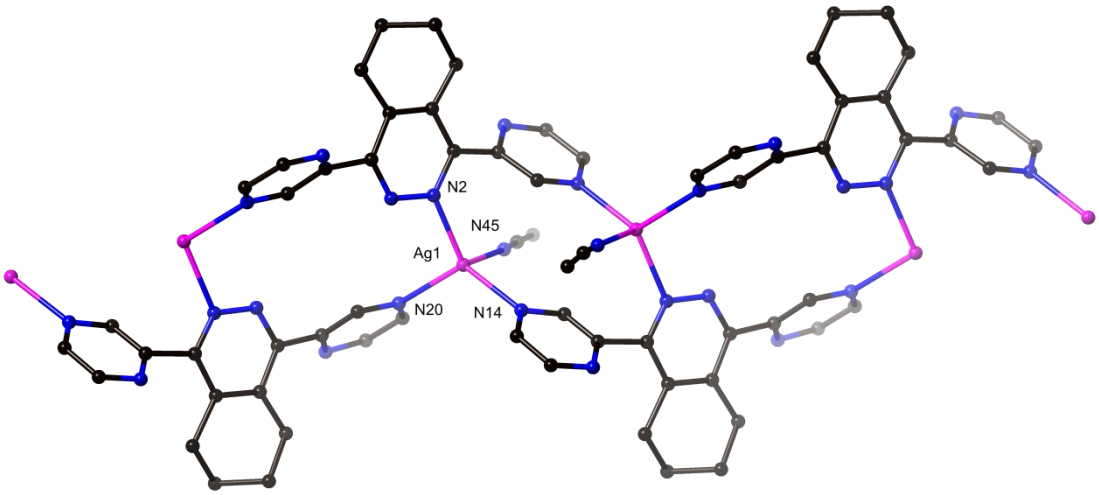

*Figure 2.33: Section of the complex **2.13** polymer showing atomic labelling. Selected bond lengths (Å)* Ag1-N2 2.292(4), Ag1-N14 2.268(4), Ag1-N20 2.335(4), Ag1-N45 2.393(5), A*and angles(°):* N2-Ag1-N45 106.79(17), N2-Ag1-N20 104.81(16), N14-Ag1-N2 130.11(15), N14-Ag1-N20 117.23(15), N14-Ag1-N45 95.45(17), N20-Ag1-N45 95.10(16).

The complex is a one-dimensional polymer as shown in figure 2.34, which propagates diagonally on the *ab* face. The pyridazine ring and fused cyclohexene ring overlap between the layered

polymeric structures however no significant interactions are observed. The non-coordinated solvates and anions are located in space between the polymeric chains with no significant interactions observed.

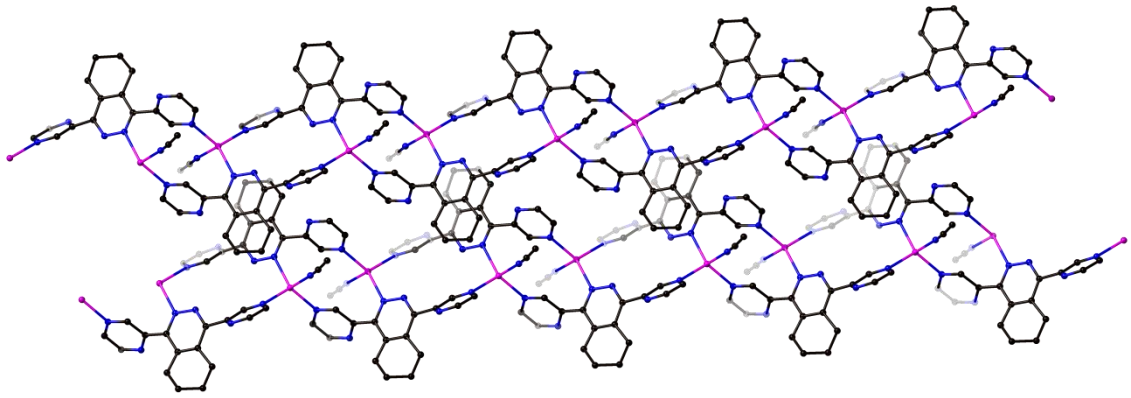

*Figure 2.34: Polymer of complex **2.13** showing the packing between two polymeric strands.*

2.6 Summary

The metallosupramolecular chemistry of Ag(I) has been investigated with a number of different molecules, **L2** - **L10**, **L13** and **L14** with a range of different architectures observed. The majority were discrete complexes with two being polymeric (**C2.5** and **C2.13**) out of a total of ten.

The complexes with the pyridyl pendant group showed increases in twisting of these groups with respect to the pyridazine ring as the fused ring size increased from cyclopentene (**2.4**) to cyclohexene (C**2.5**) and to cycloheptene (C**2.6**). However, the acenapthylene fused ring (**2.7**) has two different twists observed for the pyridazine rings, a smaller twist similar to that in the cyclopentene fused ligands (**L2**) allowing chelation to occur, and the other tilted at an angle similar to the cyclohexene fused ligand (**L3**) with no chelation observed. The results obtained for dimethylpyrazole as the pendant group show no chelation due to the steric clash of both the more sterically demanding methyl substituents and the fused components. The pyrazinyl pendant group complexes show a discrete structure for **L13** and a polymeric structure for **L14**. The extra donor atoms on **L13** are not involved in coordination resulting in a side-by-side complex as seen for **C2.2** and **C2.3** (table 2.12).[60]

Complex **2.5** is a coordination polymer, which contains subunits where the ligands are tetra-bridging ligands, refer to table 2.12. This type of connectivity is observed in half of the complexes

described in this chapter, **C2.5**, **C2.6**, **C2.8**, **C2.9**, and **C2.10**. This structural observation holds the silver atoms in close proximity for very weak Ag···Ag interactions (2.9868(3) Å – 3.2114(3) Å).

Interestingly, the reaction between **L2** and silver tetrafluoroborate in acetonitrile formed a Ag(**L2**)$_2$ complex where the ligands are coordinated in the *trans* conformation, compared to the grid like structure observed previously,[60] when the same reaction takes place in a solvent mixture. However, the reaction of the silver hexafluorophosphate and silver perchlorate with **L2** using the two different methods give the same supramolecular architecture (side-by-side complex). It was concluded that the outcome of a self-assembly between **L2** and different Ag(I) metal salts depended on two factors: (i) the counter ions of the metal salts and (ii) the solvent used, CH_3CN vs CH_2Cl_2:CH_3CN (9:1).

In seven of the structures, coordinating solvates and anions are observed, some showing bridging and bifurcating.

There is no evidence that the NMR solution studies have a strong consistent correlation with the solid state structures. However, with the 2-pyridyl series, the solution studies show a 1:1 metal-to-ligand stoichiometry that is observed in the solid state structures only when the fused ring is smaller, cyclopentene. The solution studies for the 1-(3,5-dimethylpyrazolyl) did not result in any structure determination, due to the lack of proton signals on the ligands.

Unfortunately no grid-like structures were obtained crystallographically as previously,[60,95,98] likely due to the introduction to the sterically hindering substituents. This change in architecture shows the effect of twisting of the heterocycles on the overall structural composition of complexes in this chapter. The solid state results are summarised in table 2.12. It can be concluded that there is some similarities between the solution studies and the solid state results; however, determining the structure from the solution studies has proven difficult.

*Table 2.12: Summary of the ligands complexes with silver and the metal salts required for complexation. (NB): Silver salts attempted $AgBF_4$, $AgPF_6$, $AgClO_4$, and AgOTf for each ligand. *Tetra-bridging*

C.	Ligand structure	Ag-salt	Structure	Coordi-nated anions	Cartoon Representation
2.1	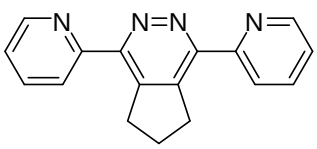 **L2**	$AgBF_4$	[2 x 2] Grid $[Ag_4(\mathbf{L2})_4]$	-	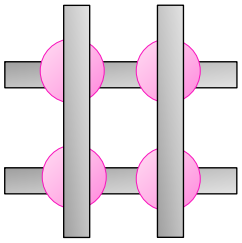
2.2		$AgPF_6$	Side-by-side $[Ag_2(\mathbf{L2})_2]$	-	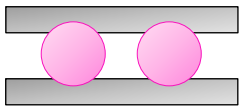
2.3		$AgClO_4$	Side-by-side $[Ag_2(\mathbf{L2})_2]$	-	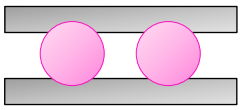
2.4		$AgBF_4$	*Trans* complex $[Ag(\mathbf{L2})_2]$	-	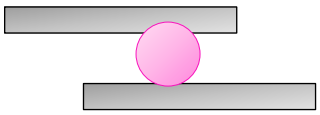
2.5	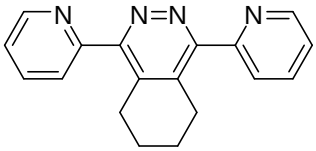 **L3**	AgOTf	Polymer containing $[Ag_4(\mathbf{L3})_2]$ subunits.	6 x OTf^-	Polymer
2.6	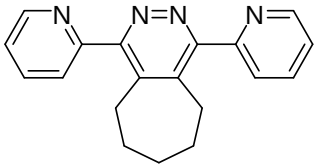 **L4**	$AgPF_6$	T-B* $[Ag_4(\mathbf{L4})_2]$	6 x MeCN	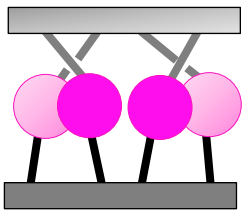

2.7	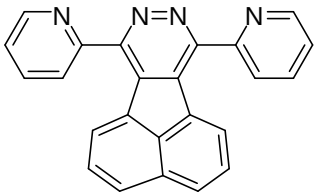 **L5**	AgOTf	$[Ag_4(\mathbf{L5})_4]$	-	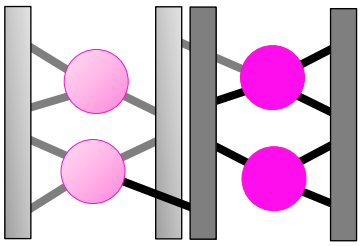
2.8	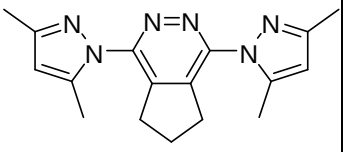 **L7**	AgOTf	T-B* $[Ag_4(\mathbf{L7})_2]$	2 x OTf^- 4 x MeCN	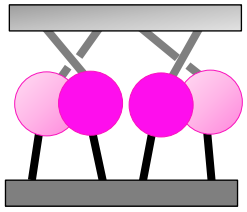
2.9	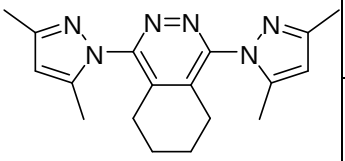 **L8**	AgOTf / $AgClO_4$	T-B* $[Ag_4(\mathbf{L8})_2]$	2 x OTf^- 4 x MeCN	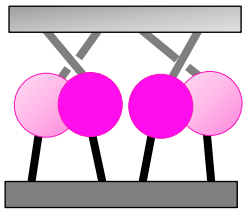
2.10	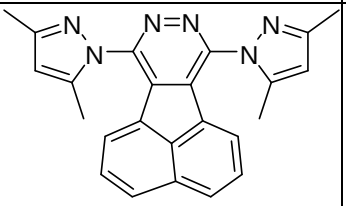 **L9**	AgOTf	T-B* $[Ag_4(\mathbf{L9})_2]$	2 x MeCN 4 x H_2O	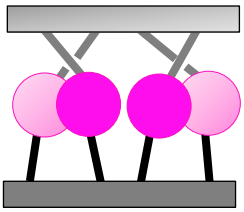
2.11	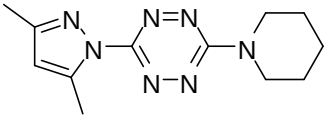 **L10**	$AgPF_6$	$[Ag(\mathbf{L10})_2]$	-	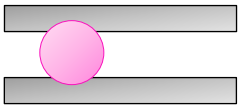
2.12	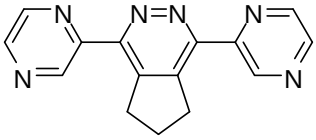 **L13**	AgOTf	Side-by-side $[Ag_2(\mathbf{L13})_2]$	2 x OTf^-	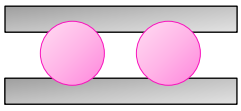
2.13	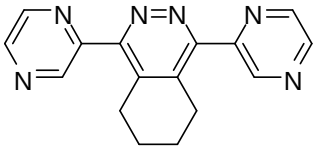 **L14**	$AgPF_6$	Polymer	1 x MeCN	Polymer

CHAPTER THREE

Copper Complexes

3.1 Introduction

The coordination chemistry of copper is dominated by its oxidation state. Cu(I) ions often prefer to adopt four coordinate geometries, commonly tetrahedral. The result of this preference is due to the d^{10} electronic configuration in which it gives the ion a spherical coordination sphere.[21] The tetrahedral geometry makes the Cu(I) ion suitable for the formation of [n x n] metallogrids with polytopic bidentate ligands. Cu(II), however is a d^9 transition metal, which has a preference for five and six coordinate geometries, square based pyramidal or trigonal bipyramidal and octahedral, respectively. Cu(II) ions have a strong tendency to have distorted geometries due to the Jahn-Teller effect.[4,21] Copper(I) halides, particularly iodide, allow the formation of polymeric complex structures with interesting inorganic coordination complexes. The anion greatly effects the overall geometry as anions such as iodide can bridge the copper atoms. Copper iodide complexes give a range of different structures, some of which are shown in figure 3.1.

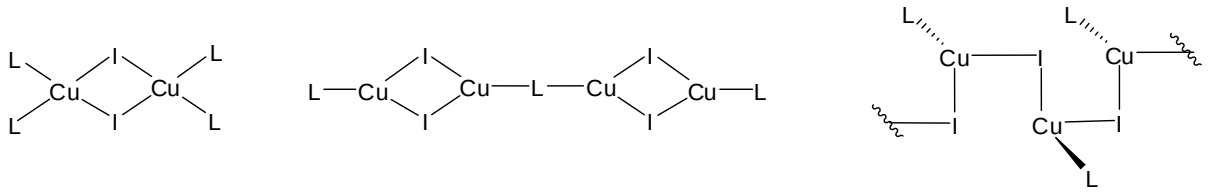

(a) (b) (c)

Figure 3.1: Selected topologies formed by copper(I) iodide involving bridging iodine atoms; (a) dinuclear; (b) polymer of dinuclear units; (c) zig zag polymeric chain.

Cu(I) and polytopic bidentate ligands are well suited to form supramolecular [n x n] grids,[30,99] due to the Cu(I) preferred tetrahedral geometry. As previously mentioned in the introduction and displayed in figure 1.4, the first [2 x 2] grid-like array was obtained with Cu(I).[30] Another grid structure published in the literature with a molecule explored in this study is the combination of Cu(I) salts with **L6**.[79] Manzano *et al.* aimed to produce a grid-like array with non-parallel facing ligands (figure 3.2b), but having open interplanar angles, in order to create host cavities with substituted pyrimidine rings. However, **L6** was also obtained to lead to parallel binding vectors with the result of a similar metallogrid as seen by Youinou *et al.* Manzano *et al.* stated that it was the first five-membered heterocyclic pendant group to pyridazine that had been published in the literature to date.[79] The grid-like array with **L6** was obtained with $Cu(MeCN)_4BF_4$ and $Cu(MeCN)_4PF_6$ (figure 3.2a).

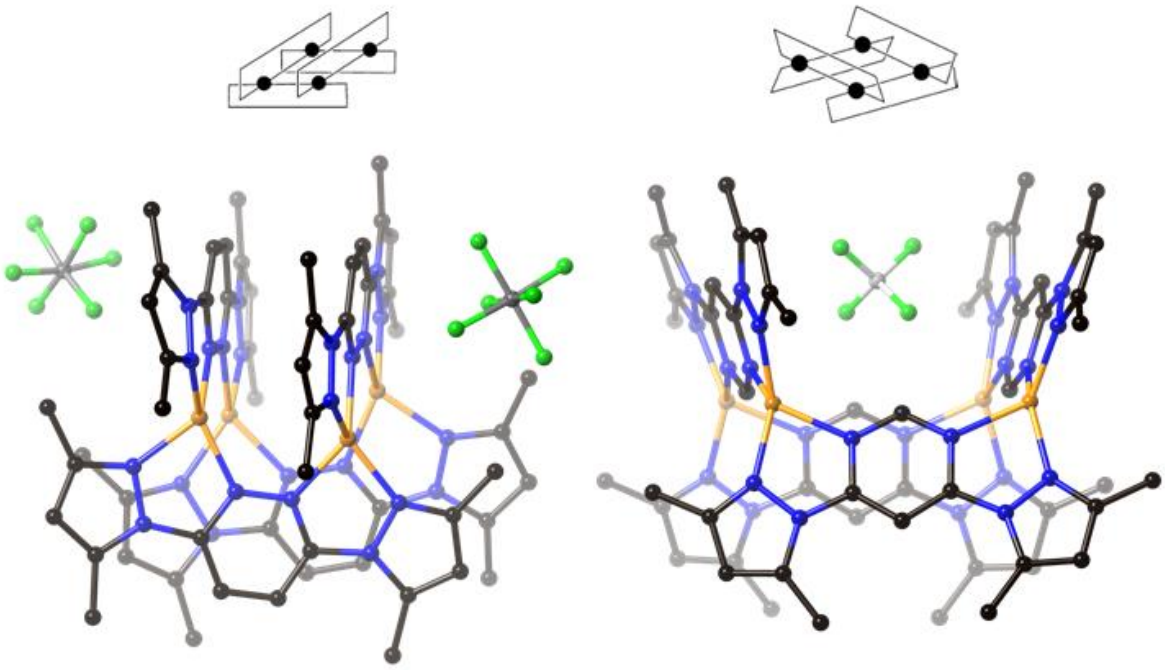

*Figure 3.2: Grid like arrays formed by Manzano et al.; (a) Parellel binding vectors with 3 and 6 pendant group substitution on pyridazine (**L6**) with Cu(I)PF_6; (b) non-parallel facing ligands with 4 and 6 pendant group substitution on pyrimidine with Cu(I)BF_4.*[79]

To the best of my knowledge there has not been any work in the literature on the molecules synthesised in this study with the copper(I) iodide metal salt. However, there has been publications on pyridazine substituted coordination polymers,[100] fused pyridazines[101] and substituted tetrazines with this metal salt forming metal organic frameworks.[102,103] In all cases, one dimensional and two dimensional complexes have formed with interesting and varied geometries.

A coordination polymer with a linear chain structural motif, reported by Song *et al.* constructed from copper(I) iodide forms when a pyridazine substituted (3,6-bis(2-pyridylthio)pyridazine) molecule is reacted with CuI. The CuI framework is described as having "butterfly shape units" (figure 3.3a) and forms due to the iodine bridge and the chelating nature of the ligand. A fused pyridazine ligand (1,2,3,6,7,8-hexahydro-cinnolino[5,4,3-*cde*]cinnoline) provides multiple binding sites for coordination into the formation of metallosupramolecular assemblies.[104] Domasevitch *et al.* form a spectacular large two-dimensional tube assembly, where the structure is built up from $Cu_{12}I_{12}$ rings stacked on top of one another interlinked by ligands (figure 3.3b).

A smaller ligand, similar to this study with 4-pyridyl pendant groups replacing the 2-pyridyl substituted in positions on a tetrazine ring was reacted with CuI forming a one-dimensional polymeric structure.[105] The ligands are linked by $Cu_2I_2(PPh_3)_2$ units (figure 3.3c). In all three examples the copper atoms have a tetrahedral geometry.

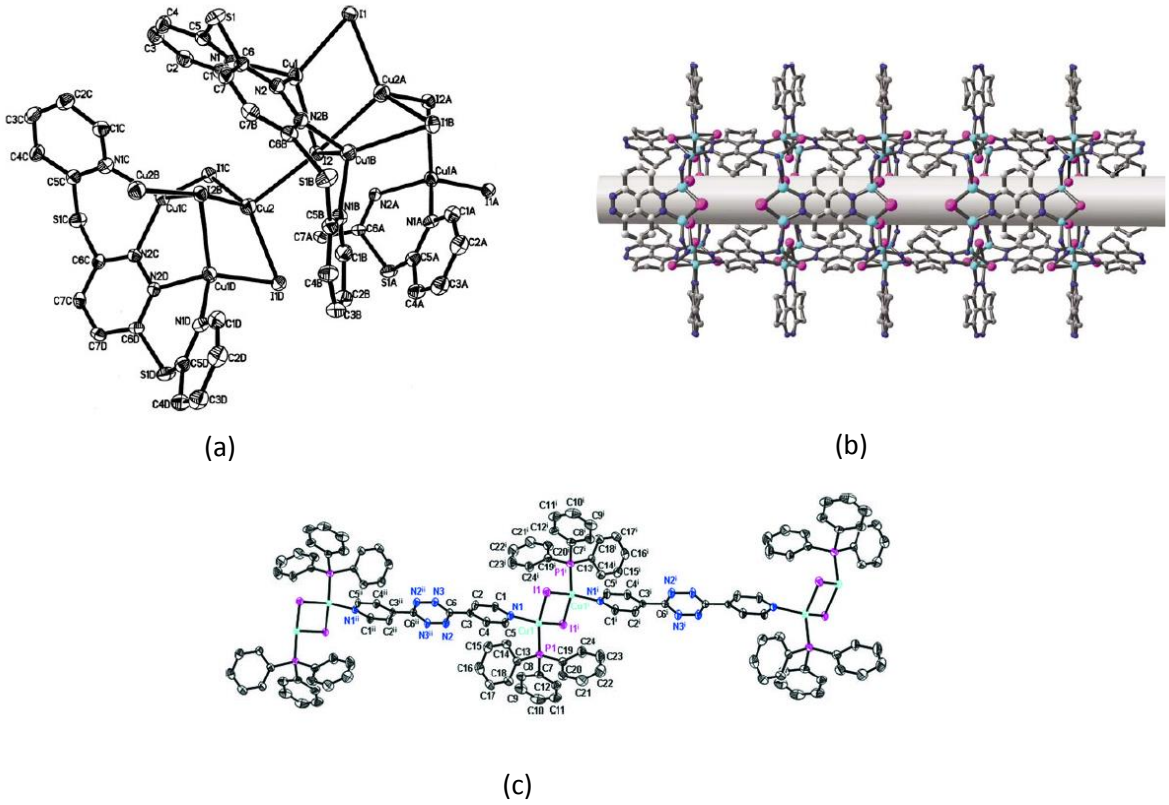

Figure 3.3: Structures of reported literature pyridazine and tetrazine CuI polymers. (a) One dimensional polymer with butterfly shape CuI bridging unit;[100] (b) Two-dimensional tube assembly with $Cu_{12}I_{12}$ framework;[104] (c) One-dimensional polymer with Cu_2I_2 bridging between tetrazine substituted molecules.[105]

Although CuI forms polymers, and while grid-like arrays are the desired structure in this study, Cu-I-Cu bridging units could separate the ligands to allow the formation of larger arrays, (figure 3.4) forming greater cavities for anions or solvates to be situated in and around.

The ligands in this study have been complexed with both tetrakis(acetonitrile)copper(I) tetrafluoroborate and copper(I) iodide.

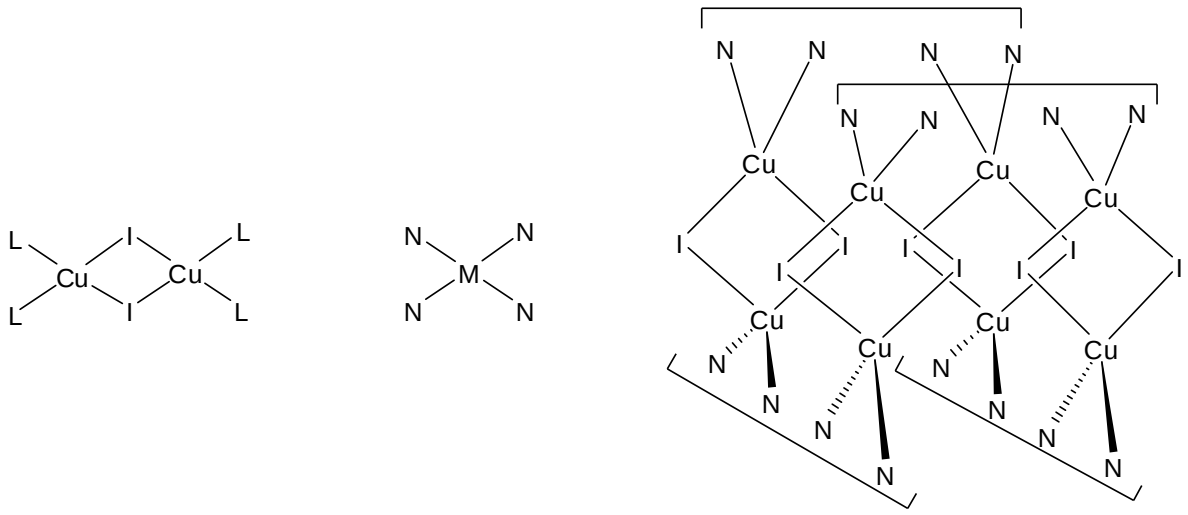

(a) (b) (c)

Figure 3.4: (a) Structure of the possible dinuclear CuI framework; (b) Structure showing how CuI has a similar bonding to the four cooradinte geometry (tetrahedral or square planar; (c) Structure showing a possible grid like structure formed with a CuI framework.

3.2 Coordination complexes

Complex 3.1 – **L2** + tetrakis(acetonitrile)copper(I) tetrafluoroborate

Complex **3.1** was obtained after diffusion of diethyl ether into the reaction mixture of **L2** and $Cu(CH_3CN)_4BF_4$ in acetonitrile, providing dark brown crystals suitable for single X-ray diffraction. These crystals analysed with a 1:1 stoichiometry.

Solution studies by NMR Spectroscopy, UV-Visible spectroscopy and electrospray ionisation-mass spectrometry were carried out for complex **3.1**. Complex **3.1** was dissolved in d_3-acetronitrile and a ^{1}H-NMR spectrum collected, analysed and compared with the ligand spectrum. The coordination induced shifts are summarised in table 3.1. The majority of the protons experience only a relatively minor downfield shift on complexation; however, two of the pyridine ring protons, H3 and H6 show a significant upfield shift of 0.55 ppm and 0.75 ppm CIS. Unfortunately, the H11 signal and the acetonitrile solvent peak is situated in the same region in the ligand spectrum, however this proton experiences a splitting into two multiplets and a downfield CIS of 0.47 ppm and 0.34 ppm on complexation. The effect of these H3 and H6 resonances shifting upfield is due to the relative switching of positions with respect to the free ligand and the delocalisation of the electrons towards the metal. The splitting of the H11 protons into two multiplets could be possibly due to hydrogen bonding interactions with nearby anions or solvates. Comparison of these shifts to the results

obtained in the silver species show similar shifts with the exception of H6, a greater shift being apparent. This observation could be due to the structure or the change in metal ion.

	H3	H4	H5	H6	H10	H11[c]
L2	8.51	7.98	7.47	8.76	3.49	2.14[c]
C3.1	7.96	7.95	7.30	8.01	3.46	2.61/2.48
CIS[b]	-0.55	-0.03	-0.17	-0.75	-0.03	+0.47/+0.34

[a] For deuterated acetonitrile solutions. [b] CIS= $^{\delta}$complex-$^{\delta}$ligand. [c] Deuterated acetonitrile overlap.

*Table 3.1: ^{1}H-NMR Chemical shifts[a] and Coordination Induced Shifts[b] of complex **3.1***

A ^{1}H-NMR titration was carried out for complex **3.1** in d_3-acetonitrile, shown in figure 3.5. This was done by adding 20 µL 0.05 mol L^{-1} aliquots of $Cu(MeCN)_4BF_4$ solution to a 500 µL of 0.01 mol L^{-1} solution of molecule **L2** until the metal to ligand ratio was 1:1. An extra equivalent was added to ensure the spectrum did not change further. The addition of 0.2 eq. resulted in a broadening of the peaks and, comparing it to the ligand, there is a broadening of the proton peaks, with only one peak (integral of two) observed in the aromatic region. No change is observed when 0.4 eq. is added. However, with 0.6 eq. of metal addition, there is a broadening of all the peaks which indicates there is more than one species formed in the solution. When the ratio is 1:1, a symmetrical complex has formed which upon addition of another equivalence of metal there is no change to the spectrum. The stoichiometric result from the titration is 1:1 metal-ligand, which is consistent with both the grid structure and the side-by-side complex.

UV-Visible spectroscopy of complex **3.1**, clearly shows a absorption maximum at 429 nm upon complexation of copper(I) ions. An observation of this has been described in the literature with the formation of gird-like structure with **L1**[30] and disubstituted pyridazine derivatives[99] with copper(I) ions. This absorbance can be assigned to the MLCT transition π-π*, this is very weak absorption compared to the ligand absorption at λ_{max} 288 nm.

ESI-MS shows many species and possible fragmentation products, $[Cu(\mathbf{L2})_2]^{+}$, $[Cu_2(\mathbf{L2})_3]^{2+}$, $[Cu_2(\mathbf{L2})_2]^{2+}$, $[Cu(\mathbf{L2})_2]^{2+}$. In the previous silver chapter, the ESI-MS showed mostly fragmented species which gives an indication that these metallosupramolecular structures are held together by weak interactions.

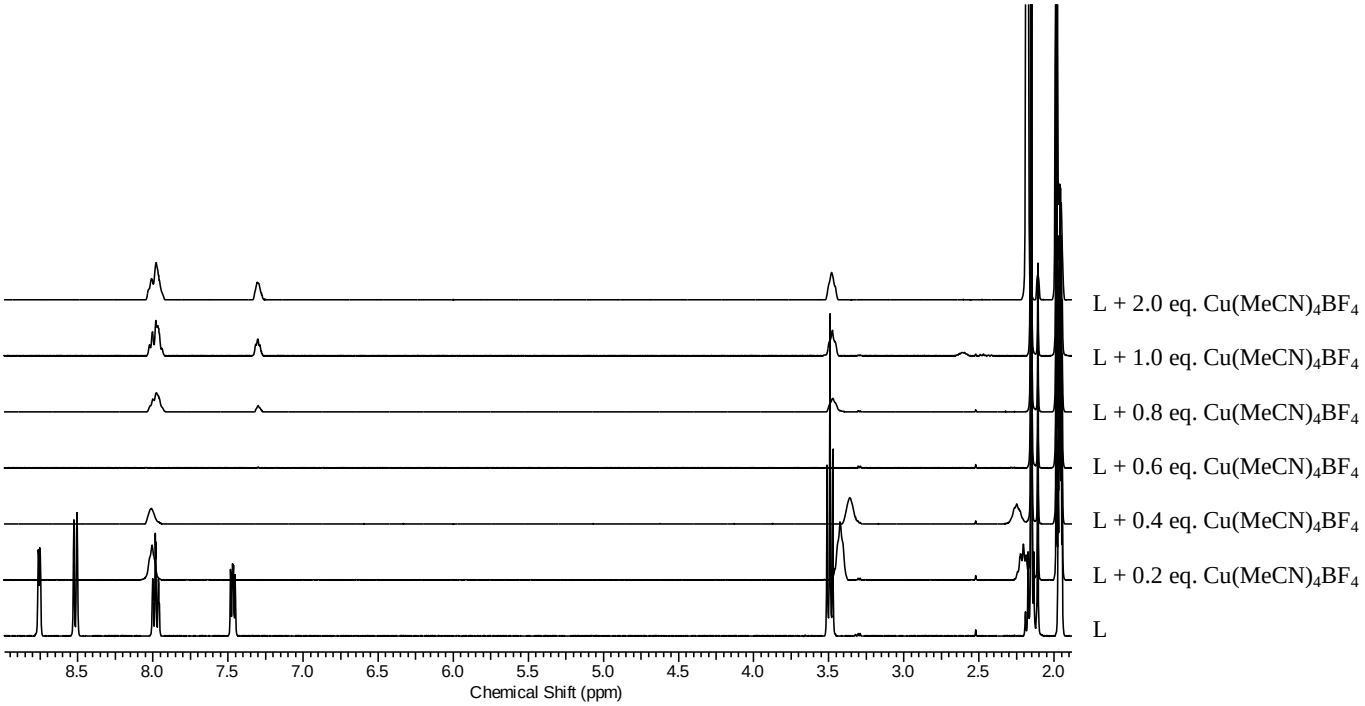

*Figure 3.5: ^{1}H-NMR titration to form complex **3.1**.*

This complex crystallised in the triclinic space group P1, despite the achiral starting materials used, which is unusual. The asymmetric unit is comprised of four [2 x 2] grid structures, each made up of four copper atoms and four molecules of **L2**. The asymmetric unit also contains ten non-coordinated acetonitrile solvate molecules and sixteen non-coordinated tetrafluoroborate anions.

The coordination geometry of the copper(I) metals is distorted tetrahedral bound to four nitrogen atoms (figure 3.6). The distortion of the metal centres arises from the enforced binding angle placed on the metal centre by the bidentate binding domains the copper to nitrogen bond lengths range from 1.971(8) Å – 2.067(8) Å with bite angles ranging from 79.2(4)° - 81.6(3)°. The pyridine rings are twisted out of the plane of the pyridazine core, ranging from 2.1(4)° - 29.2(8)°. Three of these pendant heterocycles are disordered over two sites which contribute to the larger twisting observed 11.7(5)° - 29.2(8)° for these rings. The fused cyclopentene rings have an envelope orientation, which is the most stable conformation and commonly observed in this work.

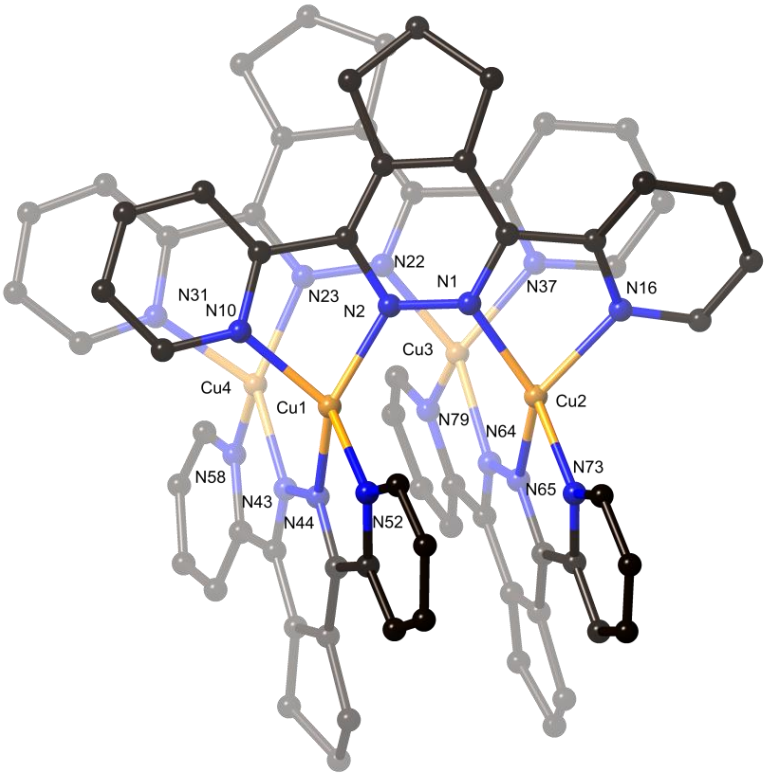

Figure 3.6: Perspective view of one of the grid structure with selected labelling shown corresponding to each of the grid structures. Solvates, anions and hydrogen atoms have been omitted for clarity.

Intramolecular offset π-π stacking interactions at distances (centroid to centroid) ranging from 3.483(10) Å – 3.890(6) Å, between the **L2** ligand rings of the grid are present as seen in figure 3.6 with the longer distances exhibiting weak interactions.

The solvate molecules and tetrafluoroborate anions are situated in space around the four grid structures, with an anion (BF_4) having a relatively weak hydrogen bonding interaction to an acetonitrile, C186-H18E···F104 2.87(3) Å (D-A), 131.1(15)°. Several anions are situated in close proximity to the grid structures with four of them involved in weak anion-π interactions. The F···pyridazine ring interactions are summarized in table 3.2.

Two of the acetonitrile solvate nitrogen atoms are facing towards the centre of two pyridazine rings in one of the grid structures, with distances of nitrogen-to-centroid of 3.061(14) Å (N184) and 2.148(15) Å (N190).

	F···plane (Å)	F···centroid (Å)	Strength of interaction
F134···pyridazine ring	3.222(15)	3.269(17)	Weak
F117···pyridazine ring	3.421(11)	3.484(11)	Very weak
F118···pyridazine ring	3.074(13)	3.531(11)	Very weak
F119···pyridazine ring	3.104(13)	3.502(11)	Very weak
F122···pyridazine ring	2.861(12)	3.048(11)	Moderate
F107···pyridazine ring	2.927(11)	3.262(10)	Weak
F109···pyridazine ring	3.387(13)	3.459(13)	Very weak

*Table 3.2: Summary of the F···pyridazine ring interactions in complex **3.1**.*

Similar to the silver series, we decided to move to sterically hindering substituents on the pendant groups, **L6**, **L7** and **L9.** These three molecules have been complexed with the two metal salts resulting in three crystal structures described below.

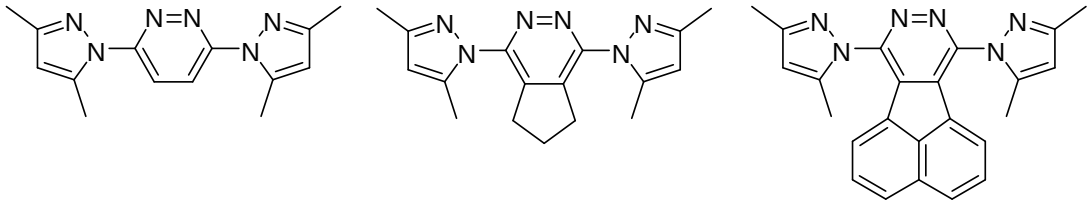

L6 **L7** **L9**

Figure 3.7: Structures of L6, L7 and L9 complexed with copper(I).

Complex 3.2 – **L6** + copper(I) iodide

Complex **3.2** was obtained by vapour diffusion of diisopropyl ether into a 1:1 metal-ligand reaction mixture of **L6** and copper iodide in acetonitrile. The crystals were analysed with a 2:1 metal to ligand stoichiometry. The crystals formed were suitable for single crystal X-ray structure determination.

Solution studies for complex **3.2** were carried out and showed only the uncoordinated ligand in both NMR and UV-Visible experiments. ESI-MS showed two Cu(I) complexes, $[Cu(\mathbf{L6})_2]^+$, $[Cu(\mathbf{L6})]^+$/$[Cu_2(\mathbf{L6})_2]^{2+}$ and one Cu(II) complexes $[Cu(\mathbf{L6})_2]^{2+}$.

The copper iodide complex, **3.2**, was the first to be obtained from this metal salt. Unfortunately, the data collected for this complex was twinned and the lattices could not be resolved, and, due to this,

the disorder of the Cu-I framework could not be successfully modelled. However, despite these problems, a description of the structure is still possible, Cu_2I_2**L6**.

Complex **3.2** crystallises in the monoclinic space group I2/m. The asymmetric unit consists of three copper(I) iodides and half of one ligand. The complex has a one dimensional polymeric structure, with the ligand molecules bridged by Cu_6I_6 units.

Two of the copper atoms of the structure are four-coordinate (Cu1 and Cu2) and the third copper (Cu3) is three coordinate. Cu1 is chelated by two nitrogen atoms and two iodine atoms. The Cu2 and Cu3 atoms form a Cu-I framework that bridges the subunit structures made up of M_4L_2, as shown in figure 3.8. Cu2 is coordinated to four iodine atoms and Cu3 is coordinated to three iodine atoms. Both Cu2 and Cu3 are located on a mirror plane and the polymer extends along the *c* axis as shown in figure 3.9.

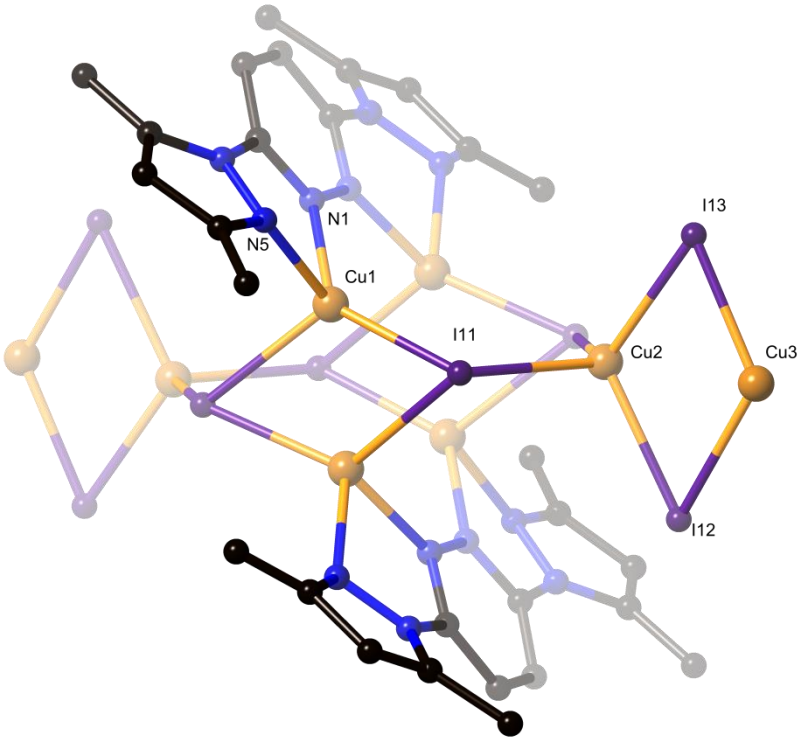

Figure 3.8: Perspective view and atom labelling of 3.2, with molecular labelling shown. Hydrogen atoms and interactions have been removed for clarity. Selected bond lengths (Å) Cu1-N1 2.063(18) Å Cu1-N5 2.11(2) Å *and angles (°):* N1-Cu1-N5 78.7(9)°.

The complex resides on a twofold axis, with figure 3.8 showing the ligands are related by the molecules being coplanar. Each ligand is chelated to two metals that are bridged by a iodide atom between the opposite metal with the two copper atoms being in close proximity for a relatively

strong interaction of 2.591(13) Å. The dimethyl-pyrazole groups on the ligand are twisted 24.1(9)° out of the plane of the pyrazine ring.

Within the polymeric structure, there is a Cu_4I_4(**L6**)$_2$ subunit which are bridged by Cu_4I_4 units. This bridging motif has not been previously reported, however, similar bridging networks that are three dimensional have been reported.[106]

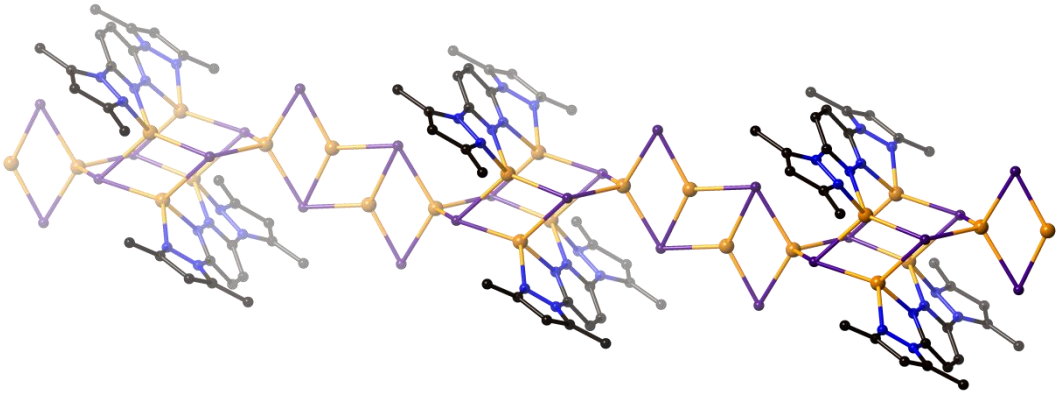

*Figure 3.9: View of the one dimensional polymeric structure down the b axis of complex **3.2**, showing the Cu-I framework between the Cu_4(**L6**)$_2$ structures.*

Complex 3.3 – **L7** + tetrakis(acetonitrile)copper(I) tetrafluoroborate

When a solution of **L7** in acetonitrile and a solution of $Cu(MeCN)_4BF_4$ in acetonitrile with a 1:1 metal-to-ligand stoichiometry were combined, a colourless solution was observed. After slow diffusion of diisopropyl ether over approximately a month, small blue crystals were obtained. These were submitted for single X-ray crystallography and a very interesting structure was observed, complex **3.3**, containing bridging acetate, the most likely source of this being the hydrolysis of acetonitrile (figure 3.10). Unfortunately, an elemental analysis was unable to be collected. In order to regrow **3.3**, copper(II) acetate was used as the metal salt, as well as mixing the two salts together, however no solid product formed. The infrared spectrum shows no acetamide intermediate which confirms the structural evidence of the acetate being coordinated.

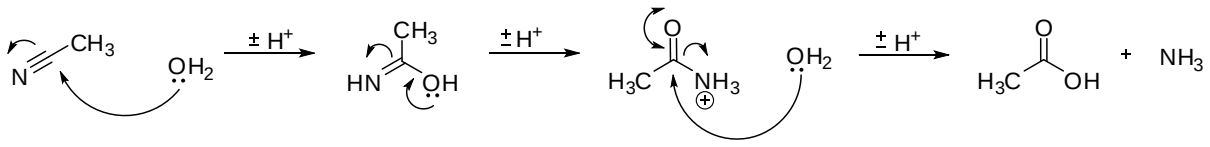

Figure 3.10: Reaction mechanism showing the slow hydrolysis of acetonitrile.

The complex crystallises in the triclinic space group P-1, with the asymmetric unit consisting of one **L7**, two and a half metal ions, two coordinated acetate molecules, one coordinated water, one bridging hydroxide molecule, two non-coordinated tetrafluoroborate and one non-coordinated acetonitrile. The small blue crystals of complex **3.3** resulted in the oxidation of copper(I) to copper(II). The structure is a Cu_5(**L7**)$_2$ with four bridging acetate molecules, two bridging hydroxides and two coordinated water molecules. The dimer can be viewed in figure 3.11.

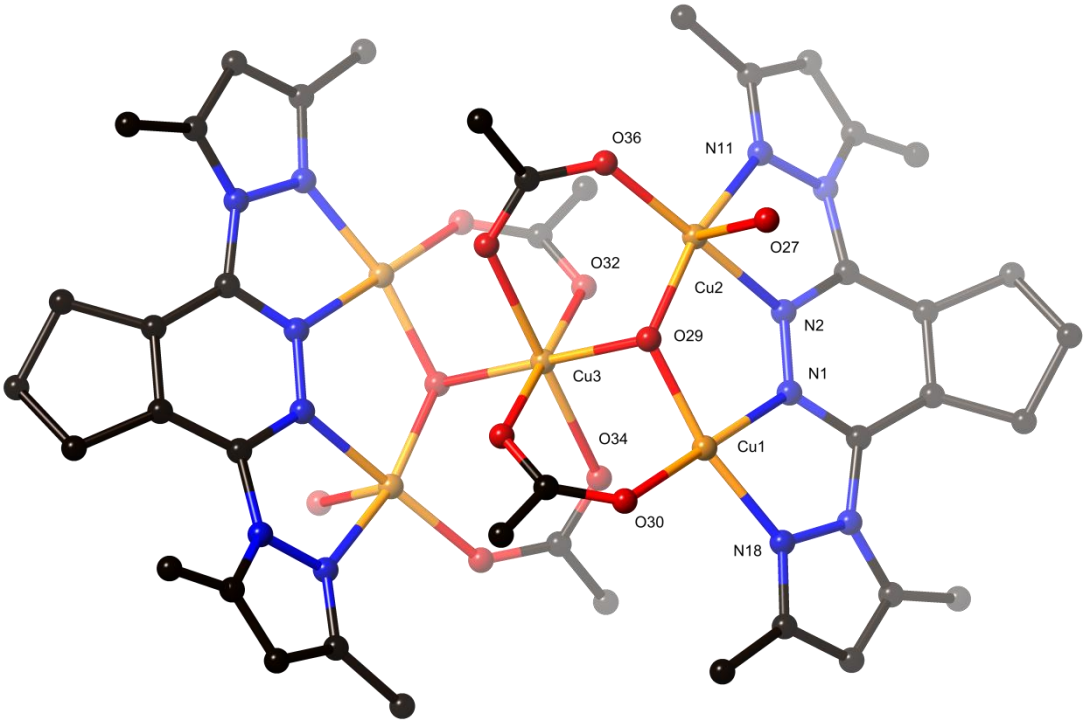

*Figure 3.11: Dimer structure of complex **3.3**, with molecular labelling shown. Hydrogen atoms, solvate anions have been omitted for clarity. Selected bond lengths (Å)* Cu1-N1 1.9971(17), Cu1-N18 1.962(2), Cu1-O29 1.9372(15), Cu1-O30 1.9372(15), Cu2-N2 2.0183(19), Cu2-N11 1.9880(19), Cu2-O27 2.3031(18), Cu2-O29 1.9417(13), Cu3-O28 2.38(4), Cu3-O29 1.9627(13), Cu3-O34 2.235(2) *and angles (°):*N1-Cu1-N18 79.36(8), N2-Cu2-N11 78.90(9).

There are three different geometries for the metals present. The first, Cu1, is in a square planar geometry coordinated to two nitrogen atoms and two oxygen atoms; one from an acetate and the other from the bridging hydroxide. Cu2 is square pyramidal, coordinated to two nitrogen atoms, to oxygen atoms, similar to Cu1, however, with the apical site being occupied by a water molecule. Lastly, Cu3 is located on a centre of inversion and has an octahedral geometry coordinated by six oxygen atoms, four of which are from the acetate molecules and the other two being hydroxides. The copper to nitrogen bond lengths to the nitrogen atoms ranging from 1.962(2) Å – 2.0183(19) Å and have bite angles of 79.36(8)° and 78.90(9)°. These angles contribute to the slight distortion of the square planar (Cu1) and square pyramidal geometries (Cu2), ~173° and ~170°, respectively.

The water molecule in the apical site of Cu2 is located perpendicular, ~92° to the square base. The octahedral angles of Cu3 is not distorted with angles of 180° and average angle of 90° for the coordinated atoms, as it occupies an inversion centre.

The pyridazine rings are parallel to each other, related by the inversion centre at Cu3. There is a slight twisting of the dimethyl-pyrazole groups of 21.37(9)° and 26.76(9)° which is due to the steric clash of the methyl groups with the cyclopentene backbone. The backbone has an envelope shape, as that has been observed previously in this work.

The two anions are situated in space and are both subject to some disorder. Two fluorine atoms are disordered over two sites in both anions with the largest occupancies being 66% and 51%. One anion is involved in two relatively strong hydrogen bonds to the coordinated water, O27-H27A···F42 2.877(4) Å (D-A), 147.87(16)° and O27-H27B···F39 2.891(2) Å (D-A), 143.33(14)°, respectively. The acetonitrile is located in close enough proximity to the bridging hydroxide and is involved in a strong hydrogen bonding interaction, O29-H29···N24 2.807(3) Å, 177.0(3)° (D-H···A).

Complex 3.4 – **L9** +copper(I) iodide

When copper iodide was reacted with **L9**, a dark brown solution formed. Vapour diffusion of diisopropyl ether resulted in small black crystals of complex **3.4** that were submitted for single X-ray diffraction studies. These crystals analysed with a 5:1 metal to ligand stoichiometry, which was the same stoichiometry which was obtained by crystallography, Cu_5I_5**L9**.

As previously described solution studies were completed for complex **3.4**, however the same results were obtained for NMR and UV-Visible as complex **3.2**.

Complex **3.4** crystallises in the monoclinic space group $P2_1/c$. The asymmetric unit contains one molecule of **L9**, five copper metals and five iodide atoms. The copper-iodide framework is constructed from Cu_5I_5 units. This framework is significantly disordered, with three copper-iodide components disordered over two sites.

The copper atoms are three or four coordinate, as shown in figure 3.12, with Cu1 and Cu3 disordered over two sites with both components having a tetrahedral geometry, bound by one nitrogen and three iodides (I1, I3, I5). Cu4 is also disordered over two parts, and a tetrahedral geometry coordinated to four iodide atoms (I1, I3, I4, I5), however, Cu4’ is three coordinate bound to three iodide (I3, I4, I5) with an interaction with an iodide atom (I2) in the fourth site (Cu4’···I2

2.851(3) Å). The other two copper atoms have not been modelled as disordered. Cu5 having the same geometry and connectivity as Cu1 and Cu3, and lastly Cu2 which is three coordinate, bound to one nitrogen and two iodide atoms with an additional site involved in a weak Cu2···I3' interaction of 3.151(7) Å.

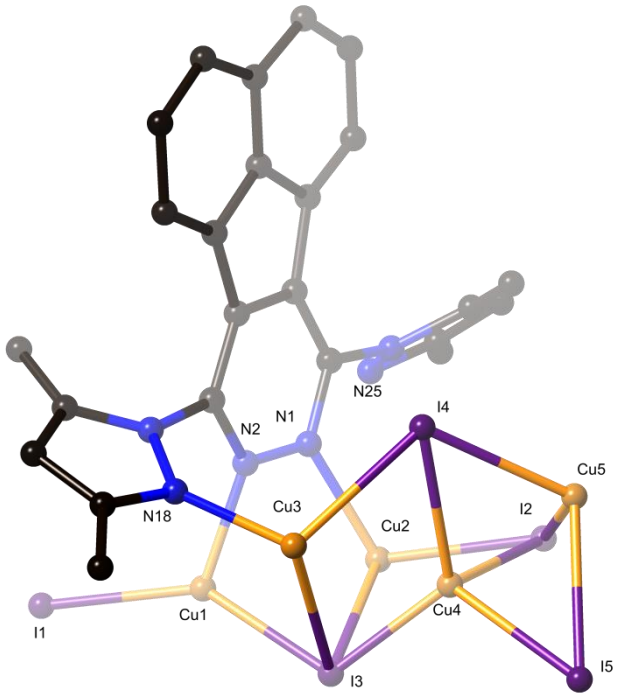

Figure 3.12: Perspective view with disordered CuI framework removed showing the selected atomic labelling for complex ***3.4****. Hydrogen atoms, disordered CuI units have been omitted for clarity. Selected bond lengths (Å):* Cu1-N2 2.019(10), Cu1'-N2 2.093(10), Cu2-N1 2.036(5), Cu3-N18 2.004(9), Cu3'-N18 2.017(9), Cu5-N25 2.003(5); *and twisting of the dimethylpyrazole pendant rings (°):* 58.47(19), 59.68(18).

The dimethyl-pyrazole groups are twisted in two different directions, 58.47(19)° and 59.68(18)°. This twisting is due to the sterically hindering methyl groups in conjunction with the fused acenaphthylene ring. The twisting of the pyridyl groups in two directions is a fundamental component for the construction of the polymer. The structure is a one-dimensional polymer, shown in figure 3.13, that extends along the *a* axis.

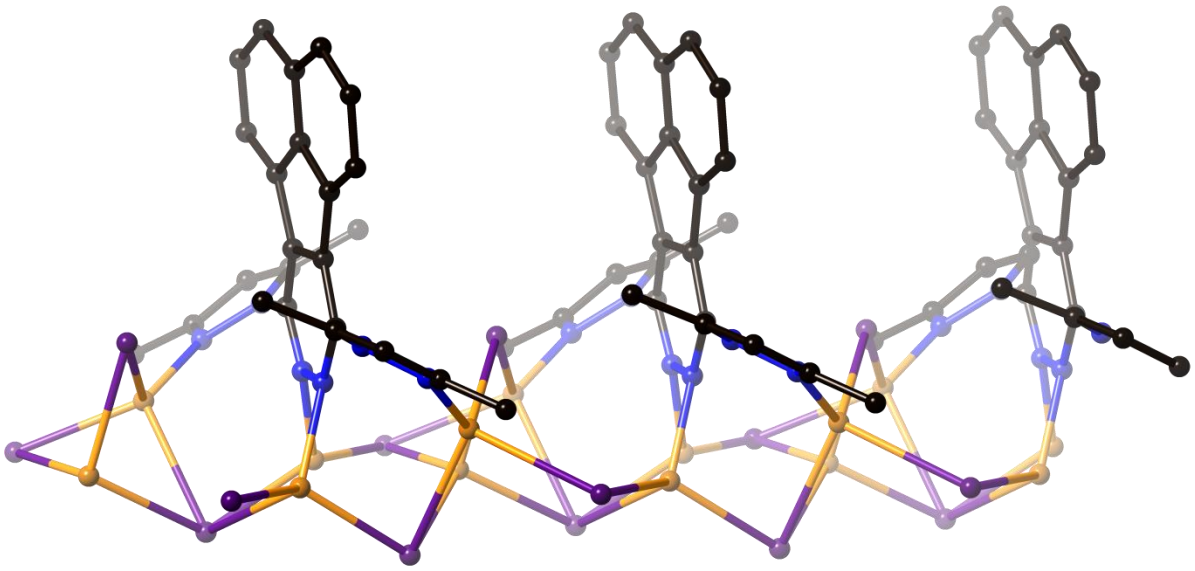

*Figure 3.13: Perspective view of the polymeric structure of complex **3.4**. Hydrogen atoms, disordered CuI units have been omitted for clarity.*

Complex 3.5– **L11** + tetrakis(acetonitrile)copper(I) tetrafluoroborate

Molecule **L11** was reacted with $Cu(MeCN)_4BF_4$ in acetonitrile which resulted in a red solution. After vapour diffusion of diethyl ether, red crystals suitable for single crystal X-ray diffraction studies were collected. Complex **3.5** analysed with a 2:1 metal to ligand stoichiometry.

Complex **3.5** crystallises in the monoclinic space group, $P2_1/c$, with the asymmetric unit consisting of one and half molecules of **L11**, one copper metal and one non-coordinated tetrafluoroborate anions. The structure is a two dimensional polymer which propagates along the *bc* plane.

The copper(I) metals are coordinated to six nitrogen atoms, two from three different ligands in a distorted octahedral geometry. This is an unusual geometry, as Cu(I) usual preferred geometry is tetrahedral.[21] The Cu-N bond lengths range from 1.955(2) Å – 2.443(2) Å. The distortion of the geometry is due to the three chelating sites, with bite angles of 70.16(8), 79.83(8)° and 79.11(8). The connectivity of the ligands is the meridional isomer shown in figure 3.4.

The core structure is a tetrazine which is different from the other ligands explored previously with copper metal salts. There is twisting of the pyrizinyl groups out from the planar tetrazine core of 7.12(8)°, 8.30(9), 14.96(9)° and 15.96(9)°, the two pendant rings are twisted in opposite directions and is imperative to the polymeric nature of the complex.

The anions are located within a box-shape cavity formed within the 2D-polymeric structure, with no significant interactions observed. The 2D-polymer framework is shown in figure 3.15.

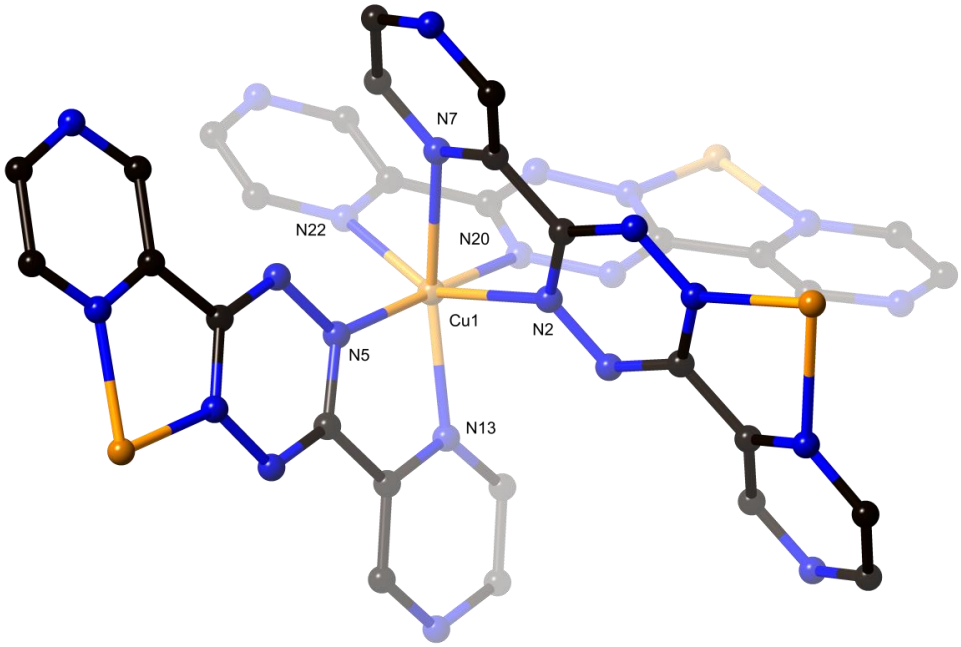

Figure 3.14: Perspective view of complex ***3.5*** *showing the distorted octahedral geometry of the copper metal with the selected atomic labelling shown. Selected bond lengths (Å)* Cu1-N2 1.955(2), Cu1-N5 1.960(2), Cu1-N7 2.090(2), Cu1-N13 2.090(2), Cu1-N20 2.242(2), Cu1-N22 2.443(2) *and angles (°)* N2-Cu1-N7 79.83(8), N5-Cu1-N13 79.11(8), N20-Cu1-N22 70.16(8).

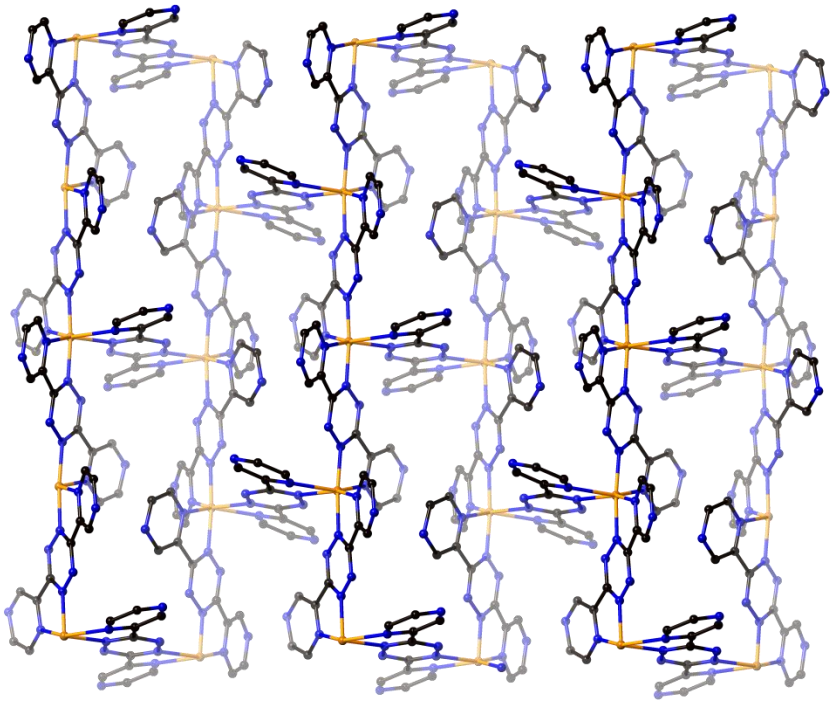

Figure 3.15: Perspective view down the a axis of the 2D polymer of complex ***3.5****.*

Complex 3.6 – **L11** + copper(I) iodide

The same molecule as complex **3.5**, (**L11**), was reacted with CuI giving a dark red/black solution. After vapour diffusion of diethyl ether into the reaction mixture, crystals suitable for small molecule X-ray diffraction were collected. Due to insufficient amount of crystals, this complex was regrown for microanalysis and this solid was analysed with a 3:1 metal-ligand stoichiometry.

Solution studies were completed for complex **3.6** as previously described, however the same results were obtained for NMR and UV-Visible as complex **3.2** showing the ligand only. From the results obtained in complex **3.2** and **3.4**, both are polymeric and showed only ligand in the NMR and UV-Visible, which would suggest a polymeric structure for complex **3.6**.

This copper iodide complex **3.6** crystallises in the monoclinic space group, $P2_1/n$. The structure is a one dimensional polymer that extends along the *b* axis, as shown in figure 3.16. The asymmetric unit consists of two copper(I) iodides and one molecule of **L11**.

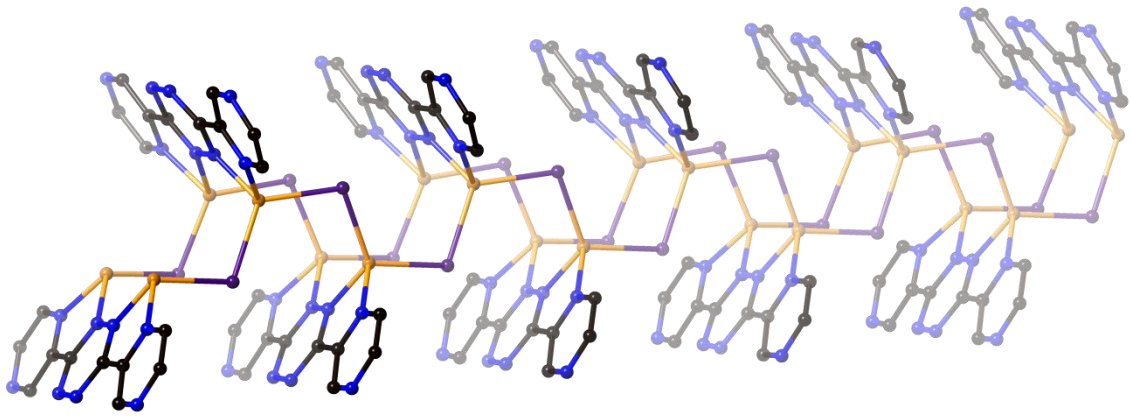

*Figure 3.16: Polymeric structure of complex **3.6** in a zig-zag topology.*

The copper metals have a distorted tetrahedral geometry and are coordinated to two nitrogen atoms and two iodides as shown in figure 3.17. The distorted geometry is the cause of the formation of five-membered chelating rings with bite angles of 79.0(2)° and 79.7(2)°. There is very little twisting of the pyrazinyl rings, 6.1(2)° and 8.5(2)° out of the plane for the tetrazine core, and the tetrazine core has a slight twist, with the torsion angle measuring 3.7(8)°.

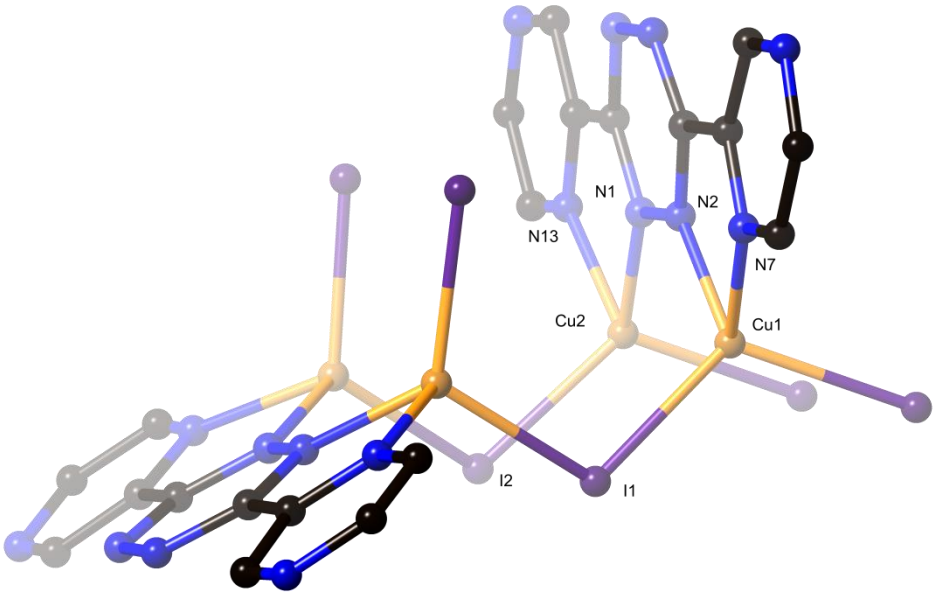

Figure 3.17: Perspective view of complex ***3.6*** *with the selected atomic labelling. Selected bond lengths (Å) Cu1-N2 2.028(6),* Cu1-N7 2.140(5), Cu1-I1 2.543(10), Cu1-I2 2.5576(11), Cu2-N1 2.017(5), Cu2-N13 2.117(6), Cu2-I1 2.5545(11), Cu1-I2 2.5323(10) *and angles (°)* N2-Cu1-N7 79.0(2), N1-Cu2-N13 79.7(2).

Complex 3.7 – **L15** + tetrakis(acetonitrile)copper(I) tetrafluoroborate

Crystals suitable for a single crystal X-ray diffraction study were obtained by vapour diffusion of diisopropyl ether into an acetonitrile solution containing one equivalent **L15** and $Cu(MeCN)_4BF_4$. Complex **3.7** analysed with a 1:1 metal to ligand stoichiometry.

NMR spectroscopy for complex **3.7** showed broadening of all peaks indicating more than one species in solution. ESI-MS showed five possible complexes $[Cu(\mathbf{L15})_2]^+$, $[Cu_2(\mathbf{L15})_3]^{2+}$, $[Cu(\mathbf{L15})]^+/[Cu_2(\mathbf{L15})_2]^{2+}$, $[Cu(\mathbf{L15})_2]^{2+}$, however a polymeric structure is predicted based on the results obtained previously.

Complex **3.7** crystallises in the monoclinic space group C2/c with the asymmetric unit containing one copper metal, one molecule of **L15**, one non-coordinated tetrafluoroborate anion and three non-coordinated acetonitrile solvates, two of which have half occupancies. The complex has a two-dimensional polymeric structure.

Each copper metal is tetrahedral and bound by four nitrogen atoms with all bond lengths ~2.0 Å and a bite angle of 79.13(6)°. Three ligand structures are required around the copper metal for this two-

dimensional polymeric structure. The connectivity of the molecules of **L15** around the metal is shown in figure 3.18.

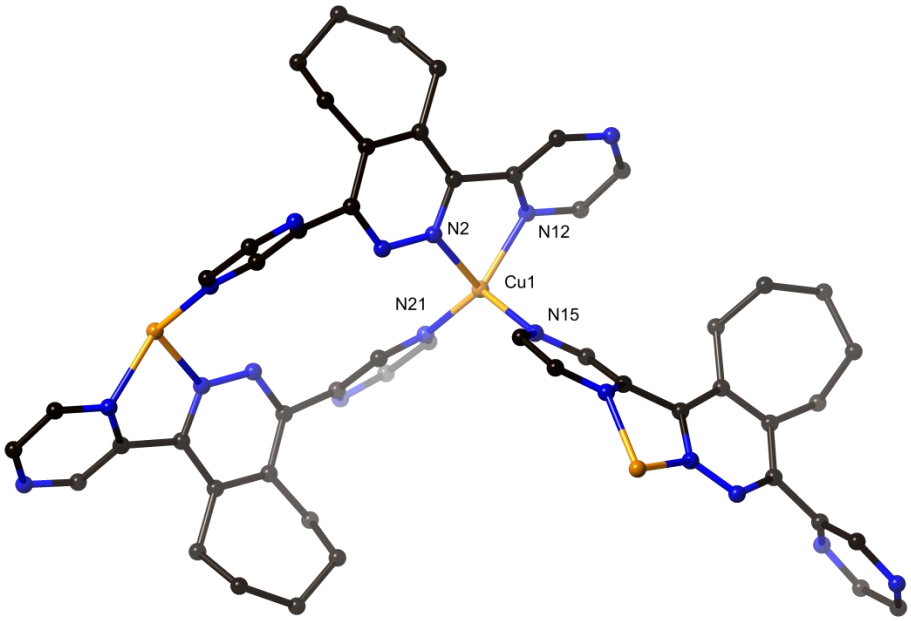

*Figure 3.18: Perspective view of the connectivity of the tetrahedral copper of complex **3.7**. Selected bond lengths (Å)* Cu1-N2 2.1203(16), Cu1-N12 2.0341(16), Cu1-N15 2.0224(16), Cu1-N12 1.9464(16) *and angles(°)* N2-Cu1-N12 79.13(6)

The chelating pyrazinyl ring is twisted out of the plane of the pyridazine core 36.60(6)°, whereas the other pyrazinyl ring has a larger twist of 61.00(6)°.

The tetrafluoroborate anion is disordered over two sites. Two of the minor occupied fluorine atoms are involved in hydrogen bonding interactions with one of the nearby acetonitrile solvates C32-H32A···F34 2.2925(17) Å (D-A), 139.3(5)° (D-H···A) and a proton located on the pyrazinyl rings C14-H14···F41 3.07(3) Å (D-A), 166.6(9)° (D-H···A). The two half occupied acetonitrile solvates are located on a symmetry point.

The conformation of the cycloheptene fused ring is in the envelope orientation which is the most stable confirmation and has been shown to form in this study. The structure of complex **3.7** is a two-dimensional polymer which propagates diagonally along the *bc* plane as shown in figure 3.19.

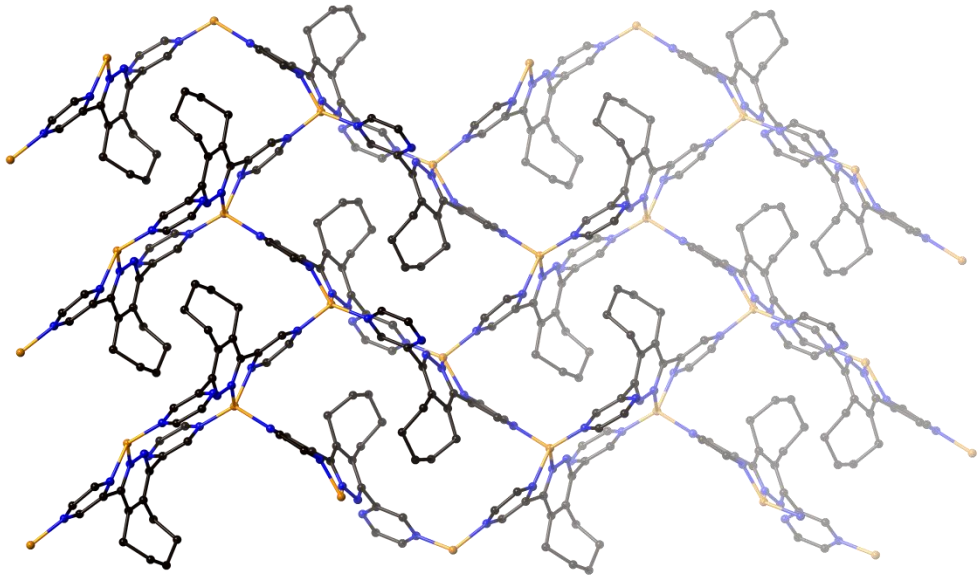

*Figure 3.19: Two-dimensional polymeric structure of complex **3.7**, view along the a-axis. Hydrogen atoms, anions and solvates have been omitted for clarity.*

3.3 Summary

The results obtained in this chapter show copper in different types of metallosupramolecular assemblies (table 3.3), with the results of one grid, five polymers and an unexpected oxidation observed from Cu(I) to Cu(II) forming a discrete M_5L_2 complex.

The grid-like assembly formed by the reaction between **L2** and $Cu(MeCN)_4BF_4$ is very similar to results published in the literature.[30,36,60] Interestingly, four different grid-structures are observed in the asymmetric unit and unusually the achiral starting material crystallises out in a chiral space group.

The increase in the sterically hindering fused rings and pendant groups has shown increase in the twisting allowing bridging, in opposite directions with respect to the pyridazine ring (**C3.4** and **C3.7**).

The polymeric structures were obtained by CuI and $Cu(MeCN)_4BF_4$, with three one-dimensional polymers and two two-dimensional polymers observed, respectively. Copper(I) usually adopts a tetrahedral coordinate geometry, however, in complex **3.5**, the copper is octahedral.

Unfortunately, no copper iodide grid-like structures were obtained however, a complex where the ligands were coplanar and were separated by Cu-I-Cu units was met with success. A summary of the solid state structures are located in table 3.3.

The majority of the solution studies resulted in ligand being observed (**C3.2**, **C3.4**, **C3.5**, **C3.6**), or a broadening of all peaks indicating a polymeric species (**C3.7**). However for complex **3.1** a few similarities with the solid state structure can be observed. NMR spectroscopy could not be completed for complex **3.3** due to the Cu(II) having a paramagnetic electron configuration.

Table 3.3: Summary of the ligands complexes with copper and the metal salts required for complexation.

C.	Ligand structure	Cu-salt	Structure
3.1	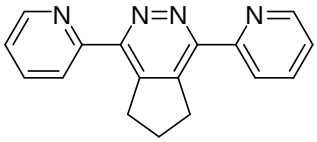 **L2**	$Cu(MeCN)_4BF_4$	$[Cu_4(\mathbf{L2})_4]^{4+}$ Metallogrid 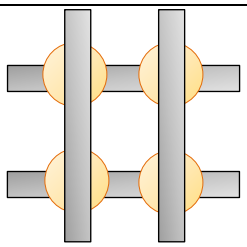
3.2	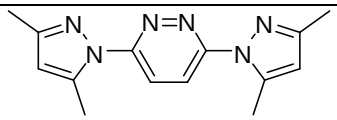 **L6**	CuI	1D Polymer
3.3	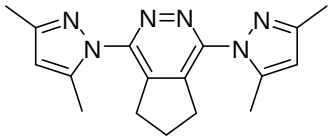 **L7**	$Cu(MeCN)_4BF_4$	$[Cu_5(\mathbf{L7})_2]^{10+}$
3.4	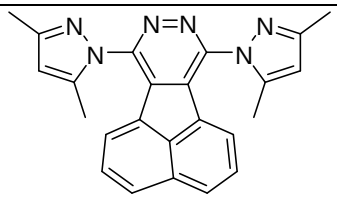 **L9**	CuI	1D Polymer
3.5	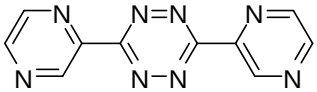 **L11**	$Cu(MeCN)_4BF_4$	2D Polymer
3.6		CuI	1D Polymer
3.7	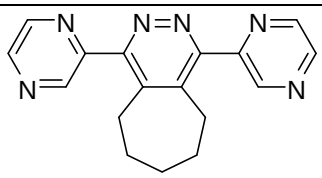 **L10**	$Cu(MeCN)_4BF_4$	2D Polymer

CHAPTER FOUR

Zinc Complexes

4.1 Introduction

The coordination chemistry of zinc has been extensively studied for many years. Earlier work has included intrinsic exploitation of chemical properties of Zn^{2+} in biological environments.[107,108] Macrocyclic polyamines demonstrated that the acidity of Zn^{2+} can be finely tuned in these structures. These properties of Zn^{2+} have led to a new area of biometric chemistry, involving novel molecular recognition, supramolecular chemistry and pharmaceutical chemistry.[109]

In the early 1980s, scientists started working on a Xenopus transcription factor, TFIIIA with the discovery of a domain associated with zinc, named the "zinc finger".[110] Since then, a number of proteins with similar domains has been investigated, with these domains being stabilised by coordination to zinc ions.[109,110] The zinc ion (Zn^{2+}) contains a filled *d* orbital, d^{10} and therefore is not involved in redox chemistry, combined with its Lewis acidity, this makes it a good candidate for biological systems.[4,111]

The supramolecular chemistry of zinc has found applications as the metal component in metal organic frameworks (MOFs),[112] which exhibit structural diversity, and have physical and chemical properties[112] including photoluminescence and porosity.[78] However, more relevant Zn^{2+} architectures to this study were completed by Lehn *et al.* in 2001, where the reaction of a polytopic ligand with three different metal ion binding domains with zinc resulted in a double helical motif (figure 4.1) rather than a grid-type assembly, which is described as a dominant/recessive behaviour of the system.[113] Zinc often adopts a distorted octahedral geometry, although tetrahedral geometries can occur.

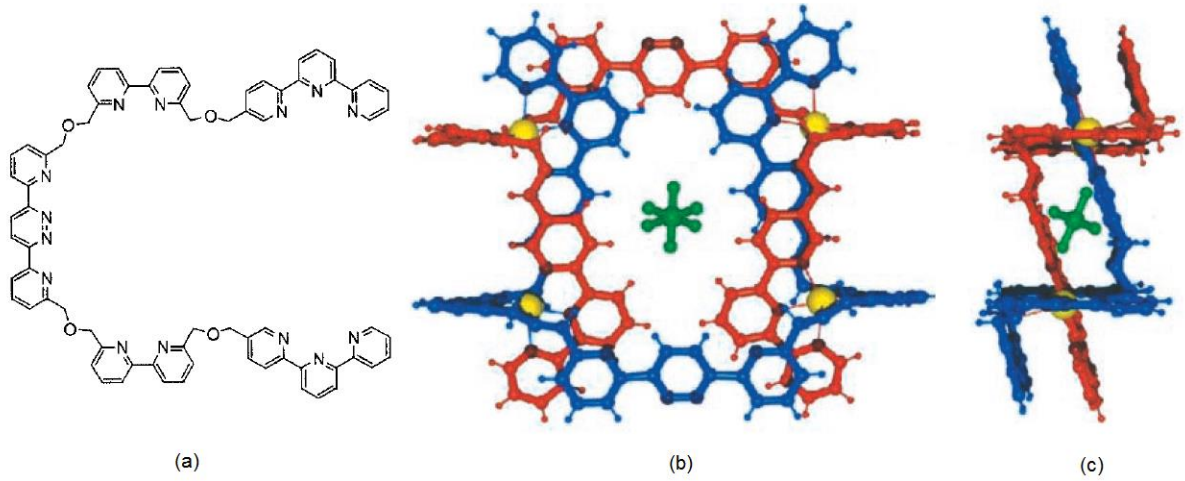

Figure 4.1: Crystal structure of the $[Zn_4(L)_2(PF_6)_8]$ circular helical complex obtained by Lehn et al. 2001;[113] (a) Ligand structure; (b) Front view with the PF_6 encapsulated inside the helical structure; (c) Side view of the complex.

Vazquez *et al.* investigated the production of larger supramolecular architectures through non-covalent aromatic interactions which resulted in a double helical structure (figure 4.2). Spectrophotometric and spectrofluorimetric studies of these were completed, leading to an understanding of their structure in solution, as well as their formation mechanism.[114]

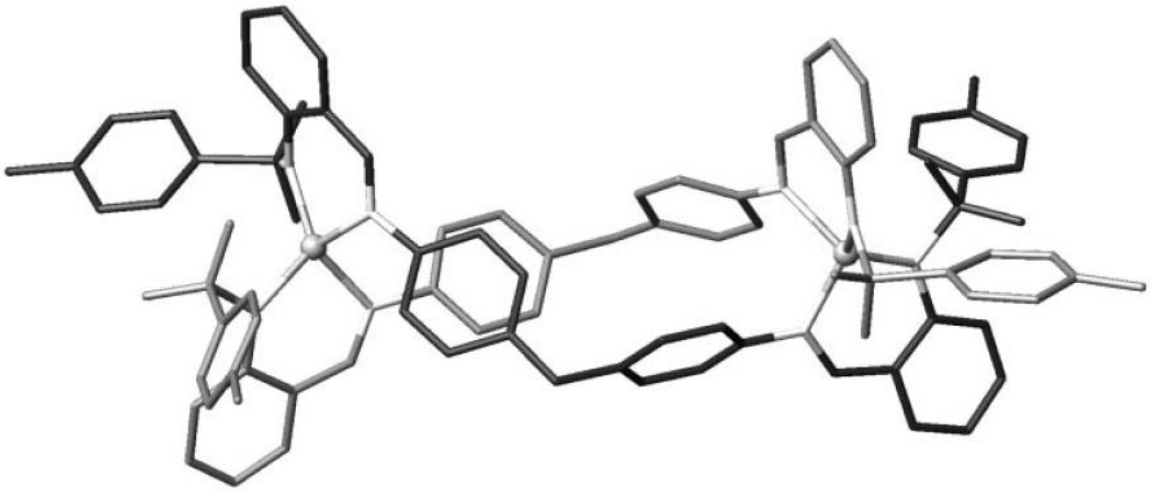

Figure 4.2: Distorted tetrahedral geometry of zinc in the double helical crystal structure obtained by Vazquez et al.[114]

The self-assembly of dinuclear Zn(II) species containing Robson-type macrocycles with varying organic subunits was reviewed by Huang *et al.* in 2006.[115] An infinite one-dimensional ladder complex formed with the reaction of 4,4'-bipyridine with the Zn(II)-macrocycle with the zinc being in an octahedral geometry (figure 4.3). Other structures described in this review show Zn^{2+} in a square based pyramidal geometry.

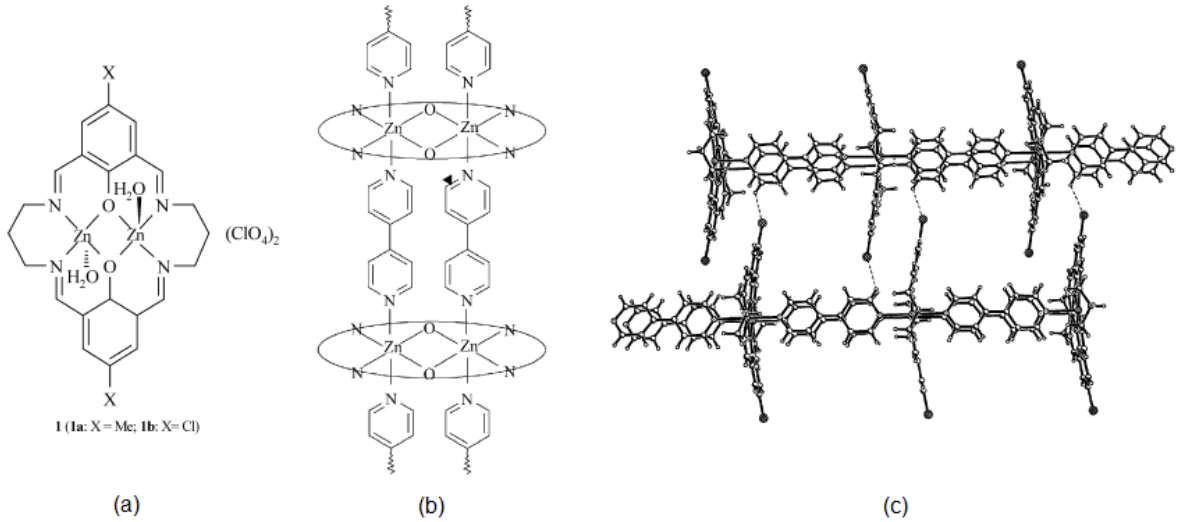

Figure 4.3: (a) Dinuclear zinc(II) Robson-type macrocycle (b) Self-assembled structure of [Zn_2(1b)(H_2O)$_2$] with 4,4'-bipyridine. (c) Perspective view of packing structure of one of the complexes.[115]

Recent work on [2 x 2] grid-like self-assembled structures,[116-118] has involved tridentate ditopic ligands with Zn(II) where the zinc adopts an octahedral geometry. Lehn *et al.* have had success forming the metallogrid shown in figure 4.4, and carried out the solution studies of this complex. The zinc metals are distorted octahedral and the structure forms N-H hydrogen bonds to nearby perchlorate anions.

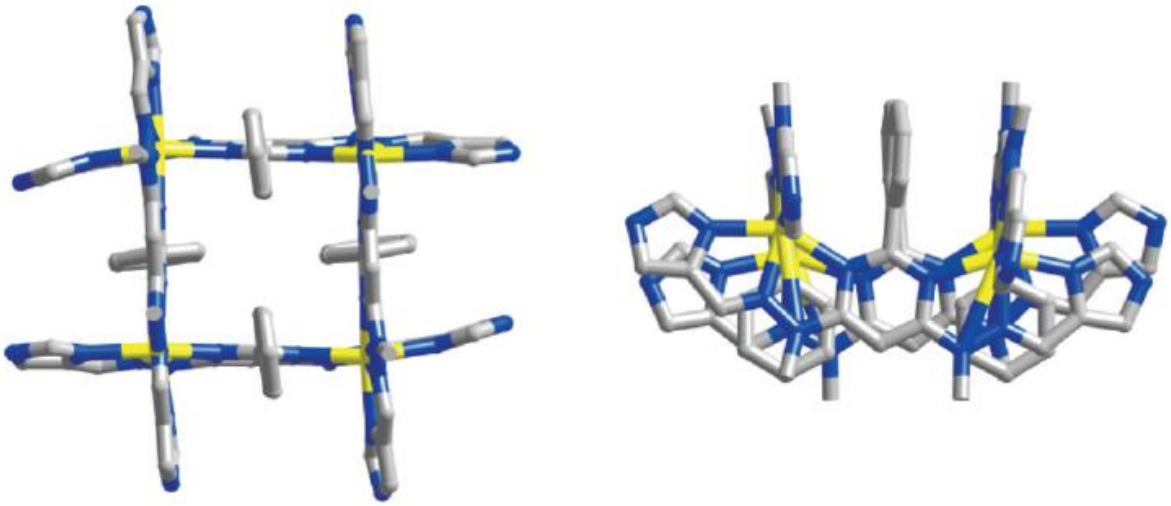

Figure 4.4: Grid-type array elucidated by Lehn et al.[118]

In the literature examples mentioned above, Zn^{2+} adopts four, five and six coordinate geometries. In biological systems the metal is often four coordinate or five coordinate when a macrocycle is involved and six coordinate in more classic coordination complexes.[21]

In this chapter, a range of self-assembled architectures formed with zinc has been investigated. The different structures formed include grids, helicates and discrete "clusters". We decided to use this metal due to its labile nature and to see if zinc behaves the same way as seen in previous chapters. As there have been no complexes with **L1**, we chose to begin our investigations here.

4.2 Coordination complexes

Complex 4.1 – **L1** + zinc perchlorate hexahydrate

X-ray crystallographic quality single crystals of complex **4.1** were grown by vapour diffusion of diisopropyl ether into the colourless reaction mixture of $Zn(ClO_4)_2.6H_2O$ with **L1** in a 1:1 ligand-metal stoichiometry in acetonitrile. This complex was obtained as crystals in very high yield (98.8%) and was analysed to have a 2:3 metal-ligand stoichiometry.

The solution chemistry of **4.1** was investigated using NMR spectroscopy and UV-Visible spectrophotometry. The complex was dissolved in d_3-acetonitrile and a ^{1}H-NMR spectrum was collected, analysed and compared with a ligand spectrum. The coordination induced shifts of these protons are summarised in table 4.1.

	H3	H4	H5	H6	H9
L1	8.71	8.00	7.52	8.77	8.67
C4.1	8.61	8.45	7.91	8.02	9.05
CIS[b]	-0.10	+0.45	+0.39	-0.75	+0.38

[a] For deuterated acetonitrile solutions. [b] CIS= $^{\delta}$complex-$^{\delta}$ligand.

*Table 4.1: ^{1}H-NMR Chemical shifts[a] and Coordination Induced Shifts[b] of complex **4.1.***

All of the protons show a change in chemical shift; two protons move upfield, H3 and H6, 0.1 ppm and 0.75 ppm, respectively, evidently showing that the coordination of zinc has a greater effect on the H6 proton, in comparison to the H3 proton. The other two pyridyl protons are shifted downfield by 0.45 ppm (H4) and 0.39 ppm (H5). The protons located on the pyridazine core experience a 0.38 ppm shift downfield. From these shifts we can conclude that the H6 protons in the complex are pointing towards the shielding zone of an aromatic ring causing this large shift.

The ^{1}H-NMR titration was done by adding 20 µL 0.05 mol L^{-1} acetonitrile aliquots of zinc perchlorate hexahydrate salt solution to a 500 µL of 0.01 mol L^{-1} acetonitrile solution of **L1** until the metal to ligand ratio was 1:1. An extra equivalent of metal was added to confirm the spectrum did not change. Shown in figure 4.5 are the NMR spectra showing the aromatic region for the titration performed to form complex **4.1**. After 0.2 equivalence (eq.) of metal salt solution is added to the ligand solution the spectrum shows only broadened peaks which is likely to be several components in equilibrium observed on the NMR time scale. However, small peaks and a few broadened peaks are present when 0.4 eq. of metal is added. Once a further 0.2 eq. (0.6 eq. in total) of metal salt solution is added, it is evident there is a formation of a symmetrical complex and there is no further change to the ^{1}H-NMR spectra with the addition to a 2:1 metal-ligand stoichiometry, giving a likely metal-to-ligand ratio of 2:3 in solution state.

A UV-Visible titration for complex **4.1** was carried out to determine if there is a trend between the solution studies, with the results displayed in figure 4.6. These show the ligand wavelength maximum at 296 nm and 256 nm and when the complex forms at a 1:1 stoichiometry there is a wavelength maximum at 299 nm and 241 nm. In the titration, with the addition of 0.2 eq., 0.4 eq., 0.6 eq. and 0.8 eq., there is continuous change observed until the ratio of metal to ligand is 1:1.

Unfortunately indicating no strong correlation between the NMR and UV-Visible titrations performed. High resolution electrospray ionisation mass spectrometry shows the possibility of two complexes of $[Zn(\mathbf{L})_3]^{2+}$ and $[Zn(\mathbf{L})_2]^{2+}$, however these could be fragments of the complex in solution.

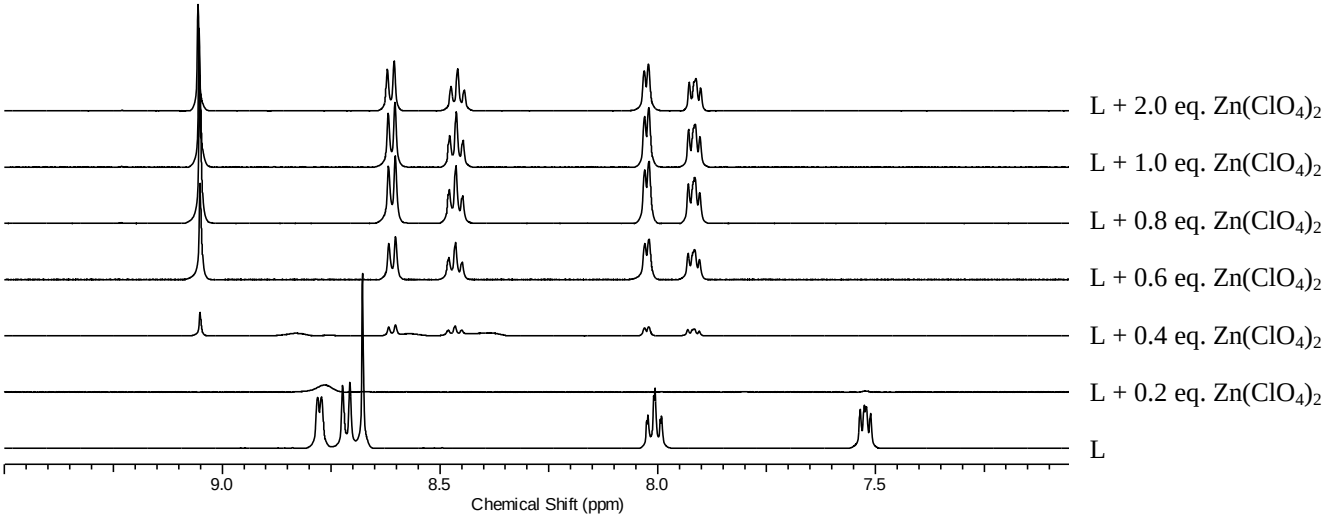

Figure 4.5: *^{1}H-NMR titration to form complex 4.1, aromatic region shown.*

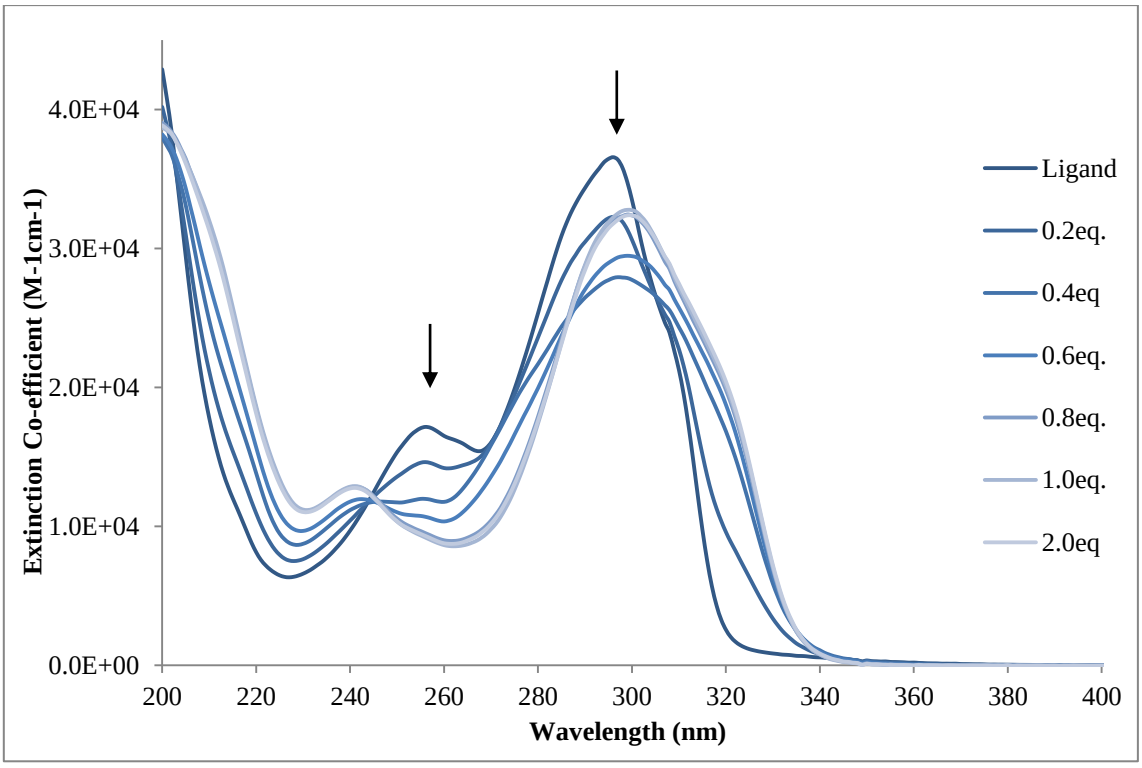

*Figure 4.6: UV-Vis spectroscopic titration plot of $Zn(ClO_4)_2$ against **L1** in acetonitrile to form complex **4.1**.*

Complex **4.1** crystallises in the orthorhombic space group, Pn. The asymmetric unit consists of four metals, six molecules of **L1**, eight non-coordinated perchlorate anions and eight non-coordinated acetonitrile solvate molecules. The metals and ligands are coordinated to form two separate triple helical subunits, with each having the formula, Zn_2(**L1**)$_3$. The molecular structure and selected atomic labelling of this complex is shown in figure 4.7.

The two helicates are different enantiomers, one is a right-handed (Δ = *P*) and the other is a left-handed (Λ = *M*) helicate, due to the noncentrosymmetric nature of the space group. The coordination geometry of the Zn(II) metals is distorted octahedral, involving six nitrogen atoms, two from each ligand forming a five-membered chelate ring. The two helical structures have similar Zn-N bond lengths and bite angles, ranging from 2.123(6) Å - 2.220(6) Å and 73.5(2)° - 75.3(2)º, respectively, which are standard bond lengths for the atoms involved. These lengths and angles are summarised in table 4.1. The distortion of the metal centres arises from the enforced binding angle placed on the metal centre by the bidentate binding domains. It can be observed that the bond lengths from the pyridyl-nitrogen to the metal are marginally smaller than that of the pyridazine-nitrogen; this is an effect of the twisting of the pyridine rings.

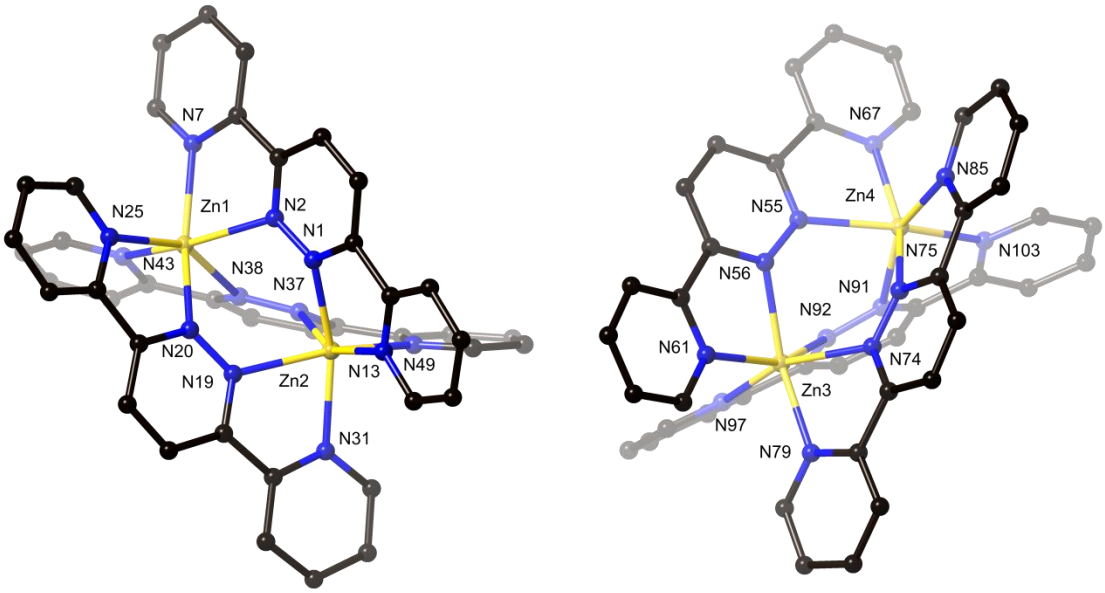

Figure 4.7: *Perspective view of complex **4.1**. All anions, solvate molecules and hydrogen bonds have been omitted for clarity. Right handed helicate (left), left handed helicate (right).*

The ligands are is in a *cis/cis-conformation* when complexed with zinc to form the helical structures, with the pyridyl groups being slightly twisted with respect the the pyridazine ring having angles measuring 7.5(2)° - 18.8(3)°. The measured torsion angles of the pyridazine ring (ranging

from 5.5(7)° - 15.7(7)°) show a bending of each ligand which is another contributor to the distorted octahedral geometry observed.

Bond lengths helicate (P)	
Zn1-N2	2.173(6)
Zn1-N7	2.144(6)
Zn1-N20	2.168(6)
Zn1-N25	2.123(6)
Zn1-N38	2.184(6)
Zn1-N43	2.141(7)
Zn2-N1	2.192(6)
Zn2-N13	2.163(6)
Zn2-N19	2.216(6)
Zn2-N31	2.162(6)
Zn2-N37	2.191(6)
Zn2-N49	2.158(6)

Bond lengths helicate (M)	
Zn3-N56	2.158(6)
Zn3-N61	2.130(6)
Zn3-N74	2.183(6)
Zn3-N79	2.152(6)
Zn3-N92	2.189(6)
Zn3-N97	2.161(6)
Zn4-N55	2.220(6)
Zn4-N67	2.167(6)
Zn4-N73	2.188(6)
Zn4-N85	2.156(6)
Zn4-N91	2.196(6)
Zn4-N103	2.151(6)

Bite angles of both helicates	
N2-Zn1-N7	74.6(2)
N20-Zn1-N25	75.2(2)
N38-Zn1-N43	74.3(2)
N1-Zn2-N13	74.1(2)
N19-Zn2-N31	73.5(2)
N37-Zn2-N49	74.1(2)
N56-Zn3-N61	75.3(2)
N74-Zn3-N70	74.3(2)
N92-Zn3-N97	74.5(2)
N55-Zn4-N67	73.5(2)
N73-Zn4-N85	73.9(2)
N91-Zn4-N103	74.2(2)

Table 4.1: *Selected bond lengths (Å) and angles (°) for complex **4.1**.*

One of the perchlorate anions, located between two of the ligands has two of the oxygen atoms involved in an anion-π interaction with distances from the anion to the pyridazine centroid as 3.026(7) Å (O110) and 3.139(7) Å (O111). An acetonitrile solvate is located on the opposite side of one of the ligands with an interaction of 3.188(10) Å (N135). The other helical structure has an acetonitrile solvate located 3.177(11) Å (N165) from the pyridazine centroid involved in a fairly weak interaction. There are no significant interactions between the other solvate molecules and perchlorate anions.

Complex **4.1** can be characterised as a triple stranded saturated homotopic helicate which has a twist of ~72°, measured as the $N_{pyridine}$-Zn-Zn-$N_{pyridine}$ torsion angle for both the P helicate and the M helicate, shown in figure 4.8.

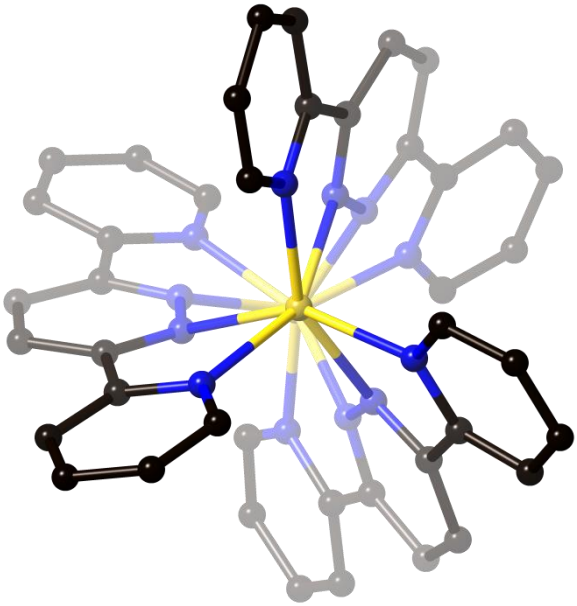

Figure 4.8: *View along the screw axis of the right handed helicate. Hydrogen atoms have been removed for clarity.*

The resulting triple helicate has a metal-to-ligand stoichiometry of 2:3 which is the same results obtained from the ^{1}H-NMR titration. The coordinated induced shifts showed a large shielding effect for H6 which was confirmed in the structure with this proton facing into the shielding zone of a nearby pyridine ring, as shown in figure 4.9, with distances ranging from the H6 protons to the centroid of a pyridine ring ranging from 3.098(3) Å – 3.390(3) Å.

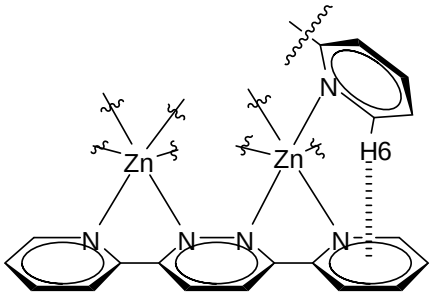

Figure 4.9: Diagram showing how H6 is oriented into the shielding zone of the pyridine pendant group.

Complex 4.2 – **L2** + zinc perchlorate hexahydrate

Colourless crystals of complex **4.2** were obtained after vapour diffusion of diisopropyl ether into the reaction mixture of **L2** and $Zn(ClO_4)_2.6H_2O$. Crystals suitable for single crystal X-ray crystallography were obtained in 54.2% yield. Unfortunately an insufficient quantity for both X-ray

crystallography and microanalysis were produced, and the solid was regrown using the same conditions and these were analysed with a 1:1 metal-ligand stoichiometry.

The same solution studies, for complex **4.2** were completed as previously described. Complex **4.2** was dissolved in d_3-acetonitrile and a ^{1}H-NMR spectrum was collected and the coordination induced shifts are summarised in table 4.2. Comparisons of the complex to the ligand show H6 having the greatest shift downfield by 0.80 ppm. The other protons experience shifts upfield by 0.36 ppm and 0.41 ppm, for H5 and H4, respectively, whilst H3 experiences a negligible shift. The alkyl protons also are affected with CIS downfield shift of 0.11 ppm for H10 and 0.73 ppm for H11. From the H6 shift and the results previously observed in complex **4.1**, indicates the structure to be a helicate. The shift observed for H11 protons, likely indicates interactions with nearby solvates and anions.

	H3	H4	H5	H6	H10	H11
L2	8.51	7.98	7.47	8.76	3.49	2.14[c]
C4.2	8.46	8.39	7.83	7.96	3.60	2.87[c]
CIS[b]	-0.05	+0.41	+0.36	-0.80	+0.11	+0.73

[a] For deuterated acetonitrile solutions. [b] CIS= $^{\delta}$complex-$^{\delta}$ligand. [c] Deuterated acetonitrile overlap.

*Table 4.2: ^{1}H-NMR Chemical shifts[a] and Coordination Induced Shifts[b] of complex **4.2***

A ^{1}H-NMR titration was done using the same method as previously described. Shown in figure 4.10 are the ^{1}H-NMR spectra for the titration, indicating a trend for metal salt addition similar to complex **4.1**, with the first 0.2 eq. addition with a broadening of peaks seen, appearance of peaks with 0.4 eq. added and then no further change seen after 0.6 eq. is added. This indicates the likely formation of M_2L_3 helical structure in solution.

A UV-Visible spectroscopic titration was carried for complex **4.2** and the results are displayed in figure 4.11. This shows a shift from the lowest energy transition from the free ligand 288 nm to 299 nm at a ratio of 1:1 metal to ligand. Peaks form in the shoulder region at 207 nm and 245 nm corresponding to a ligand to ligand charge transfer (LCT). Note that there is a lack of isosbestic points; however, the spectrum does not change after a metal-to-ligand stoichiometry is 2:3.

The two titrations show similarities in complex formation, with a 2:3 metal-ligand stoichiometry supported by both results. The ESI-MS for complex **4.2** show the same results as complex **4.1**.

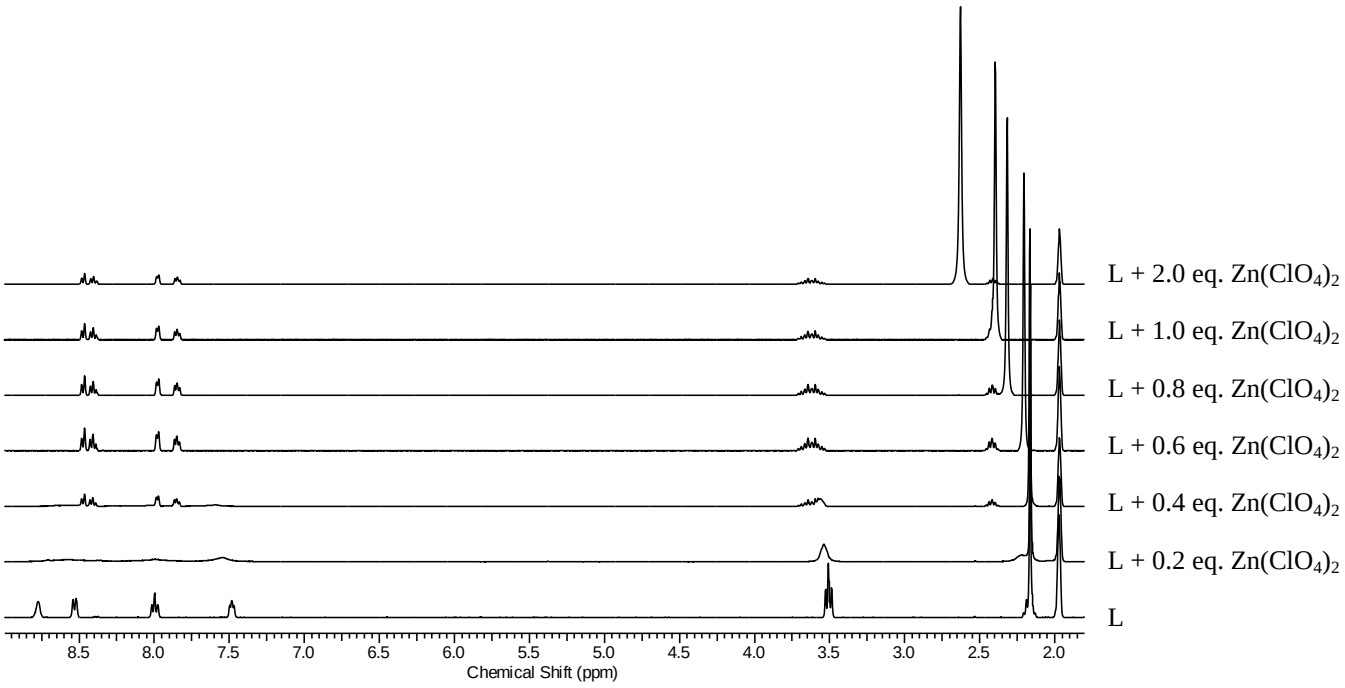

*Figure 4.10: ^{1}H-NMR titration to form complex **4.2**.*

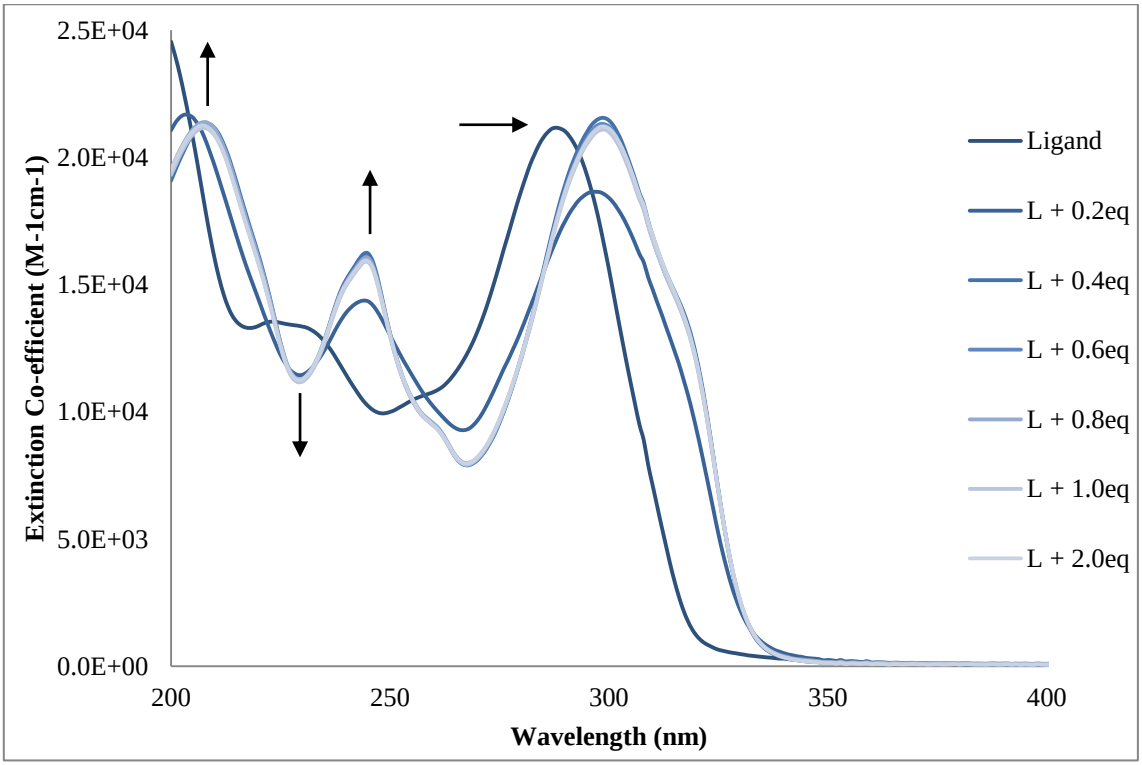

*Figure 4.11: UV-Vis spectroscopic titration plot of $Zn(ClO_4)_2$ against **L2** in acetonitrile to form complex **4.2**.*

The colourless crystals of complex **4.2** were suitable for single X-ray structure analysis and crystallise in the orthorhombic space group, Aba2. The asymmetric unit contains two zinc metals and three ligand molecules with a triple helical structure, as well as, four non-coordinated

perchlorate anions and three non-coordinated acetonitrile solvate molecules. The helical structure, as shown in figure 4.12, is the left handed (M=Λ) helicate, although the other enantiomer will be present due to the achiral space group. This stoichiometry obtained in the crystal structure is different from the microanalysis, due to the complex having to be regrown.

The bond lengths are of typical length for zinc to nitrogen (2.137(4) Å - 2.219(4) Å), as seen previously for zinc complexes (Zn-$N_{pyridine}$ and Zn-$N_{pyridazine}$).[106] The connectivity to the zinc metal is very similar to the previous complex **4.1**, with the zinc metal being distorted octahedral and having two nitrogen atoms from each ligand to form the helicate.

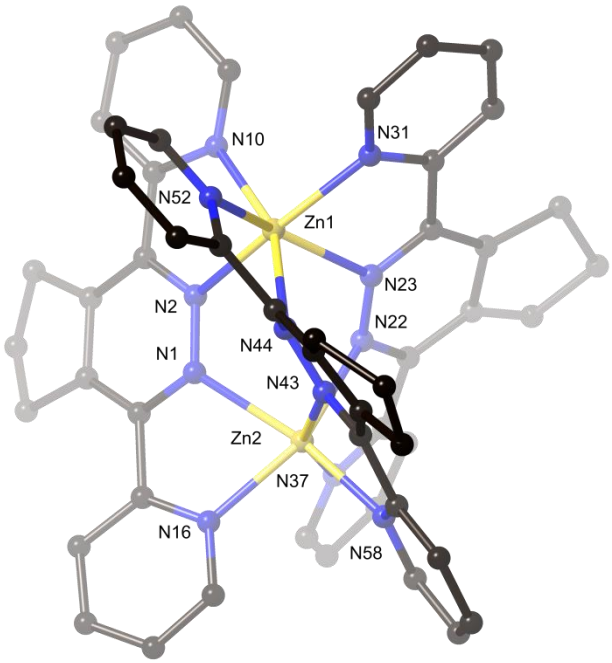

Figure 4.12: Crystal structure of the asymmetric unit of complex ***4.2.*** *All anions, solvate molecules and hydrogen bonds have been omitted for clarity. Selected bond lengths (Å):* Zn1-N2 2.153(4), Zn1-N10 2.150(4), Zn1-N23 2.165(4), Zn1-N31 2.148(4), Zn1-N44 2.191(4), Zn1-N52 2.156(4), Zn2-N1 2.219(4), Zn2-N16 2.140(4), Zn2-N22 2.212(4), Zn2-N37 2.149(4), Zn2-N43 2.137(4), Zn2-N58 2.139(4) *and angles (°):* N2-Zn1-N10 74.80(16), N23-Zn1-N31 73.51(14), N44-Zn1-N52 74.76(15), N1-Zn2-N16 73.64(15), N22-Zn2-N37 73.73(15), N23-Zn2-N58 74.64(15).

The fused cyclopentene ring has an envelope conformation, which is the most stable for this five-membered ring as seen previously. The pyridine rings of **L2** are slightly twisted out of the plane of the pyridzine ring, 6.92(16)° - 28.07(15)°, due to the helical structure and the strain forced upon the rigid ligand. The torsion angles of the $N_{pyridine}$-C-C-$N_{pyridazine}$ range from 2.7(5)° - 22.6(4)°. The twisting observed could potentially be influenced by the fused cyclopentene backbone due to steric clash of the H···H interaction between the backbone and the pyridyl groups (H···H ranging from

2.08891(2) Å – 2.46544(3) Å and C···C ranging from 3.120(8) Å – 3.193(10) Å). The pyridazine core are also twisted with angles 3.6(5)°, 6.9(5)° and 7.0(5)°.

Three of the perchlorate anions are situated in the cavities produced by the helical structure (figure 4.13), along with two of the acetonitrile solvates. These anions are involved in hydrogen bonding interactions with protons located on the pendant groups and the fused cyclopentene ring. The interactions are summarised in table 4.3. The interactions that the perchlorates are involved in are mostly with H5 of the ligand, shows moderately strong hydrogen bonding interactions. There are interactions observed with H4 and H11, however these interactions are weak, as well as interactions between the anions and acetonitrile solvates.

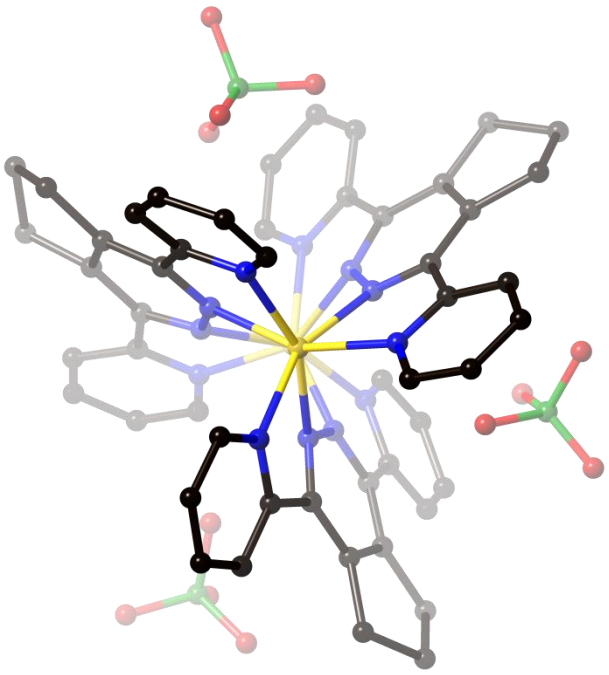

*Figure 4.13: View down the screw axis of the complex **4.2**. Figure emphasising the cavities in which the perchlorates are located. Hydrogen atoms have been removed for clarity.*

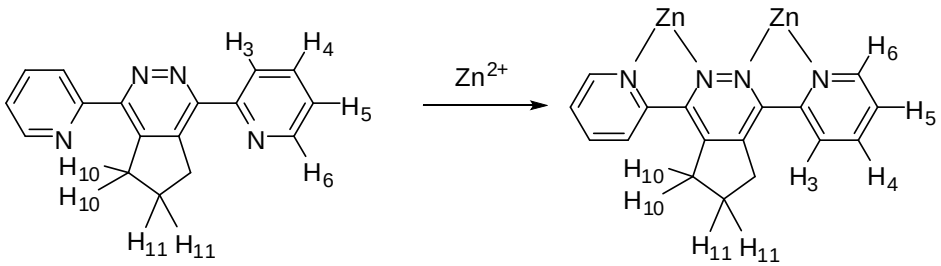

*Figure 4.14: Proton labelling on the ligand molecule, **L2**.*

D-H···A	D-A (Å)	D-H···A (°)	D-atom type
C41-H41···O66	3.355(9)	149.9(4)	'H4' on ligand
C40-H40···O65	3.163(6)	145.4(4)	'H5' on ligand
C62-H62···O76	3.231(7)	135.5(4)	'H5' on ligand
C56-H56···O80	3.177(7)	120.3(3)	'H5' on ligand
C19-H19···O83	3.397(7)	158.5(5)	'H5' on ligand
C48-H48B···O83	3.377(7)	136.1(4)	'H11' on ligand
C89-H89B···O73	3.354(10)	152.6(5)	MeCN-N
C86-H86A···O70	3.331(8)	146.9(5)	MeCN-N

*Table 4.3: Summary of the hydrogen bonding interactions observed between perchlorate anions and protons on **L2** as well as with solvates in close proximity, labelled protons are shown in figure 4.14.*

Complex **4.2** is a triple helicate as suggested in the solution work, having solution spectroscopy results very similar to the previous complex **4.1**. The helicate can be described in the same way, as a triple stranded saturated homotopic helicate with a similar helical twist of ~77°, measuring from the $N_{pyridine}$-Zn-Zn-$N_{pyridine}$. The structure shows that the H6 protons on the ligands are indeed facing into a shielding zone of an aromatic ring in close proximity, distances from H6 to the centroid of the pyridine ring ranging from 2.999(2) Å – 3.296(2) Å, as observed on the ^{1}H-NMR CIS for this proton (table 4.2). The structure also shows interactions between the H4, H5 and H11 protons with anions which could explain the reason for these CIS. The twisting of the pyridyl rings are seen to remove any clash between the H3 and H10.

Complex 4.3 – **L3** + zinc perchlorate hexahydrate

The reaction **L3** with $Zn(ClO_4)_2.6H_2O$ gave complex **4.3** which was isolated after vapour diffusion of diisopropyl ether, giving a 61.3% yield of colourless plate-like crystals suitable for single crystal X-ray diffraction studies. These crystals were analysed with a 1:1 metal-ligand stoichiometry.

^{1}H-NMR spectroscopy and UV-Visible spectrophotometry were completed for this complex and analysed by titration studies. The complex was firstly dissolved in d_3-acetonitrile and the NMR spectrum collected and compared to the ligand spectrum. The coordination induced shifts are summarised in table 4.4. The complex shows different shifts to the previous two complexes described in this chapter. The coordination of zinc has the greatest effect on the H3 protons with a

downfield induced shift of 0.55 ppm, rather than the H6 for complexes **4.1** and **4.2**. The other protons experience a 0.33 ppm downfield shift for both H4 and H5 and an upfield shift for H6 of 0.25 ppm. The allyl protons are split after zinc is bound to the ligand, H10 into two multiplets and H11 split into two singlets.

	H3	H4	H5	H6	H10	H11
L3	7.88	7.98	7.48	8.72	2.94	1.80
C4.3	8.43	8.31	7.81	8.47	3.18/3.32	1.62/2.13
CIS[b]	+0.55	+0.33	+0.33	-0.25	+0.25/+0.38	-0.18/+0.33

[a] For deuterated acetonitrile solutions. [b] CIS= $^{\delta}$complex-$^{\delta}$ligand.

*Table 4.4: ^{1}H-NMR Chemical shifts[a] and Coordination Induced Shifts[b] of complex **4.3**.*

Firstly from these shifts, the H6 is not the proton that experiences the greatest shift which was seen in both complexes **4.1** and **4.2**. From this it can be concluded that the structure is unlikely to be helical. The effect seen on the chemical shifts could be due to the rotation of the pyridyl groups to allow chelation. The splitting observed for the fused backbone could be due to hydrogen bonding interactions with nearby anions or solvates.

A ^{1}H-NMR titration was completed in the same way as described in the complexes **4.1** and **4.2**, with the addition of metal to ligand until the ratio was 1:1. The same concentrations were used and the same procedures carried out. Shown in figure 4.15 is the ^{1}H-NMR titration for complex **4.3**.

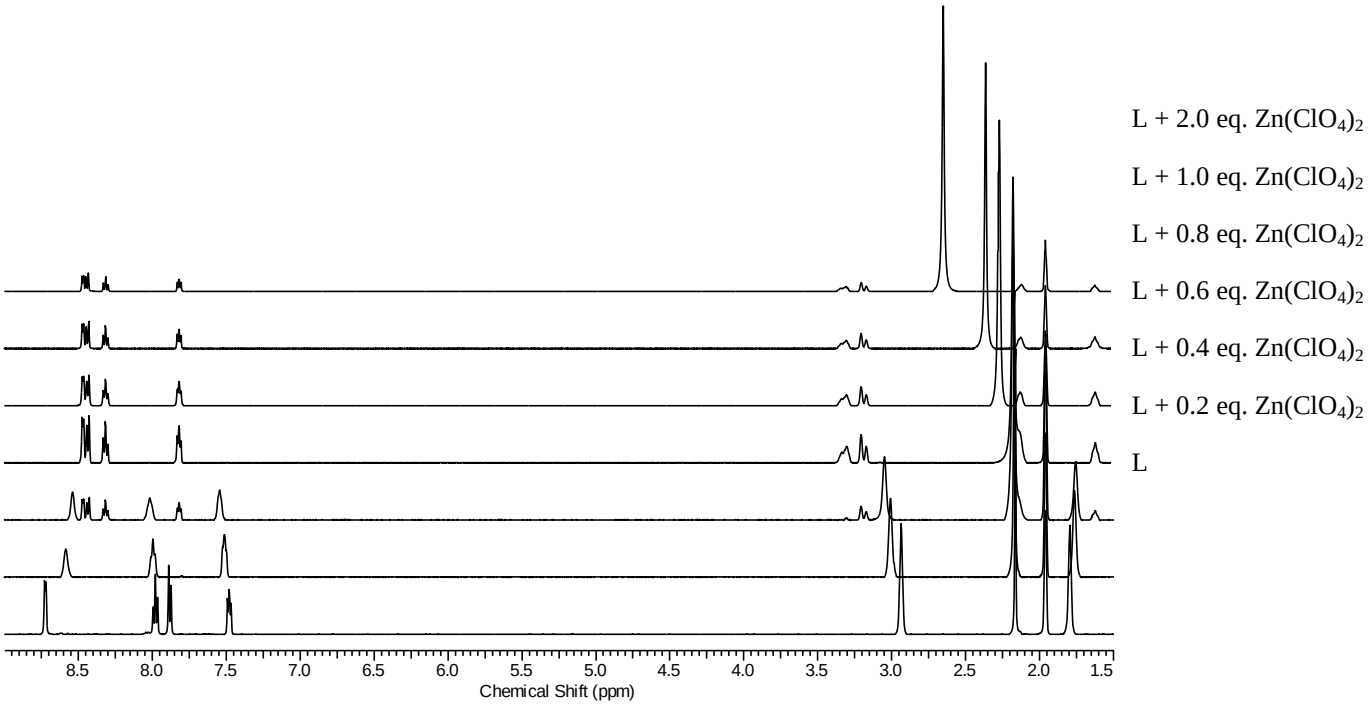

Figure 4.15: ^{1}H-NMR titration to form complex 4.3.

When 0.2 eq. of metal is added to the ligand, the spectra show slight broadening of the peaks. However, when 0.4 eq. is added seven peaks are observed, representing more than one structure present in solution with integral values in the aromatic region of 2, 1, 1, 1, 2, 1, and 2 which indicates two species in solution. With another 0.2 eq. being added, 0.6 eq. in total, there is a disappearance of minor product from the spectra, which once again shows a symmetrical product. There are small shifts until a 1:1 metal-ligand stoichiometry is completed, which could signify a side-by-side structure or a grid-like structure.

UV/Visible spectroscopy titration was completed (figure 4.16), showing a decrease in the absorption at 271 nm and 215 nm and an increase at lower energy wavelengths 296 nm and 241 nm. When 0.4 eq. of metal is added there is no change indicating similar results to complex **4.2** with no isosbestic points being observed. Unfortunately the titrations do not support each other in metal equivalence addition (See 0.4 eq. spectra), however the overall stoichiometry is maintained. High resolution mass spectrometry indicates the possibility of two species, $[Zn(\mathbf{L3})_3]^{2+}$ and $[Zn(\mathbf{L3})_2]^{2+}$, which again could be fragmented parts of the overall complex.

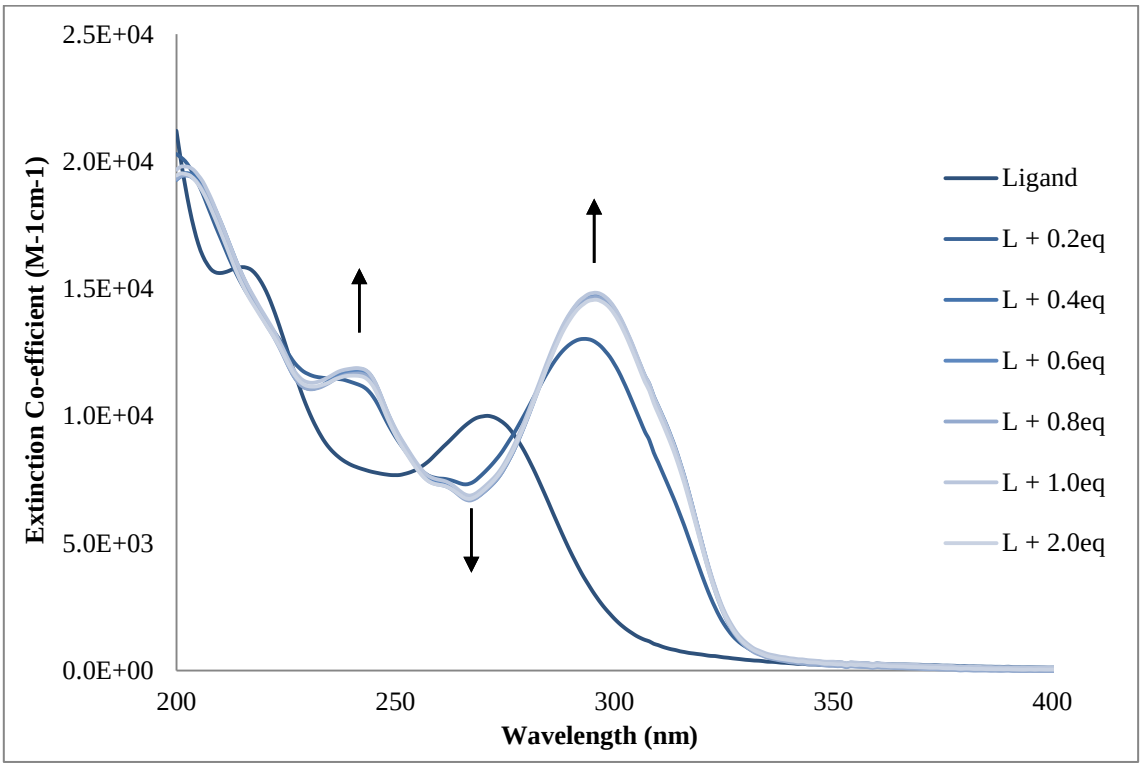

*Figure 4.16: UV-Vis spectroscopic titration plot of $Zn(ClO_4)_2$ against ligand **L3** in acetonitrile. to form complex **4.3**.*

The complex crystallises in the monoclinic space group $P2_1/n$, with the asymmetric unit containing four molecules **L3** and four zinc atoms that are connected by two bridging hydroxides and two bridging water molecules. The asymmetric unit also contains six non-coordinated perchlorate

anions, two water molecules and three non-coordinated acetonitrile solvent molecules. The grid-like structure of complex **4.3** is shown in figure 4.17.

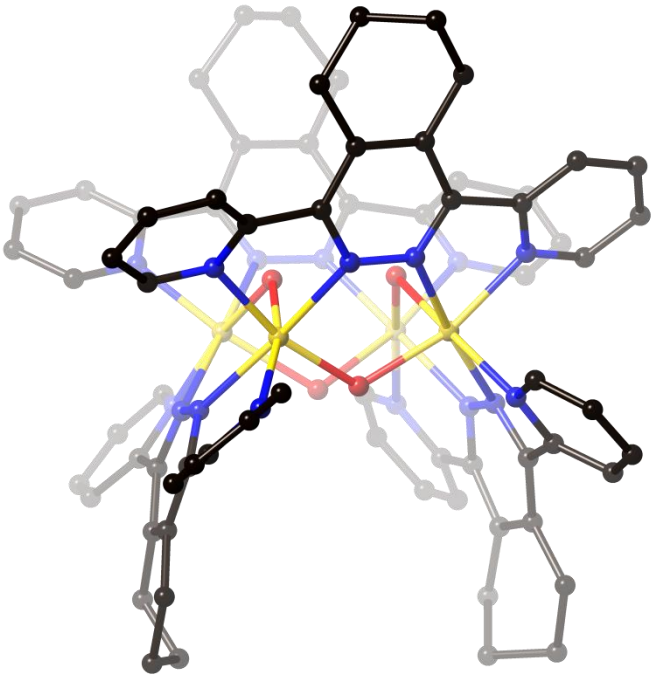

*Figure 4.17: Perspective view of complex **4.3**, showing the discrete grid-like structure. All anions, solvate molecules, hydrogen bonds and minor disorder on the backbone have been omitted for clarity.*

The hydrogen atoms of the bridging hydroxide and water were located based on peaks in the difference map using possible hydrogen bonding interactions with anions and solvates in close proximity to aid in determining their positions. The hydrogen atoms were refined with distance restraints. Knowledge of these bridging atoms was essential to balance the charge of the structure, with the four unique Zn^{2+} ions requiring six perchlorate anions and two bridging hydroxides.

All four zinc metals have an octahedral geometry and are coordinated to four nitrogen atoms and two oxygen atoms. The nitrogen atoms are from two separate ligands forming chelating rings. Zinc prefers being six-coordinate[21] and binds to two oxygen atoms from the solvent for this to occur. The Zn-N and Zn-O bond lengths range from 2.109(4) Å - 2.215(4) Å and 2.043(3) Å - 2.162(3) Å, respectively. The shorter lengths, Zn1-O92 (2.046(3) Å) and Zn4-O92, (2.043(3) Å), correspond to the wider angle seen for the bridging hydroxides, Zn1-O92-Zn4 114.71(16)º. The bond lengths and angles are summarised in table 4.5.

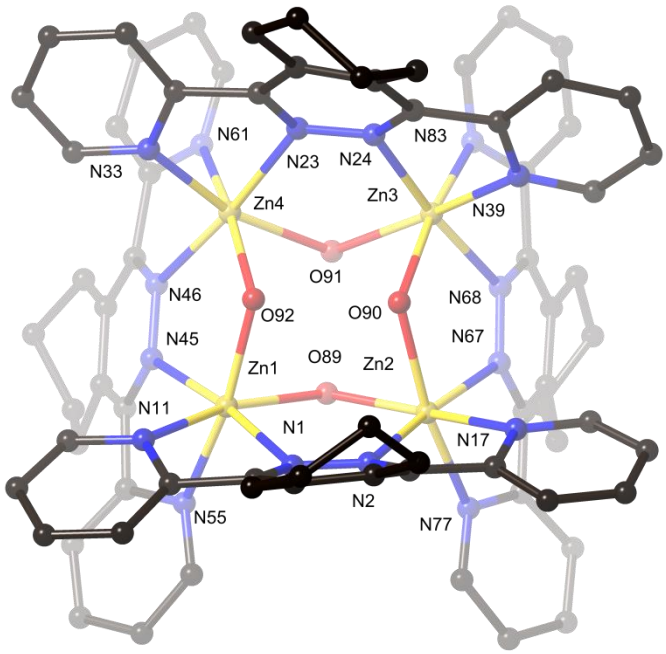

*Figure 4.18: Grid structure of complex **4.6** with atomic labelling.*

Bond Lengths			
Zn1-O89	2.148(3)	Zn3-O90	2.153(3)
Zn1-O92	2.046(3)	Zn3-O91	2.067(3)
Zn1-N1	2.215(4)	Zn3-N24	2.152(3)
Zn1-N11	2.126(4)	Zn3-N39	2.141(4)
Zn1-N45	2.173(4)	Zn3-N68	2.180(3)
Zn1-N55	2.120(4)	Zn3-N83	2.109(4)
Zn2-O89	2.081(3)	Zn4-O91	2.120(3)
Zn2-O90	2.162(3)	Zn4-O92	2.043(3)
Zn2-N2	2.140(3)	Zn4-N23	2.207(4)
Zn2-N17	2.115(4)	Zn4-N33	2.164(4)
Zn2-N67	2.133(3)	Zn4-N46	2.191(4)
Zn2-N77	2.109(4)	Zn4-N61	2.139(4)

Bite Angles	
N11-Zn1-N1	74.25(15)
N55-Zn1-N45	74.55(14)
N17-Zn2-N2	76.15(14)
N77-Zn2-N67	75.69(13)
N39-Zn3-N24	75.83(14)
N83-Zn3-N68	75.76(14)
N33-Zn4-N23	74.17(15)
N61-Zn4-N46	74.57(15)

Bridging Oxygen Angles	
Zn2-O89-Zn1	112.58(13)
Zn3-O90-Zn2	109.12(12)
Zn3-O91-Zn4	113.22(13)
Zn4-O92-Zn1	114.71(16)

Table 4.5: Selected bond lengths (Å) and angles (º) for complex 4.3

Ligand **L3** contains a fused cyclohexene ring which can exist in two chair conformations; however, disorder is only evident in one of the four ligands seen in this complex. The increase in the fused ring size by one -CH_2-, from complex **4.2** (cyclopentene) to **4.3** (cyclohexene) has resulted in a larger twisting of the pyridyl groups out of the pyridazine core, ranging from 22.13(15)° - 36.83(18)°. This has also resulted in a grid-like complex compared to the helical structure seen in the previous two complexes (**4.1** and **4.2**). This is the first metallogrid complex with bridging

oxygen atoms from hydroxides and water molecules to be observed, for bis-bidentate ligands. The closest structure reported in the literature is by Kurup *et al.*,[119] where a tridentate ligand was synthesised with a carbonyl located in the centre to be the oxygen bridging mode. The connectivity of the zinc ion reported[119] is octahedral bound to four nitrogen atoms and two oxygen atoms. The same bonding atoms are seen here in complex **4.3**; however, the oxygen atoms are not connected to the ligand.

The anions are situated in space around the structure, with two perchlorate anions and one acetonitrile solvate located in two cavities formed by the ligands fused cyclohexene rings that are parallel to each other in the grid-like structure. Within these two cavities, hydrogen bonding interactions are observed as well as between the bridging atoms (figure 4.19). A summary of these interactions is located in table 4.6.

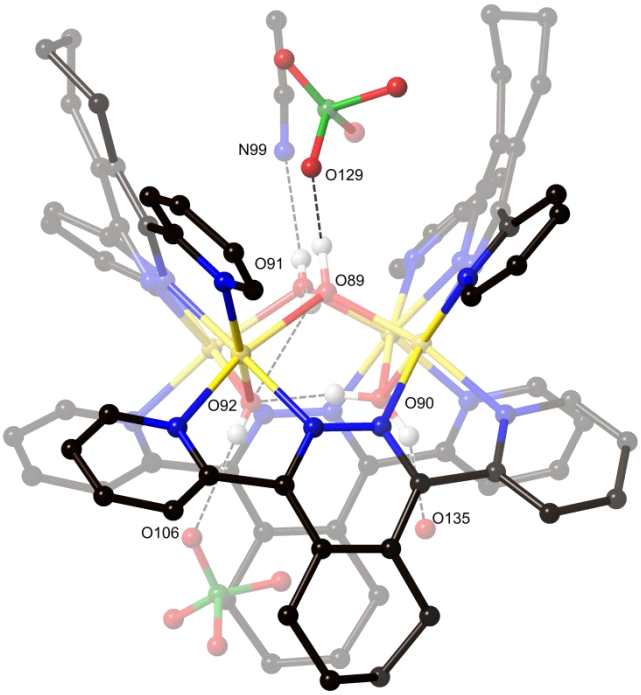

Figure 4.19: Hydrogen bonding interactions between the anion and solvates located in the two cavities formed by the parallel ligands of complex ***4.3****. Other solvates, anions and hydrogen atoms not involved in these interactions have been removed for clarity.*

The stronger hydrogen bonding interactions are between the bridging hydroxides and water molecules due to the structure holding these atoms in close proximity, O89-H89A···O91 2.520(4) Å, 150(17)° and O90-H90B···O92 2.542(5), 163(8). There is a hydrogen bond between the bridging hydroxide and the acetonitrile (N99), which is located at an angle 172(7)° and the bond length indicates a relatively strong H-bonding interaction.[10,11] The perchlorate anion to the bridging hydroxide shows a stronger H-bonding interaction compared to the other perchlorate anion to the

bridging water molecule. The major occupied solvate water molecule (87%) is involved in two hydrogen bonding interactions; one to a bridging hydroxide and the other to a nearby acetonitrile (O135-H13A···N93 2.499(17) Å, 136(6)°.

Bridging Molecule Type	D-H···A	Acceptor Molecule	D-A (Å)	D-H···A (°)
Hydroxides	O91-H91···N99	MeCN	2.847(7)	172(7)
	O92-H92···O106	ClO_4^-	2.847(7)	168(4)
Water	O89-H89B···O129	ClO_4^-	2.732(10)	128(16)
	O89-H89A···O91	^-OH	2.520(4)	150(17)
	O89-H89A···O92	^-OH	2.796(5)	121(14)
	O90-H90A···O135	H_2O (free)	2.652(7)	154(9)
	O90-H90B···O92	^-OH	2.542(5)	163(8)

*Table 4.6: Hydrogen bonding interactions observed in complex **4.3**.*

The ^{1}H-NMR titration and microanalysis indicate a 1:1 stoichiometry which is confirmed by the solid state structure. The twisting of the pyridyl pendant groups with respect to the pyridazine ring to remove any potential steric clash between the pyridyl protons and the fused cyclohexene ring. There were no interactions between the H10 and H11 protons with non-coordinated solvates or anions; however the proximity of anions, held within the cleft could lead to differentiation between these protons (inside versus outside).

Complex 4.4 – **L4** + zinc perchlorate hexahydrate

The complex **4.4** was isolated from vapour diffusion of diisopropyl ether into the reaction mixture of **L4** and $Zn(ClO_4)_2.6H_2O$ in acetonitrile. The colourless crystals analysed with a 1:1 metal-ligand stoichiometry.

Solution studies for complex **4.4** were carried out similar to the complexes described in this chapter. The coordination induced shifts are summarised in table 4.7. The CIS show a sizeable shift of all the pyridine ring protons in comparison to minor shifts for the fused cycloheptene ring. All of the protons experience downfield CIS, with an exception of proton H6 moving upfield which is very similar to the shifts associated with complex **4.3**. The protons on the fused cycloheptene ring show a splitting for H11 which could be due to an interaction with nearby anions or solvates, as previously seen in complex **4.3**.

	H3	H4	H5	H6	H10	H11	H12[c]
L4	7.86	7.98	7.49	8.73	3.00	1.71	1.89[c]
C4.4	8.12	8.32	7.82	8.42	3.32	1.87/1.76	2.00[c]
CIS[b]	+0.26	+0.34	+0.33	-0.31	+0.32	+0.16/+0.05	+0.11[c]

[a] For deuterated acetonitrile solutions. [b] CIS= $^{\delta}$complex-$^{\delta}$ligand. [c] Deuterated acetonitrile overlap.

*Table 4.7: ^{1}H-NMR Chemical shifts[a] and Coordination Induced Shifts[b] of complex **4.4.***

The ^{1}H-NMR titration was carried out with the same procedure and concentrations as described in complex **4.1**. The ^{1}H-NMR titration performed for complex **4.4** is shown in figure 4.20. The collated spectra show the same results as described in complex **4.3**. The addition of 0.2 eq. of metal salt solution the spectrum shows a broadening of the peaks. After 0.4 eq. is added there are seven peaks observed in the aromatic region which corresponds to more than one structure in solution, similar to complex **4.3**, these could be a helical and a grid-like structures. After 0.6 eq. is added, there is a loss of one species and the symmetry of one species is observed. A 1:1 metal-ligand stoichiometry is shown by this spectrum.

The UV-Visible data show a decrease in the two ligand peaks (λ_{max} = 269, 219 nm) and an increase of two peaks (λ_{max} = 291, 238 nm) further in the visible spectrum during the titration of metal equivalence added to the ligand seen in figure 4.21.

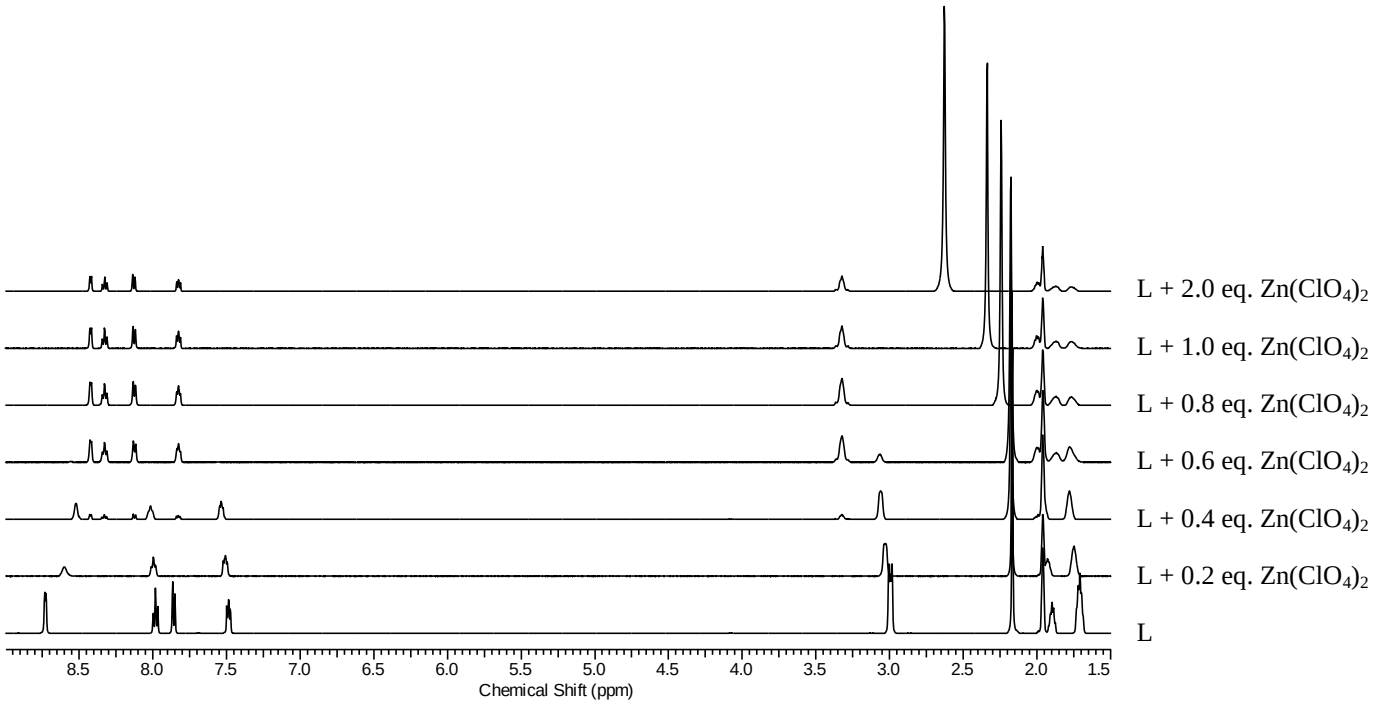

Figure 4.20: NMR titration to form complex 4.4.

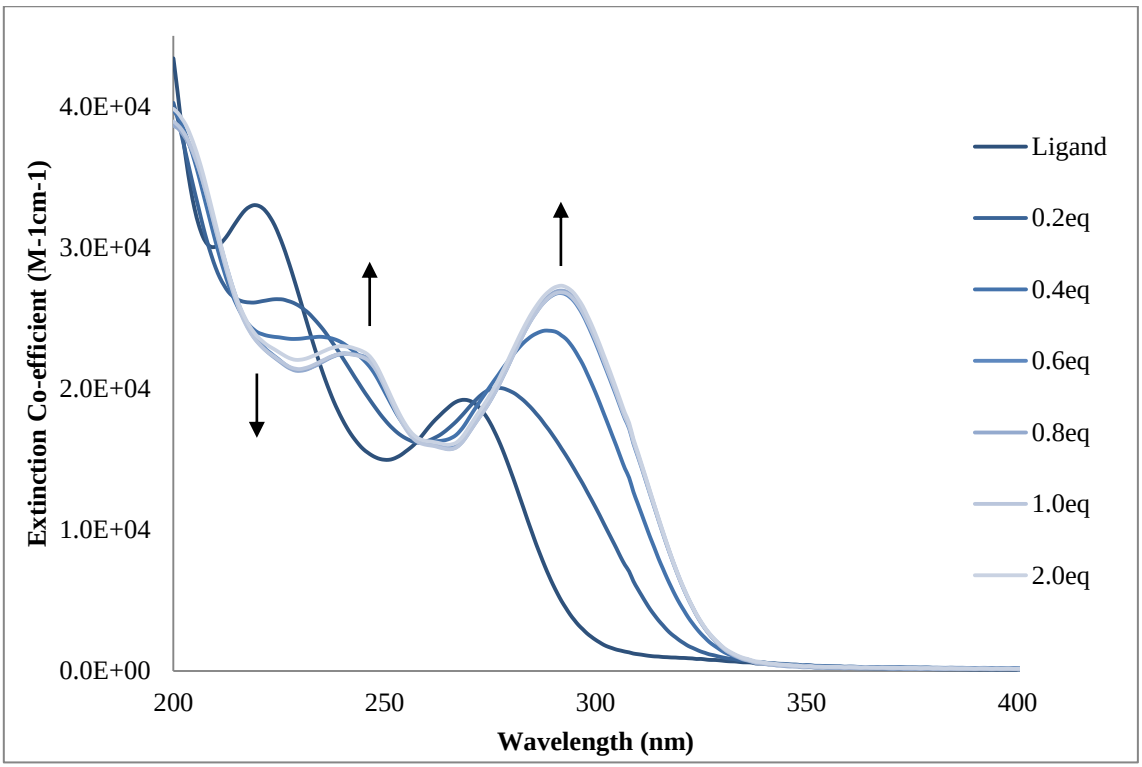

*Figure 4.21: UV-Vis spectroscopic titration plot of $Zn(ClO_4)_2$ against **L4** in acetonitrile to form complex **4.4**.*

The two titrations performed match well in metal equivalence addition to the ligand to form the complex in solution. A 1:1 metal-ligand stoichiometry is supported by both titrations. In complex **4.3** the high resolution mass spectrometry did not show a 1:1 ratio but a grid-structure was demonstrated. Nevertheless, the results for complex **4.4** ESI-MS show a ratio of 1:1 metal to ligand.

This complex, **4.4**, crystallises in the triclinic space group P-1, and has a grid-like structure, as shown in figure 4.22. The asymmetric unit contains four molecules of **L4**, bound to four zinc metals with two hydroxide and two water bridging atoms, as well as six perchlorate anions, seven non-coordinated acetonitrile and one water molecule.

The structure formed is similar to complex **4.3**. The hydrogen atoms on the hydroxide and water bridging atoms were located and refined as previously described for complex **4.3**. The coordinate geometry of the zinc metals are the same, coordinated to four nitrogen atoms and two oxygen atoms. The bond lengths and angles range from 2.025(3) Å – 2.205(3) Å and 74.91(14)° - 76.52(13)°, respectively and are summarised in table 4.8. The measurements are very similar which correspond to the same effects as previously mentioned and will not be discussed any further.

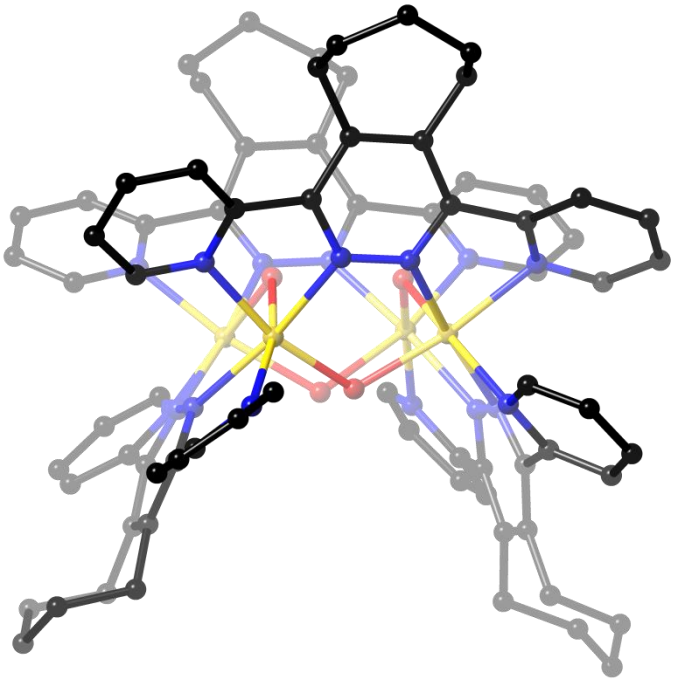

Figure 4.22: Grid-like crystal structure of complex **4.4**. *All anions, solvate molecules, hydrogen bonds, disorder on the backbone has been omitted for clarity.*

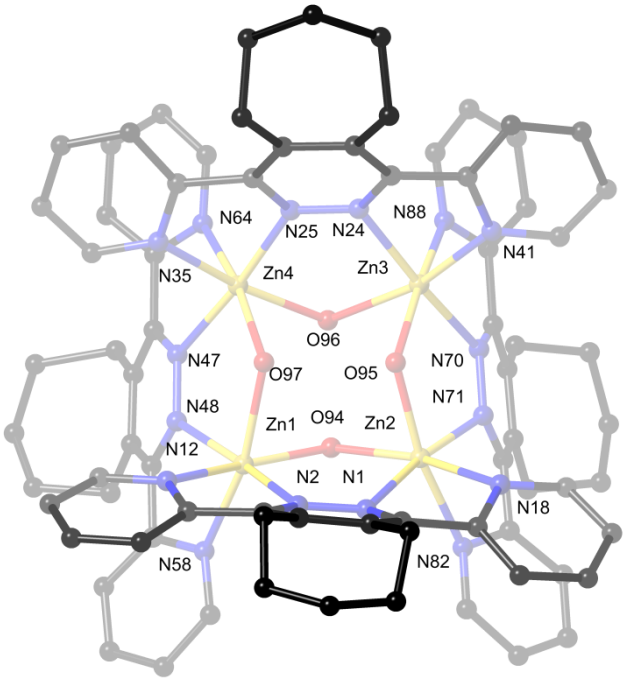

Figure 4.23: Complex ***4.4*** *with the selected atomic labelling.*

Bond Lengths			
Zn1-O94	2.025(3)	Zn3-O95	2.029(3)
Zn1-O97	2.205(3)	Zn3-O96	2.187(3)
Zn1-N2	2.157(3)	Zn3-N70	2.146(4)
Zn1-N58	2.128(3)	Zn3-N88	2.139(4)
Zn1-N48	2.170(3)	Zn3-N24	2.175(4)
Zn1-N12	2.142(3)	Zn3-N41	2.133(4)
Zn2-O94	2.052(3)	Zn4-O97	2.098(3)
Zn2-O95	2.074(3)	Zn4-O96	2.131(3)
Zn2-N18	2.198(3)	Zn4-N47	2.140(3)
Zn2-N71	2.156(3)	Zn4-N25	2.138(3)
Zn2-N1	2.159(3)	Zn4-N64	2.134(4)
Zn2-N82	2.200(4)	Zn4-N35	2.133(4)

Bite Angles	
N12-Zn1-N2	75.15(13)
N58-Zn1-N48	75.48(13)
N35-Zn4-N25	76.51(15)
N64-Zn4-N47	76.52(13)
N1-Zn2-N18	74.92(13)
N71-Zn2-N82	75.08(13)
N41-Zn3-N24	75.44(15)
N88-Zn3-N70	74.91(14)

Bridging Oxygen Angles	
Zn1-O94-Zn2	114.10(13)
Zn4-O97-Zn1	110.44(12)
Zn3-O95-Zn2	113.97(13)
Zn4-O96-Zn3	110.39(12)

*Table 4.8: Selected bond lengths (Å) and angles (º) for complex **4.4***

As described in the asymmetric unit, there are 4 bridging atoms; two water molecules and two hydroxides which contribute to the overall charge as discussed for complex **4.3**. These components within the structure are involved in hydrogen bonding interactions with nearby solvates and anions located in the cavities formed by the grid structure, (one perchlorate anion and one acetonitrile solvate in each cavity). These hydrogen bonding interactions are summarised in table 4.9.

Bridging Molecule Type	D-H···A	Acceptor Molecule	D-A (Å)	D-H···A (°)
Hydroxides	O94-H94···O122	ClO_4^-	2.924(4)	167(4)
	O95-H95···O100	ClO_4^-	2.813(7)	159(4)
Water	O96-H96B···O94	^-OH	2.564(3)	165(6)
	O96-H96A···N133	MeCN	2.766(5)	178(6)
	O97-H97A···O95	^-OH	2.534(4)	169(7)
	O97-H97B···N151	MeCN	2.678(5)	174(6)

*Table 4.9: Hydrogen bonding interactions observed in complex **4.4**.*

A very strong hydrogen bonding interaction is observed between one of the bridging water atoms (O96) with an acetonitrile (N133). However, the bond lengths between the hydroxides and water bridging atoms are relatively short in comparison due to the structure holding them in close proximity to one another. The other hydrogen bonding interactions are moderately strong, with the strongest being bridging water molecules with nearby acetonitrile solvates, followed by an

interaction between the hydroxide and the bridging waters and a weaker interaction observed between the hydroxides and nearby perchlorate anions.

The remaining perchlorate anions are not involved in hydrogen bonding, and are situated in the cavities formed by the fused cycloheptene ring and the twisting of the pyridine groups. The cycloheptene ring forms an envelope shape that helps form the occupied cavities. These anions do not show any significant interactions, with the closest possible being between the disordered perchlorate and disordered cycloheptene ring with distances of 3.60(6) Å (C77-O126) and 3.15(6) Å (C77-O125) confirming no adequate interaction.

The solution studies for complex **4.4** indicate the possible 1:1 metal to ligand stoichiometry. This is confirmed by the solid state structure as a grid-like structure. The effects associated with the CIS are similar to that of complex **4.3** with the same solid structure and similar solution studies observations.

Complex 4.5 – **L5** + zinc perchlorate hexahydrate

$Zn(ClO_4)_2.6H_2O$ with **L5** resulted in yellow crystalline material when diethyl ether was diffused into the reaction mixture in dichloromethane:acetonitrile (9:1). The crystals suitable for single crystal X-ray diffraction analysed with a 1:3 metal-ligand stoichiometry.

NMR spectroscopy and UV-Visible spectrophotometry were completed on crystals obtained for this complex, **4.5**. This complex was sparingly soluble in solvents; however it could be dissolved in d_6-DMSO and a ^{1}H-NMR spectrum of **4.5** shows only the ligand with no coordination observed. This observation may be due to the strong donor solvent, DMSO, however, ESI-MS indicates two possible complexes, $[Zn(\mathbf{L5})_2]^{2+}$ and $[Zn(\mathbf{L5})_3]^{2+}$. Due to the ligand and metal being insoluble in the same solvent, a ^{1}H-NMR titration was attempted using a solvent mixture. Unfortunately, during the titration precipitation occurred. UV-Visible spectroscopy was carried out and showed only the ligand, as seen in the ^{1}H-NMR.

This complex, **4.5**, crystallises in the monoclinic space group $P2_1/n$. The asymmetric unit contains one metal, three molecules of **L5**, two non-coordinated perchlorate anions and two non-coordinated solvate molecules, one acetonitrile and one dichloromethane.

As seen previously in the first two complexes within this chapter **4.1** and **4.2**, the coordination of the zinc metal in the helical structures is distorted octahedral with two nitrogen donor atoms from each ligand. The same coordination is observed in this complex **4.5**, the difference however is only

one metal is seen in this complex. The structure observed is a facial (*fac*) coordinated complex, as shown in figure 4.24. The complex formation being *fac* is unusual as it is statistically the less favourable isomer. The bond lengths for this complex range from 2.111(2) Å - 2.198(2) Å, bite angles from 74.82(8)º - 76.72(8)º and angles of opposite nitrogen atoms from 161.29(8)º - 168.05(9)º.

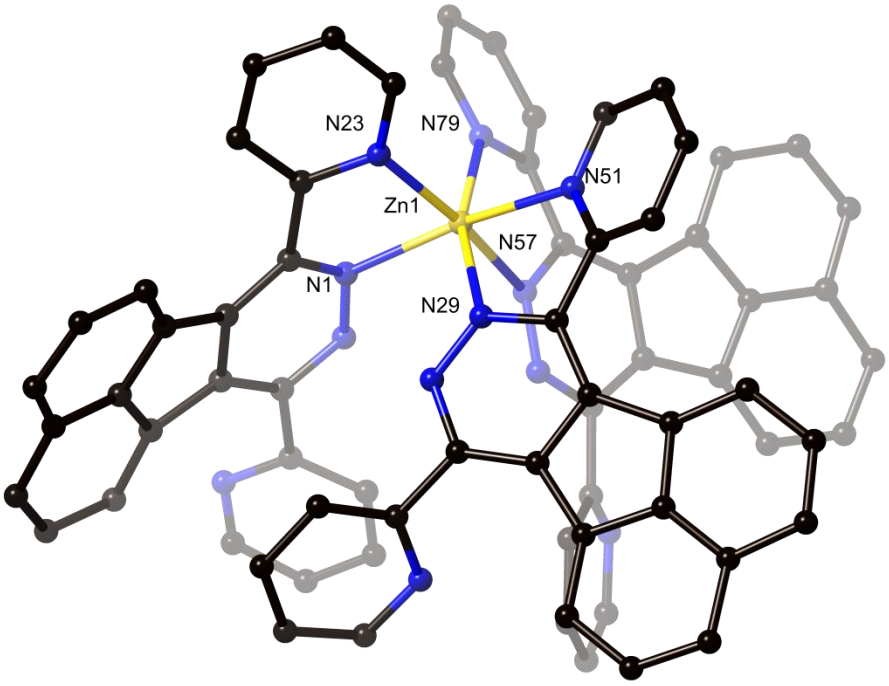

Figure 4.24. *Complex 4.5 helical structure showing the facial arrangement of the ligands and octahedral geometry. All anions, solvate molecules and hydrogen bonds have been omitted for clarity. Selected bond lengths (Å)* Zn1-N1 2.133(2), Zn1-N23 2.135(2), Zn1-N29 2.140(2), Zn1-N51 2.198(2), Zn1-N57 2.194(2), Zn1-N79 2.111(2) *and angles (º)* N1-Zn1-N23 76.72(8), N29-Zn1-N51 74.82(8), N79-Zn1-N57 76.68(8), N1-Zn1-N51 163.59(8), N23-Zn1-N57 168.05(9), N29-Zn1-N79 161.29(8).

Previous work by Cooke *et al.* showed substituted pyridazines forming *fac* and *mer* forms with ruthenium(II) and iron (II).[76] Facial isomers of coordination polymers have proven to be most valuable due to their C_3 symmetry giving greater control over directionality, however, this is statistically unfavourable in *tris* complexes.[76] Wiezman *et al.* developed a synthesis for selective *fac* isomer formation using a cyclic template for orienting the ligand strands.[120] However, in this complex, there is no cyclic template for orienting the structure; nevertheless a metal could be a potential template, two metals forming a triple helicate. However the rigid and sterically hindered fused ring on the ligand allows only one metal to bind upon crystallization.

The rigid acenaphthylene fused to the pyridazine ring enforces planarity on the core, which has, very little twisting 0.3(3)° – 2.6(3)° in comparison to the other helical structures within this chapter. The coordinated pyridyl-groups on the ligands show a five-membered chelation evident throughout this chapter. These three coordinated pyridyl groups are twisted out of the plane of the pyridazine core 26.85(9)°, 28.31(9)° and 31.66(9)° compared to the non-coordinated pyridyl groups being twisted 126.20(9)°, 136.78(9)° and 145.87(10)°. The twisting is due to the steric clash associated with the fused acenapthyl-group. The coordinated pyridyl groups have the potential H···H clash and the twisting relieves this resulting in distances between the two hydrogen atoms, ~2.16 Å. The non-coordinated pyridyl groups have a steric clash with the backbone N···H as well as a potential H-bond through the nitrogen but the twisting is too large for any interaction to occur.[7,10]

The anions and solvate molecules are situated around the complex structure (non-coordinated) which is a result of crystal packing effects.

Unfortunately solution studies were unable to be completed, however the ESI-MS results did indicate a 1:3 metal-to-ligand ratio which was the structure obtain by X-ray crystallography. Interestingly, the complex in coordinated as a *fac* isomer which is less favourable than the *mer* isomer. Metal temptation could be the reason for this complex formation.

Complex 4.6 – **L10** + zinc perchlorate hexahydrate

We decided to use the molecule, **L10** again to determine connectivity of this potential ligand with zinc. Different stoichiometric mixtures were set up of molecule **L10** and $Zn(ClO_4)_2.6H_2O$; 1:1, 1:2 and 1:3 metal-ligand ratios giving red solutions in acetonitrile. The metal-ligand stoichiometry 1:2 was the only successful mixture in growing crystals resulting in complex **4.6**. Crystals were grown by vapour diffusion of diisopropyl ether, resulting in large red needles, suitable for single X-ray diffraction. This successful combination may be due to the methyl substituents on the pyrazole heterocycle blocking the coordination of another ligand. This complex was synthesised to verify the coordination of the dimethyl-pyrazole group and see what zinc coordination preferences would be.

The same solution studies were carried out for complex **4.6**. The same procedures were adopted as described in complex **4.1**. Complex **4.6** was dissolved in d_3-acetonitrile and a ^{1}H-NMR spectrum collected and analysed with comparisons to the ligand spectrum with the coordination induced shifts shown in table 4.10. All protons experience a CIS, with H4 and H7 experiencing the greatest shifts both downfield by 0.32 ppm. The other methyl group proton, H6, experiences a smaller shift upfield. This shift could be due to the protons facing into the shielding zone of an aromatic region,

or interaction with nearby solvates or anions. H13 on the piperidyl- ring has a CIS upfield of 0.18 ppm; however the other protons on this ring have relatively small CIS of 0.08 ppm (H14) and 0.02 ppm (H15). These upfield shifts could potentially be due to these protons interacting with nearby solvates and anions.

	H4	H6	H7	H13	H14	H15
L10	6.15	2.28	2.44	3.98	1.73	1.78
C4.6	6.47	2.39	2.72	3.80	1.65	1.76
CIS[b]	+0.32	-0.11	+0.32	-0.18	-0.08	-0.02

[a] For deuterated acetonitrile solutions. [b] CIS= $^{\delta}$complex-$^{\delta}$ligand.

*Table 4.10: ^{1}H-NMR Chemical shifts[a] and Coordination Induced Shifts[b] of complex **4.6**.*

A ^{1}H-NMR titration was performed showing the coordinated induced shifts described above (figure 4.25). When the first 0.2 eq. of metal was added to the ligand, the spectrum shows a broadening of the peaks indicating an equilibrium of several species in solution. With the addition of 0.4 eq. the spectrum shows a symmetrical molecule and a shift of peaks upfield and downfield. There is no change observed to the spectrum after the addition of 0.6 eq. of metal. The stoichiometry is approximately 1:2 metal to ligand.

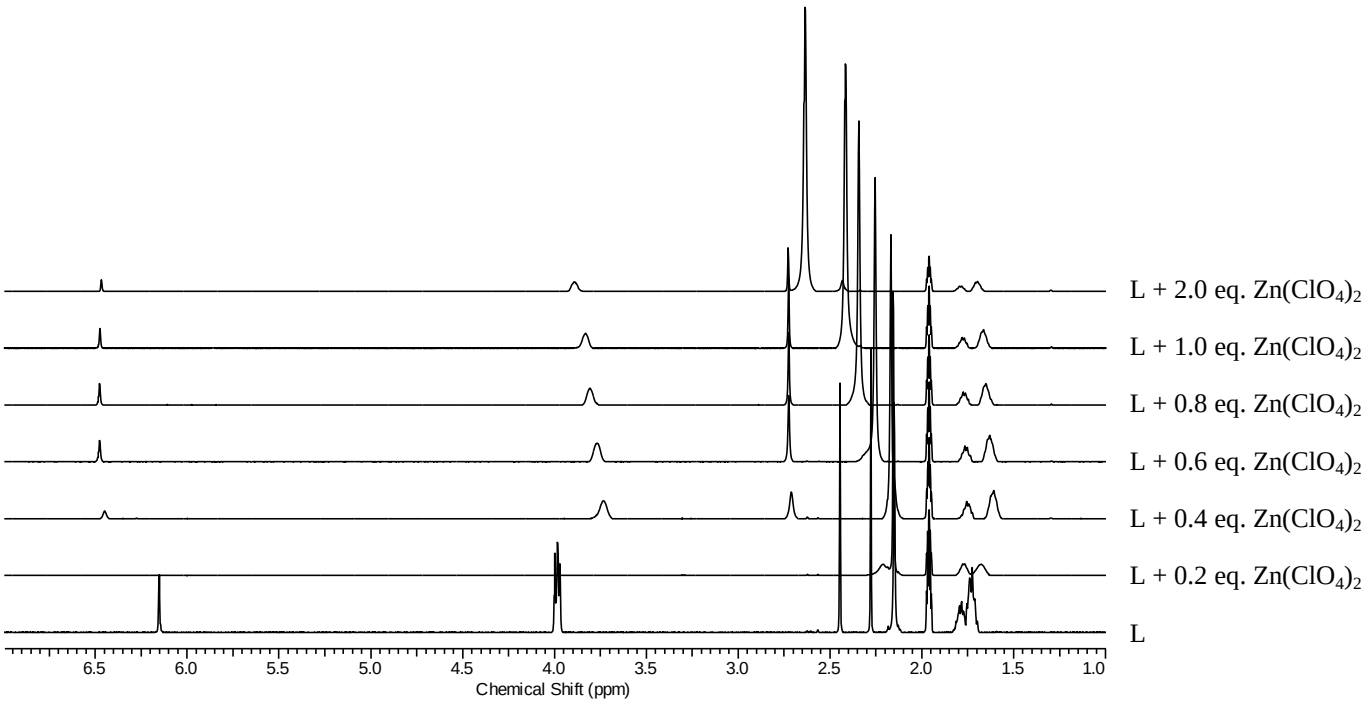

*Figure 4.25: ^{1}H-NMR titration to form complex **4.6**.*

The UV-Visible titration (figure 4.26) shows isosbestic points which clearly shows the formation of one complex in solution. The ligand spectrum shows maximum absorbance at 426 nm and 279 nm

with the loss of these peaks when the complex forms and maximum absorbance at 464 nm, 293 nm and 233 nm.

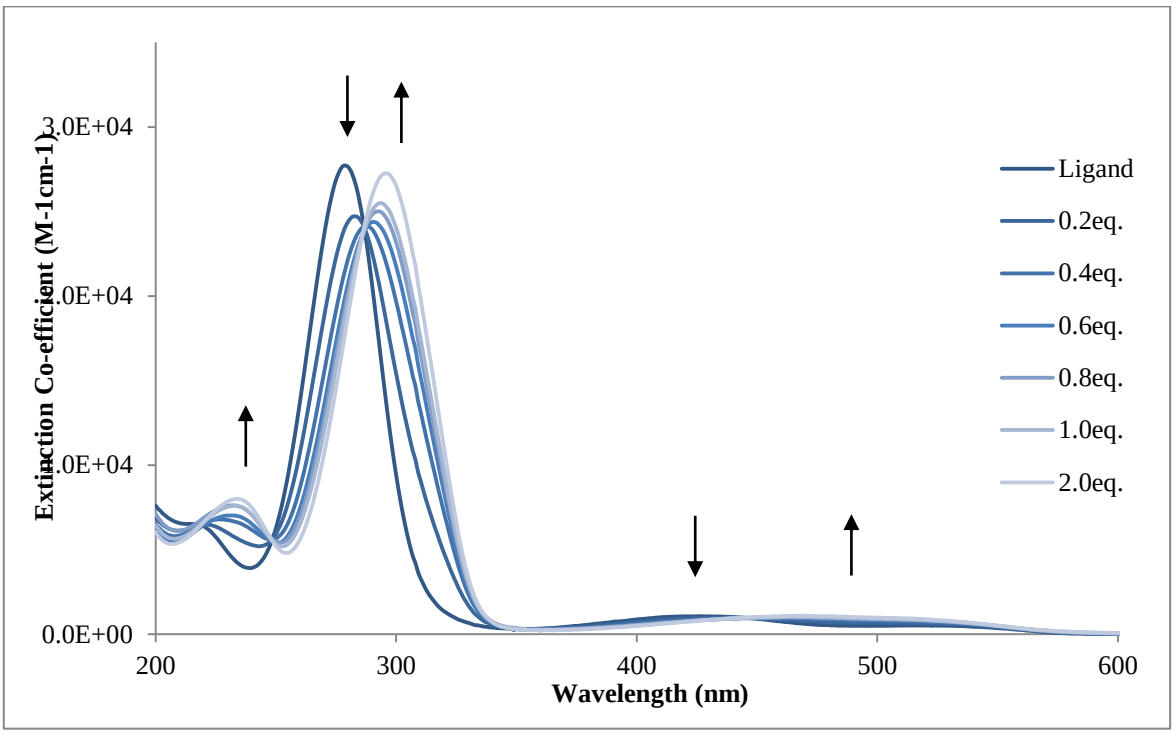

*Figure 4.26: UV-Vis spectroscopic titration plot of $Zn(ClO_4)_2$ against **L10** in acetonitrile to form complex **4.6**.*

The ESI-MS studies indicate a number of possible complexes in solution, $[Zn(\mathbf{L})_3(ClO_4)]^+$, $[Zn(\mathbf{L})_2(ClO_4)]^+$, $[Zn(\mathbf{L})_3]^{2+}$ and $[Zn(\mathbf{L})_2]^{2+}$. When the solution studies' data is collated, the possible metal to ligand stoichiometries could be 1:1 (UV-Visible) and 1:2 (NMR).

Complex **4.6**, crystallised in a triclinic space group P-1 with the asymmetric unit containing one zinc atom, two molecules of **L10**, two uncoordinated perchlorate anions and three acetonitrile solvent molecules; two of which are coordinated to zinc and one that is hydrogen bonded to one of the anions. The structure of this complex is shown in figure 4.27.

Zinc has a preference to be octahedral and this is shown in this complex. The zinc metal is coordinated to six nitrogen atoms, two from each ligand forming five membered chelating rings and the other two from the coordinated acetonitrile solvates. The bond lengths to the metal atom range from 2.0956(14) Å - 2.2722(13) Å. The shorter lengths are the nitrogen atoms bound to the coordinated solvent and the larger lengths being the nitrogen atoms of the tetrazine core structure. The pendant dimethylpyrazole groups are twisted out of the plane of the tetrazine core at angles of 10.88(6)° and 16.49(7)°, which is due to the sterically hindering methyl groups and chelating angle to the metal. The ligands are coordinated in a transoid manner resulting in the piperidinyl groups on

opposite sides. One of the piperidinyl groups is disordered in the two chair forms, with 71% being the larger occupancy.

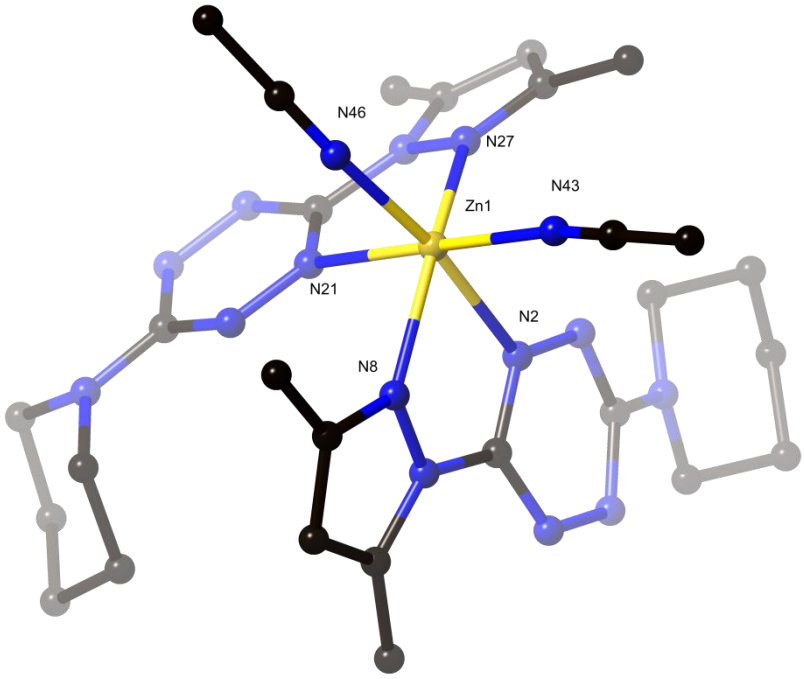

Figure 4.27: Perspective view of complex ***4.6****. All anions, solvate molecules, hydrogen bonds and minor occupancies have been omitted for clarity. Selected bond lengths (Å):* Zn1-N2 2.1968(12), Zn1-N8 2.1339(12), Zn1-N21 2.2722(13), Zn1-N27 2.1428(14), Zn1-N43 2.0956(14), Zn1-N46 2.0679(14) *and angles (°):* N2-Zn1-N8 74.64(5), N21-Zn1-N27 73.88(5).

There are two perchlorate anions, one of which is disordered over two sites with the larger occupancy being 84%. The non-coordinated acetonitrile molecule is in close proximity to this disordered perchlorate and has a strong hydrogen bond to one of the minor disordered oxygen atoms with the components measuring O62···H51a 1.998(16) Å. The perchlorate anions are located between the subunits with a significant number of interactions between the anions and the subunits. These H-bonding interactions are summarised in table 4.11, with the strongest interaction observed being between a major occupied perchlorate as the acceptor to a methyl group proton, 3.291(3) Å (D-A), 170.17(12)° (D-H···A).

The solution studies for complex **4.6** indicates a 1:2 metal-to-ligand stoichiometry from the ^{1}H-NMR titration, although the H13 proton signal is showing a small shift, this may be due to the different conformations of the piperidyl-ring. The ESI-MS results also showed the possibility of this stoichiometry; however, it was uncertain if this was a fragment of a larger complex. The solid state structure was only obtained with the ratio of 1:2 (metal-to-ligand), which indicates that it is the only stable solid state structure.

D-H···A	D-A (Å)	D-H···A (°)	D-atom type	Major/Minor ClO_4^-
C18-H18A···O56	3.509(3)	172.21(12)	'H14' on ligand	Fully Occupied
C31-H31C···O63	3.296(3)	132.53(12)	Methyl-H	Fully Occupied
C12-H12A···O62	3.239(19)	123.9(3)	Methyl-H	Minor
C12-H12A···O61	3.291(3)	170.17(12)	Methyl-H	Major
C45-H45A/C···O61	3.391(3)	139.44(12)	MeCN	Major
C45-H45C···O59	3.137(3)	125.68(12)	MeCN	Major
C13-H13A···O54	3.396(3)	144.31(11)	Methyl-H	Fully Occupied
C10-H10···O65	3.365(3)	149.31(12)	H4	Major
C35-H35A···O64	3.327(14)	159.1(4)	'H14' on ligand	Minor
C51-H51A···O62	2.898(17)	155.3(6)	-	Fully Occupied

*Table 4.11: Summary of the hydrogen bonding interactions observed in complex **4.6**.*

Complex 4.7 – **L6** + zinc perchlorate hexahydrate

The reaction of **L6** with $Zn(ClO_4)_2$ resulted in a colourless solution and after vapour diffusion of diethyl ether, crystals of complex **4.7** were obtained that were suitable for single X-ray crystallography. The complex analysed with a 2:3 metal-ligand stoichiometry.

NMR spectroscopy, UV-Visible spectrophotometry and ESI-Mass Spectrometry were completed for the solution studies analysis of complex **4.7**. The coordination induced shifts are shown in table 4.12. Protons H10 and H4 experience downfield shifts of 0.24 ppm and 0.17 ppm respectively. The two methyl groups do not experience significant CIS downfield (0.11 ppm and 0.12 ppm, for H6 and H7, respectively). The shifts of the protons indicate complexation but no significant structural features can be determined.

	H4	H6[c]	H7	H10
L6	6.16	2.28	2.67	8.19
C4.7	6.33	2.39[c]	2.79	8.43
CIS[b]	+0.17	+0.11	+0.12	+0.24

[a] For deuterated acetonitrile solutions. [b] CIS= $^{\delta}$complex-$^{\delta}$ligand. [c] Solvent overlap.

*Table 4.12: ^{1}H-NMR Chemical shifts[a] and Coordination Induced Shifts[b] of complex **4.7***

A ^{1}H-NMR titration was carried out for complex **4.7**, shown in figure 4.28b, using the same procedure as complex **2.1**. Interestingly, a different spectrum is observed to the dissolved complex

(figure 4.28a). The addition of 0.2 eq. and 0.4 eq. metal salt solutions indicates more than one species in solution as there is broadening of all peaks. The 0.6 eq. and 0.8 eq. additions show small broadened peaks indicating two possible complex species in solution. When the addition of metal salt is at a 1:1 metal-to-ligand ratio, there is distinctly two species in solution, the smaller peak at 8.57 ppm has an integral value of 10% of the peak at 8.44 ppm. The peak at 6.50 ppm has a similar integral value difference to the peak at 6.36 ppm. When these proton signals are compared to the dissolved complex spectrum, it indicates that the smaller integral is possibly a side product. The UV-Visible titration, displayed in figure 4.29, shows a decrease in the ligand wavelength maximum at 281 nm and an increase in a wavelength maximum at 289 nm. There are no observed isosbestic points and the titration does not indicate a specific metal to ligand stoichiometry.

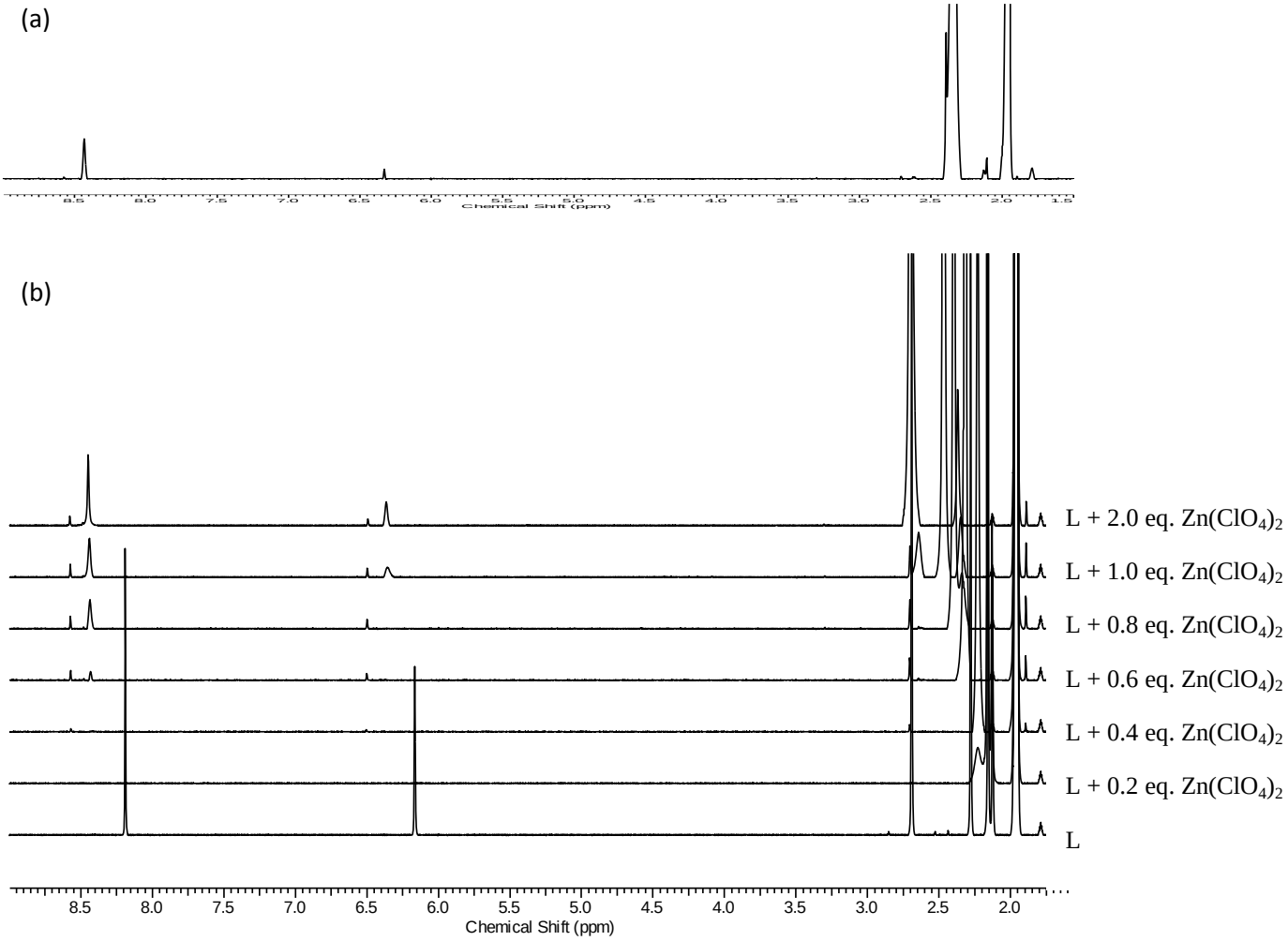

Figure 4.28: (a)[1]H-NMR of complex 4.7; (b) [1]H-NMR titration to form complex 4.7.

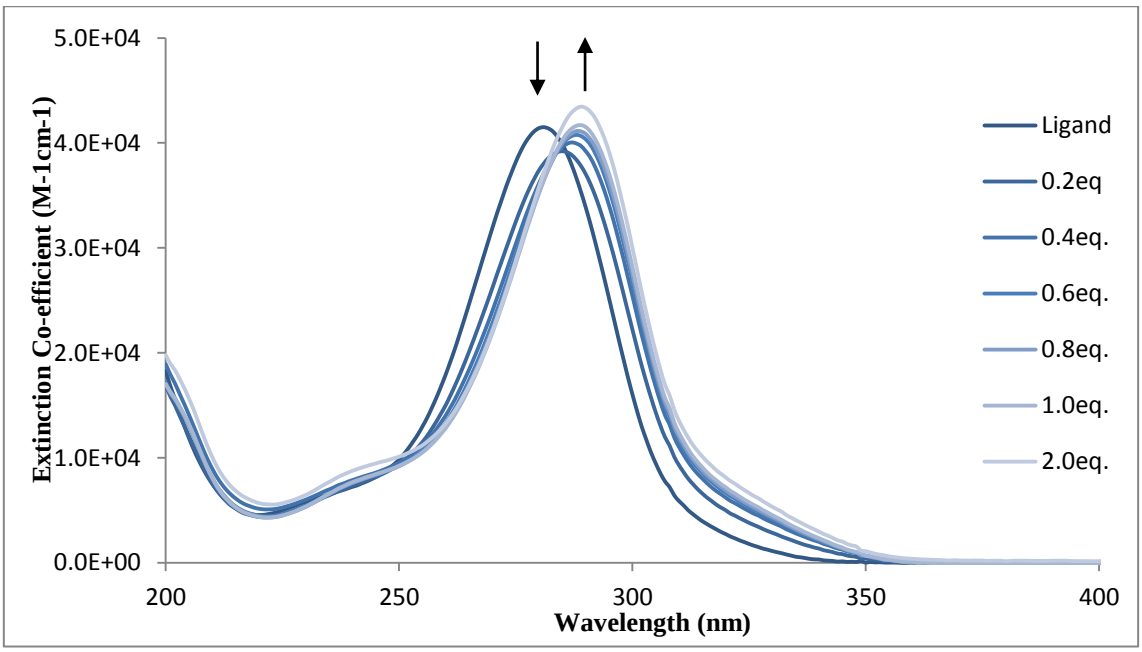

*Figure 4.29: UV-Vis spectroscopic titration plot of $Zn(ClO_4)_2$ against **L6** in acetonitrile to form complex **4.7**.*

Complex **4.7** crystallises in the trigonal space group, P-3c1. The asymmetric unit consists of three zinc metals with a third occupancy for each, one and a half molecules of **L6** and three perchlorate anions; two with half occupancies and the third disordered over two sites with the largest occupancy, 90%. Two discrete triple helical structures, $[Zn_2(\mathbf{L6})_3]$ are present in complex **4.7**. The two helices are of different enantiomers, with the right handed (Δ = *P*) helicate located along a threefold axis and the left handed (Λ = *M*) helicate is positioned on a three-fold rotation axis. All four zinc metals are octahedral, coordinated to six nitrogen atoms, two from each ligand forming bite angles, ~73°. The two helical structures are shown in figure 4.30 with the selected atomic labelling. The bond lengths to the nitrogen atoms range from 2.103(3) Å – 2.208(3) Å, with the small lengths being the nitrogen located on the dimethyl-pyrazole groups. The chelating angles are smaller than previously seen for the pyridine group, ~73° compared to ~75°; this difference is due to the change to a five-membered heterocyclic ring. The dimethyl-pyrazole rings of **L6** are slightly twisted (12.4(4)° for *M*-helicate and 12.68(14)° and 17.31(15)° for *P*-helicate), due to the twisting to form the helicate.

The anions are located in space with no significant interactions between other components in the complex.

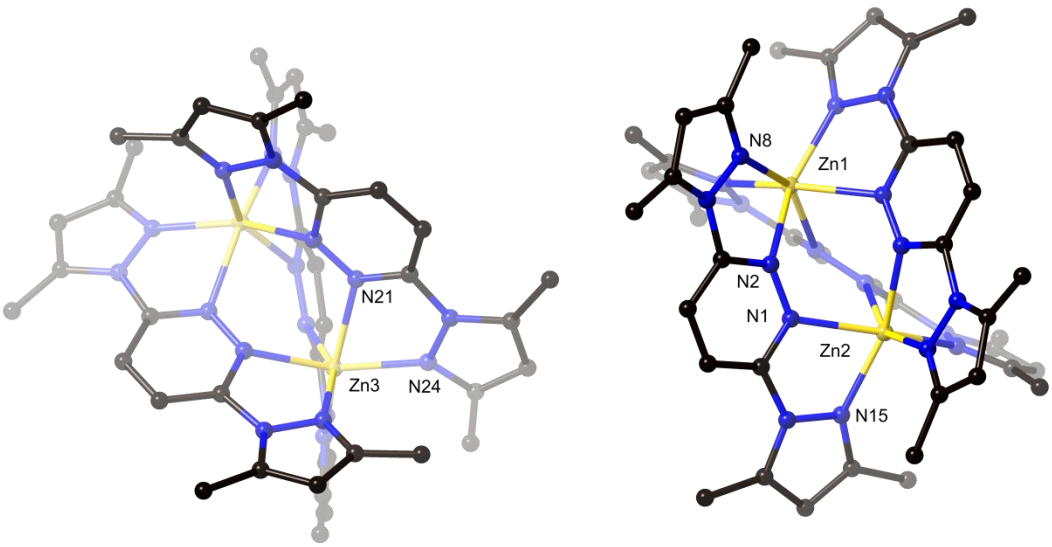

Figure 4.30: The two independent helical structures of complex ***4.7****. All anions, solvate molecules and hydrogen bonds have been omitted for clarity. Left handed helicate (left), right handed helicate (right). Selected bond lengths (Å):* Zn1-N2 2.208(3), Zn1-N8 2.116(3), Zn2-N1 2.189(3), Zn2-N15 2.103(3), Zn3-N21 2.183(3), Zn3-N24 2.113(3) *and angles (°):* N2-Zn1-N8 72.53(11), N1-Zn2-N15 72.98(11), N21-Zn3-N24 73.29(11).

Solution studies for complex **4.6**, indicated two possible species in solution, and it could possibly be a helicate and grid structure. The resulting solid state structure is a triple stranded saturated homotopic helicate. This species could be explored further into understanding the other species in solution, including the minor peaks evident in the ^{1}H-NMR titration.

Complex 4.8 – **L11** + zinc perchlorate hexahydrate

The next complex was investigated to determine if zinc would form polymeric species or discrete species with molecule **L11**, and what coordination geometry would the metal ion prefer when additional donor atoms are added to the pendant groups (pyrazine). Red needle like crystals of complex **4.8** were obtained upon vapour diffusion of diethyl ether into the red reaction solution of **L11** and $Zn(ClO_4)_2$ in acetonitrile. These crystals seemed to lose solvent quickly, however they were able to be obtained in reasonable yield (57.7%) and were analysed to have a 1:1 metal-ligand stoichiometry.

Solution studies were completed for complex **4.8**, as described previously. The complex was dissolved in d_3-acetonitrile and a ^{1}H-NMR spectrum collected and compared to the ligand spectrum. The coordination induced shifts are summarised in table 4.13, with all protons experiencing a

downfield shift of 0.29 ppm, 0.12 ppm, and 0.05 ppm, for H3, H6 and H5, respectively. Thus indicating no shielding of protons, however these shifts could be due to interactions with nearby solvates and anions.

	H3	H5	H6
L11	9.84	8.93	8.97
C4.8	10.13	8.98	9.09
CIS[b]	+0.29	+0.05	+0.12

[a] For deuterated acetonitrile solutions. [b] CIS= $^{\delta}$complex-$^{\delta}$ligand. [c] Solvent overlap.

*Table 4.13. ^{1}H-NMR Chemical shifts[a] and Coordination Induced Shifts[b] of complex **4.8***

A ^{1}H-NMR titration was carried out for complex **4.8**, however no consistent results can be determined due to the likely formation of a polymeric structure. The ESI-MS results show three possible fragmented products, $[Zn(\mathbf{L11})_2]^{2+}$, $[Zn(\mathbf{L11})ClO_4]^{+}$ and $[Zn(\mathbf{L11})_2(ClO_4)]^{+}$.

Complex **2.8** crystallises in the monoclinic space group $P2_1/a$, with the asymmetric unit consisting of one metal, one molecule of **L11**, two coordinated acetonitrile solvates, two non-coordinated acetonitrile solvates and two perchlorate anions.

The zinc metal adopts an octahedral geometry to two pyrazinyl-nitrogen's, two tetrazine-nitrogen's and two acetonitrile solvates, as displayed in figure 4.31. The Zn-N bond lengths to the N from the solvates are marginally smaller than the ligand nitrogen atoms (2.068(4) Å and 2.106(4) Å compared with 2.117(4) Å - 2.299(4) Å) which show similar results to what was observed in the tetrazine complex **4.6**.

The pyrazinyl pendant groups are twisted out of the plane of the tetrazine core 4.08(14)° and 4.97(14)° which is the smallest twist observed when zinc is the coordinated metal. The planar ligand with no hindering substituents is the reason for this small twist. This ligand as previously mentioned in the introduction has more donor atoms, which has the potential to bridge different subunits and has the potential to form polymeric structures. Complex **4.8** is a one-dimensional polymer shown in figure 4.32, that propagates along the *a* axis. The perchlorate anions and solvates are located in space with no significant interactions observed.

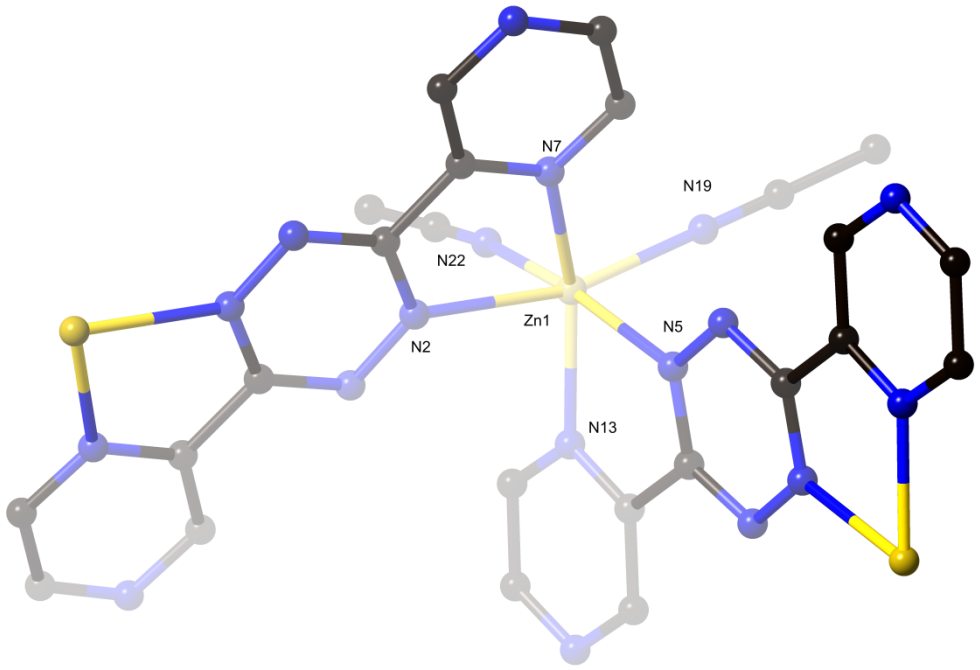

Figure 4.31: Perspective view of complex 4.8, showing the distorted octahedral coordination of the zinc metal. Selected bond lengths (Å): Zn1-N2 2.255(4), Zn1-N5 2.299(4), Zn1-N7 2.117(4), Zn1-N13 2.151(4), Zn1-N19 2.106(4), Zn1-N22 2.068(4) *and angles (°):* N2-Zn1-N7 74.72(14), N5-Zn1-N13 73.15(13).

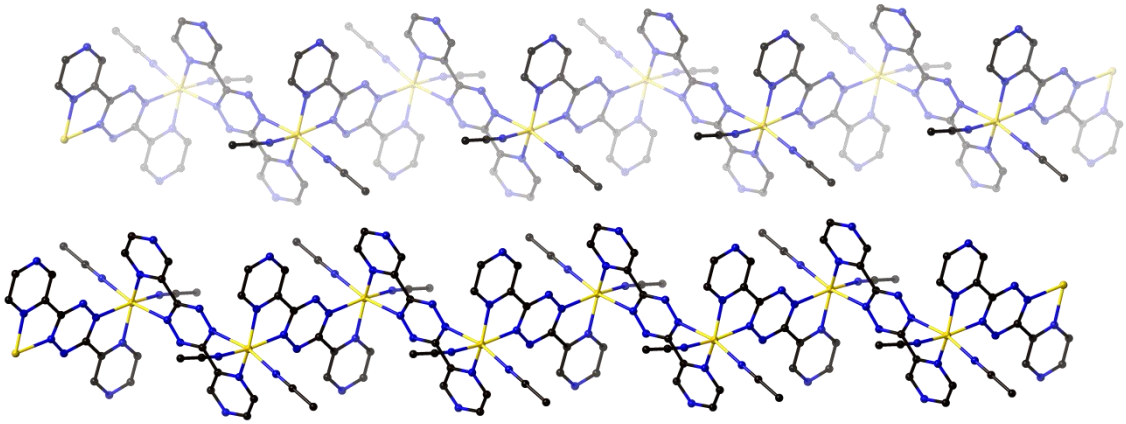

Figure 4.32: One dimensional polymeric structure showing two polymers side by side.

4.5 Summary

A range of metallosupramolecular assemblies formed with Zn(II), with a range of different ligands, **L1** - **L6**, **L10** and **L11**. Unexpected formations of three helical structures were obtained with the pyridazine ring ligands, **L1** and **L6** and the cyclopentene fused ring molecule **L2**. Interestingly a

grid structure was obtained with the larger fused rings, cyclohexene and cycloheptene with the pyridine pendant rings.

Similar to the silver complexes, the increase in the size of substituents at the 4- and 5- positions fused ring system from hydrogens (pyridazine) to cyclopentene, cyclohexene, and cycloheptene showed an increase in the twisting of the coordinated pendant groups from an average of ~12° to an average of ~33°. This however shows different structures to the other chapters, as zinc triple helicates are observed in the less hindering groups, compared to two grid structures.[36,60] The larger fused ring systems form grid-like complexes instead, refer to table 4.14.

All structures obtained showed zinc in a six-coordinated octahedral geometry with, in a few structures, solvates (acetonitrile, water and hydroxides) coordinated to obtain this preference and to balance the charge of the complex.

The metallogrids obtained for complex **4.3** and **4.4** are the first grids to be obtained with bridging hydroxides and water molecules.

Overall it can be concluded that there is more of a link between the solution studies and solid state results with zinc(II) as the metal. After the resolution of the first complex **4.1**, due to similar coordination induced shifts in the ^{1}H-NMR, it was possible that the **4.2** solid state complex was also a helicate. It was possible that a different structure would be seen in complex **4.3** and **4.4** due to different CIS observed, and indeed this was the case. However, unfortunately the prediction of the dimethylpyrazole molecules and pyrazine molecules with Zn(II) were unable to be predicted, as very little to no CIS were observed and this could be due to the lack of appropriate protons for the analysis.

A summary of the structures obtained with each ligand is shown in table 4.14. The differences in structures are due to the sterically hindering substituents and conformational strain of the ligands, as well as zinc metals coordination preferences

Table 4.14: Summary of the ligands complexed with zinc and the structures identified by X-ray crystallography. All complexation occurred with $Zn(ClO_4)_2$.

C.	Ligand structure	Structure		
4.1	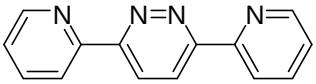 **L1**	$[Zn_2(\mathbf{L1})_3]^{4+}$ Triple helicate	-	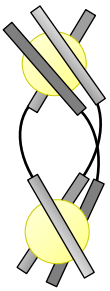
4.2	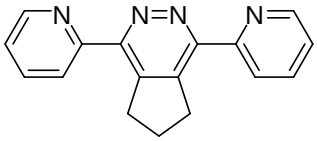 **L2**	$[Zn_2(\mathbf{L2})_3]^{4+}$ Triple helicate	-	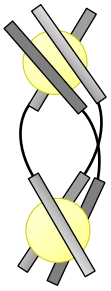
4.3	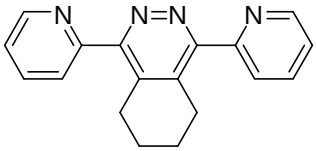 **L3**	$[Zn_4(\mathbf{L3})_4]^{6+}$ Metallogrid	2 x ^{-}OH 2 x H_2O	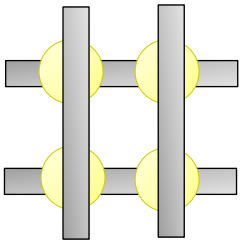
4.4	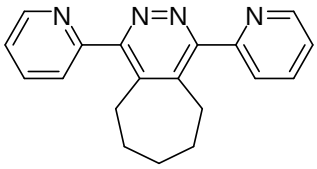 **L4**	$[Zn_4(\mathbf{L4})_4]^{6+}$ Metallogrid	2 x ^{-}OH 2 x H_2O	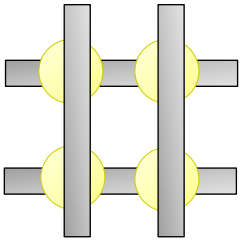
4.5	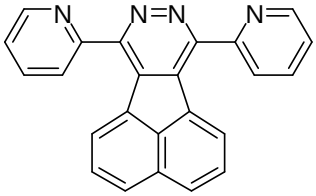 **L5**	$[Zn(\mathbf{L5})_3]^{2+}$ Facial isomer	-	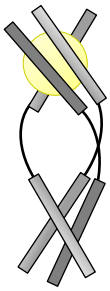

4.6	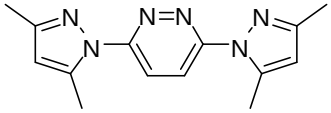 **L6**	$[Zn_2(\mathbf{L6})_3]^{4+}$ Triple helicate	-	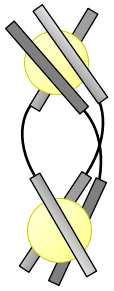
4.7	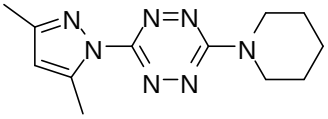 **L10**	$[Zn(\mathbf{L10})_2]^{2+}$	2 x MeCN	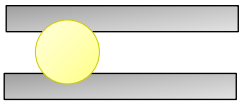
4.8	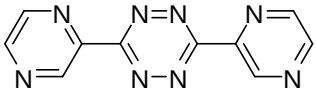 **L11**	2D Polymer	2 x MeCN	Polymer

CHAPTER FIVE

Conclusion and Future Work

Present study

This thesis investigated twenty-five new metallosupramolecular architectures prepared from sixteen ligands showing that a wide range of structures are possible with the three selected d^{10} metals, silver(I), copper(I) and zinc(II). The approach to form these architectures utilised metal-to-ligand coordination bonds between the N-donor atoms on the heterocyclic ligands and the selected metal atoms.

It was hoped that grid-like arrays would form due to the specific design of the rigid ligands and the preferred coordinate geometries of the metals. Also it was hoped to determine structures in solution by comparing the solid state results with the coordination induced shifts and information obtained from the ^{1}H-NMR spectroscopy and UV-Visible spectrophotometry titrations.

The majority of the complexes analysed by single crystal X-ray structure analysis are discrete structures (seventeen) and the other eight are polymeric.

The polymeric structures were observed when coordinating atoms were used, and also, when more donor atoms were introduced within the ligand (pyrazine as the pendant group). Interestingly, tetra-bridging ligands were observed to form with Ag(I) when the sterically hindering fused ring and methyl groups were introduced on the ligand. Within these structures, Ag···Ag interactions are observed as the metals are held in close proximity. The larger fused rings, cyclohexene and cycloheptene formed grid like structures with zinc, however, the attempts to crystallise Cu(I) complexes with these ligands were unsuccessful. The pyridazine substituted ligands, resulted in grid like structures (Ag(I)[60], Cu(I)), side-by-side complexes (Ag(I)), and helicates (Zn(II)).

It should be noted that the complexes with the cyclohexene fused ring ligands took longer to crystallise and were modelled to be disordered in the two different chair conformations, compared to both the cyclopentene and cycloheptene fused ring systems which were both observed in an envelope conformation. These crystals on average were obtained in less time, with the exception for complex **3.3** (the oxidation of Cu(I) to Cu(II)).

It can be concluded that there is no real evidence to link the solution studies and the solid state structures. The ligands containing the pyridine rings as the pendant groups give more evidence from the solution studies, to predict the possible solid state structures. However, silver being promiscuous and adopting a range of geometries, two, three, four and five coordinate observed in this study, no definite conclusions can be made. In the zinc chapter, there is more of a link between the solution studies and the determined solid state structures, with stoichiometric comparisons being observed.

Thus, the seventeen ligands prepared for this thesis were investigated with the aim of forming interesting metallosupramolecular architectures. The variety of metals and ligands allowed this, and the structures were investigated by X-ray crystallography.

Future work

Purification of 7,10-bis(2-pyrazinyl)-8,9-difluoranthene (figure 5.1) was unable to be completed due to time restrictions, however it would be interesting to observed the effect the extra donor atoms have on the overall metallosupramolecular architecture formed with the d^{10} metals explored in this study. Larger ligands with pyrazole-pyridine as the pendant group on a pyridazine ring has recently been reported in the literature,[121] however, no complexation has been attempted with the metals mentioned within this thesis. The molecule 3,6-bis(3-pyridyl-1-pyrazolyl)-1,2,4,5-tetrazine (figure 5.1) could also be synthesised and a Diels-Alder reaction done to synthesise sterically hindering components, as seen in this study to the pyridazine ring. It would be interesting to investigate the metallosupramolecular self-assembly of these potential ligands.

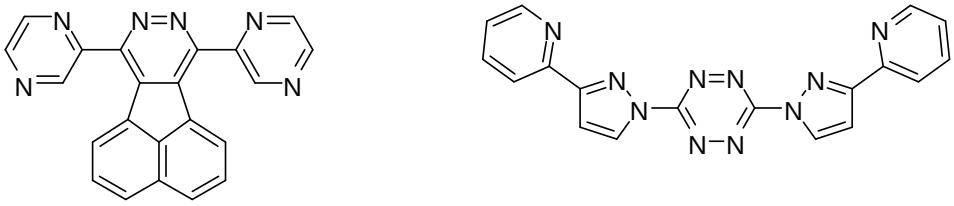

7,10-bis(2-pyrazinyl)-8,9-difluoranthene 3,6-bis(3-pyridyl-1-pyrazolyl)-1,2,4,5-tetrazine

Figure 5.1: Potential molecules for future work.

Other d^{10} metals could be investigated with the molecules synthesised and complexation with **L16**. The exploration into knowledge of structure in solution can be done in further detail.

These ligands and complexes have the potential to be luminescent. Luminescence of the complexes was tested at room temperature; however no luminescence was observed and is therefore not discussed here. Low temperature luminescence would be another future direction for this work into potential applications.

CHAPTER SIX

Experimental Methods

6.1 General Experimental

All reagents and starting materials were reagent grade, obtained from commercial sources and used as received, unless otherwise stated. Elemental analysis was carried out by the Campbell Microanalytical Laboratory, located at The University of Otago. Melting points were obtained on a Electrothermal melting point apparatus and are uncorrected.

Nuclear Magnetic Resonance

NMR spectra were recorded at 23°C on Varian INOVA 400 or Varian Unity INOVA 500 spectrometers, operating for ^{1}H, at 400 MHz and 500 MHz, respectively and for ^{13}C, at 100 MHz and 125 MHz, respectively. Commercially available deuterated solvents ($CDCl_3$, CD_3CN and DMSO) were used to dissolve all samples for analysis. Chemical shifts in this thesis are described in parts per million (ppm), and were referenced to the appropriate residual solvent peaks. Tetramethylsilane (TMS) were used as an internal reference. When required, COSY, 1-D TOCSY, HSQC and HMBC experiments were performed using standard Varian and Agilent pulse sequences available on both spectrometers.

Mass Spectrometry

Electrospray ionisation mass spectra (ESI MS) were recorded by Dr. Marie Squire on either a DIONEX ultimate 3000 or Bruker MaXis 4G spectrometer, both of which operated in high resolution positive ion electrospray mode. The samples were dissolved in HPLC grade acetonitrile or methanol and were submitted with the required concentrations.

Infrared Spectroscopy

All infrared spectroscopy were recorded on a Bruker ALPHA FT-IR spectrometer with diamond ATF configuration, DTGS 4000-430 cm^{-1}. The samples collected 8 scans at 4 cm^{-1} resolution. Where necessary the products were made finer for the IR collection.

UV/Visible Spectroscopy

UV/Visible spectra were recorded on a Varian CARY 100 Bio UV/Visible spectrophotometer in the range 800-200 nm in either acetonitrile or dichloromethane. The samples were measured at room temperature in quartz curvettes with a path length of 1 cm.

X-ray Crystallography

Refinement data is presented in Appendix 1. X-ray crystallographic data collection and refinement was carried out on an Oxford-Agilent SuperNova instrument with focused microsource Cu Kα (λ= 1.51418 Å) radiation or Mo Kα (λ0.71073 Å) and ATLAS CCD area detector. All structures were solved using direct methods with SHELXS[122] and refined on F^2 using all data by full matrix least-squares procedures with SHELXL-97[123] within OLEX-2.3.[124] Non-hydrogen atoms were refined with anisotropic displacement parameters. Hydrogen atoms were placed in calculated positions or manually assigned from residual electron density where appropriate unless otherwise stated. The functions minimised were Σ*w*(*F2*o-*F2c)*, with *w* = [σ2(F2o) + *a*P2 + *bP*]-1, where *P* = [max(Fo)2 + 2F2c]/3. Graphical representations of crystallographic data were prepared using Olex2. The isotropic displacement parameters are 1.2 times the isotropic equivalent of their carrier atoms. The reported refinement values may change upon publications. Selected bond lengths and angles are listed in the discussion of the structures. Graphical representations of crystallographic data were prepared using the CrystalMaker. The remaining measurements for distances and angles, as well as other information such as atom coordinates, anisotropic displacement parameters and hydrogen atom coordinates are available from the Chemistry Department, University of Canterbury on request.

6.2 Ligands

The following compounds were prepared by literature procedures:

3,6-di(2-pyridyl)pyridazine **L1**,[54] 1,4-di(pyridin-2-yl)-6,7-dihydro-5H-cyclopenta[d]pyridazine **L2**,[54] 1,4-di(pyridin-2-yl)-5,6,7,8-tetrahydrophthalazine **L3**,[54] 1,4-di(pyridin-2-yl)-6,7,8,9-tetrahydro-5H-cyclohepta[*d*]pyridazine **L4**,[54] 7,10-di(pyridin-2-yl)-8,9-difluoranthene **L5**,[55] 1,4-bis(3,5-dimethylpyrazol-1-yl)-6,7-dihydro-5*H*-cyclopenta[*d*]pyridazine **L7**,[57] 1,4-bis(3,5-dimethylpyrazol-1-yl)-5,6,7,8-tetrahydrophthalazine **L8**,[57] 7,10-bis(3,5-dimethyl-1*H*-pyrazol-1-yl)-8,9-diazafluoranthene **L9**,[55] 3-(3,5-dimethyl-1*H*-pyrazol-1-yl)-6-(1-piperidinyl)- 1,2,4,5-tetrazine **L10**,[58] 3,6-bis(2-pyrazinyl)-1,2,4,5-tetrazine **L11**.[125]

3,6-bis(3,5-dimethylpyrazolyl)pyridazine **L6**

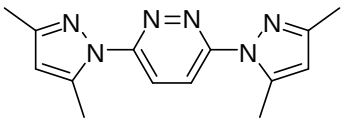

This molecule was synthesised adopting a slight modification of the literature procedure of Rusinov *et al.*.[57] A solution of 3,6-bis(3,5-dimethylpyrazol-1-yl)-1,2,4,5-tetrazine (0.5g, 1.85mmol) with ethyl vinyl ether (0.753 g, 10.44 mmol) in dry toluene (5 mL) was heated in a pressure tube to 120°C for one hour. During this time, the reaction colour went from pink to mustard yellow. The reaction mixture was cooled to room temperature, solid impurities were filtered and the filtrate was evaporated under reduced pressure to give the desired product as an off-white solid. This off-white solid was recrystallized from methanol resulting in a white fluffy product. (0.3114 g, 63%). ^{1}H-NMR and Mass Spectrometry analysis are consistent with the reported literature.

3,6-bis(2-pyrazinyll)pyridazine **L12**

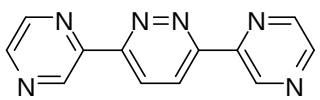

Adopting the method constructed for L6; To a dry pressure tube, 3,6-bis(2-pyrazinyl)-1,2,4,5-tetrazine (0.37 g, 1.55 mmol) with ethyl vinyl ether (0.753 g, 10.44 mmol) was added, followed by dry toluene (5 mL) then heated overnight at 120°C. During this time, the reaction colour went from pink to a pale yellow colour. The reaction mixture was cooled to room temperature, and the solid precipitate filtered. The off white solid was dried under the high vac. and analysed to be pure. Yield: 85.8%. Mp: 332°C.

^{1}H-NMR (400 MHz, $CDCl_3$) δ 9.98 (s, 2H, H_3), 8.72-8.68(m, 6H, $H_{5,6,9}$). ^{13}C-NMR (100 MHz, $CDCl_3$) δ 157.23 (C_8), 148.44 (C_2), 145.731(C_5), 143.95(C_3), 143.76(C_6), 125.49(C_9). IR ν/cm^{-1}:

3075br/w, 1578w, 1481w, 1400m, 1157m, 1086m, 1016s, 841s, 489w, 421s. ESI-MS: Found M^+ 237.0888, $C_{12}H_8N_6$ requires M^+ 237.0883. UV-Visible (CH_3CN) λ_{max} (ε) 296 nm (25240), 251 nm (4435).

1,4-bis(2-pyrazinyl)-6,7-dihydro-5*H*-cyclopenta[*d*]pyridazine **L13**

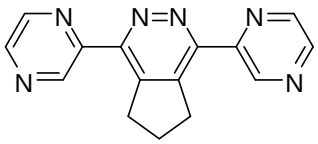

To an over dried Schlenk tube, 3,6-bis(2-pyrazinyl)-1,2,4,5-tetrazine (0.45 g, 1.89 mmol) and cyclopentanone (0.39 g, 5.13 mmol) was added under N_2. Dry DMSO (5ml) was then added, followed by proline (0.005 g). The Schlenk tube was then fitted to a condenser with a N_2 balloon. The reaction mixture was heated to 100°C for 48 hours during which the colour went from a red/pink colour to a dark brown. Once cooled to room temperature, the solution was added to water (50ml), extracted with ethyl acetate (100 mL) and the organic layer separated. The aqueous layer was again washed with ethyl acetate (100 mL) then separated. The organic layers were combined, washed with water (2 x 50 mL), then brine (50 mL), dried with $MgSO_4$, concentrated under reduced pressure to give a light brown product. This was recrystallized from methanol to give a fluffy light brown solid. Yield: 49.7%. Mp: 180°C.

^{1}H-NMR (400 MHz, $CDCl_3$) δ 9.87(s, 2H, H_3), 8.70-8.66(m, 4H, $H_{5,6}$), 3.53(t, *J*=7.8 Hz, H_{10}), 2.25-2.17(m, 2H, H_{11}). ^{13}C-NMR (100 MHz, $CDCl_3$) δ 153.71(C_8), 151.07(C_2), 146.60(C_9), 145.10(C_3), 144.37(C_5), 143.23(C_6), 33.19(C_{10}), 25.07(C_{11}). IR ν/cm^{-1}: 1362w, 1111w, 1013m, 855w, 445m. ESI-MS: Found M^+ 277.1194, $C_{15}H_{12}N_6$ requires M^+ 277.1196. UV-Visible (CH_3CN) λ_{max} (ε) 292 nm (20859), 217 nm (11372). Analysis: Calc. for $C_{15}H_{12}N_6$: C, 65.21; H, 4.38; N, 30.42. Found: C, 64.97; H, 4.33; N, 30.47.

1,4-di(2-pyrazinyl)-5,6,7,8-tetrahydrophthalazine **L14**

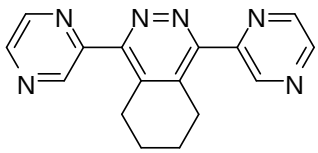

3,6-Bis(2-pyrazinyl)-1,2,4,5-tetrazine (0.44 g, 1.85 mmol) and cyclohexene (0.3 g, 3.70 mmol) was added to a dry pressure tube, followed by dry toluene (5 mL). The reaction mixture was heated to 150°C for three days. The pressure tube was cooled to room temperature and the solid impurities filtered. The filtrate was removed under reduced pressure and the oily product washed with hot methanol, filtered impurities and then the solvent was removed under reduced pressure to yield the product. Yield: 38.3%. Mp: 113°C.

^{1}H-NMR (400 MHz, $CDCl_3$-d_3) δ 9.32(s, 2H, H_3), 8.67(s, 4H, $H_{5,6}$), 3.08(s, 4H, H_{10}), 1.84(s, 4H, H_{11}). ^{13}C-NMR (100 MHz, $CDCl_3$) δ 156.04(C_8), 151.82(C_2), 146.21(C_3), 144.30(C_5), 142.73(C_6), 138.79(C_9), 26.69(C_{10}), 21.42(C_{11}). IR ν/cm^{-1}: 3373br/m, 3287br/w, 2921br/w, 1667w, 1372m, 1138m, 1017s, 860m, 766w. ESI-MS: Found M^+ 291.1353, $C_{16}H_{14}N_6$ requires M^+ 291.1353. UV-Visible (CH_3CN) λ_{max} (ε) 278 nm (18659), 215 nm (18806). Analysis: Calc. for $C_{16}H_{14}N_6.1/4CH_2Cl_2.2/3H_2O$: C, 60.32; H, 4.93; N, 25.97. Found: C, 60.40; H, 4.81; N, 25.60.

1,4-di(2-pyrazinyl)-6,7,8,9-tetrahydro-5H-cyclohepta[*d*]pyridazine **L15**

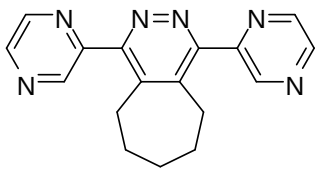

Adopting the same method, as for L12, 3,6-bis(2-pyrazinyl)-1,2,4,5-tetrazine (0.46 g, 1.91 mmol) and cycloheptanone (0.44 g, 4.40 mmol) was added under N_2 to an oven dried schlenk tube. Dry DMSO (5ml) was then added, followed by proline (0.005 g). The schlenk tube was then fitted to a condenser with a N_2 balloon. The reaction mixture was heated to 100°C for six days. Once cooled to room temperature, the precipitate was filtered was washed with the filtrate and then cold methanol yielding the product as an off white solid. Yield: 47.7%. Mp: 208°C

^{1}H-NMR (400 MHz, $CDCl_3$) δ 9.27(s, 2H, H_3), 8.68(s, 4H, $H_{5,6}$), 3.09(t, J=4.9 Hz, 4H, H_{10}), 1.92(d, J=5.5 Hz, 2H, H_{12}), 1.78(d, J=4.3 Hz, 4H, H_{11}). ^{13}C-NMR (100 MHz, $CDCl_3$) δ 165.06(C_8), 152.17(C_2), 146.23(C_3), 144.22(C_9), 144.15(C_5), 143.07(C_6), 31.63(C_{12}), 29.47(C_{10}), 26.06(C_{11}). IR ν/cm^{-1}: 2911br/w, 2841w, 1473w, 1372w, 1096m, 1017m, 882w, 763w. ESI-MS: Found M^+ 305.1514, $C_{17}H_{16}N_6$ requires M^+ 305.1509. UV-Visible (CH_3CN) λ_{max} (ε) 277 nm (25240), 219 nm (26182). Analysis: Calc. for $C_{17}H_{16}N_6$: C, 67.09; H, 5.30; N, 27.61. Found: C, 66.62; H, 5.17; N, 27.49.

3,6-bis(pyrazolyl)-1,2,4,5-tetrazine **L16**

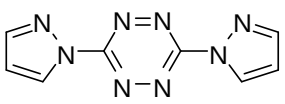

3,6-Bis(3,5-dimethylpyrazol-1-yl)-1,2,4,5-tetrazine (0.44 g, 1.63 mmol) and pyrazole (1.26 g, 18.51 mmol) were added under N_2 to an over dried schlenk tube. The mixture was kept in a molten state at 100°C for 5 hours. The reaction mixture was cooled to room temperature and left to stand overnight. The solid remains were washed with pet ether and then washed with acetonitrile. The solid product was then extracted into DCM (50 mL) and washed with water (5 x 50 mL). The organic layer was separated, dried with $MgSO_4$ and the solvent removed in *vacuo* to give a solid pink product. Yield: 62.5%. Mp: 255°C.

^{1}H-NMR (400 MHz, $CDCl_3$) δ 8.73(d, *J*=2.4 Hz, 2H, H_3), 8.04(s, 2H, H_5), 6.70(s, 2H, H_4). ^{13}C-NMR (100 MHz, $CDCl_3$) δ 158.76(C_2), 146.04(C_5), 129.58(C_3), 110.78(C_4). IR *ν*/cm^{-1}: 3146w, 3127w, 3103w, 1477m, 1395m, 1025m, 917m, 774s, 606s. ESI-MS: Found M^+ 215.0789, $C_8H_6N_8$ requires M^+ 215.0788. UV-Visible (CH_3CN) λ_{max} (ε) 368 nm (1264), 285 nm (36323). Analysis: Calc. for $C_8H_6N_8$: C, 44.86; H, 2.82; N, 52.32. Found: C, 44.69; H, 2.84; N, 52.02.

6.3 Complexes with silver

$AgBF_4$ with 1,4-di(pyridin-2-yl)-6,7-dihydro-5H-cyclopenta[d]pyridazine, viz **2.1**

Silver tetrafluoroborate (10.1 mg, 0.052 mmol) and **L2** (13.6 mg, 0.050 mmol) were dissolved separately in dichloromethane and acetonitrile (9:1, 3 mL) and acetonitrile (3 mL), respectively, heated, and then combined to give the complex mixture. Crystals suitable for single crystal analysis were prepared by vapour diffusion of pentane into the mixture. Yield: 69.1%. Mp: 232°C.

ESI-MS: 851.0573 $[Ag_2(\mathbf{L2})_2(BF_4)]^+$, 655.1492 $[Ag(\mathbf{L2})_2]^+$, 519.0874 $[Ag_2(\mathbf{L2})_3]^{2+}$, 381.0267 $[Ag(\mathbf{L2})]^+$/$[Ag_2(\mathbf{L2})_2]^{2+}$, 275.1291 $[(\mathbf{L2})H]^+$. IR *ν*/cm^{-1}: 2957br/w, 1590w, 1467w, 1380w, 1032br/s, 789m, 743m, 519m. UV-Visible (CH_3CN) λ_{max} 288nm. Analysis: Calc. for $C_{17}H_{14}N_4.AgBF_4$: C, 40.74; H, 3.03; N, 10.86. Found: C, 41.16; H, 3.06; N, 11.15.

$AgPF_6$ with 1,4-di(pyridin-2-yl)-6,7-dihydro-5H-cyclopenta[d]pyridazine, viz **2.2**

A hot solution of silver hexafluorophosphate (7.55 mg, 0.030 mmol) in dichloromethane and acetonitrile (9:1, 1 mL) was added to a hot solution of **L2** (7.28 mg, 0.028 mmol) in dichloromethane (1 mL), forming a pale yellow solution. After vapour diffusion of pentane into the reaction mixture, crystals formed which were suitable for X-ray diffraction studies. Yield: 53.6%. Mp: 227°C.

^{1}H-NMR (500 MHz, CD_3CN) δ 8.70(s, 1H, H_6), 8.10-8.05(m, 2H, $H_{3,4}$), 7.62(s, 1H, H_5), 3.34(t, *J*=7.5 Hz, 2H, H_{10}), 2.17-2.16(m, 2H, H_{11}). ^{13}C-NMR (125 MHz, CD_3CN) δ 152.47(C_2), 150.60(C_6), 147.54(C_9), 138.26(C_4), 125.61(C_5), 124.85(C_3), 33.42(C_{10}), 24.61(C_{11}). IR *ν*/cm^{-1}: 2967br/w, 1588w, 1387w, 1133w, 827s, 554s. UV-Vis: (CH_3CN) λ_{max} (ε) 288 nm (14003). ESI-MS: 909.0179 $[Ag_2(\mathbf{L2})_2](PF_6)$, 655.1493 $[Ag(\mathbf{L2})_2]^+$, 381.0264 $[Ag(\mathbf{L2})]^+$/$[Ag_2(\mathbf{L2})_2]^{2+}$, 275.1288 $[(\mathbf{L2})H]^+$. Analysis: Calc. for $C_{17}H_{14}N_4.AgPF_6$: C, 38.73; H, 2.68; N, 10.63. Found: C, 39.00; H, 2.66; N, 10.62.

$AgClO_4$ with 1,4-di(pyridin-2-yl)-6,7-dihydro-5H-cyclopenta[d]pyridazine, viz **2.3**

Reaction of **L2** (13.60 mg, 0.050 mmol) in hot dichloromethane (1 mL) and silver perchlorate (11.66 mg, 0.056 mmol) in hot dichloromethane and acetonitrile (9:1) were combined. Large crystals were obtained that were suitable for single X-ray diffraction after vapour diffusion of pentane into the reaction mixture. Yield: 63.0%. Mp: 245°C.

^{1}H-NMR (500 MHz, CD_3CN) δ 8.69(s, 1H, H_6), 8.09-8.06(m, 2H, $H_{3,4}$), 7.62(s, 1H, H_5), 3.34(t, *J*=7.1 Hz, 2H, H_{10}), 2.19-2.18(m, 2H, H_{11}). ^{13}C-NMR (125 MHz, CD_3CN) δ 154.61(C_2), 152.57(C_8), 150.36(C_6), 147.21(C_9), 138.03(C_4), 125.32(C_5), 124.55(C_3), 33.33(C_{10}), 24.48(C_{11}). IR *v*/cm^{-1}: 2968br/w, 1593w, 1386w, 1068br/s, 788m, 618s. UV-Vis: (CH_3CN) λ_{max} (ε) 288 nm (28263). ESMS: 863.0007 [Ag_2(**L2**)$_2$](ClO4), 655.1483 [Ag(**L2**)$_2$]$^+$, 381.0206 [Ag(**L2**)]+/[Ag_2(**L2**)$_2$]$^{2+}$, 275.1287 [(**L2**)H]$^+$. Analysis: Calc. for $C_{17}H_{14}N_4.AgClO_4.H_2O$: C, 40.86; H, 3.23; N, 11.21. Found: C, 40.52; H, 2.78; N, 11.24.

$AgBF_4$ with 1,4-di(pyridin-2-yl)-6,7-dihydro-5H-cyclopenta[d]pyridazine, viz **2.4**

Reaction of **L2** (2.92 mg, 0.015 mmol) and silver tetrafluoroborate (4.11 mg, 0.015 mmol) were dissolved in d_3-aceteonitile for NMR analysis. Overnight, yellow crystals formed in the NMR tube suitable for single crystal X-ray analysis. Yield: 54.2%. Mp: 242°C

^{1}H-NMR (500 MHz, CD_3CN) δ 8.61(d, *J*=4.6 Hz, 1H, H_6), 8.03-8.02(m, 2H, $H_{3,4}$), 7.56(dd, *J*=8.8 Hz, 4.3 Hz, 1H, H_5), 3.28(t, *J*=7.4 Hz, 2H, H_{10}), 2.15-2.11(m, 2H, H_{11}). ^{13}C-NMR (125 MHz, CD_3CN) δ 154.44(C_2), 151.97(C_8), 150.56(C_6), 147.39(C_9), 138.18(C_4), 125.54(C_5), 124.77(C_3), 33.28(C_{10}), 24.52(C_{11}). IR *v*/cm^{-1}: 2970br/w, 1587w, 1444w, 1378w, 1047br/s, 787m, 738m, 614w. UV-Vis: (CH_3CN) λ_{max} (ε) 288 nm (27047). ESI-MS: 851.0569 [Ag_2(**L2**)$_2$](BF_4), 519.0875 [Ag_2(**L2**)$_3$]$^{2+}$, 381.0267 [Ag(**L2**)]$^+$/[Ag_2(**L2**)$_2$]$^{2+}$, 275.1288 [(**L2**)H]$^+$. Analysis: Calc. for $C_{17}H_{14}N_4.AgBF_4$: C, 43.54; H, 3.01 N, 11.95. Found: C, 43.53; H, 3.20; N, 12.59.

AgOTf with 1,4-di(pyridin-2-yl)-5,6,7,8-tetrahydrophthalazine, viz **2.5**

A reaction mixture was obtained by a hot solution of silver triflate (9.77 mg, 0.038 mmol) in dichloromethane and acetonitrile (9:1, 1 mL), added to a hot solution of **L3** (10.00 mg, 0.035 mmol) in hot dichloromethane (1 mL). Crystals were collected by vapour diffusion of diisopropyl ether

into the reaction mixture prepared, that were acceptable for single X-ray crystallography. Yield: 40.1% Mp: 222°C.

^{1}H-NMR (500 MHz, CD_3CN) δ 8.56(d, *J*=4.9 Hz, 1H, H_6), 8.01(t, *J*=7.7 Hz, 1H, H_4), 7.77(d, *J*=7.8 Hz, 1H, H_3), 7.52(m, 1H, H_5), 2.79(s, 1H, H_{10}), 1.76(s, 1H, H_{11}). ^{13}C-NMR (125 MHz, CD_3CN) δ 158.52(C_8), 153.11(C_2), 150.35(C_6), 139.56(C_9), 137.74(C_4), 125.38(C_3), 124.97(C_5), 26.89(C_{10}), 20.90(C_{11}). IR ν/cm^{-1}: 2950br/w, 1595w, 1244s, 1149s, 1025s, 791w, 633s, 514w. UV-Vis: (CH_3CN) λ_{max} (ε) 271 nm (27070). ESMS: 941.0365 $[Ag_2(\mathbf{L3})_2](CF_3SO_3)$, 540.1112 $[Ag_2(\mathbf{L3})_3]^{2+}$, 395.0421 $[Ag_2(\mathbf{L3})_2]^{2+}$, 289.1447 $[(\mathbf{L3})H]^{+}$. Analysis: Calc. for $C_{18}H_{16}N_4$.AgOTf.H_2O.DCM: C, 37.06; H, 3.11 N, 8.64. Found: C, 37.32; H, 2.63; N, 8.89.

<u>$AgPF_6$ with 1,4-di(pyridin-2-yl)-6,7,8,9-tetrahydro-5H-cyclohepta[*d*]pyridazine, viz **2.6**</u>

A reaction mixture of silver hexafluorophosphate (25.79 mg, 0.102 mmol) in hot dichloromethane and acetonitrile (9:1, 1 mL) and **L4** (11.18 mg, 0.037 mmol) in hot dichloromethane (1 mL) gave crystals after vapour diffusion of pentane. The crystals obtained were suitable for single molecule X-ray crystallography. Yield: 58.7%. Mp: 220°C.

^{1}H-NMR (500 MHz, CD_3CN) δ 8.57(d, *J*=4.6 Hz, 1H, H_6), 8.01(t, *J*=7.7 Hz, 1H, H_4), 7.63(d, *J*=7.8 Hz, 1H, H_3), 7.54(dd, *J*=6.8 Hz, 5.6Hz, 1H, H_5), 2.87(t, *J*=5.1 Hz, 2H, H_{10}), 1.95-1.90(m, 2H, H_{12}), 1.71-1.67(m, 2H, H_{11}). ^{13}C-NMR (125 MHz, CD_3CN) δ 158.28(C_8), 153.35(C_2), 150.57(C_6), 144.86(C_9), 137.87(C_4), 125.73(C_3), 124.92(C_5), 31.07(C_{12}), 29.94(C_{10}), 25.42(C_{11}). IR ν/cm^{-1}: 2943br/w, 2267br/w, 1596w, 1007br/m, 825s, 555m. UV-Vis: (CH_3CN) λ_{max} (ε) 269 nm (18979), 219 nm (30875). ESI-MS: 965.0798 $[Ag_2(\mathbf{L4})_2](PF_6)$, 561.1349 $[Ag_2(\mathbf{L4})_3]^{2+}$, 409.0578 $[Ag(\mathbf{L4})]^{+}$/$[Ag_2(\mathbf{L4})_2]^{2+}$, 303.1604 $[(\mathbf{L4})H]^{+}$. Analysis: Calc. for $C_{19}H_{18}N_4$.$AgPF_6$: C, 29.03; H, 2.84; N, 8.46. Found C, 28.44; H, 2.50; N, 8.39.

<u>AgOTf with 7,10-di(pyridin-2-yl)-8,9-difluoranthene, viz **2.7**</u>

Two solutions, one of molecule **L5** (12.00mg, 0.0335mmol) in hot dichloromethane (2ml) and another of silver triflate (16.00mg, 0.0623mmol) in hot dichloromethane and acetonitrile (9:1) were added together to form the reaction mixture. Crystals suitable for X-ray crystallography were obtained after vapour diffusion of diisopropyl ether. Yield: 52.1%. Mp: >360°C.

^{1}H-NMR (400 MHz, DMSO) δ 8.95(d, *J*=4.3 Hz, 2H, H_6), 8.30-8.18(m, 8H, $H_{11,3,13,4}$), 7.80-7.73(m, 4H, $H_{12,5}$). ^{13}C-NMR (100 MHz, DMSO) δ 155.57(C_2), 149.83(C_6), 138.39(C_4), 131.77(C_{11}), 129.38(C_{13}), 129.00(C_{12}), 125.60(C_5), 125.22(C_3). IR *ν*/cm^{-1}: 3389br/w, 3067br/w, 1592w, 1416w, 1221s, 1142m, 1025s, 771m, 634s. **ESI-MS**: 825.1495 [Ag(**L5**)$_2$]$^+$, 645.0883 [Ag$_2$(**L5**)$_3$]$^{2+}$, 465.0264 [Ag(**L5**)]$^+$/[Ag$_2$(**L5**)$_2$]$^{2+}$, 359.1289 [(**L5**)H]$^+$. UV-Visible (DMSO) λ_{max} (ε) 368 nm (11912), 326 nm (11610), 271 nm (25892), 256 nm (25103). Analysis: Calc. for $(C_{24}H_{14}N_4)_3AgOTf.CH_2Cl_2.2H_2O$: C, 42.41; H, 2.74; N, 7.61. Found: C, 42.38; H, 2.28; N, 7.85.

AgOTf with 1,4-bis(3,5-dimethylpyrazol-1-yl)-6,7-dihydro-5*H*-cyclopenta[*d*]pyridazine, viz **2.8**

Silver triflate (10.00 mg, 0.032 mmol) in hot acetonitrile (2 mL) was added to **L7** (8.40 mg, 0.033 mmol) in hot acetonitrile (2 mL) to form a colourless reaction mixture. Vapour diffusion of diisopropyl ether yielded crystals suitable for single X-ray crystallography. Yield: 53.1%. Mp: 253°C.

^{1}H-NMR (500 MHz, CD_3CN) δ 6.17(s, 2H, H_4), 3.20-3.17(m, 4H, H_8), 2.47(s, 6H, H_2/H_1), 2.28(s, 6H, H_1/H_2), 2.20-2.19(m, 2H, H_9). ^{13}C-NMR (125 MHz, CD_3CN) δ 152.93(C_6), 150.68(C_3/C_5), 144.32(C_7), 142.34(C_5/C_3), 107.97(C_4), 32.44(C_8), 23.59(C_9), 12.83(C_1/C_2), 12.03(C_2/C_1). IR *ν*/cm^{-1}: 2980br/w, 1565w, 1403m, 1251s, 1146s, 1026s, 805w, 634s, 515m. ESI-MS: 725.2557 [Ag(**L7**)$_2$]$^+$, 415.0799 [Ag(**L7**)]$^+$/[Ag$_2$(**L7**)$_2$]$^{2+}$, 309.1825 [(**L7**)H]$^+$. UV-Visible (CH_3CN) λ_{max} (ε) 273 nm (51758). Analysis: Calc. for $(C_{17}H_{20}N_6)_2(AgOTf_2)_2.3H_2O$: C, 36.5; H, 3.91; N, 14.19. Found: C, 36.06; H, 3.46; N, 13.79.

AgOTf with 1,4-bis(3,5-dimethylpyrazol-1-yl)-5,6,7,8-tetrahydrophthalazine, viz **2.9**

Silver triflate (10.7 mg, 0.033 mmol) and **L8** (12.2 mg, 0.047 mmol) were dissolved separately in acetonitrile (2 mL), heated, and then combined to give a reaction mixture. Crystals suitable for single crystal analysis were prepared by vapour diffusion of pet ether into the mixture. Yield: 40.6%. Mp: 284°C.

^{1}H-NMR (500 MHz, CD_3CN) δ 6.18 (s, 2H, H_4), 2.62 (s, 4H, H_{11}), 2.28-2.26 (m, 12H, $H_{6,7}$), 1.78 (s, 4H, H_{12}). ^{13}C-NMR (100 MHz, CD_3CN) δ 155.03 (C_9), 150.37 (C_3/C_5), 142.17 (C_5/C_3), 139.35 (C_{10}), 106.71 (C_4), 24.41 (C_{11}), 20.47 (C_{12}), 12.77 (C_6/C_7), 10.77 (C_7/C_6). IR *ν*/cm^{-1}: 2950br/w, 1562w, 1400w, 1253m, 1149m, 1027s, 803w, 635s. ESI-MS: 751.2870 [Ag(**L8**)$_2$]$^+$, 431.0945 [Ag(**L8**)]$^+$/[Ag$_2$(**L8**)$_2$]$^{2+}$, 323.1977 [(**L8**)H]$^+$. UV-Visible (CH_3CN) l_{max} (e) 262 nm (20092).

Analysis: Calc. for $(C_{18}H_{22}N_6)_2.AgOTf_4.CH_3CN$: C, 29.44; H, 2.76; N, 10.63. Found: C, 29.12; H, 2.85; N, 11.10.

AgOTf with 7,10-bis(3,5-dimethyl-1*H*-pyrazol-1-yl)-8,9-diazafluoranthene, viz **2.10**

A hot solution of silver triflate (5.53 mg, 0.022 mmol) in dichloromethane/acetonitrile (9:1, 2 mL) was added to a hot solution of **L9** (6.30 mg, 0.016 mmol) in hot dichloromethane/acetonitrile (9:1, 2 mL) with a pale yellow solution resulting. After vapour diffusion of petroleum ether into the reaction mixture, yellow crystals were obtained suitable for single crystal X-ray determination studies. Yield: 50.4%. Mp: 316°C.

^{1}H-NMR (400 MHz, CD_3CN) δ 8.30(d, *J*=8.3 Hz, 2H, H_{12}), 7.92(d, *J*=7.0 Hz, 2H, H_{14}), 7.82(t, *J*=7.9 Hz, 2H, H_{13}), 6.37(s, 2H, H_{14}), 2.43-2.45(m, 12H, $H_{6,7}$). ^{13}C-NMR (100 MHz, CD_3CN) δ 157.39 (C_9), 151.18 (C_5), 143.01 (C_3), 138.49 (C_{11}), 131.70 (C_{12}), 131.42 (C_{15}), 129.13 (C_{14}), 128.84 (C_{13}), 121.10 (C_{10}), 107.88 (C_4), 12.83 (C_6), 11.24 (C_7). IR v/cm^{-1}: 3479b/w, 1581w, 1420m, 1257s, 12132, 1156s, 1018s, 776n, 634s ESI-MS: 1539.2965 $[Ag_2(\mathbf{L9})_3OTf]^+$, 1285.4313 $[Ag(\mathbf{L9})_3]^+$, 1149.1119 $[Ag_2(\mathbf{L9})_2OTf]^{2+}$, 893.2561 $[Ag(\mathbf{L9})_2]^+$, 696.1678 $[Ag_2(\mathbf{L9})_3]^{2+}$, 540.1061 $[Ag(\mathbf{L9})CH_3CN]^+$, 500.0799 $[Ag(\mathbf{L9})]^+/[Ag_2(\mathbf{L9})_2]^{2+}$, 393.1821 $[(\mathbf{L})H]^+$. UV-Visible (CH_3CN) l_{max} (e) 369 nm (15533), 325 nm (15317), 263 nm (35944), 242 nm (49473). Analysis: Calc. for $(C_{24}H_{20}N_6)_2.AgOTf_4.2H_2O$: C, 33.78; H, 2.40; N, 9.09. Found: C, 33.31; H, 2.40; N, 8.94.

$AgPF_6$ with 3-(3,5-dimethyl-1*H*-pyrazol-1-yl)-6-(1-piperidinyl)- 1,2,4,5-tetrazine, viz **2.11**

Reaction of **L10** (10.96 mg, 0.060 mmol) in hot acetonitrile (2 mL) and silver hexafluorophosphate (12.95 mg, 0.067 mmol) in hot acetonitrile (2 mL) were combined. Large block-like red crystals were obtained, that were suitable for single X-ray diffraction after vapour diffusion of diisopropyl ether into the reaction mixture.

^{1}H-NMR (400 MHz, CD_3CN) δ 6.26(s, 1H, H_4), 3.95(t, *J*=5.3 Hz, 4H, H_9), 2.50(s, 3H, H_1), 2.33(s, 3H, H_2), 1.78(d, *J*=3.9 Hz, 2H, H_{11}), 1.71(d, *J*=5.1 Hz, 4H, H_{10}). ^{13}C-NMR (100 MHz, CD_3CN) δ 160.47(C_7), 155.42(C_6), 152.05(C_3), 143.07(C_5), 109.36(C_4), 44.61(C_9), 25.12(C_{10}), 23.97(C_{11}), 13.08(C_1), 12.46(C_2). **ESI-MS**: 625.2161 $[Ag(\mathbf{L10})_2]^+$, 407.0856 $[Ag(\mathbf{L10})]^+(CH_3CN)$, 366.0598 $[Ag(\mathbf{L10})]^+$, 260.1627 $[(\mathbf{L10})H]^+$.

AgOTf with 1,4-bis(2-pyrazinyl)-6,7-dihydro-5*H*-cyclopenta[*d*]pyridazine, viz **2.12**

Silver triflate (5.01 mg, 0.018 mmol) in hot acetonitrile (2 mL) was added to a hot solution of **L13** (4.60 mg, 0.018 mmol) in acetonitrile (2 mL). Vapour diffusion of diethyl ether resulted in crystals suitable for single crystal X-ray diffraction studies. Yield: 60.8%. Mp: 238°C

^{1}H-NMR (400 MHz, CD_3CN) δ 9.71 (s, 2H, H_3), 8.75 (s, 2H, H_6), 8.71 (s, 2H, H_5), 3.49 (t, J=15.6, 7.8 Hz, 4H, H_{10}), 2.20-2.13 (m, 2H, H_{11}). ^{13}C-NMR (100 MHz, CD_3CN) δ 153.88 (C_8), 151.00 (C_2), 146.72 (C_9), 144.73 (C_3/C_5), 144.61 (C_5/C_3), 143.67 (H_6), 32.81 (C_{10}), 23.80 (C_{11}). IR ν/cm^{-1}: 3068b/w, 1435w, 1373w, 1251s, 1157s, 1018s, 854m, 766w, 633s, 515m. ESI-MS: 916.9859 $[Ag_2(\mathbf{L13})_2(OTf)]^+$, 659.1303 $[Ag(\mathbf{L13})]^+$, 383.0170 $[Cu(\mathbf{L13})]^+$/$[Cu_2(\mathbf{L13})_2]^{2+}$, 277.1198 $[(\mathbf{L13})H]^+$. UV-Visible (CH_3CN) λ_{max} (ε) 293 nm (36498), 219 nm (20449). Analysis: Calc. for $(C_{15}H_{12}N_6)$AgOTf: C, 36.04; H, 2.27; N, 15.76. Found: C, 36.03; H, 2.31; N, 16.02.

$AgPF_6$ with 1,4-di(2-pyrazinyl)-5,6,7,8-tetrahydrophthalazine, viz **2.13**

Silver hexafluorophosphate (8.63 mg, 0.030 mmol) in hot acetonitrile (2 mL) was added to solution containing **L14** (10.27 mg, 0.041 mmol) in hot acetonitrile (2 mL). Crystals suitable for single crystal X-ray determination were obtained after diisopropyl ether into the reaction mixture. Yield: 52.7%. Mp: 225°C.

IR ν/cm^{-1}: 2942w/b, 1384w, 1144w, 1022w, 824s/b, 554s. ESI-MS: 687.1614 $[Ag(\mathbf{L14})_2]^+$, $[Ag(\mathbf{L14})]^+$/$[Ag_2(\mathbf{L14})_2]^{2+}$, 291.1351 $[(\mathbf{L14})H]^+$. UV-Visible (CH_3CN) λ_{max} (ε) 279 nm (50008), 215 nm (50151). Analysis: Calc. for $(C_{16}H_{14}N_6)_2(AgPF_6)_2.C_2H_5NO$: C, 35.65; H, 2.90; N, 15.90. Found: C, 35.95; H, 2.82; N, 15.96

6.4 Complexes with copper

$Cu(MeCN)_4BF_4$ with 1,4-di(pyridin-2-yl)-6,7-dihydro-5H-cyclopenta[d]pyridazine, viz **3.1**

A warm solution of tetrakis(acetonitrile)copper(I) tetrafluoroborate (11.35 mg, 0.036 mmol) in acetonitrile (1 mL) was added to a warm solution of **L2** (10.00 mg, 0.036 mmol) in acetonitrile (1 mL). Crystals suitable for X-ray diffraction were obtained by diffusing diethyl ether into the reaction mixture. Yield: 57.7%. Mp: >350°C.

^{1}H-NMR (500 MHz, CD_3CN) δ 8.03-7.94(m, 3H, $H_{6,3,4}$), 7.30(t, *J*=5.9 Hz, 1H, H_5), 3.49-3.43(m, 2H, H_{10}), 2.65-2.58(m, 1H, H_{11a}), 2.52-2.44(m, 1H, H_{11b}). ^{13}C-NMR (125 MHz, CD_3CN) δ 151.41(C_8), 149.78(C_6), 148.39(C_2), 147.97(C_9), 139.49(C_4), 128.52(C_5), 126.14(C_3), 35.04(C_{10}), 24.44(C_{11}). ESI-MS: 761.1066 $[Cu_2(\mathbf{L2})_2](BF_4)$, 611.1736 $[Cu(\mathbf{L2})_2]^+$, 475.1115 $[Cu_2(\mathbf{L2})_3]^{2+}$, 337.0508 $[Cu_2(\mathbf{L2})_2]^{2+}$, 305.5860 $[Cu(\mathbf{L2})_2]^{2+}$, 275.1283 $[(\mathbf{L2})H]^+$. IR *v*/cm^{-1}: 3553br/w, 2956br/w, 1594w, 1463w, 1368w, 1274w, 1046br/s, 787m, 741w, 619s. UV-Visible (CH_3CN) λ_{max} (ε) 429 (8474), 288nm (136248). Analysis: Calc. for $C_{17}H_{14}N_4.CuBF_4.H_2O$: C, 46.12; H, 3.63; N, 12.66. Found: C, 46.27; H, 3.44; N, 12.59.

CuI with 3,6-bis(3,5-dimethylpyrazolyl)pyridazine, viz **3.2**

Copper iodide (7.1 mg, 0.037 mmol) and **L6** (9.98 mg, 0.037 mmol) were dissolved separately in hot acetonitrile (3 mL) and then combined to give a dark brown complex mixture. Vapour diffusion of diisopropyl ether into the reaction mixture yielded crystals suitable for single X-ray crystallography. Yield: 80.8%. Mp: 297°C.

IR *v*/cm^{-1}: 3430br/w, 3084w, 1567m, 1426s, 1341m, 1061m, 969m, 837m, 793s, 484s. ESI-MS: 599.2177 $[Cu(\mathbf{L6})_2]^+$, 331.0725 $[Cu(\mathbf{L6})]^+/[Cu_2(\mathbf{L6})_2]^{2+}$, 299.6078 $[Cu(\mathbf{L6})_2]^{2+}$, 269.1508 $[(\mathbf{L6})H]^+$. UV-Visible (CH_3CN) λ_{max} (ε) 281 nm (38917), 245 nm (32191). Analysis: Calc. for $(C_{14}H_{16}N_6)Cu_2I_2.MeCN$: C, 27.84; H, 2.77; N, 14.20. Found: C, 28.13; H, 2.68; N, 13.76.

$Cu(MeCN)_4BF_4$ with 1,4-bis(3,5-dimethylpyrazol-1-yl)-6,7-dihydro-5*H*-cyclopenta[*d*]- pyridazine, viz **3.3**

Tetrakis(acetonitrile)copper(I) tetrafluoroborate (10.28 mg, 0.033 mmol) in hot acetonitrile (2 mL) was added to a hot solution of **L7** (10.03 mg, 0.033 mmol) in acetonitrile (2 mL) forming a colourless reaction mixture. Vapour diffusion of diisopropyl ether yielded small blue crystals that were suitable for single crystal X-ray analysis. Yield: 13.9%. Mp: >360°C.

IR *v*/cm^{-1}: 1574w, 1417m, 1049br/s, 680w, 444s. ESI-MS: 679.2802 $[Cu(\mathbf{L7})_2]^+$, 526.1917 $[Cu_2(\mathbf{L7})_3]^{2+}$, 371.1044 $[Cu(\mathbf{L7})]^+/[Cu_2(\mathbf{L7})_2]^{2+}$, 309.1828 $[(\mathbf{L7})H]^+$.

CuI with 7,10-bis(3,5-dimethyl-1*H*-pyrazol-1-yl)-8,9-diazafluoranthene, viz **3.4**

Copper iodide (6.10 mg, 0.032 mmol) and **L9** (9.80 mg, 0.025 mmol) were dissolved separately in hot acetonitrile (3 mL) and then combined. Crystals suitable for X-ray diffraction were obtained by vapour diffusion of diisopropyl ether into the reaction mixture. Yield: 90.8%. Mp: >360°C.

IR ν/cm^{-1}: 1575m, 1415s, 1088m, 1039w, 826m, 772s. ESI-MS: 847.2795 [Cu(**L9**)$_2$]$^{2+}$, 652.1919 [Cu$_2$(**L9**)$_3$]$^{2+}$, 456.1037 [Cu(**L9**)]$^+$/[Cu$_2$(**L9**)$_2$]$^{2+}$, 393.1821 [(**L9**)H]$^+$. UV-Visible (CH_3CN) l $_{max}$ (e) 268 nm (7175), 244 nm (72678). Analysis: Calc. for ($C_{24}H_{20}N_6$)Cu_5I_5.MeCN: C, 22.53; H, 1.67; N, 7.08. Found: C, 22.66; H, 1.63; N, 6.62.

Cu(MeCN)$_4$BF$_4$ with 3,6-bis(2-pyrazinyl)-1,2,4,5-tetrazine, viz **3.5**

L11 (7.85 mg, 0.033 mmol) and tetrakis(acetonitrile)copper(I) tetrafluoroborate (10.1 mg, 0.032 mmol) were dissolved separately in hot acetonitrile and then added together forming a red solution (4 mL). After vapour diffusion of diethyl ether was completed, red needle-like crystals were obtained, suitable for determination of single crystal X-ray analysis. Yield: 73.8%. Mp: >360°C.

^{1}H-NMR (500vMHz, CD_3CN) δ 9.86 (s, 2H, H_6), 8.97-8.95 (m, 4H, $H_{3,5}$). ^{13}C-NMR (125 MHz, CD_3CN) δ 163.28 (C_8), 147.91 (C_5), 145.80 (C_2), 145.43 (C_6/C_3), 145.38 (C_3/C_6). IR ν/cm^{-1}: 1381m, 1145m, 1051s, 862w, 608w, 520w, 454s. ESI-MS: 604.0016 [Cu$_2$(**L11**)$_2$]$^+$, 539.0724 [Cu(**L11**)$_2$]$^+$, 342.0270 [Cu$_1$(**L11**)CH_3CN]$^+$, 300.9993 [Cu(**L11**)]$^+$, 269.5358 [Cu(**L11**)$_2$]$^{2+}$, 239.0785 [(**L11**)H]$^+$. UV-Visible (CH_3CN) λ_{max} (ε) 535 nm (379), 292 nm (26633). Analysis: Calc. for ($C_{10}H_8N_8$)$CuBF_4$: C, 30.91; H, 1.56; N, 28.84. Found: C, 31.04; H, 1.63; N, 28.80.

CuI with 3,6-bis(2-pyrazinyl)-1,2,4,5-tetrazine, viz **3.6**

The warm solution of copper iodide (9.81 mg, 0.041 mmol) in acetonitrile (2 mL) was added to a warm solution of the **L11** (12.01 mg, 0.063 mmol) in acetonitrile (2 mL) forming a dark red/brown reaction solution. Vapour diffusion of diethyl ether into the reaction mixture yielded crystals suitable for single crystal X-ray crystallographic studies. Yield: 95.1%. Mp: 324°C.

IR ν/cm^{-1}: 1359w, 1292w, 1159w, 1028w, 832w, 605w, 435s. ESI-MS: 728.9070 [Cu$_2$(**L11**)$_2$I]$^+$, 602.0027 [Cu$_2$(**L11**)$_2$]$^{2+}$, 539.0728 [Cu$_1$(**L**)$_2$]$^+$, 342.0272 [Cu(**L11**)ClO_4]$^{2+}$, 300.9996 [Cu(**L11**)]$^+$, 239.0785 [(**L11**)H]$^+$. Analysis: Calc. for ($C_{10}H_8N_8$)Cu_3I_3.MeCN: C, 16.94; H, 1.07; N, 14.82. Found: C, 17.27; H, 1.13; N, 14.59.

$Cu(MeCN)_4BF_4$ with 1,4-di(2-pyrazinyl)-6,7,8,9-tetrahydro-5H-cyclohepta[*d*]pyridazine, viz **3.7**

Tetrakis(acetonitrile)copper(I) tetrafluoroborate (8.78 mg, 0.028 mmol) in hot dichloromethane/acetonitrile (9:1, 2 mL) was added to a warm dichloromethane/acetonitrile solution (9:1, 2 mL) containing **L15** (9.63 mg, 0.031 mmol). Crystals suitable for single crystal X-ray diffraction studies were obtained by vapour diffusion of diisopropyl ether. Yield: 83.8%. Mp: 260°C

IR ν/cm^{-1}: 2922b/w, 1382w, 1048s, 731w, 520w, 423w. ESI-MS: 821.1501 $[Cu_2(\mathbf{L15})_2BF_4]^+$, 671.2180 $[Cu(\mathbf{L15})_2]^+$, 520.1449 $[Cu_2(\mathbf{L15})_3]^{2+}$, 408.0999 $[Cu(\mathbf{L15})CH_3CN]^{2+}$, 367.0730 $[Cu(\mathbf{L15})]^+/[Cu_2(\mathbf{L15})_2]^{2+}$, 335.6084 $[Cu(\mathbf{L15})_2]^{2+}$, 305.1512 $[(\mathbf{L15})H]^+$. UV-Visible (CH_3CN) λ_{max} (ε) 277 nm (23877), 210 (39515). Calc. for $(C_{17}H_{16}N_6)CuBF_4.C_3H_7NOCl_2$: C, 40.12; H, 3.87; N, 16.38. Found: C, 39.68; H, 3.56; N, 16.43.

6.5 Complexes with zinc

$Zn(ClO_4)_2$ with 3,6-di(2-pyridyl)pyridazine, viz **4.1**

Two solutions, **L1** (9.82 mg, 0.042 mmol) in hot acetonitrile (2 mL) and zinc perchlorate hexahydrate (15.89 mg, 0.043 mmol) in hot acetonitrile (2 mL) were added together to form the reaction mixture. Crystals were obtained by vapour diffusion of diisopropyl ether into the complex mixture that were suitable for single X-ray crystallography. Yield: 98.9%. Mp: >360°C.

^{1}H-NMR (400 MHz, CD_3CN) δ 9.05(s, 2H, H_9), 8.61(d, J=7.8 Hz, 2H, H_3), 8.45(td, J=7.9 Hz, 1.6Hz, 2H, H_4), 8.02(d, J=4.7 Hz, 2H, H_6), 7.91(t, J=5.8 Hz, 2H, H_5). ^{13}C-NMR (100 MHz, CD_3CN) δ 155.25(C_8), 149.88(C_6), 146.33(C_2), 143.00(C_4), 137.71(C_9), 129.82(C_5), 125.73(C_3). IR ν/cm^{-1}: 1605w, 1459w, 1425w, 1061br/m, 774w, 618m. ESI-MS: 383.0998 $[Zn(\mathbf{L1})_3]^{2+}$, 266.0552 $[Zn(\mathbf{L1})_2]^{2+}$, 235.0985$[(\mathbf{L1})H]^+$. UV-Visible (CH_3CN) λ_{max} (ε) 299 nm (32781), 242 nm (12888). Analysis: Calc. for $(C_{14}H_{10}N_4)_3(Zn(ClO_4)_2)_2.2H_2O$: C, 39.8; H, 2.70; N, 13.26. Found: C, 40.18; H, 2.74; N, 13.57.

$Zn(ClO_4)_2$ with 1,4-di(pyridin-2-yl)-6,7-dihydro-5H-cyclopenta[d]pyridazine, viz **4.2**

Zinc perchlorate hexahydrate (14.04 mg, 0.037 mmol) and **L2** (10.21 mg, 0.037 mmol) were dissolved separately in acetonitrile (2 mL), heated, and then combined to give a colourless solution.

Crystals suitable for single crystal analysis were prepared by vapour diffusion of diethyl ether into the complex mixture. Yield: 73.6%. Mp: 244°C.

^{1}H-NMR (500 MHz, CD_3CN) δ 8.46(d, *J*=8.4 Hz, 1H, H_3), 8.39(t, *J*=7.8 Hz, 1H, H_4), 7.96(d, *J*=5.2 Hz, 1H, H_6), 7.83(t, *J*=6.4 Hz, 1H, H_5), 3.68-3.53(m, 2H, H_{10}), 3.43-2.32(m, 2H, H_{11}). ^{13}C-NMR (125 MHz, CD_3CN) δ 152.83(C_9), 151.96(C_8), 150.00(C_6), 146.97(C_2), 142.62(C_4), 129.04(C_5), 127.43(C_3), 34.08(C_{10}), 23.80(C_{11}). IR ν/cm^{-1}: 3423br/w, 1602w, 1391w, 1261w, 1055br/s, 1014m, 793w, 618s. ESI-MS: 711.1211 $[Zn(\mathbf{L2})_2](ClO_4)_2$, 443.1469 $[Zn(\mathbf{L2})_3]^{2+}$, 306.0862 $[Zn(\mathbf{L2})_2]^{2+,}$ 275.1294 $[(\mathbf{L2})H]^{+}$. UV-Visible (CH_3CN) λ_{max} (ε) 298 nm (23835), 245 nm (18000), 207 nm (23596). **Analysis:** Calc. for $C_{17}H_{14}N_4.Zn(ClO_4)_2.2MeCN$: C, 40.63; H, 3.25; N, 11.42. Found: C, 40.61; H, 3.59; N, 11.06.

$Zn(ClO_4)_2$ with 1,4-di(pyridin-2-yl)-5,6,7,8-tetrahydrophthalazine, viz **4.3**

L3 (10.00 mg, 0.035 mmol) and zinc perchlorate hexahydrate (13.29 mg, 0.035 mmol) were both dissolved in hot acetonitrile and combined to give a colourless solution. Suitable crystals for single crystal structural analysis were obtained by diffusion of diisopropyl ether into the reaction mixture. Yield: 61.3%. Mp: 298°C.

^{1}H-NMR (500 MHz, CD_3CN-d_3) δ 8.47(d, *J*=5.2 Hz, 1H, H_6), 8.43(d, *J*=8.3 Hz, 1H, H_3), 8.31(t, *J*=7.9 Hz, 1H, H_4), 7.81(t, *J*=6.4 Hz, 1H, H_5), 3.32(t, *J*=8.6 Hz, 1H, H_{10a}), 3.18(d, *J*=17.1 Hz, 1H, H_{10b}), 2.13(s, 2H, H_{11a}), 1.62(s, 2H, H_{11b}). ^{13}C-NMR (125 MHz, CD_3CN) δ 154.23(C_8), 150.65(C_6), 147.22(C_2), 145.96(C_9), 141.83(C_4), 128.47(C_5), 128.43(C_3), 29.48(C_{10}), 20.48(C_{11}). IR ν/cm^{-1}: 3434br/w, 1601w, 1392w, 1258w, 1073br/s, 789w, 751w, 619s. ESI-MS: 739.1527 $[Zn(\mathbf{L3})_2(ClO_4)]^{+}$, 464.1705 $[Zn(\mathbf{L3})_3]^{2+}$, 320.1017 $[Zn(\mathbf{L3})_2]^{2+}$, 289.1450 $[(\mathbf{L3})H]^{+}$. UV-Visible (CH_3CN) λ_{max} (ε) 296 nm (25746), 242 nm (20740). Analysis: Calc. for $C_{18}H_{16}N_4.Zn(ClO_4)_2$: C, 39.12; H, 2.92; N, 10.14. Found: C, 38.74; H, 3.51; N, 10.31.

$Zn(ClO_4)_2$ with 1,4-di(pyridin-2-yl)-6,7,8,9-tetrahydro-5H-cyclohepta[*d*]pyridazine, viz **4.4**

Zinc perchlorate hexahydrate (12.53 mg, 0.034 mmol) was dissolved in hot acetonitrile (1 mL), then combined with molecule, **L4** (9.07 mg, 0.030 mmol) dissolved in hot acetonitrile (1 mL). Crystals were obtained by vapour diffusion of diisopropyl ether into the reaction mixture that were suitable for single X-ray diffraction. Yield: 64.1%. Mp: 266°C.

^{1}H-NMR (500 MHz, CD_3CN) δ 8.42(d, *J*=5.2 Hz, 1H, H_6), 8.32(t, *J*=7.8 Hz, 1H, H_4), 8.12(d, *J*=8.1 Hz, 1H, H_3), 7.82(dd, *J*=7.1 Hz, 5.9Hz, 1H, H_5), 3.32(s, 2H, H_{10}), 2.00(m, 2H, H_{11}), 1.87(s, 1H, H_{11a}), 1.76(s, 1H, H_{11b}). ^{13}C-NMR (125 MHz, CD_3CN) δ 154.44(C_8), 151.59(C_9), 150.36(C_6), 147.97(C_2), 142.01(C_4), 128.41(C_3), 128.25(C_5), 30.91(C_{10}), 30.61(C_{11}), 24.73(C_{12}). IR *ν*/cm^{-1}: 3478br/w, 1599w, 1477w, 1389w, 1053br/s, 792w, 619s. ESI-MS: 767.1843 [Zn(**L4**)$_2$](ClO_4), 485.1941 [Zn(**L4**)](ClO_4), 334.1174 [Zn(**L4**)$_2$]$^{2+}$, 303.1611 [(**L4**)H]$^{+}$. UV-Visible (CH_3CN) λ_{max} (ε) 292 nm (15082), 241 nm (12681). Analysis: Calc. for ($C_{19}H_{18}N_4$)Zn(ClO_4)$_2$.6H_2O: C, 33.82; H, 4.48; N, 8.3. Found: C, 33.88; H, 4.08; N, 8.12.

<u>Zn(ClO_4)$_2$ with 7,10-di(pyridin-2-yl)-8,9-difluoranthene, viz **4.5**</u>

Zinc perchlorate hexahydrate (10.92 mg, 0.030 mmol) in hot dichloromethane and acetonitrile (9:1, 1 mL) was added to molecule **L5** (10.99 mg, 0.031 mmol) in hot dichloromethane (1 mL) to form the complex mixture. Vapour diffusion of diethyl ether yielded crystals suitable for single X-ray crystallography. Yield: 41.3%. Mp: 263°C.

IR *ν*/cm^{-1}: 3559br/w, 1601w, 1418w, 1383w, 1058br/s, 788m, 753m, 620s. ESI-MS: 879.1208 [Zn(**L5**)$_2$(ClO_4)]$^{+}$, 569.1468 [Zn(**L5**)$_3$]$^{2+}$, 390.0859 [Zn(**L5**)$_2$]$^{2+}$, 359.1283 [(**L5**)H]$^{+}$. UV-Visible (DMSO) λ_{max} (ε) 369 nm (23195), 325 nm (22615), 308 nm (27007), 271 nm (48964). Analysis: Calc. for ($C_{24}H_{14}N_4$)$_3$Zn(ClO_4)$_2$.CH_2Cl_2: C, 60.1; H, 2.97; N, 11.52. Found: C, 59.95; H, 3.24; N, 11.61.

<u>Zn(ClO_4)$_2$ with 3-(3,5-dimethyl-1*H*-pyrazol-1-yl)-6-(1-piperidinyl)-1,2,4,5-tetrazine, viz **4.6**</u>

Zinc perchlorate hexahydrate (10.00 mg, 0.027 mmol) in hot dichloromethane and acetonitrile (9:1, 2 mL) was added to **L10** (10.00 mg, 0.055 mmol) in hot dichloromethane (2 mL) to form a reaction mixture. Vapour diffusion of diethyl ether yielded crystals suitable for single X-ray diffraction analysis. Yield: 47.3%. Mp: 139°C.

^{1}H-NMR (400 MHz, CD_3CN) δ 6.47(s, 1H, H_4), 3.80(s, 4H, H_9), 2.72(s, 3H, H_2), 2.39(s, 3H, H_1), 1.76(d, *J*=4.7 Hz, 2H, H_{11}), 1.65(s, 4H, H_{10}). ^{13}C-NMR (100 MHz, CD_3CN) δ 160.69(C_7), 154.46(C_3), 151.53(C_6), 144.70(C_5), 122.32(C_4), 44.91(C_9), 24.98(C_{10}), 23.75(C_{11}), 13.74(C_2), 12.52(C_1). IR *ν*/cm^{-1}: 3386br/w, 1568w, 1495w, 1394w, 1272w, 1037br/s, 758w, 619m. ESI-MS: 940.3407 [Zn(**L10**)$_3$](ClO_4), 681.1867 [Zn(**L10**)$_2$](ClO_4), 420.6955 [Zn(**L10**)$_3$]$^{2+}$, 291.1179 [Zn(**L10**)$_2$]$^{2+,}$ 260.1616 [(**L10**)H]$^{+}$.]$^{+}$. UV-Visible (CH_3CN) λ_{max} (ε) 464 nm (1032), 293 nm

(25488), 233 (7598). Analysis: Calc. for $C_{24}H_{34}N_{14}.ZnClO_4.2H_2O$: C, 35.20; H, 4.68; N, 23.94. Found C, 35.10; H, 4.67; N, 23.86.

$Zn(ClO_4)_2$ with 3,6-bis(3,5-dimethylpyrazolyl)pyridazine, viz **4.7**

L6 (8.72 mg, 0.032 mmol) and zinc perchlorate hexahydrate (13.20 mg, 0.035 mmol) were both dissolved in hot acetonitrile and combined. Crystals suitable for single crystal X-ray analysis were obtained by diffusion of diisopropyl ether into the reaction mixture. Yield: 42.2%. Mp: >360°C.

^{1}H-NMR (400 MHz, CD_3CN) δ 8.43 (s, 2H, H_{10}), 6.33 (s, 2H, H_4), 2.79 (s, 6H, H_7), 2.39 (s, 6H, H_6). ^{13}C-NMR (100 MHz, CD_3CN) δ 155.41 (C_8), 142.12 (C_5), 140.24 (C_3), 122.80 (C_9), 107.31 (C_4), 13.88 (C_7), 12.64 (C_6). IR ν/cm^{-1}: 1593w, 1473w, 1436w, 1357w, 1075w, 1075br/s, 803w, 620s. **ESI-MS**: 699.1644 $[Zn(\mathbf{L6})_2(ClO_4)]^+$, 434.1795 $[Zn(\mathbf{L6})_3]^{2+}$, 300.1077 $[Zn(\mathbf{L6})_2]^{2+}$, 269.1509 $[(\mathbf{L6})H]^+$. UV-Visible (CH_3CN) λ_{max} (ε) 289 nm (41695). Analysis: Calc. for $(C_{14}H_{16}N_6)_3(Zn(ClO_4)_2)_2.4H_2O$: C, 35.89; H, 4.02; N, 17.94. Found: C, 36.3; H, 3.76; N, 17.85.

$Zn(ClO_4)_2$ with 3,6-bis(2-pyrazinyl)-1,2,4,5-tetrazine, viz **4.8**

The reaction of **L11** (4.47 mg, 0.019 mmol) and $Zn(ClO_4)_2$ (5.93 mg, 0.016 mmol) were dissolved separately in hot acetonitrile and then added together. Upon vapour diffusion of diethyl ether, red crystals suitable for single X-ray diffraction studies were obtained. Yield: 57.5% Mp: >360°C.

^{1}H-NMR (400 MHz, CD_3CN) δ 9.99 (s, 2H, H_3), 9.09 (s, 2H, H_6) 8.99(s, 2H, H_5). ^{13}C-NMR (100 MHz, CD_3CN) δ 148.99 (C_6), 145.73 (C_3), 145.00 (C_5). IR ν/cm^{-1}: 3483m/b, 3325w/b, 3185m/b, 1638b/w, 1380m, 1075s, 1057s, 933w, 622m. ESI-MS: 639.0205 $[Zn(\mathbf{L11})_2(ClO_4)]^+$, 400.9482 $[Zn(\mathbf{L11})ClO_4]^+$, 270.0351 $[Zn(\mathbf{L11})_2ClO_4]^+$, 239.0785 $[(\mathbf{L11})H]^+$. UV-Visible (CH_3CN) λ_{max} (ε) 535 nm (534), 292 nm (33260), 244 nm (10778). Analysis: Calc. for $(C_{10}H_8N_8)Zn(ClO_4)_2.4H_2O$: C, 20.90; H, 2.46; N, 19.50. Found: C, 21.07; H, 2.57; N, 19.16.

References

(1) Lehn, J. M. *Angew. Chem. Int. Edn.* **1988**, *27*, 89-112.

(2) Wilson, A. J. *Ann. Rep. Prog. Chem. Sect. B* **2008**, 164-183.

(3) Dalgarno, S. J. *Ann. Rep. Prog. Chem. Sect. B* **2010**, 197-215.

(4) Chang. R. *Chemistry*; McGraw-Hill, 2009.

(5) Cram, D. J. *Science* **1988**, *240*, 760-767.

(6) Pedersen, C. J. *Angew. Chem. Int. Ed. Engl* **1988**, *27*, 1021-1027.

(7) Steed, J. W., Atwood J. L., Gale, P. A. *Definition and Emergence of Supramolecular Chemistry. Supramolecular Chemistry: From Molecules to Nanomaterials.*; John Wiley and Sons Ltd., 2012.

(8) Lehn, J. *Science* **1993**, *260*, 1762-1763.

(9) Janiak, C. *Dalton* **2000**, 3885-3896.

(10) Steiner, T. *Angew. Chem. Int. Edn.* **2002**, *41*, 49-76.

(11) Nishio, M.; Umezawa, Y.; Honda, K.; Tsuboyama, S.; Suezawa, H. *CrystEngComm* **2009**, *11*, 1757-1788.

(12) Treadway, C. R.; Hill, M. G.; Barton, J. K. *Chem. Phys.* **2002**, *281*, 409-428.

(13) Sherrington, D. C.; Taskinen, K. A. *Chem. Soc. Rev.* **2001**, *30*, 83-93.

(14) Constable, E. C. *Chem. Ind.* **1994**, 56-59.

(15) Whitesides, G. M.; Grzybowski, B. *Science* **2002**, *295*, 2418-2421.

(16) Lehn, J.-M. *Angew. Chem. Int. Edn.* **1990**, *29*, 1304-1319.

(17) Holliday, B. J.; Mirkin, C. A. *Angew. Chem. Int. Edn.* **2001**, *40*, 2022-2043.

(18) Wender, P. A.; Harmata, M. *Silver in organic chemistry*; John Wiley & Sons, 2011.

(19) Steel, P. J.; Fitchett, C. M. *Coord. Chem. Rev.* **2008**, *252*, 990-1006.

(20) Young, A. G.; Hanton, L. R. *Coord. Chem. Rev.* **2008**, *252*, 1346-1386.

(21) Housecroft, C. E.; Sharpe, A. G. *Inorganic Chemistry*; 3rd ed.; Pearson Education Limited: Harlow, England, 2008.

(22) Li, S.-S.; Northrop, B. H.; Yuan, Q.-H.; Wan, L.-J.; Stang, P. J. *Acc. Chem. Res.* **2009**, *42*, 249-259.

(23) Lee, J.-S. *Physica E. Low Dimens. Syst. Nanostruct.* **2013**, *51*, 94-103.

(24) Pardo, E.; Ruiz-Garcia, R.; Cano, J.; Ottenwaelder, X.; Lescouezec, R.; Journaux, Y.; Lloret, F.; Julve, M. *Dalton Trans.* **2008**, 2780-2805.

(25) Albrecht, M.; Fiege, M.; Osetska, O. *Coord. Chem. Rev.* **2008**, *252*, 812-824.

(26) Suh, M. P.; Cheon, Y. E.; Lee, E. Y. *Coord. Chem. Rev.* **2008**, *252*, 1007-1026.

(27) Roy, B.; Bairi, P.; Nandi, A. K. *RSC Adv.* **2014**, *4*, 1708-1734.

(28) Wessjohann, L. A.; Rivera, D. G.; Coll, F. *J. Org. Chem.* **2006**, *71*, 7521-7526.

(29) Trant, A. G.; Baddeley, C. J. *J. Phys. Chem. C* **2010**, *115*, 1025-1030.

(30) Youinou, M. T.; Rahmouni, N.; Fischer, J.; Osborn, J. A. *Angew. Chem. Int. Edn.* **1992**, *31*, 733-735.

(31) Hannon, M. J.; Painting, C. L.; Errington, W. *Chem. Commun.* **1997**, 307-308.

(32) Sauvage, J.-P. *Acc. Chem. Res.* **1998**, *31*, 611-619.

(33) Fujita, M. *Acc. Chem. Res.* **1998**, *32*, 53-61.

(34) Albrecht, M. *Chem. Rev.* **2001**, *101*, 3457-3497.

(35) Fujita, M.; Sasaki, O.; Mitsuhashi, T.; Fujita, T.; Yazaki, J.; Yamaguchi, K.; Ogura, K. *Chem. Commun.* **1996**, 1535-1536.

(36) Schottel, B. L.; Chifotides, H. T.; Shatruk, M.; Chouai, A.; Perez, L. M.; Bacsa, J.; Dunbar, K. R. *J. Am. Chem. Soc.* **2006**, *128*, 5895-5912.

(37) Baxter, P. N. W.; Lehn, J.-M.; Fischer, J.; Youinou, M.-T. *Angew. Chem. Int. Edn.* **1994**, *33*, 2284-2287.

(38) Marquis, A.; Kintzinger, J.-P.; Graff, R.; Baxter, P. N. W.; Lehn, J.-M. *Angew. Chem. Int. Edn.* **2002**, *41*, 2760-2764.

(39) Baxter, P. N. W.; Lehn, J.-M.; Baum, G.; Fenske, D. *Chem. Eur. J.* **2000**, *6*, 4510-4517.

(40) Dawe, L. N.; Shuvaev, K. V.; Thompson, L. K. *Inorg. Chem.* **2009**, *48*, 3323-3341.

(41) Dawe, L. N.; Shuvaev, K. V.; Thompson, L. K. *Chem. Soc. Rev.* **2009**, *38*, 2334-2359.

(42) Dey, S. K.; Abedin, T. S. M.; Dawe, L. N.; Tandon, S. S.; Collins, J. L.; Thompson, L. K.; Postnikov, A. V.; Alam, M. S.; Müller, P. *Inorg. Chem.* **2007**, *46*, 7767-7781.

(43) Ruben, M.; Rojo, J.; Romero-Salguero, F. J.; Uppadine, L. H.; Lehn, J.-M. *Angew. Chem. Int. Edn.* **2004**, *43*, 3644-3662.

(44) Onions, S. T.; Frankin, A. M.; Horton, P. N.; Hursthouse, M. B.; Matthews, C. J. *Chem. Commun.* **2003**, 2864-2865.

(45) Milway, V. A.; Abedin, S. M. T.; Niel, V.; Kelly, T. L.; Dawe, L. N.; Dey, S. K.; Thompson, D. W.; Miller, D. O.; Alam, M. S.; Muller, P.; Thompson, L. K. *Dalton Trans.* **2006**, 2835-2851.

(46) Kramer, R.; Lehn, J. M.; Marquis-Rigault, A. *Proc. Natl. Acad. Sci.* **1993**, *90*, 5394-5398.

(47) Dawe, L. N.; Abedin, T. S. M.; Kelly, T. L.; Thompson, L. K.; Miller, D. O.; Zhao, L.; Wilson, C.; Leech, M. A.; Howard, J. A. K. *J. Mater. Chem.* **2006**, *16*, 2645-2659.

(48) Hardy, J. G. *Chem. Soc. Rev.* **2013**, *42*, 7881-7899.

(49) Lehn, J. M.; Rigault, A.; Siegel, J.; Harrowfield, J.; Chevrier, B.; Moras, D. *Proc. Natl. Acad. Sci.* **1987**, *84*, 2565-2569.

(50) Piguet, C.; Bernardinelli, G.; Hopfgartner, G. *Chem. Rev.* **1997**, *97*, 2005-2062.

(51) Piguet, C. *Journal of Inclusion Phenomena* **1999**, *34*, 361-391.

(52) Stadler, A.-M.; Burg, C.; Ramirez, J.; Lehn, J.-M. *Chem. Commun.* **2013**, *49*, 5733-5735.

(53) Eicher, T., Hauptmann, S. *The Chemistry of Heterocycles*; Second ed.; WILEY-VCH, 2003.

(54) Xie, H.; Zu, L.; Oueis, H. R.; Wang, H. L. J.; Wang, W. *Org. Lett.* **2008**, *10*, 1923-1926.

(55) Rahanyan, N.; Linden, A.; Baldridge, K. K.; Siegel, J. S. *Org. Biomol. Chem.* **2009**, *7*, 2082-2092.

(56) Li, Y.; Asadi, A.; Perrin, D. M. *J. Fluorine Chem.* **2009**, *130*, 377-382.

(57) Rusinov, G. L.; Ishmetova, R. I.; Latosh, N. I.; Ganebnych, I. N.; Chupakhin, O. N.; Potemkin, V. A. *Russ. Chem. Bull.* **2000**, *49*, 355-362.

(58) Glidewell, C.; Lightfoot, P.; J. L. Royles, B.; M. Smith, D. *J. Chem. Soc., Perkin Trans. 2* **1997**, *0*, 1167-1174.

(59) Rusinov, G. L.; Latosh, N. I.; Ganebnykh, I. I.; Ishmetova, R. I.; Ignatenko, N. K.; Chupakhin, O. N. *Russ. J. Org. Chem.* **2006**, *42*, 757-765.

(60) Bodman, S. E., Ferguson, J. L., Crowther, A. C., Geraghty, P. B., Fitchett, C. M. *Dalton Trans.* **2014**, *Submitted*.

(61) Constable, E. C.; Housecroft, C. E.; Kariuki, B. M.; Neuburger, M.; Smith, C. B. *Aust. J. Chem.* **2003**, *56*, 653-655.

(62) Mastropietro, T. F.; Marino, N.; Armentano, D.; De Munno, G.; Yuste, C.; Lloret, F.; Julve, M. *Cryst. Growth Des.* **2012**, *13*, 270-281.

(63) Sung, N.-D.; The Industry and Academic Cooperation In Chungnamnational University Iac , S. Korea . 2007; pp 17 pp.

(64) Ball, P. W.; Blake, A. B. *J. Chem. Soc. A* **1969**, 1415-1422.

(65) Andrew, J. E.; Ball, P. W.; Blake, A. B. *Chem. Commun.* **1969**, 143-4.

(66) Ball, P. W.; Blake, A. B. *J. Chem. Soc., Dalton Trans.* **1974**, 852-859.

(67) Tsukada, N.; Sato, T.; Mori, H.; Sugawara, S.; Kabuto, C.; Miyano, S.; Inoue, Y. *J. Organomet. Chem.* **2001**, *627*, 121-126.

(68) Ghedini, M.; Neve, F.; Longeri, M.; Bruno, M. C. *Inorg. Chim. Acta* **1988**, *149*, 131-138.

(69) Ghumaan, S.; Sarkar, B.; Patra, S.; Parimal, K.; van Slageren, J.; Fiedler, J.; Kaim, W.; Lahiri, G. K. *Dalton Trans.* **2005**, 706-712.

(70) Ghedini, M.; Neve, F.; Lanfredi, A. M. M.; Ugozzoli, F. *Inorg. Chim. Acta* **1988**, *147*, 243-250.

(71) Lanfredi, A. M. M.; Tiripicchio, A.; Ugozzoli, F.; Ghedini, M.; Neve, F. *J. Chem. Soc., Dalton Trans.* **1988**, 651-656.

(72) Ghedini, M.; Neve, F.; Bruno, M. C. *Inorg. Chim. Acta* **1988**, *143*, 89-93.

(73) El-Qisairi, A. K.; Qaseer, H. A.; Zaghal, M. H.; Kana'n, S. M.; Atfah, M. A. *J. Coord. Chem.* **2007**, *60*, 1165-1171.

(74) Zaghal, M. H.; Abu-Obeid, M. A.; Atfah, M. A.; El-Qisairi, A. K.; Qaseer, H. A.; Ali, B. F. *Transit. Metal Chem.* **2001**, *26*, 517-522.

(75) Esmadi, F.; Al-Hamid, A. *Transit. Metal Chem.* **1994**, *19*, 571-574.

(76) Cooke, G.; O Maille, G. M.; Quesada, R.; Wang, L.; Varughese, S.; Draper, S. M. *Dalton Trans.* **2011**, *40*, 8206-8212.

(77) Gil, B.; Cooke, G. A.; Nolan, D.; O Maille, G. M.; Varughese, S.; Wang, L.; Draper, S. M. *Dalton Trans.* **2011**, *40*, 8320-8327.

(78) Yu, Q.; Zhang, A.-S.; Hu, T.-L.; Bu, X.-H. *Solid State Sci.* **2010**, *12*, 1484-1489.

(79) Manzano, B. R.; Jalaton, F. A.; Ortiz, I. M.; Soriano, M. L.; De la Torre, F. G.; Elguero, J.; Maestro, M. A.; Mereiter, K.; Claridge, T. D. W. *Inorg. Chem.* **2008**, *47*, 413-428.

(80) Gupta, G.; Prasad, K. T.; Das, B.; Yap, G. P. A.; Rao, K. M. *J. Organomet. Chem.* **2009**, *694*, 2618-2627.

(81) Gao, H.; Zhang, Z.-H.; Jiang, P.; Li, X.-R. *Transit. Metal Chem.* **2006**, *31*, 1088-1092.

(82) Thompson, L. K.; Tandon, S. S.; Manuel, M. E. *Inorg. Chem.* **1995**, *34*, 2356-66.

(83) Thompson, L. K.; Lee, F. L.; Gabe, E. J. *Inorg. Chem.* **1988**, *27*, 39-46.

(84) Mandal, S. K.; Thompson, L. K.; Hanson, A. W. *J. Chem. Soc., Chem. Commun.* **1985**, 1709-11.

(85) Thompson, L. K.; Woon, T. C.; Murphy, D. B.; Gabe, E. J.; Lee, F. L.; Le Page, Y. *Inorg. Chem.* **1985**, *24*, 4719-25.

(86) Cherdantseva, E. V.; Starichenko, D. V.; Slepukhin, P. A.; Ishmetova, R. I.; Shvachko, Y. N.; Korolev, A. V.; Rusinov, G. L.; Ustinov, V. V.; Matern, A. I.; Charushin, V. N. *Russ. Chem. Bull.* **2010**, *59*, 717-723.

(87) Oxtoby, N. S.; Blake, A. J.; Champness, N. R.; Wilson, C. *Proc. Natl. Acad. Sci.* **2002**, *99*, 4905-4910.

(88) Oxtoby, N. S.; Blake, A. J.; Champness, N. R.; Wilson, C. *Dalton Trans.* **2003**, 3838-3839.

(89) Oxtoby, N. S.; Champness, N. R.; Wilson, C. *CrystEngComm* **2005**, *7*, 284-288.

(90) Sarkar, B.; Frantz, S.; Kaim, W.; Duboc, C. *Dalton Trans.* **2004**, 3727-3731.

(91) Sarkar, B.; Kaim, W.; Schleid, T.; Hartenbach, I.; Fiedler, J. *Z. Anorg. Allg. Chem.* **2003**, *629*, 1353-1357.

(92) Cherdantseva, E. V.; Nesterova, A. V.; Matern, A. I.; Buldakova, L. Y.; Yanchenko, M. Y.; Ishmetova, R. I.; Rusinov, G. L. *Russ. J. Gen. Chem.* **2010**, *80*, 1860-1863.

(93) Fitchett, C. M.; Steel, P. J. *Dalton Trans.* **2006**, 4886-4888.

(94) Gulbransen, J. L.; Fitchett, C. M. *CrystEngComm* **2012**, *14*, 5394-5397.

(95) Price, J. R.; Lan, Y.; Jameson, G. B.; Brooker, S. *Dalton Trans.* **2006**, 1491-1494.

(96) Fitchett, C. M.; Richardson, C.; Steel, P. J. *Org. Biomol. Chem.* **2005**, *3*, 498-502.

(97) Steed, J. W.; Atwood, J. L. *Supramolecular chemistry*; John Wiley & Sons, 2009.

(98) Schottel, B. L.; Chifotides, H. T.; Shatruk, M.; Chouai, A.; Pérez, L. M.; Bacsa, J.; Dunbar, K. R. *J. Am. Chem. Soc.* **2006**, *128*, 5895-5912.

(99) Hoogenboom, R.; Kickelbick, G.; Schubert, U. S. *Eur. J. Org. Chem.* **2003**, 4887-4896.

(100) Song, R.-F.; Sun, Y.-Y.; Yang, J.; Yang, X.-Y. *J. Inorg. Organomet. P.* **2011**, *21*, 237-243.

(101) Domasevitch, K. V.; Solntsev, P. V.; Krautscheid, H.; Zhylenko, I. S.; Rusanov, E. B.; Chernega, A. N. *Chem. Commun.* **2012**, *48*, 5847-5849.

(102) Lu, Z.-Z.; Zhang, R.; Li, Y.-Z.; Guo, Z.-J.; Zheng, H.-G. *J. Am. Chem. Soc.* **2011**, *133*, 4172-4174.

(103) Lu, Z.-Z.; Zhang, R.; Pan, Z.-R.; Li, Y.-Z.; Guo, Z.-J.; Zheng, H.-G. *Chem. Eur. J.* **2012**, *18*, 2812-2824, S2812/1-S2812/18.

(104) Solntsev, P. V.; Sieler, J.; Krautscheid, H.; Domasevitch, K. V. *Dalton Trans.* **2004**, 1153-1158.

(105) Zhang, J. *Acta Cryst.* **2010**, *E66*, m1480.

(106) Allen, F. H.; Bellard, S.; Brice, M.; Cartwright, B. A.; Doubleday, A.; Higgs, H.; Hummelink, T.; Hummelink-Peters, B.; Kennard, O.; Motherwell, W. *Acta Cryst.* **1979**, *B35*, 2331-2339.

(107) Maret, W.; Li, Y. *Chem. Rev.* **2009**, *109*, 4682-4707.

(108) Maret, W. *J Trace Elements in Medicine and Biology* **2005**, *19*, 7-12.

(109) Aoki, S.; Kimura, E. *Chem. Rev.* **2004**, *104*, 769-788.

(110) Hanas, J.; Larabee, J.; Hocker, J. In *Zinc Finger Proteins*; Iuchi, S., Kuldell, N., Eds.; Springer US, 2005; pp 39-46.

(111) Frausto da Silva, J. J. R. W., R. J. P *The Biological Chemistry of the Elements*: Oxford, U.K., 1991.

(112) James, S. L. *Chem. Soc. Rev.* **2003**, *32*, 276-288.

(113) Funeriu, D. P.; Rissanen, K.; Lehn, J.-M. P. *Proc. Natl. Acad. Sci.* **2001**, *98*, 10546-10551.

(114) Vazquez, M.; Bermejo, M. R.; Licchelli, M.; Gonzalez-Noya, A. M.; Pedrido, R. M.; Sangregorio, C.; Sorace, L.; Garcia-Deibe, A. M.; Sanmartin, J. *Eur. J. Inorg. Chem.* **2005**, 3479-3490.

(115) Huang, W.; Zhu, H.-B.; Gou, S.-H. *Coord. Chem. Rev.* **2006**, *250*, 414-423.

(116) Hardy, J. G.; Cao, X.-y.; Harrowfield, J.; Lehn, J.-M. *New J. Chem.* **2012**, *36*, 668-673.

(117) Stefankiewicz, A. R.; Harrowfield, J.; Madalan, A.; Rissanen, K.; Sobolev, A. N.; Lehn, J.-M. *Dalton Trans.* **2011**, *40*, 12320-12332.

(118) Stefankiewicz, A. R.; Rogez, G.; Harrowfield, J.; Sobolev, A. N.; Madalan, A.; Huuskonen, J.; Rissanen, K.; Lehn, J.-M. *Dalton Trans.* **2012**, *41*, 13848-13855.

(119) Kurup, M. R. P. P.; Fun, H.-K. *Inorg. Chem.Comm.* **2007**, *10*, 324-328.

(120) Weizman, H.; Libman, J.; Shanzer, A. *J. Am. Chem. Soc.* **1998**, *120*, 2188-2189.

(121) Anna, V. R.; Prasad, K. T.; Wang, P.; Rao, K. M. *J. Chem. Sci.* **2012**, *124*, 565-575.

(122) Sheldrick, G. *Acta Cryst.* **2008**, *A64*, 112-122.

(123) Sheldrick, G. *Göttingen University: Göttingen, Germany* **1997**.

(124) Dolomanov, O. V.; Bourhis, L. J.; Gildea, R. J.; Howard, J. A.; Puschmann, H. *J. Appl. Cryst.* **2009**, *42*, 339-341. (125) Thebault, F.; Blake, A. J.; Wilson, C.; Champness, N. R.; Schroeder, M. *New J. Chem.* **2006**, *30*, 1498-1508.

Appendices

Crystal data and structural refinement details

Table A1. Crystal data and structure refinement for **2.4**, **2.5**, **2.6**, **2.7** and **2.8**.

Compound	**2.4**	**2.5**	**2.6**	**2.7**	**2.8**
Empirical formula	$C_{34}H_{28}AgBF_4N_8$	$C_{20}H_{16}Ag_2F_6N_4O_6S_2$	$C_{52}H_{58}Ag_4Cl_4F_{24}N_{14}P_4$	$C_{106}H_{66}Ag_4Cl_4F_{12}N_{18}O_{12}S_4$	$C_{46}H_{52}Ag_4F_{12}N_{16}O_{12}S_4$
Formula weight	743.32	802.23	2032.27	2713.28	1808.74
Radiation Source	MoKα	MoKα	MoKα	MoKα	MoKα
Temperature (K)	120.0(1)	120.0(1)	120.0(1)	120.0(1)	120.0(1)
Crystal system	triclinic	Monoclinic	triclinic	triclinic	monoclinic
Space group	P-1	$P2_1/c$	P-1	P-1	$P2_1/c$
Unit cell dimensions: a (Å)	7.71106(11)	9.07079(16)	10.8982(3)	10.9636(2)	11.6261(3)
b (Å)	13.2156(2)	19.5058(4)	13.6051(4)	15.3060(4)	20.0170(4)
c (Å)	15.3394(2)	14.1587(2)	13.9044(4)	16.7266(6)	14.0058(3)
α (°)	78.1499(12)	90	109.105(3)	114.371(3)	90
β (°)	81.8731(12)	98.5136(16)	94.572(2)	98.952(2)	101.620(2)
γ (°)	77.2010(13)	90	109.494(3)	97.955(2)	90
Volume($Å^3$)	1484.31(4)	2477.54(8)	1794.63(10)	2460.75(13)	3192.64(11)
Z	2	4	1	1	2
Density (calculated) (Mg/m^3)	1.663	2.151	1.8803	1.831	1.8814
Absorption coefficient (mm^{-1})	0.746	1.842	1.423	1.077	1.444
F(000)	752	1568	998.1	1352	1787
Crystal size (mm)	0.21 × 0.05 × 0.05	0.18 × 0.13 × 0.04	0.31 × 0.25 × 0.12	0.08 × 0.04 × 0.04	0.19 × 0.16 × 0.12
Theta range for data collection (°)	5.446 to 55°	5.434 to 54.998°	5.48 to 55°	5.242 to 54.998°	5.42 to 55°
Reflections collected	41522	46419	45550	41624	107902
Independent reflections [R(int)]	6804 [0.0294]	5688 [0.0317]	8236 [0.0281]	11288 [0.0421]	7321 [0.0375]
Observed reflections (I>2s(I))	6544	5262	7506	9981	6762
Data / restraints / parameters	6804/0/517	5688/0/380	8236/0/459	11288/6/760	7321/0/428
Goodness-of-fit on F^2	0.68	1.055	1.046	1.157	1.063
R_1 [I>2σ (I)]	0.0217	0.0291	0.0307	0.0774	0.0385
wR2 (all data)	0.0648	0.0789	0.0853	0.1892	0.1118
Flack Parameter					

Table A2. Crystal data and structure refinement for **2.9**, **2.10**, **2.11**, **2.12** and **2.13**.

Compound	**2.9**	**2.10**	**2.11**	**2.12**	**2.13**
Empirical formula	$C_{48}H_{64}Ag_4F_{12}N_{16}O_{16}S_4$	$C_{56}H_{54}Ag_4F_{12}N_{14}O_{20}S_4$	$C_{96}H_{137}Ag_4F_{24}N_{56}P_4$	$C_{32}H_{22}Ag_2F_6N_{12}O_6S_2$	$C_{38}H_{37}Ag_2F_{12}N_{15}OP_2$
Formula weight	1908.87	2030.85	3086.97	1064.47	1225.5
Radiation Source	MoKα	MoKα	MoKα	CuKα	CuKα
Temperature (K)	120.0(1)	287.0(1)	120.0(1)	120.0(1)	120.0(1)
Crystal system	monoclinic	triclinic	triclinic	triclinic	triclinic
Space group	C2/c	P-1	P-1	P-1	P-1
Unit cell dimensions: a (Å)	32.147(2)	12.17101(18)	11.5597(3)	8.3324(8)	9.2760(2)
b (Å)	11.8130(2)	12.88618(19)	18.4198(6)	10.4247(5)	12.1244(3)
c (Å)	24.7278(13)	13.2277(3)	30.7766(9)	10.9392(13)	12.3076(2)
α (°)	90	100.5726(14)	98.910(3)	90.097(8)	99.2660(17)
β (°)	129.510(10)	107.9861(15)	96.708(2)	90.487(9)	107.610(2)
γ (°)	90	107.7327(13)	104.439(3)	111.397(7)	107.624(2)
Volume($Å^3$)	7244.9(10)	1789.11(5)	6186.3(3)	884.68(15)	1207.80(5)
Z	4	1	2	1	1
Density (calculated) (Mg/m^3)	1.75	1.885	1.657	1.998	1.685
Absorption coefficient (mm^{-1})	1.282	1.307	0.782	10.865	7.988
F(000)	3808	1008	3138	526	610
Crystal size (mm)	0.37 × 0.17 × 0.09	0.16 × 0.09 × 0.05	0.39 × 0.25 × 0.18	0.13 × 0.05 × 0.03	0.10 × 0.08 × 0.05
Theta range for data collection (°)	6.086 to 55°	5.554 to 76.072°	5.342 to 54.998°	8.082 to 134.992°	7.846 to 134.998°
Reflections collected	47062	83772	64811	4350	18737
Independent reflections [R(int)]	7305 [0.0393]	18710 [0.0406]	28337 [0.0518]	2692 [0.0561]	4349 [0.0371]
Observed reflections (I>2s(I))	6553	15216	20572	2608	4212
Data / restraints / parameters	7305/18/494	18710/0/501	28337/36/1672	2692/24/271	4349/0/334
Goodness-of-fit on F^2	1.081	1.056	1.074	1.259	1.135
R_1 [I>2σ (I)]	0.0536	0.0419	0.0653	0.1399	0.0476
wR2 (all data)	0.1714	0.1188	0.1648	0.3686	0.1452
Flack Parameter					

Table A3. Crystal data and structure refinement for **3.1**, **3.2**, **3.3**, **3.4** and **3.5**.

Compound	**3.1**	**3.2**	**3.3**	**3.4**	**3.5**
Empirical formula	$C_{292}H_{241}B_{16}Cu_{16}F_{64}N_{74}O_2$	$C_{27.5}H_{25}N_{2.5}O_{2.5}Cu_{0.5}I_{0.5}$	$C_{46}H_{62}B_4Cu_5F_{16}N_{14}O_{12}$	$C_{96}H_{80}Cu_{19}I_{20}N_{24}$	$C_{15}H_9BCuF_4N_{12}$
Formula weight	7224.13	525.72	1668.03	5315.1	507.69
Radiation Source	MoKα	CuKα	MoKα	CuKα	CuKα
Temperature (K)	120.0(1)	120.0(1)	120.0(1)	120.0(1)	120.0(1)
Crystal system	triclinic	monoclinic	triclinic	monoclinic	monoclinic
Space group	P1	$P2_1/m$	P-1	$P2_1/c$	$P2_1/c$
Unit cell dimensions: a (Å)	14.7322(4)	8.9739(9)	10.8673(5)	7.22168(9)	11.0689(4)
b (Å)	22.2070(5)	18.4291(11)	11.3077(5)	19.6955(2)	12.2929(4)
c (Å)	22.9447(6)	14.0028(10)	13.0768(4)	21.8731(3)	13.2159(4)
α (°)	83.469(2)	90	86.073(3)	90	90
β (°)	80.733(2)	99.055(8)	81.280(3)	91.1657(12)	97.784(3)
γ (°)	79.395(2)	90	73.733(4)	90	90
Volume($Å^3$)	7254.6(3)	2287.0(3)	1524.20(11)	3110.46(7)	1781.69(11)
Z	1	4	1	1	4
Density (calculated) (Mg/m^3)	1.654	1.527	1.817	2.837	1.893
Absorption coefficient (mm^{-1})	1.259	6.431	1.836	42.784	2.455
F(000)	3647	1074	841	2435	1012
Crystal size (mm)	0.39 × 0.18 × 0.10	0.09 × 0.04 × 0.02	0.17 × 0.16 × 0.09	0.27 × 0.02 × 0.01	0.30 × 0.10 × 0.10
Theta range for data collection (°)	5.31 to 50.5°	6.392 to 148.474°	5.234 to 75.512°	6.04 to 148.89°	8.062 to 134.938°
Reflections collected	104152	13510	46802	32971	6374
Independent reflections [R(int)]	52365 [0.0418]	4625 [0.0555]	15553 [0.0335]	6260 [0.0556]	3199 [0.0219]
Observed reflections (I>2s(I))	40087	2590	11046	5723	2930
Data / restraints / parameters	52365/27/4281	4625/0/165	15553/7/489	6260/0/420	3199/0/298
Goodness-of-fit on F^2	1.017	3.493	1.041	1.035	0.892
R_1 [I>2σ (I)]	0.0589	0.1986	0.0482	0.0378	0.0417
wR2 (all data)	0.1516	0.567	0.1409	0.1075	0.1178
Flack Parameter	-0.012(4)				

Table A4. Crystal data and structure refinement for **3.6**, **3.7**, **4.1**, **4.2** and **4.3**.

Compound	**3.6**	**3.7**	**4.1**	**4.2**	**4.3**
Empirical formula	$C_{10}H_6Cu_2I_2N_8$	$C_{168}H_{168}B_8Cu_8F_{32}N_{64}$	$C_{100}H_{84}Cl_8N_{32}O_{32}Zn_4$	$C_{56}H_{49.5}Cl_4N_{14.5}O_{16}Zn_2$	$C_{78}H_{77}Cl_6N_{19}O_{30}Zn_4$
Formula weight	619.11	4286.45	2791.07	1454.14	2234.76
Radiation Source	CuKα	MoKα	MoKα	CuKα	CuKα
Temperature (K)	120.0(1)	120.0(1)	120.0(1)	120.0(1)	287.0(1)
Crystal system	monoclinic	monoclinic	monoclinic	orthorhombic	monoclinic
Space group	$P2_1/n$	C2/c	Pn	Aba2	$P2_1/n$
Unit cell dimensions: a (Å)	9.3549(3)	26.6151(11)	18.7724(6)	24.7037(3)	16.7902(5)
b (Å)	6.8766(2)	9.1830(2)	24.8564(8)	22.0120(3)	22.1991(4)
c (Å)	23.2528(10)	22.5893(8)	12.3412(3)	21.7668(4)	27.0999(7)
α (°)	90	90	90	90	90
β (°)	92.478(4)	121.956(6)	90	90	92.979(2)
γ (°)	90	90	90	90	90
Volume($Å^3$)	1494.45(10)	4684.3(4)	5758.6(3)	11836.3(3)	10087.2(4)
Z	4	1	2	8	4
Density (calculated) (Mg/m^3)	2.752	1.52	1.61	1.632	1.472
Absorption coefficient (mm^{-1})	36.034	0.991	1.102	3.378	3.254
F(000)	1144	2184	2840	5944	4560
Crystal size (mm)	0.08 × 0.04 × 0.03	0.37 × 0.21 × 0.07	0.25 × 0.21 × 0.07	0.45 × 0.29 × 0.24	0.32 × 0.20 × 0.11
Theta range for data collection (°)	7.612 to 134.988°	5.614 to 54.992°	5.374 to 54.988°	6.74 to 134.996°	6.054 to 148.02°
Reflections collected	7123	30657	46220	28948	57739
Independent reflections [R(int)]	2687 [0.0411]	5381 [0.0278]	24699 [0.0337]	9258 [0.0406]	19796 [0.0234]
Observed reflections (I>2s(I))	2332	4949	22295	8800	15219
Data / restraints / parameters	2687/0/199	5381/12/372	24699/14/1631	9258/1/838	19796/10/1308
Goodness-of-fit on F^2	1.104	1.024	1.116	1.034	1.104
R_1 [I>2σ (I)]	0.0366	0.0362	0.055	0.0348	0.0739
wR2 (all data)	0.0946	0.1015	0.1313	0.0925	0.2424
Flack Parameter			0.028(4)	0.002(9)	

Table A5. Crystal data and structure refinement for **4.4**, **4.5**, **4.6**, **4.7** and **4.8**.

Compound	**4.4**	**4.5**	**4.6**	**4.7**	**4.8**
Empirical formula	$C_{88}H_{93}Cl_6N_{22}O_{29}Zn_4$	$C_{75}H_{47}Cl_4N_{13}O_8Zn$	$C_{84}H_{96}Cl_8N_{36}O_{32}Zn_4$	$C_{30}H_{42}Cl_2N_{17}O_8Zn$	$C_{18}H_{18}Cl_2N_{12}O_8Zn$
Formula weight	2397.02	1465.42	2667.04	905.07	666.71
Radiation Source	CuKα	CuKα	CuKα	MoKα	CuKα
Temperature (K)	120.0(1)	120.0(1)	120.0(1)	120.0(1)	287.0(1)
Crystal system	triclinic	monoclinic	trigonal	triclinic	monoclinic
Space group	P-1	$P2_1/n$	P-3c1	P-1	$P2_1/a$
Unit cell dimensions: a (Å)	14.0182(2)	17.67741(18)	18.9678(6)	12.0791(5)	11.5181(4)
b (Å)	15.9372(2)	14.09011(13)	18.9678(6)	12.9316(5)	23.0673(6)
c (Å)	24.4801(3)	26.4871(2)	25.6502(8)	15.0230(4)	11.6719(4)
α (°)	101.3748(11)	90	90	69.951(3)	90
β (°)	95.3521(12)	102.4076(9)	90	71.302(3)	118.451(5)
γ (°)	96.5500(11)	90	120	70.590(4)	90
Volume($Å^3$)	5288.90(13)	6443.22(11)	7992.0(5)	2021.77(14)	2726.59(19)
Z	2	4	3	2	4
Density (calculated) (Mg/m^3)	1.505	1.511	1.662	1.487	1.624
Absorption coefficient (mm^{-1})	3.146	2.651	3.703	0.809	3.654
F(000)	2458	3000	4092	938	1352
Crystal size (mm)	0.25 × 0.11 × 0.05	0.29 × 0.11 × 0.05	0.13 × 0.05 × 0.01	0.80 × 0.31 × 0.22	0.50 × 0.10 × 0.10
Theta range for data collection (°)	6.12 to 147.824°	5.51 to 134.992°	5.38 to 134.988°	5.646 to 65.822°	7.666 to 134.996°
Reflections collected	59792	33461	42474	23937	49069
Independent reflections [R(int)]	20892 [0.0311]	11579 [0.0219]	4817 [0.1005]	13481 [0.0253]	4903 [0.0594]
Observed reflections (I>2s(I))	18029	9959	3304	10950	4350
Data / restraints / parameters	20892/42/1454	11579/30/1013	4817/12/433	13481/0/604	4903/0/427
Goodness-of-fit on F^2	1.07	1.025	1.007	1.034	1.07
R_1 [I>2σ (I)]	0.0636	0.0489	0.0454	0.0402	0.0713
wR2 (all data)	0.1863	0.1361	0.1135	0.1064	0.19
Flack Parameter					